

PB96144415  


Publication No. FHWA-RD-94-098  
August 1995

---

# Issues Impacting Bridge Painting: An Overview



U.S. Department of Transportation  
**Federal Highway Administration**

Research and Development  
Turner-Fairbank Highway Research Center  
6300 Georgetown Pike  
McLean, Virginia 22101-2296

REPRODUCED BY: **NTIS**  
U.S. Department of Commerce  
National Technical Information Service  
Springfield, Virginia 22161

## FOREWORD

This report presents a review of issues associated with bridge painting. The review takes into consideration paint debris containment problems, worker exposure and safety considerations, general environmental problems associated with bridge painting, and new regulations which have been designed to limit volatile emissions and the use of toxic ingredients in bridge paints. Recommendations and conclusions regarding the various factors assessed are presented.



Charles J. Nemmers, Director  
Office of Engineering and Highway  
Operations Research and Development

## NOTICE

This Document is disseminated under the sponsorship of the Department of Transportation in the interest of information exchange. The United States Government assumes no liability for its contents or use thereof.

The contents of this report reflect the views of the contractor who is responsible for the accuracy of the data presented herein. The contents do not necessarily reflect the official policy of the Department of Transportation.

This report does not constitute a standard, specification, or regulation.


The United States Government does not endorse products or manufacturers. Trade or manufacturers' names appear herein only because they are considered essential to the object of this document.

## GENERAL DISCLAIMER

This document may have problems that one or more of the following disclaimer statements refer to:

- This document has been reproduced from the best copy furnished by the sponsoring agency. It is being released in the interest of making available as much information as possible.
- This document may contain data which exceeds the sheet parameters. It was furnished in this condition by the sponsoring agency and is the best copy available.
- This document may contain tone-on-tone or color graphs, charts and/or pictures which have been reproduced in black and white.
- The document is paginated as submitted by the original source.
- Portions of this document are not fully legible due to the historical nature of some of the material. However, it is the best reproduction available from the original submission.



1. Report No. FHWA-RD-94-098		PB96-144415 		3. Recipient's Catalog No.	
4. Title and Subtitle ISSUES IMPACTING BRIDGE PAINTING: AN OVERVIEW		5. Report Date		6. Performing Organization Code	
7. Author(s) Thomas F. Bernecki, George M. Nichols, David Prine, Gary Shubinsky and Alan Zdunek		8. Performing Organization Report No.		10. Work Unit No. (TRAIS) 3E4C0222	
9. Performing Organization Name and Address BIRL Northwestern University 1801 Maple Avenue Evanston, IL 60201-3135		11. Contract or Grant No. DTFH61-92-C-00033		13. Type of Report and Period Covered Final Report July 1992 - January 1994	
12. Sponsoring Agency Name and Address Office of Engineering Research and Development Federal Highway Administration 6300 Georgetown Pike McLean, Virginia 22101-2296		14. Sponsoring Agency Code		15. Supplementary Notes Contracting Officer's Technical Representative (COTR): John W. Peart, HNR-20	
16. Abstract This final report documents the findings of a research program designed to collect and critically assess information on issues impacting bridge painting.  Life-cycle costs and performance were used to assess the economics of maintenance painting. These assessments are made difficult (uncertain) because performance data and hidden application costs are extremely variable. The variability of coating performance can be improved by better control of preparation quality.  Paint-removal assessments were made based largely on field operations. A few tests involving environmental chambers were conducted. Test conditions and pros and cons of the various procedures are critically summarized. Regarding worker safety, recommendations are made for close monitoring and control of the particles generated during surface preparation, especially when techniques such as steel-grit blasting and laser ablation are used for cleaning.  Paint debris digestion procedures followed by atomic absorption spectroscopy is the best way to determine total lead in a paint film. The toxicity characteristic leaching procedure (TCLP) is currently the best method for classifying paint, but may not be a reliable indicator of future resistance to leaching. Steel blast media is recyclable and stabilizes lead; proprietary additives work well in reducing leachable lead in the TCLP. Long-term stability of lead-containing debris has not been validated.  With the exception of thermal spray coatings, the lack of performance data, i.e., long-term durability data, is a major problem in using advanced coating systems. Advantages and disadvantages of thermal spray coatings are summarized. Modified accelerated testing procedures to determine coating durability were identified that could improve the correlation between laboratory tests and corresponding field tests.  Several sensor technologies were considered in an effort to identify techniques that could improve the quality of applied coatings. The methods evaluated included monochrome CCD (to determine the degree of surface rusting), color CCD to assess the cleanliness of blast-cleaned surfaces, and thermal-wave images to evaluate the condition of the substrate beneath the coating prior to paint removal.					
17. Key Words Bridge painting, paint removal/disposal, pollution, blasting, volatile organic compounds, life-cycle costs, worker safety, alternate coatings, accelerated tests.			18. Distribution Statement No restrictions. This document is available to the public through the National Technical Information Service, Springfield, VA 22161.		
19. Security Classif. (of this report) Unclassified		20. Security Classif. (of this page) Unclassified		21. No. of Pages 172	22. Price

# SI\* (MODERN METRIC) CONVERSION FACTORS

## APPROXIMATE CONVERSIONS TO SI UNITS

## APPROXIMATE CONVERSIONS FROM SI UNITS

Symbol	When You Know	Multiply By	To Find	Symbol
<b>LENGTH</b>				
in	inches	25.4	millimeters	mm
ft	feet	0.305	meters	m
yd	yards	0.914	meters	m
mi	miles	1.61	kilometers	km
<b>AREA</b>				
in <sup>2</sup>	square inches	645.2	square millimeters	mm <sup>2</sup>
ft <sup>2</sup>	square feet	0.093	square meters	m <sup>2</sup>
yd <sup>2</sup>	square yards	0.836	square meters	m <sup>2</sup>
ac	acres	0.405	hectares	ha
mi <sup>2</sup>	square miles	2.59	square kilometers	km <sup>2</sup>
<b>VOLUME</b>				
fl oz	fluid ounces	29.57	milliliters	mL
gal	gallons	3.785	liters	L
ft <sup>3</sup>	cubic feet	0.028	cubic meters	m <sup>3</sup>
yd <sup>3</sup>	cubic yards	0.765	cubic meters	m <sup>3</sup>
<b>MASS</b>				
oz	ounces	28.35	grams	g
lb	pounds	0.454	kilograms	kg
T	short tons (2000 lb)	0.907	megagrams (or "metric ton")	Mg (or "t")
<b>TEMPERATURE (exact)</b>				
°F	Fahrenheit temperature	$5(F-32)/9$ or $(F-32)/1.8$	Celcius temperature	°C
<b>ILLUMINATION</b>				
fc	foot-candles	10.76	lux	lx
fl	foot-Lamberts	3.426	candela/m <sup>2</sup>	cd/m <sup>2</sup>
<b>FORCE and PRESSURE or STRESS</b>				
lbf	poundforce	4.45	newtons	N
lbf/in <sup>2</sup>	poundforce per square inch	6.89	kilopascals	kPa

Symbol	When You Know	Multiply By	To Find	Symbol
<b>LENGTH</b>				
mm	millimeters	0.039	inches	in
m	meters	3.28	feet	ft
m	meters	1.09	yards	yd
km	kilometers	0.621	miles	mi
<b>AREA</b>				
mm <sup>2</sup>	square millimeters	0.0016	square inches	in <sup>2</sup>
m <sup>2</sup>	square meters	10.764	square feet	ft <sup>2</sup>
m <sup>2</sup>	square meters	1.195	square yards	yd <sup>2</sup>
ha	hectares	2.47	acres	ac
km <sup>2</sup>	square kilometers	0.386	square miles	mi <sup>2</sup>
<b>VOLUME</b>				
mL	milliliters	0.034	fluid ounces	fl oz
L	liters	0.264	gallons	gal
m <sup>3</sup>	cubic meters	35.71	cubic feet	ft <sup>3</sup>
m <sup>3</sup>	cubic meters	1.307	cubic yards	yd <sup>3</sup>
<b>MASS</b>				
g	grams	0.035	ounces	oz
kg	kilograms	2.202	pounds	lb
Mg (or "t")	megagrams (or "metric ton")	1.103	short tons (2000 lb)	T
<b>TEMPERATURE (exact)</b>				
°C	Celcius temperature	$1.8C + 32$	Fahrenheit temperature	°F
<b>ILLUMINATION</b>				
lx	lux	0.0929	foot-candles	fc
cd/m <sup>2</sup>	candela/m <sup>2</sup>	0.2919	foot-Lamberts	fl
<b>FORCE and PRESSURE or STRESS</b>				
N	newtons	0.225	poundforce	lbf
kPa	kilopascals	0.145	poundforce per square inch	lbf/in <sup>2</sup>

\* SI is the symbol for the International System of Units. Appropriate rounding should be made to comply with Section 4 of ASTM E380.

## TABLE OF CONTENTS

CHAPTER 1: INTRODUCTION . . . . .	1
CHAPTER 2: TASK A - ECONOMIC EVALUATION . . . . .	3
Introduction . . . . .	3
Background . . . . .	3
Model Development . . . . .	4
Life-Cycle Cost Model Development . . . . .	5
LCC Model Applications . . . . .	7
Expanded Spreadsheet Model . . . . .	11
Summary and Conclusions . . . . .	16
CHAPTER 3: TASK B - WORKER PROTECTION/PAINT REMOVAL . . . . .	21
Introduction . . . . .	21
Discussion . . . . .	21
Paint-Removal Methods . . . . .	21
IDOT Paint-Removal Demonstration-Testing Protocol . . . . .	29
Initial Tests . . . . .	30
Tests Conducted During the Paint-Removal . . . . .	30
Tests Conducted After Paint Removal . . . . .	30
Analysis of Paint and Steel for Lead by X-Ray Fluorescence . . . . .	31
Water-Jet Cleaning Results . . . . .	32
Air-Sampling Tests for VOCs Generated During Grit Blasting Within Confinement . . . . .	32
Airborne Grit-Blast Debris Particulate Sampling and Analysis . . . . .	33
Effectiveness of Paint-Removal Procedures . . . . .	39
Julien Dubuque Bridge at Dubuque, Iowa . . . . .	55
CHAPTER 4: TASK C - EVALUATION OF PROCEDURES FOR ANALYSIS AND DISPOSAL OF LEAD-BASED PAINT-REMOVAL DEBRIS . . . . .	69
Introduction . . . . .	69
Discussion . . . . .	70
Waste Analysis Methods . . . . .	70
Analysis of the Existing Paint . . . . .	70
Samples of Existing Paint From I-55 . . . . .	71
Existing Paint Analysis by Energy-Dispersive X-Ray Analysis . . . . .	71
TCLP Analysis of the Paint Debris . . . . .	74

**TABLE OF CONTENTS (continued)**

Waste Treatment . . . . .	75
Iron Stabilization of Lead-Based Paint Debris . . . . .	76
TCLP and Optical Analysis of Paint Debris Samples . . . . .	77
Conclusions and Suggestions . . . . .	80
<b>CHAPTER 5: TASK D - ADVANCED COATINGS . . . . .</b>	<b>83</b>
Introduction . . . . .	83
Background . . . . .	83
Dilemmas Facing Fabrication Shops . . . . .	85
Increased Shop Painting . . . . .	85
Containment for Maintenance Painting . . . . .	85
Fabrication Shop Problems . . . . .	85
Regulation of Fabrication Shops . . . . .	86
Overcoating . . . . .	87
Factors Affecting Performance and Durability of Overcoating Systems . . . . .	88
Adhesion/Cohesion . . . . .	88
Surface Contamination . . . . .	88
Thermal Spray Technology . . . . .	89
Introduction . . . . .	89
Thermal Spray Coatings . . . . .	89
Thermal Spray Materials . . . . .	92
Zinc . . . . .	92
Aluminum . . . . .	92
Zinc/Aluminum . . . . .	93
Sealers . . . . .	93
Infrastructural Applications of Thermal Spray Technology . . . . .	93
Thermal Spraying of Steel Bridges: A Short History . . . . .	95
Test-Panel Preparation . . . . .	96
Conclusions and Recommendations . . . . .	97
<b>CHAPTER 6: TASK E - ACCELERATED TESTING . . . . .</b>	<b>103</b>
Background . . . . .	103
Types of Coating Failure . . . . .	103
Coating Properties . . . . .	104
Coating Evaluation . . . . .	105
Objectives and Approach . . . . .	107
Materials and Procedures . . . . .	107



**TABLE OF CONTENTS (continued)**

Test-Panel Preparation . . . . .	107
Coating Type and Application . . . . .	109
Electrolyte Preparation . . . . .	110
Accelerated Test Procedure Identification and Modification . . . . .	110
Immersion Experiment . . . . .	110
Immersion Test Procedure . . . . .	110
Cyclic Test I . . . . .	110
Cyclic Test I Procedure . . . . .	112
Cyclic Test II . . . . .	112
Cyclic Test II Procedure . . . . .	114
Results and Discussion . . . . .	115
Immersion Experiments . . . . .	115
Thermally Sprayed Coatings . . . . .	115
Pb/Alkyd and VOC-Compliant Coatings . . . . .	119
Cyclic Accelerated Tests . . . . .	121
Non-Flat Panel Results . . . . .	122
Flat-Panel Results . . . . .	128
Visual Rating . . . . .	128
EIS Analysis . . . . .	128
Conclusions and Recommendations . . . . .	137
CHAPTER 7: TASK F - PRODUCTIVITY IMPROVEMENT . . . . .	141
Introduction . . . . .	141
Degree of Surface Rusting . . . . .	141
Evaluation of Blast-Cleaned Surface . . . . .	142
Quantitative Measurement of Damaged Area . . . . .	142
Infrared Thermography . . . . .	149
Introduction . . . . .	149
Disbondment of Existing Paint Systems . . . . .	149
Conclusion and Recommendations . . . . .	152
APPENDIX A: DESCRIPTION OF ELECTROCHEMICAL TECHNIQUES . . . . .	157
Electrochemical Impedance Spectroscopy . . . . .	157
Linear Polarization . . . . .	157
Potentiodynamic Polarization . . . . .	160
REFERENCES . . . . .	161

## LIST OF FIGURES

Figure 1.	EUAC versus life expectancy for various interest rates. . . .	8
Figure 2.	EUAC versus initial cost for various life expectancies, i=7%, e=4%. . . . .	8
Figure 3.	EUAC versus initial cost for various life expectancies, i=10%, e=4%. . . . .	9
Figure 4.	EUAC versus initial cost for various life expectancies, i=10%, e=0%. . . . .	9
Figure 5.	EUAC for overcoating compared to full lead removal. . . . .	10
Figure 6.	Formulas in maintenance painting life-cycle cost model. . . .	12
Figure 7.	Maintenance painting life-cycle costs: overcoating(10-percent surface corrosion), 6-yr durability. . . . .	13
Figure 8.	Maintenance painting life-cycle costs: overcoating (10 -percent surface corrosion), 10-yr durability. . . . .	14
Figure 9.	Maintenance painting life-cycle costs: overcoating (10 -percent surface corrosion), 15-yr durability. . . . .	15
Figure 10.	Maintenance painting life-cycle costs: total lead removal. . .	17
Figure 11.	Maintenance painting life-cycle costs: thermal spray [0.15 to 0.20 mm (0.006 - 0.008 in) pure zinc, Phenolic Sealer]. . . .	18
Figure 12.	Laser paint-removal test apparatus set up beneath the laser beam. . . . .	24
Figure 13.	Flask used for laser paint removal (after treating the painted steel surface for 15 min). . . . .	25
Figure 14.	SEM photomicrograph of fine soot deposited on the interior walls of the containment flask. . . . .	26
Figure 15.	SEM photomicrograph of fine soot deposited on the stainless steel base of the containment flask. . . . .	26
Figure 16.	SEM photomicrograph of fine soot deposited on the vacuum seal of the containment flask. . . . .	27
Figure 17.	Photographs at x 10 magnification of two different spots on the surface of the painted steel 1 s after laser treatments prior to cleaning off the char residue. . . . .	28

LIST OF FIGURES (continued)

Figure 18. Photograph at x 7 magnification of a spot on the surface of the painted steel after 1-s laser treatment and after cleaning off the char residue. . . . . 29

Figure 19. Coulter number percentage particle-size histogram of airborne dust samples collected within grit-blasting confinement zone during blasting. . . . . 35

Figure 20. Elzone™ number percentage particle-size analysis of airborne dust sample #1 collected within grit-blasting confinement zone during blasting. . . . . 36

Figure 21. Elzone™ number percentage particle-size analysis of airborne dust sample #2 collected within grit-blasting confinement zone during blasting. . . . . 36

Figure 22. Elzone™ volume percentage particle-size analysis of airborne dust sample #1 collected within grit-blasting confinement zone during blasting. . . . . 37

Figure 23. Elzone™ volume percentage particle-size analysis of airborne dust sample #2 collected within grit-blasting confinement zone during blasting. . . . . 37

Figure 24. SEM micrograph showing particle sizes using the acetone dispersion technique. . . . . 38

Figure 25. SEM micrograph showing particle sizes using carbon tape dispersion technique. . . . . 40

Figure 26. EDX analysis and SEM micrograph of airborne particulates collected within confinement zone during blasting. . . . . 41

Figure 27. EDX analysis and SEM micrograph of 650- $\mu\text{m}$  particles collected on filter within confinement zone during blasting. . . . . 42

Figure 28. EDX analysis and SEM micrograph of 25- $\mu\text{m}$  particle collected on filter within confinement zone during blasting. . . . . 43

Figure 29. EDX analysis and SEM micrograph of 5- $\mu\text{m}$  particle collected on filter within confinement zone during blasting. . . . . 44

Figure 30. EDX analysis and SEM micrograph of 6- $\mu\text{m}$  particle collected on filter within confinement zone during blasting. . . . . 45

Figure 31. EDX analysis and SEM micrograph of 35- $\mu\text{m}$  particle collected on filter within confinement zone during blasting. . . . . 46

Figure 32. EDX analysis and SEM micrograph of 4- $\mu\text{m}$  particle collected on filter within confinement zone during blasting. . . . . 47

**LIST OF FIGURES (continued)**

Figure 33. EDX analysis and SEM micrograph, 50- $\mu\text{m}$ particle collected on filter within confinement zone during blasting. . . . .	48
Figure 34. EDX analysis and SEM micrograph of 270- $\mu\text{m}$ particle collected on filter within confinement zone during blasting. . . . .	49
Figure 35. EDX analysis and SEM micrograph of 55- $\mu\text{m}$ particle collected on filter within confinement zone during blasting. . . . .	50
Figure 36. EDX analysis and SEM micrograph of 1- $\mu\text{m}$ particle collected on filter within confinement zone during blasting. . . . .	51
Figure 37. EDX analysis and SEM micrograph of 1- $\mu\text{m}$ particle collected on filter within confinement zone during blasting. . . . .	52
Figure 38. EDX analysis and SEM micrograph of 1- $\mu\text{m}$ particle collected on filter within confinement zone during blasting. . . . .	53
Figure 39. EDX analysis and SEM micrograph of 1- $\mu\text{m}$ particle collected on filter within confinement zone during blasting. . . . .	54
Figure 40. Scaffolding and grit-blasting confinement structure built for Julien Dubuque Bridge paint-removal job. . . . .	57
Figure 41. Low-magnification SEM photomicrographs of paint debris samples. . . . .	58
Figure 42. Low-magnification optical photographs of paint debris samples. . . . .	59
Figure 43. EDX analysis of paint debris samples from Julien Dubuque job. . . . .	60
Figure 44. SEM photomicrographs of magnetically separated paint debris particles < 45 $\mu\text{m}$ in diameter at magnifications of x 500, x 5,000, and x 50,000. . . . .	62
Figure 45. SEM photomicrographs of air-separated paint debris particles < 45 $\mu\text{m}$ in diameter at magnifications of x 500, x 5,000, and x 50,000. . . . .	63
Figure 46. SEM photomicrographs of vacuum-blast paint debris particles < 45 $\mu\text{m}$ in diameter at magnifications of x 500, x 5,000, and x 50,000. . . . .	64
Figure 47. EDX analysis of 0.5- $\mu\text{m}$ magnetically separated particles . . .	65
Figure 48. EDX analysis of 0.5- $\mu\text{m}$ air-separated particles. . . . .	66
Figure 49. EDX analysis of 0.5- $\mu\text{m}$ vacuum-blast particles . . . . .	67

## LIST OF FIGURES (continued)

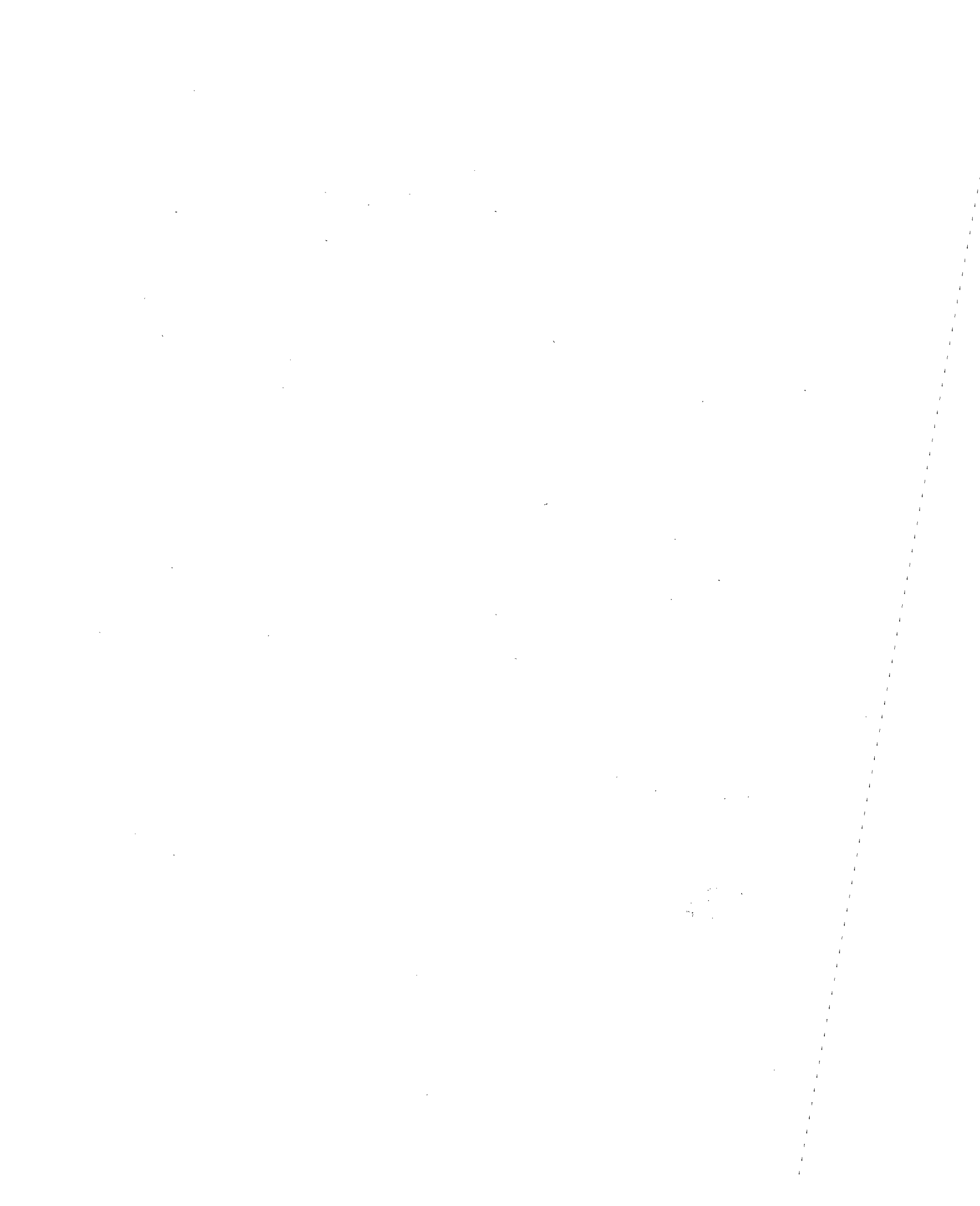
Figure 50. Inner surface of paint chip samples (x 20 magnification). . .	72
Figure 51. Paint debris from different removal methods (x 20 magnification). . . . .	79
Figure 52. NIST model of elements affecting paint durability . . . . .	84
Figure 53. Thermal spray process. . . . .	90
Figure 54. Splat structure. . . . .	90
Figure 55. Relevant thermal spray processes. . . . .	91
Figure 56. Estimated service life for Al and Al MCC thermal spray coatings. . . . .	93
Figure 57. Estimated service life for Zn and 85/15 Zn/Al thermal spray coatings. . . . .	94
Figure 58. Grit-blasted surface of steel plate. . . . .	100
Figure 59. Thermally sprayed zinc coating . . . . .	100
Figure 60. Thermally sprayed aluminum coating. . . . .	101
Figure 61. Thermally sprayed 85/15 zinc/aluminum alloy. . . . .	101
Figure 62. Thermally sprayed EAA copolymer. . . . .	102
Figure 63. Steel test panel with typical bridge geometries. . . . .	108
Figure 64. Corrosion cell used in immersion experiments. . . . .	111
Figure 65. Representative EIS Nyquist plots for the immersion experiments. . . . .	116
Figure 66. Electrochemical properties for the thermally sprayed coating in the immersion experiments. . . . .	118
Figure 67. Electrochemical properties for the Pb/alkyd and VOC-compliant coatings in immersion experiments. . . . .	120
Figure 68. Before-and-after photographs of the coated, non-flat test panels subjected to cyclic tests I and II. . . . .	123
Figure 69. Before-and-after photographs of the coated, non-flat test panels subjected to cyclic tests I and II. . . . .	129
Figure 70. Electrochemical parameters for the thermally sprayed coatings in the cyclic tests . . . . .	133

### LIST OF FIGURES (continued)

Figure 71. Electrochemical parameters for the VOC-compliant coating in the cyclic tests (GB means grit-blasted surface, MS means millscale surface). . . . .	136
Figure 72. Results of image analysis of standard for rust grade 9 (0.03 -percent rust). . . . .	143
Figure 73. Results of image analysis of standard for rust grade 8 (.01 -percent rust). . . . .	143
Figure 74. Results of image analysis of standard for rust grade 6 (1 -percent rust). . . . .	144
Figure 75. Results of image analysis of standard for rust grade 4 (10 -percent rust). . . . .	144
Figure 76. Histogram of red element. . . . .	145
Figure 77. Histogram of blue element. . . . .	146
Figure 78. Histogram of green element. . . . .	147
Figure 79. Schematic of color CCD camera system to measure damaged area. . . . .	148
Figure 80. Photograph of girder section showing damaged paint. . . . .	150
Figure 81. Calculated damaged area. . . . .	151
Figure 82. Schematic of infrared thermography system. . . . .	153
Figure 83. Section of girder used to evaluate infrared thermographs. . .	154
Figure 84. Delaminated paint on the I-Beam. . . . .	155
Figure 85. Some elements of electrochemical impedance spectroscopy. . . .	158
Figure 86. Representative potentiodynamic polarization scan for mild -steel rod in electrolyte. . . . .	160

## LIST OF TABLES

Table 1.	Summarizing life-cycle costs for three overcoat life expectancies. . . . .	16
Table 2.	Paint-removal methods. . . . .	22
Table 3.	Chloride content of water samples from I-Beam surfaces before and after water-jet cleaning. . . . .	33
Table 4.	Composition of various size particles collected on a filter within the grit-blast confinement zone. . . . .	55
Table 5.	Comparison of paint-removal methods. . . . .	56
Table 6.	EDX analysis of paint chips from I-55 in Chicago, Illinois. . .	73
Table 7.	Analysis of paint debris for lead by the TCLP method. . . . .	78
Table 8.	Metallized zinc bridges. . . . .	95
Table 9.	Thermally sprayed samples. . . . .	98
Table 10.	Paint systems. . . . .	98
Table 11.	Important factors and types of coating failure. . . . .	103
Table 12.	ASTM methods for evaluating paint and coating systems. . . . .	106
Table 13.	Summary of experimental materials. . . . .	108
Table 14.	Number of test specimens for immersion experiments. . . . .	110
Table 15.	Number of test panels for cyclic tests. . . . .	113
Table 16.	Summary of cyclic experiments. . . . .	114
Table 17.	ASTM-D610 visual corrosion rating for the non-flat test panels. . . . .	127
Table 18.	ASTM visual corrosion rating for the flat test panels. . . . .	133





## CHAPTER 1: INTRODUCTION

The economic health of a nation is dependent on its ability to engage in commerce. This ability is directly related to the capability of its infrastructure to efficiently and safely respond to the demands placed upon it, not only by its users, but also by the environment. A recent survey (1993) indicates that of the nearly 600,000 bridges tabulated, just over 190,000 bridges were considered substandard.<sup>(1)</sup> While the reasons for this classification are varied, a growing number are the result of the presence of lead-containing paints previously applied for corrosion protection. Both recently adopted and proposed future regulations have resulted from a growing awareness of the need to protect the environment from uncontrolled pollution, and to safeguard the health of workers engaged in renovation as well as that of the general populace. In 1992, Congress requested that the Federal Highway Administration (FHWA) commission, through the competitive bid process, a study to evaluate the state of technology as it pertains to the rehabilitation of bridges. In particular, the study was to evaluate how lead-containing paints are removed and tested, and to evaluate alternative coating techniques. To this end, six technical and three management and reporting tasks were initiated. The technical tasks performed were:

Task A-Economic Evaluation

Task B-Worker Protection/Paint Removal

Task C-Waste Treatment and Disposal

Task D-Alternative Coatings

Task E-Accelerated Testing

Task F-Productivity Improvement

The evaluation of coatings, materials, and processes for the rehabilitation of bridges is based on their ability to meet regulatory standards, perform in the field, and be economical.

Task A developed an economic model by which rehabilitation options can be ranked in terms of long-term benefits versus present-day expenditures. As with any study, information has been gathered from the literature and by experiments done in the laboratory. However, only when tested in the field can such information be validated. To that end, in cooperation with the Illinois Department of Transportation (IDOT), field tests for the various tasks were performed on a stretch of I-55 near Wood Avenue in Chicago, Illinois. Several methods of paint removal were tested as part of task B, and debris was collected for analysis in task C. Several selected alternative coating systems typified by painted and metallized panels were deployed at the test site for environmental exposure testing as part of task D. Furthermore, the feasibility of extending laboratory testing into the field was evaluated as part of task E. Finally, the deployment of sensors in the field to evaluate surface preparation and the condition of existing paint systems was successfully demonstrated as part of task F.



## CHAPTER 2: TASK A - ECONOMIC EVALUATION

### Introduction

The objective of task A was to perform an economic study of the highway bridge maintenance painting problem. A major goal of this task was to develop economic models that can be used to provide a rational framework for the evaluation of alternatives in the maintenance painting of steel bridges. To accomplish the objective, an extensive study of steel bridge maintenance practices was conducted. The purpose of this effort was to acquire cost data and detailed information on practices and performance experience, and to gain a better understanding of the bridge maintenance problems as viewed from the owner's perspective. This study has included a literature search and a series of meetings and discussions with various groups and individuals within the bridge maintenance community, including various State highway department personnel, representatives of the paint industry, the Steel Structures Painting Council (SSPC) and bridge painting contractors. Site visits have been made in Illinois, Wisconsin, and Kentucky. The site visits included bridges that were undergoing total lead-containing paint removal within a containment structure, and bridges that were being overcoated. These two categories represent the most commonly employed alternatives currently being pursued by bridge owners. The data and experience from the bridge maintenance painting study were used to formulate the models and to provide input data for the completed models.

### Background

Over 40 percent of the steel bridges in the United States are painted with lead-containing paints. In Illinois alone, over 2800 steel bridges that are owned by Illinois Department of Transportation (IDOT) fall into this category. This number can double or triple for States that have large numbers of rivers or extensive coastal areas. In the past, lead-containing paint provided a reliable economical solution to the long-term corrosion protection of these structures. Painting did not represent a major item in bridge maintenance, and a maintenance paint job that lasted 5 to 7 years was adequate. Recent concerns over the effects of lead as a toxic substance in the environment have resulted in a dramatic increase in the dollars spent by owners in areas associated with lead-containing paint removal. Open sand/grit blasting followed by repainting of the structure is no longer an acceptable solution. Potential solutions to the maintenance of these structures may follow one of the alternatives listed below:

1. Allow the paint to deteriorate, with potential loss of steel, until replacement of the structure is required.
2. Remove all of the lead-containing paint using negative-pressure containment and re-paint.<sup>(2)</sup>
3. Spot clean, wash, spot prime, and overcoat the steel.<sup>(3)</sup>

A variation on strategy 2 that is also currently practiced in specific situations, particularly on old bridges with only a few years left prior to replacement, is the spot-repair approach wherein bad areas of paint/corrosion are removed using vacuum power tools or localized containment and are then

repainted.<sup>(4)</sup> This is essentially an installment-plan version of number 2 that becomes less economically sound as containment, erection, and removal costs increase due to more stringent regulations.

The cost-effective solution must be chosen by careful evaluation of many complex and sometimes interacting factors. Maintenance costs of these structures have been severely impacted by the need to protect the environment. For example open blasting and repainting with a typical alkyd paint system prior to 1985 might have cost \$10.76 to \$20.52/m<sup>2</sup> (\$1.00 to \$2.00/ft<sup>2</sup>). Maintenance painting of the same structure with negative-pressure containment, total lead removal and repainting in 1993 may cost \$75.32 to \$161.40/m<sup>2</sup> (\$7.00 to \$15.00/ft<sup>2</sup>). Replacement of the bridge's superstructure can cost \$322.80 to \$538.00/m<sup>2</sup> (\$30.00 to \$50.00/ft<sup>2</sup>), while total replacement may cost \$430.40 to \$860.80/m<sup>2</sup> (\$40.00 to \$80.00/ft<sup>2</sup>).

In the past, the maintenance painting approach that was the cheapest in the short term was usually the one chosen. No consideration was typically given to factors such as life-cycle cost. The current situation involves painting costs that have dramatically increased by factors of two to three, and in some cases, as much as tenfold. Reality is that maintenance budgets have essentially remained frozen; therefore, the choice of the correct maintenance painting alternative becomes critical. Serious consideration must be given to factors such as long-term performance of coating systems and life-cycle costs.

It is this latter consideration that is the driving force behind this study. In the following sections, we will review the development of the economic models for evaluation of steel bridge maintenance painting.

#### Model Development

Two paths were pursued in the development of economic models for evaluation of steel bridge painting alternatives. They were:

- \* Classical engineering economics.
- \* Multi-parameter models that include additional factors beyond purely economic ones.

Development work on the first category is complete. A life-cycle cost model that computes equivalent uniform annual cost (EUAC) has been developed. Sensitivity analysis has been performed, and a generic chart has been produced that will allow alternatives to be compared on the basis of initial cost per square foot and expected lifetime. The second approach to model development was based on a model developed by the National Institute of Standards and Technology (NIST) using the analytic hierarchy process (AHP) decision-aiding method. Its chief positive feature is the ability to include both financial and non-financial quantitative factors as well as non-quantitative factors in the decision-making process. Work on this approach to modeling is in process. Members of the Coating Center Advisory Committee have received copies of the NIST software and we are using a team approach in developing categories, criteria, and weighing factors for the AHP model. The initial response to this approach was favorable. However, as development proceeded with the life-cycle cost (LCC) model, which would provide one of the key criteria in the AHP

model, we discovered that there were serious problems with the LCC input data. These problems are discussed in detail later in this report. These findings led us to conclude that under these circumstances, the time and money could be better spent refining the LCC model before AHP can profitably be employed.

### Life-Cycle Cost Model Development

A life-cycle cost model has been developed using Microsoft Excel™. The model uses traditional engineering economics procedures to evaluate investment alternatives. It has long been recognized that this approach, which makes use of the cost-of-money concept, tends to penalize long-term alternatives. Such is the case particularly when interest rates are higher than about 7 percent. It is not the purpose of this report to enter into a lengthy discussion of the philosophical correctness or incorrectness of this approach to evaluating alternatives. The chief attraction to using this approach is that it is widely accepted and thus provides a rational means for comparison that has a high degree of acceptance.

The bridge maintenance painting process consists of a series of cash flows that occur over the life of the structure. Our model applies an escalation factor to these cash flows to take into account the effects of inflation. The cash flows are represented as cost per square foot. This quantity is the most commonly available measurement of maintenance painting costs. It includes all of the cost components of the paint job, such as mobilization, traffic control, access, surface preparation, paint application, etc. Due to the realities of contracting for maintenance painting, detailed breakdowns of the individual components that comprise the cost per square foot are seldom available. These costs vary widely with bridge size, type, and location. Since a large amount of cost data is available on a square-footage basis, and this approach seems better related to readily observable factors, we decided to base our model on cost per square foot.

The second variable to apply to our economic analysis is the expected lifetime for the maintenance paint job. The future cash flows are spaced in time by the life expectancy of the applied coating system. Each future cash flow is inflated by the escalation factor by using the following equation:

$$FC = IC(1+e)^{np} \tag{1}$$

where

<i>FC</i>	=	future cash flow
<i>IC</i>	=	initial cost
<i>e</i>	=	escalation rate (inflation)
<i>np</i>	=	number of periods (years)

The cash flows will repeat until we reach the nearest multiple of the life expectancy that is less than the remaining life of the bridge. The future cash flows are brought back to the present by computing the present value of each of them. The equation that is used for this is:

$$PV = \frac{FC}{(1+i)^{np}} \quad (2)$$

where

- $PV$  = present value of a future cash flow ( $FC$ )
- $i$  = interest rate
- $np$  = number of periods (years)

Then, we calculate the total present value of the lifetime maintenance costs for the bridge by summing the present values.

$$TPV = \sum_{(n=1)}^{n=\text{integer } \frac{L}{l}} PV_n \quad (3)$$

where

- $TPV$  = total present value
- $L$  = life expectancy of the bridge
- $l$  = life expectancy of the coating

$$EUAC = TPV \frac{i(1+i)^L}{(1+i)^L - 1} \quad (4)$$

Finally, using equation 4, we annualize the  $TPV$  over the lifetime ( $L$ ) of the bridge using the interest rate ( $i$ ) and we get the equivalent uniform annual cost (EUAC) in dollars per square foot.

A sensitivity analysis has been conducted using the above-described life-cycle cost model. The effects of coating life expectancy on EUAC for a range of interest rates were explored. The case chosen for our analysis is a typical overcoating job. The cost used is \$21.52/m<sup>2</sup> (\$2.00/ft<sup>2</sup>). We chose an inflation rate of 4 percent and an interest rates of 6 percent, 7 percent, and 10 percent, respectively. The life expectancy of the bridge was 90 years. The sensitivity analysis varied the coating life expectancy in 1-year increments from 6 to 30 years. The lowest estimate given by various highway department personnel is 6 years. Any life expectancy lower than 6 years would represent a serious failure of the coating system. An extremely optimistic life expectancy for any paint system in a typical midwest environment is 30

years. The results of the analysis are summarized in figure 1.

The analysis clearly shows that improvements in the life expectancy for the coating system have a strong effect on EUAC in the range of 6 to 15 years, with the effect rapidly diminishing after 15 years. The effects of changing the interest rate are also clearly shown. Again, the strongest effect on EUAC by a change in interest rate is in the 6- to 15-year range of life expectancy.

### LCC Model Applications

The basic life-cycle cost model discussed in the previous section has been used to produce a chart that plots EUAC versus initial cost for a range of coating life expectancies. The resultant chart contains a family of EUAC curves for initial cost, ranging from \$0.00 to \$215.20/m<sup>2</sup> (\$0.00 to \$20.00/ft<sup>2</sup>) for life expectancies of 6, 10, 15, 25, and 40 years, respectively. An example is shown in figure 2.

The chart in figure 2 can be used to compare various coating strategies on the basis of the initial cost of application and the expected lifetime for the coating. The strong sensitivity of life-cycle costs to the life expectancy of the coating is readily apparent from examining this figure. For example, a coating system that has a \$26.90/m<sup>2</sup> (\$2.50/ft<sup>2</sup>) initial cost and a life expectancy of 6 years has a life-cycle cost of \$10.76/m<sup>2</sup>/yr (\$1.00/ft<sup>2</sup>/yr) for its remaining life. If we could extend the life expectancy to 10 years, we could afford to spend approximately \$43.04/m<sup>2</sup> (\$4.00/ft<sup>2</sup>) and still maintain the same life-cycle cost. Another way of utilizing this chart would be to compare two different coating systems, one with an initial cost of \$107.60/m<sup>2</sup> (\$10.00/ft<sup>2</sup>) and another with an initial cost of \$43.04/m<sup>2</sup> (\$4.00/ft<sup>2</sup>). Let us assume that the \$43.04/m<sup>2</sup> (\$4.00/ft<sup>2</sup>) system has a life expectancy of 10 years. To be competitive, the \$107.60/m<sup>2</sup> (\$10.00/ft<sup>2</sup>) system would have to have a life expectancy of approximately 40 years. All of the above is true for the financial parameters chosen, interest rate of 7 percent interest and an inflation rate of 4 percent. The interest rate and inflation rate tend to counteract each other. If the interest rate rises, but inflation remains the same, the slopes of the curves decrease and the sensitivity to changes in life expectancies longer than 15 years decreases. This effect is shown in figure 3.

This figure shows the same range of initial costs and life expectancies as shown in figure 2 except that the interest rate has been increased to 10 percent and the inflation rate is held at 4 percent. The effect of changing the inflation rate can be seen in figure 4, where we have held interest constant at 10 percent and reduced the inflation rate to 0 percent.

Here we can clearly see that the slopes are decreased and any advantage between 25- and 40-year life expectancy has disappeared and, in fact, there is little advantage to extending life expectancy beyond 15 years under these financial conditions. In any case, one has no control over these purely financial factors and, furthermore, over an extended lifetime of a structure, we can be certain that significant variation will occur. The purpose of this model is simply to allow uniform comparisons to be made under present conditions.

### Life-Cycle Cost Sensitivity Analysis

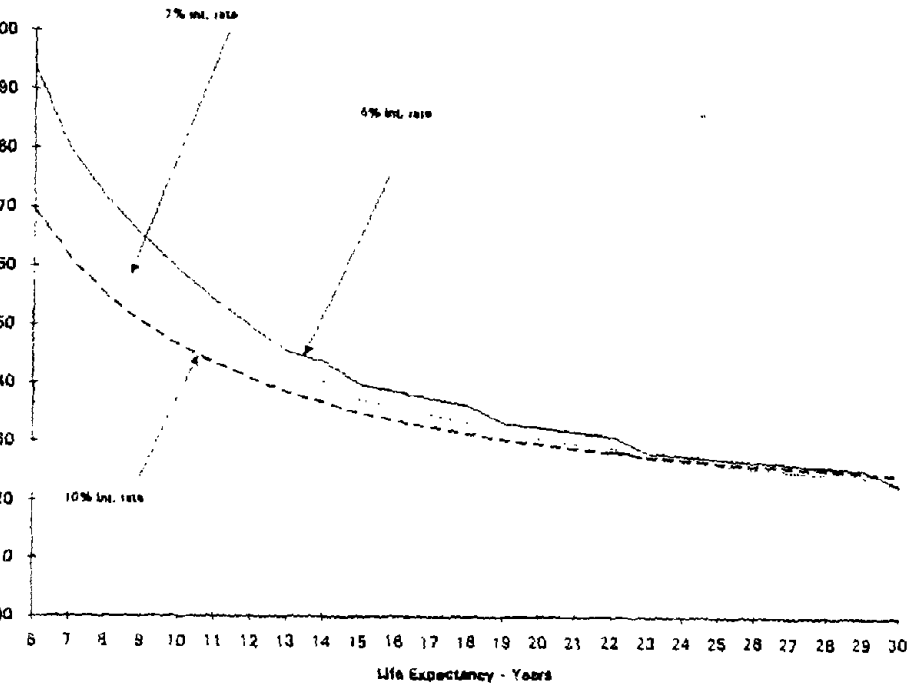
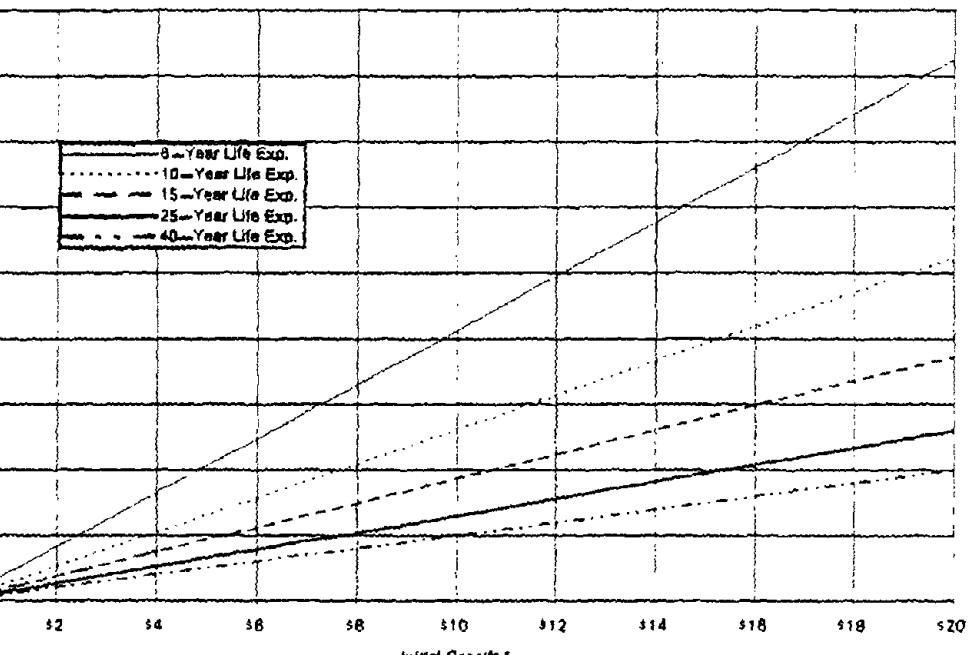
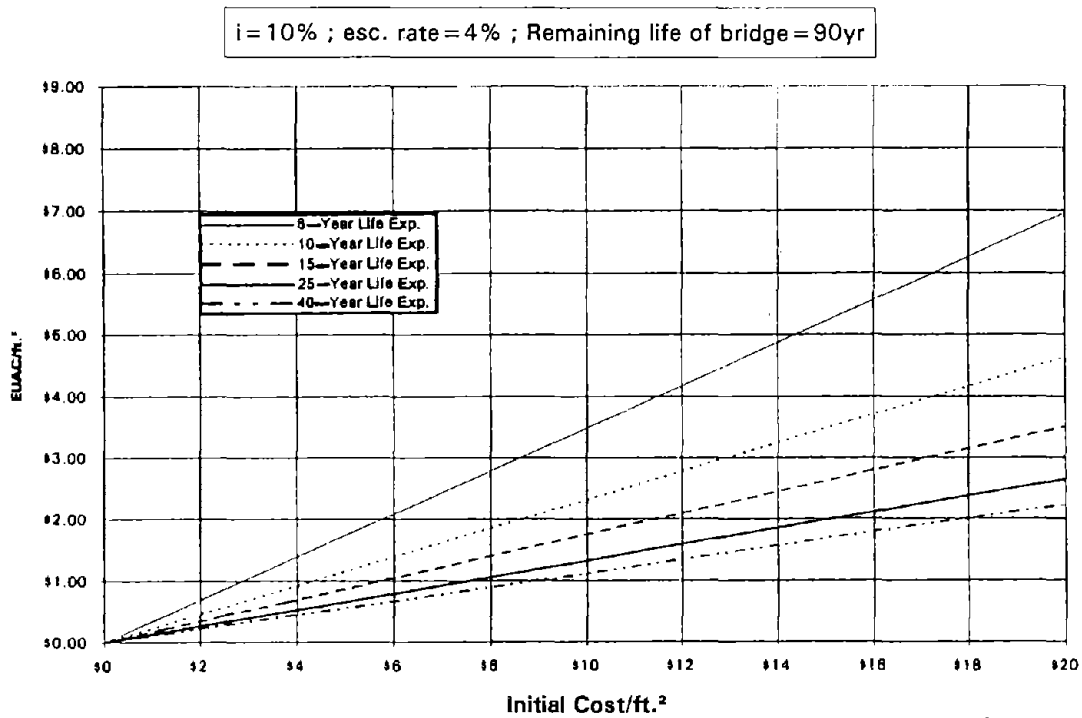


Figure 1. EUAC versus life expectancy for various interest rates.

$i = 7\%$  ;  $acc. rate = 4\%$  ; Remaining life of bridge = 90yr

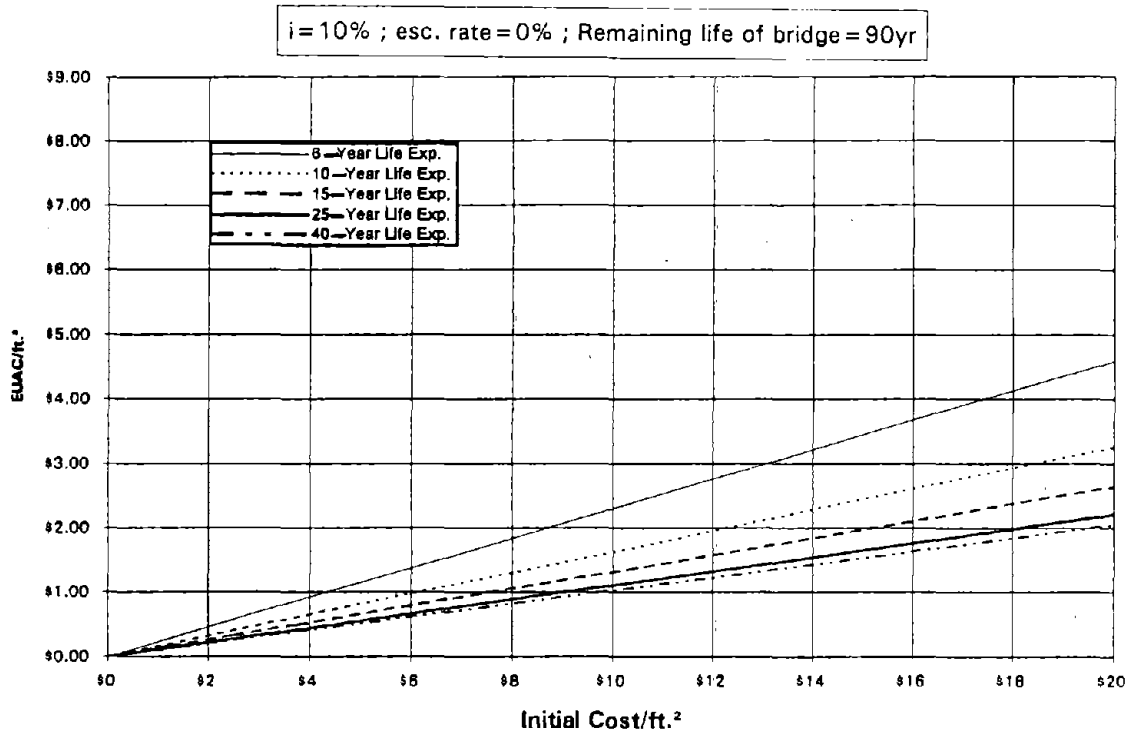






$\$1.00/\text{ft}^2 = \$10.75/\text{m}^2$

Figure 3. EUAC versus initial cost for various life expectancies,  $i=10\%$ ,  $e=4\%$ .



$\$1.00/\text{ft}^2 = \$10.75/\text{m}^2$

Figure 4. EUAC versus initial cost for various life expectancies,  $i=10\%$ ,  $e=0\%$ .

The EUAC versus initial cost chart can also be used to compare coating alternatives and to define the allowable ranges of initial cost and life expectancy for a candidate to be competitive on the basis of life-cycle costs with another candidate. In figure 5, we see the chart for an interest rate of 7 percent and an inflation rate of 4 percent, with two regions of the chart that represent overcoating and full lead removal.

In this figure, we can see that for the cheapest overcoat job with a poor performance of only 6 years life expectancy, we would have to get 25 years out of even the cheapest total lead-removal job for the two approaches to be competitive on the basis of life-cycle costs. This approach could be used to evaluate any new coating alternative with an existing one. The chart would tell us what we would have to get in life expectancy out of a new candidate system that might be more expensive than an existing system for it to be life-cycle cost-competitive. This approach could also be used to tell us how much we can afford to spend to increase the life expectancy of a system. For example, if a \$21.52/m<sup>2</sup> (\$2.00/ft<sup>2</sup>) system is giving us only 6 years of life expectancy, we can afford to spend up to \$43.04/m<sup>2</sup> (\$4.00/ft<sup>2</sup>) to extend the life to only 10 years. This latter observation should have an impact on how State highway departments look at the question of warranted paint jobs. Some paint companies offer warranties that typically cover 10 years. The warrantee adds a cost increment to the paint job. The life-cycle cost approach of comparing these two alternatives says that the increment could be

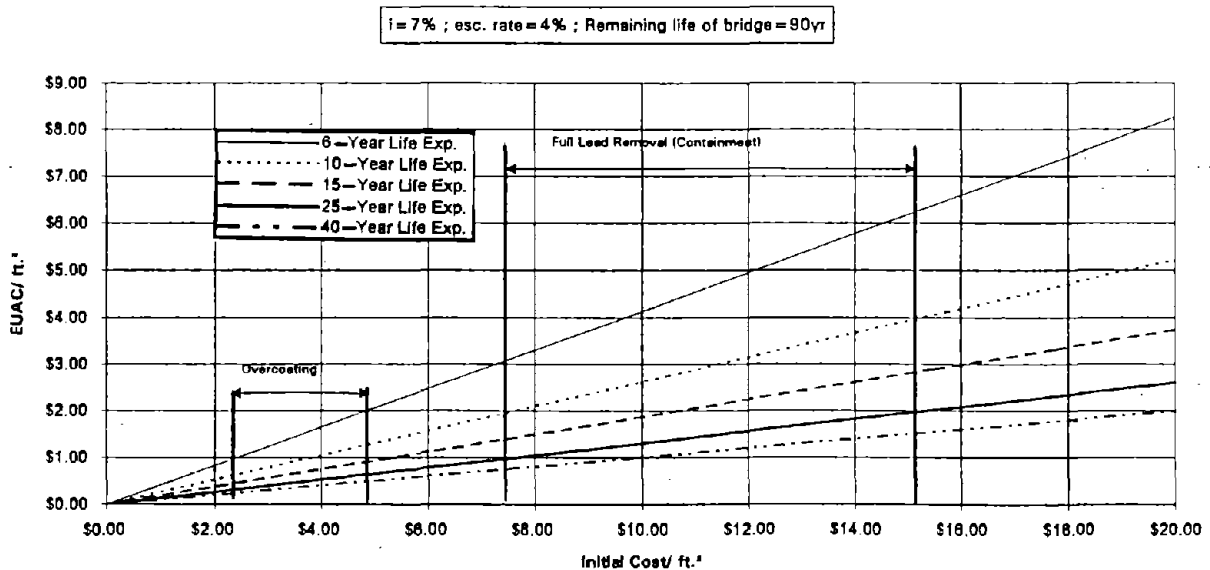


Figure 5. EUAC for overcoating compared to full lead removal.

as high as 100 percent (certainly, considerably more than is typically charged for a warrantee) for the case shown above. The allowable margin for increased cost to get increases in life expectancy decreases as we go to higher initial life expectancy.

These examples have shown that an application of a simple life-cycle cost method can add significant insight to the consideration of various alternatives in the maintenance painting of steel bridges.

### Expanded Spreadsheet Model

The basic life-cycle cost model based on present value analysis discussed above was expanded to allow input of more detailed cost data and to allow exploration of mixed coating strategies. Seven individual cost-item categories are available for input. Each cost-item category can be assigned an individual escalation (inflation) factor to account for the fact that labor and non-labor items may have different escalation rates. An eighth cost category is available, Lump Sum Costs, in case detailed data are unavailable. The escalation factor used for the lump sum cost is a weighted average of the other seven escalation rates. The weighing factors are taken from detailed cost information provided by several sources, including both painting consultants and highway departments.<sup>(5,6,7)</sup> An additional refinement of the model is the ability to use different costs and coating life expectancies for each of the maintenance paint cycles. The current implementation covers up to 10 repaint cycles and is easily expandable both for additional repaint cycles as well as more detailed cost components. The resultant output includes both the total present value (TPV) and the equivalent uniform annual cost, (EUAC). As in the previously discussed model, the computation is accomplished using a Microsoft Excel™ spreadsheet. Figure 6 shows a portion of the spreadsheet with the Excel™ formulas printed in the appropriate cells. Several case studies using the spreadsheet model have been done and a discussion of them follows.

The first case shown in figures 7, 8, and 9 compares the overcoating process for a bridge with 10 percent surface corrosion for overcoat life expectancies of 6, 10, and 15 years, respectively. The bridge has 60 years of remaining life, and the interest rate is assumed to be 7 percent. Cost data are taken from Angeloff.<sup>(5)</sup> The model shows that, as expected, the life-cycle costs are profoundly affected by the life expectancy of the applied process. Table 1 summarizes these results.

The next case study considers a bridge that has degraded beyond the point where overcoating is a viable option. Here we compare a typical total lead removal with containment and conventional painting (figure 10) with the same total lead-removal process, but with thermal spray, an advanced coating process, evaluated in task D (figure 11). The paint data are taken from Oregon DOT, and Angeloff and Kay.<sup>(4,5,8)</sup> The thermal spray process utilizes coating material that costs \$21.09/m<sup>2</sup> (\$1.96/ft<sup>2</sup>) as compared to the conventional paint system's \$5.38/m<sup>2</sup> (\$0.50/ft<sup>2</sup>) cost. The coating application costs are also higher for the thermal spray [\$15.49 versus 10.76/m<sup>2</sup> (\$1.44 versus \$1.00/ft<sup>2</sup>)]. In fact, the total initial cost of the thermal spray is 8 percent higher than the conventional paint job [\$203.90

	A	B	C	D	E	F	G
1	Maintenance Painting Cost/ft <sup>2</sup> (Yr)	Exp. Rates					
2	Lump Sum Cost (\$/ft <sup>2</sup> )	$= (6*B3 + 2*B4 + B5 + 10*B6 + 4*B7 + 4*B8 + 8*B9)/41$	0	0	0		
3	Surface Preparation (Labor + Material)(\$/ft <sup>2</sup> )	0.0394	3.07	3.07	3.07		
4	Coating Application (Labor)(\$/ft <sup>2</sup> )	0.04	1.44	1.44	1.44		
5	Coating Material(\$/ft <sup>2</sup> )	0.0191	1.90	1.90	1.90		
6	Containment & Air Filtration System(\$/ft <sup>2</sup> )	0.03	6	6	6		
7	Rigging(\$/ft <sup>2</sup> )	0.03	1.04	1.04	1.04		
8	Mobilization(\$/ft <sup>2</sup> )	0.03	2.44	2.44	2.44		
9	Hazardous Waste Storage & Disposal(\$/ft <sup>2</sup> )	0.06	3	0	0		
10	Coating Life Expectancy(Years)		30	30	30		
11	Remaining Bridge Life(Years)	60					
12	Interest Rate	0.07					
13	TPV	$= F27$					
14	EJAC	$= PMT(B12, B11, -B13)$					
15							
16							
17	Year	0	= C10	= C10	= C10 + D10		
18		$= C2*(1 + B2)^C17$	$= D2*(1 + B2)^D17$	$= E2*(1 + B2)^E17$			
19		$= C3*(1 + B3)^C17$	$= D3*(1 + B3)^D17$	$= E3*(1 + B3)^E17$			
20		$= C4*(1 + B4)^C17$	$= D4*(1 + B4)^D17$	$= E4*(1 + B4)^E17$			
21		$= C5*(1 + B5)^C17$	$= D5*(1 + B5)^D17$	$= E5*(1 + B5)^E17$			
22		$= C6*(1 + B6)^C17$	$= D6*(1 + B6)^D17$	$= E6*(1 + B6)^E17$			
23		$= C7*(1 + B7)^C17$	$= D7*(1 + B7)^D17$	$= E7*(1 + B7)^E17$			
24		$= C8*(1 + B8)^C17$	$= D8*(1 + B8)^D17$	$= E8*(1 + B8)^E17$			
25		$= C11*(1 + B9)^C17$	$= D8*(1 + B9)^D17$	$= E9*(1 + B9)^E17$			
26	Re-Paint Cost	$= SUM(C18:C25)$	$= SUM(D18:D25)$	$= SUM(E18:E25)$			
27	Present Value	$= C26/((1 + B9)^12)^C17$	$= D26/((1 + B9)^12)^D17$	$= E26/((1 + B9)^12)^E17$	$= SUM(C27:E27)$	TPV	

$$\$1.00/\text{ft}^2 = \$10.76/\text{m}^2$$

Figure 6. Formulas in maintenance painting life-cycle cost model.

Maintenance Painting Cost / Cycle	Esc. Rates	1	2	3	4	5	6	7	8	9	10
Lump Sum Cost	3.75%	\$0.00	\$0.00	\$0.00	\$0.00	\$0.00	\$0.00	\$0.00	\$0.00	\$0.00	\$0.00
Surface Preparation (Labor + Material)	3.94%	\$0.60	\$0.60	\$0.60	\$0.60	\$0.60	\$0.60	\$0.60	\$0.60	\$0.60	\$0.60
Coating Application (Labor)	4.00%	\$1.18	\$1.18	\$1.18	\$1.18	\$1.18	\$1.18	\$1.18	\$1.18	\$1.18	\$1.18
Coating Material	1.91%	\$0.59	\$0.59	\$0.59	\$0.59	\$0.59	\$0.59	\$0.59	\$0.59	\$0.59	\$0.59
Containment & Air Filtration System	3.00%	\$0.03	\$0.03	\$0.03	\$0.03	\$0.03	\$0.03	\$0.03	\$0.03	\$0.03	\$0.03
Rigging	3.00%	\$1.04	\$1.04	\$1.04	\$1.04	\$1.04	\$1.04	\$1.04	\$1.04	\$1.04	\$1.04
Mobilization	3.00%	\$0.13	\$0.13	\$0.13	\$0.13	\$0.13	\$0.13	\$0.13	\$0.13	\$0.13	\$0.13
Hazardous Waste Storage & Disposal	6.00%	\$0.03	\$0.03	\$0.03	\$0.03	\$0.03	\$0.03	\$0.03	\$0.03	\$0.03	\$0.03
Coating Life Expectancy		6	6	6	6	6	6	6	6	6	6
Remaining Bridge Life	60										
Interest Rate	7.00%										
TPV	\$16.97										
EUAC	\$1.21										
<b>Note: All costs are on a per-square-foot basis.</b>											
	Year	0	6	12	18	24	30	36	42	48	54

$$\$1.00/\text{ft}^2 = \$10.75/\text{m}^2$$

Figure 7. Maintenance painting life-cycle costs: overcoating (10-percent surface corrosion), 6-yr durability.

Maintenance Painting Cost / Cycle	Esc. Rates	1	2	3	4	5	6	7	8	9	10
Lump Sum Cost	3.75%	\$0.00	\$0.00	\$0.00	\$0.00	\$0.00	\$0.00				
Surface Preparation (Labor + Material)	3.94%	\$0.60	\$0.60	\$0.60	\$0.60	\$0.60	\$0.60				
Coating Application (Labor)	4.00%	\$1.18	\$1.18	\$1.18	\$1.18	\$1.18	\$1.18				
Coating Material	1.91%	\$0.59	\$0.59	\$0.59	\$0.59	\$0.59	\$0.59				
Containment & Air Filtration System	3.00%	\$0.03	\$0.03	\$0.03	\$0.03	\$0.03	\$0.03				
Rigging	3.00%	\$1.04	\$1.04	\$1.04	\$1.04	\$1.04	\$1.04				
Mobilization	3.00%	\$0.13	\$0.13	\$0.13	\$0.13	\$0.13	\$0.13				
Hazardous Waste Storage & Disposal	6.00%	\$0.03	\$0.03	\$0.03	\$0.03	\$0.03	\$0.03				
Coating Life Expectancy		10	10	10	10	10	10				
Remaining Bridge Life	60										
Interest Rate	7.00%										
TPV	\$10.86										
EUAC	\$0.77										
<b>Note: All costs are on a per-square-foot basis.</b>											
Year	0	10	20	30	40	50	60	60	60	60	60

$$\$1.00/\text{ft}^2 = \$10.75/\text{m}^2$$

Figure 8. Maintenance painting life-cycle costs: overcoating (10-percent surface corrosion), 10-yr durability.

Maintenance Painting Cost / Cycle	Est. Rates	1	2	3	4	5	6	7	8	9	10
Lump Sum Cost	3.75%	\$0.00	\$0.00	\$0.00	\$0.00						
Surface Preparation (Labor + Material)	3.94%	\$0.60	\$0.60	\$0.60	\$0.60						
Coating Application (Labor)	4.00%	\$1.18	\$1.18	\$1.18	\$1.18						
Coating Material	1.91%	\$0.59	\$0.59	\$0.59	\$0.59						
Containment & Air Filtration System	3.00%	\$0.03	\$0.03	\$0.03	\$0.03						
Rigging	3.00%	\$1.04	\$1.04	\$1.04	\$1.04						
Mobilization	3.00%	\$0.13	\$0.13	\$0.13	\$0.13						
Hazardous Waste Storage & Disposal	6.00%	\$0.03	\$0.03	\$0.03	\$0.03						
Coating Life Expectancy		15	15	15	15						
Remaining Bridge Life	60										
Interest Rate	7.00%										
TPV	\$7.83										
EUAC	\$0.56										
<b>Note: All costs are on a per-square-foot basis.</b>											
	Year	0	15	30	45	60	60	60	60	60	60

$$\$1.00/\text{ft}^2 = \$10.75/\text{m}^2$$

Figure 9. Maintenance painting life-cycle costs: overcoating (10-percent surface corrosion), 15-yr durability.

versus \$188.30/m<sup>2</sup> (\$18.95 versus \$17.50/ft<sup>2</sup>)]. The resulting life-cycle costs, however, clearly favor thermal spray. This occurs because the life expectancy is doubled by going to thermal spray.

### Summary and Conclusions

The application of life-cycle cost considerations to the maintenance coating of steel bridges represents a major departure from the current practice of basing coating decisions on lowest initial cost. The spreadsheet model developed here can be exercised for a variety of possibilities and provides some interesting observations. A major problem becomes apparent upon a careful examination of the data that feeds the model. The cost and performance data are highly variable and considerable doubt exists about the validity of comparisons between different sources. The reasons for these problems are many. The costs are seldom available in a detailed breakout format. Typically, the cost data are simply a lump sum that may be transformed to a unit cost per area if the surface area is provided. Some States still use the practice of expressing coating costs as a cost per ton of steel. This practice stems from the commonly used approach applied to new construction. Given the wide range of geometries used in bridge construction, conversion of cost per ton to cost per square foot is difficult. Another major factor in the variability of the cost data is the presence of hidden costs. For example, we may consider two similar bridges with the same surface preparation and coating system that have different accessibility limitations. In one case, access for painting is unrestricted, while in the other case, painting can only be performed during periods of minimal traffic disruption. For the first bridge, scaffolding and containment can be erected and left in place until the job is complete, while the second bridge requires the scaffolding and containment to be assembled and disassembled before and after each daily painting period. If all other costs remain identical, these two jobs could easily differ by two or three times in cost per square foot. Another source of hidden costs results from typical contractor practices that stem from cash-flow problems. Contractors will typically shift labor costs to purchased materials so that they can front-load their invoicing. This practice introduces large variations in hardware and material costs.

Performance data is also badly clouded. The judgment of when a coating system has failed can be very subjective, particularly if no uniform quantitative standards exist for judging failure. The current study being conducted by Ocean City Research, under FHWA funding, addresses this problem to some degree and should result in better, more objective coating system performance data. A very important consideration in judging coating system performance is to

**Table 1. Summarizing life-cycle costs for three overcoat life expectancies.**

Life Expectancy	TPV	EUAC (\$/ft <sup>2</sup> )
6 Years	\$16.97	\$ 1.21
10 Years	\$10.86	\$ 0.77
15 Years	\$ 7.83	\$ 0.56

$$\text{\$1.00/ft}^2 = \text{\$10.75/m}^2$$



Maintenance Painting Cost / Cycle	Disc. Rate	1	2	3	4	5	6	7	8	9	10
Lump Sum Cost	3.75%	\$0.00	\$0.00	\$0.00	\$0.00	\$0.00					
Surface Preparation (Labor + Material)	3.94%	\$3.00	\$3.00	\$3.00	\$3.00	\$3.00					
Coating Application (Labor)	4.00%	\$1.00	\$1.00	\$1.00	\$1.00	\$1.00					
Coating Material	1.91%	\$0.50	\$0.50	\$0.50	\$0.50	\$0.50					
Containment & Air Filtration System	3.00%	\$6.00	\$6.00	\$6.00	\$6.00	\$6.00					
Rigging	3.00%	\$2.00	\$2.00	\$2.00	\$2.00	\$2.00					
Mobilization	3.00%	\$2.00	\$2.00	\$2.00	\$2.00	\$2.00					
Hazardous Waste Storage & Disposal	6.00%	\$3.00	\$0.00	\$0.00	\$0.00	\$0.00					
Coating Life Expectancy		15	15	15	15	15					
Remaining Bridge Life		60									
Interest Rate		7.00%									
TPV		\$35.67									
EUAC		\$2.54									
<b>Note: All costs are on a per-square-foot basis.</b>											
	Year	0	15	30	45	60	75	75	75	75	75

$\$1.00/\text{ft}^2 = \$10.75/\text{m}^2$

Figure 10. Maintenance painting life-cycle costs: total lead removal.

Maintenance Painting Cost / Cycle	Fac. Rates	1	2	3	4	5	6	7	8	9	10
Lump Sum Cost	3.75%	\$0.00	\$0.00	\$0.00							
Surface Preparation (Labor + Material)	3.94%	\$3.07	\$3.07	\$3.07							
Coating Application (Labor)	4.00%	\$1.44	\$1.44	\$1.44							
Coating Material	1.91%	\$1.96	\$1.96	\$1.96							
Containment & Air Filtration System	3.00%	\$6.00	\$6.00	\$6.00							
Rigging	3.00%	\$1.04	\$1.04	\$1.04							
Mobilization	3.00%	\$2.44	\$2.44	\$2.44							
Hazardous Waste Storage & Disposal	6.00%	\$3.00	\$0.00	\$0.00							
Coating Life Expectancy		30	30	30							
Remaining Bridge Life		60									
Interest Rate		7.00%									
TPV		\$26.20									
EUAC		\$1.87									
<b>Note: All costs are on a per-square-foot basis.</b>											
	Year	0	30	60	90	90	90	90	90	90	90

$$\$1.00/\text{ft}^2 = \$10.75/\text{m}^2$$

Figure 11. Maintenance painting life-cycle costs: thermal spray [0.15 to 0.20 mm (0.006 - 0.008 in) pure zinc, Phenolic Sealer].

ensure that uncontrolled variables such as surface preparation are minimized. The development of improved global and local sensors to ascertain the condition of the prepared surface prior to coating application will aid this aspect of judging performance. A very important aspect of sensor development is the provision for traceability of data. Current visual inspection does not provide this important feature.

Additional consideration needs to be given to contracting practices. If life-cycle cost methods are to provide meaningful comparisons of alternatives, reliable cost data must be available. One approach that might aid the situation would be uniform coating contract standards that require detailed cost breakouts of the elements of the project. These cost elements need to hold up to audit standards so that hidden costs cease to exist. This process will not be popular with painting contractors, but if we are going to employ life-cycle costs as a criteria for judging coating alternatives, we must be sure that the data (cost and performance) are accurate and that we are indeed comparing alternatives on a rational basis.



## CHAPTER 3: TASK B - WORKER PROTECTION/PAINT REMOVAL

### Introduction

The objective of task B was to review current worker health and safety practices pertaining to the removal of lead-based paint from existing structures. This included reviewing containment concepts and methods of testing the relative efficiency and safety of different types of paint-removal methods. Development of a test chamber to assess the relative merits of various removal techniques also was suggested in the initial plan. The objectives were achieved by: (1) assessing information obtained from State and Federal DOT personnel, the general literature (including Steel Structure Painting Council (SSPC) publications), and materials and equipment suppliers, (2) conducting and participating in field paint-removal and recoating trials, (3) observation and assessment of contract bridge repainting operations done in cooperation with State departments of transportation, especially the Illinois Department of Transportation (IDOT), and (4) performing laboratory tests and analysis of samples from the various field operations in addition to samples prepared in the laboratory.

The program plans were reviewed with an advisory committee consisting of experts in the field, including State DOT representatives from Oregon, Illinois, and Kentucky; the U.S. Army Corps of Engineers; paint and thermal spray companies; and the FHWA program monitor. The consensus of the committee was that it would be difficult to develop and qualify a universal test chamber to accurately assess the relative merits of paint-removal techniques within the time and funds allocated to this task in this program. It was agreed, however, that a controlled-environment chamber could be valuable for certain removal-method evaluations as well as for paint-application control studies. Thus, the majority of the paint-removal/worker-protection analyses were based on field operations, and a lesser number of analyses were based on chamber tests. Valuable information also was provided by the Iowa, Kentucky, Louisiana, North Carolina, and Wisconsin DOTs.

### Discussion

#### Paint-Removal Methods

There are many methods of paint removal, including abrasive or grit blasting, water jets, handtools, power tools, chemical stripping, and heat. Each of these general methods consists of a number of subcategories as shown in table 2.

An excellent comparison of many of the attributes of these methods is given in the *Industrial Lead-Paint Removal Handbook* by K.A. Trimmer (see chapter 5, table 4). Additional comparisons based on our work in this program are provided later.

In the past, the most common paint-removal method has been abrasive or grit blasting. It is fast, and it removes paint, corrosion, and millscale to produce a clean surface with a good profile for recoating. Its main disadvantage is that it produces large volumes of dust. The dust contains very fine particulates from which the environment and the workers must be protected. The cost of this protection is high. Today, continuous blasting

Table 2. Paint-removal methods.

---

---

A. Grit-Blasting Options:

1. Open to environment,\* vacuum attachment, or total confinement.
2. Expendable or recyclable abrasive.
3. Wet or dry.
4. Water soluble or insoluble blast media.
5. Silica, slag, steel, silicon carbide, salt, or plastic media.
6. Single component, additives, blends, or mixtures.

B. Water-Jet Options:

1. Low, medium, high, or ultra-high pressure.
2. Heated or ambient temperature.
3. With or without abrasive injection.
4. With or without additives such as detergent.

C. Handtools Options:

1. Knife, chisel, brush, etc.

D. Power-Tools Options:

1. Open to environment or vacuum attachment.
2. Needle gun, roto-peen, abrasive disc.

E. Chemical-Stripping Options:

1. Solvent, gel, or paste.
2. Open to environment or within confinement.

F. Heat (or Light) Options:

1. Flame, heat gun, laser, high-energy light, induction, etc.
  2. Embrittle, burn, or pyrolyze.
  3. Open to environment, off-gas scrubbing, or within confinement.
- 
- 

\* No longer acceptable.

without containment will generate particulates in excess of the U.S. Environmental Protection Agency (EPA) regulations. An alternative is vacuum blasting without confinement, but the removal rates are greatly reduced (approximately 80 percent). The added weight of the vacuum attachment tires the operator and the added bulk reduces mobility. In case of containment, building and moving the confinement structures are both costly and time-consuming. In both cases, the used blast media and the paint debris need to be separated so the media can be recycled and the volume of hazardous waste can be reduced. This significantly reduces the cost of treatment and disposal of the waste.

Steel grit often is selected because it can be recycled repeatedly because of a low breakdown rate. It gives a good surface profile, and provides temporary

stabilization against leaching of lead from the debris as measured by the toxicity characteristic leaching procedure (TCLP) test. Steel-grit blasting produces large numbers of paint debris particles with diameters of less than 1.0  $\mu\text{m}$ . As discussed in greater detail later, size analysis of the particles collected on a filter within the blast confinement area showed that more than 50 percent of the particles had diameters of less than 1.0  $\mu\text{m}$ . Elemental analysis of these fine particles shows that they contain lead. It is difficult to determine how many particles with diameters less than 0.3  $\mu\text{m}$  are produced by the blasting operation because such small particles pass through most filters and common particle size analysis techniques are not applicable below 0.3  $\mu\text{m}$ . Particulates that contain lead/chromium and have diameters less than 0.3  $\mu\text{m}$  would present a hazard to the worker because: (1) they would not be totally removed by standard high efficiency particle absolute (HEPA) filters, which are rated 99.97 percent efficient down to 0.3- $\mu\text{m}$  size particles, (2) they would be difficult to contain within the confinement structure, and (3) they would produce contamination at greater distances from the work site.

Despite problems associated with grit blasting, its high removal rate outweighs the additional costs associated with worker and environmental protection when compared with other paint-removal options. In general, blasting within confinement is the method of choice when complete paint removal is specified, while vacuum blasting may be selected for spot-preparation requirements. In this process, it is difficult to recover all dust and debris with the vacuum system. Very few additives are used in grit blasting. One exception is the addition of a material such as Blastox™, which has been shown to help stabilize the lead in the paint debris against leaching in the TCLP test. A negative aspect of Blastox™ is the need to keep it dry; when wet it clogs the blasting system.

Water jets can be used to remove loose paint and rust, as well as salt, dirt, and soils. Advantages of this method are: (1) the degree of loose paint and rust removal can be altered by adjusting the water pressure, (2) the paint usually comes off in chips so that these chips can be collected on a porous tarp, while allowing the water to pass through, (3) the water temperature can be adjusted, and (4) it is relatively inexpensive. Disadvantages are: (1) the method, by itself, is not suitable for total paint, corrosion, and millscale removal; (2) it does not produce any surface profile; and (3) care must be taken to be sure all hazardous debris is contained and properly disposed. Paint removal by handtools gives a minimally prepared surface. This may be satisfactory provided good surface-tolerant paints are available and limited coating lifetimes are acceptable. Handtool removal is probably the most operator sensitive of the removal methods. It has the advantage of producing the least debris and the debris that is produced can be easily collected on tarps.

Chemical stripping is used in certain cases, depending on bridge type and location. It is used most often to remove paint from tanks. This process involves messy, dangerous acidic or alkaline materials, often as gels, which are hazardous and require thorough rinsing and proper disposal.

Paint removal by laser was examined in the laboratory using a Coherent EFA51, 1500-W, continuous-wave CO<sub>2</sub> laser. The substrates (test samples) were 102-mm (4-in) square or 51-mm by 102-mm (2-in by 4-in) rectangular sections of

painted steel cut from bridge girders that had been taken out of service and stored by the Illinois Department of Transportation. The existing paint was a three-layer system consisting of a red-lead/alkyd primer, a leafing aluminum/phenolic matrix intermediate coating, and a green-pigmented, non-leafing aluminum/phenolic topcoat. The test samples were placed within a glass confinement system with a zinc selenide (ZnSe) window so that all byproducts from the removal process were contained. The containment system consisted of a 2-L glass filter flask with side tubulation and the bottom cut off. The test sample was placed on a steel-base plate to which the flask was sealed by vacuum-bagging tacky tape. The ZnSe window was sealed to the top of the flask and the side arm led through a Tenax™ adsorbent tube to a Tedlar™ gas bag. The apparatus is shown in figure 12.

The laser beam covered a 6.4-mm (1/4-in) diameter area of the sample surface. It was found that approximately 1 s of laser operation was sufficient to remove the paint without damage to the steel. Thus, the sample was moved to expose a different spot on the surface after each 1-s irradiation until sufficient byproduct could be collected for analysis.

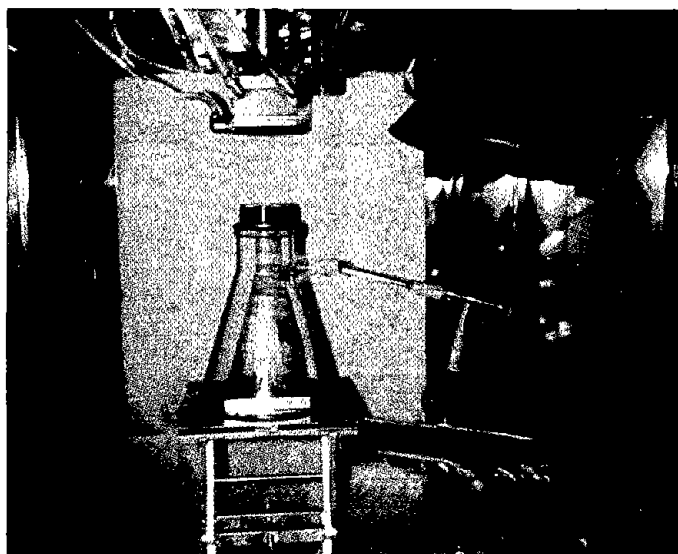


Figure 12. Laser paint-removal test apparatus set up beneath the laser beam.



Each time the laser beam impinged upon the painted surface, the paint burned with a yellow, sooty flame that rose 76 to 102 mm (3-4 in) above the painted surface. Visibility through the flask was reduced with each application of the laser. This was due to the fine soot that formed and was deposited on the sides of the flask. It scattered light within the flask and was deposited on the inner walls of the flask as shown in figure 13. Larger, heavy soot particles fell to the bottom of the system, depositing on the base plate as well as on the painted sample itself.

Samples of the soot were collected from various parts of the apparatus and were analyzed by scanning electron microscopy (SEM) and energy dispersive x-ray (EDX). SEM micrographs of soot from the walls of the flask, from the base plate, and from the area where the byproduct gases escaped from the flask are shown in figures 14, 15, and 16, respectively. By comparing the particle sizes with the 10- $\mu\text{m}$  bar on the photos, it is evident that particles with diameters much less than 1  $\mu\text{m}$  are prevalent. In fact, the larger particles appear to be agglomerates of finer particles.

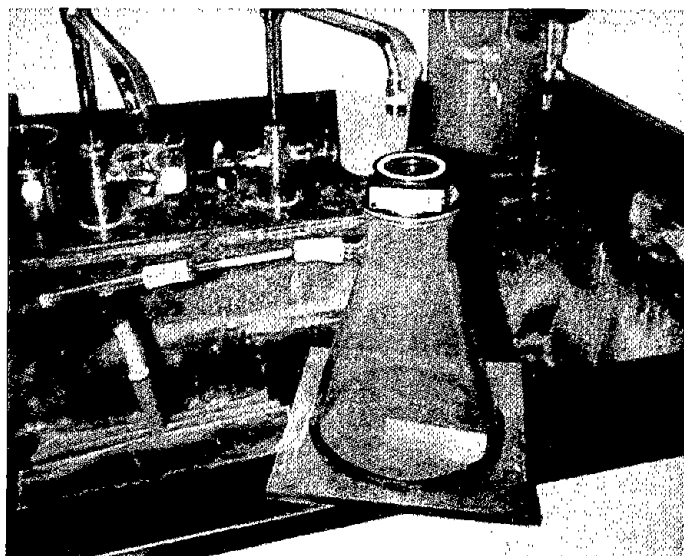


Figure 13. Flask used for laser paint removal (after treating the painted steel surface for 15 min).

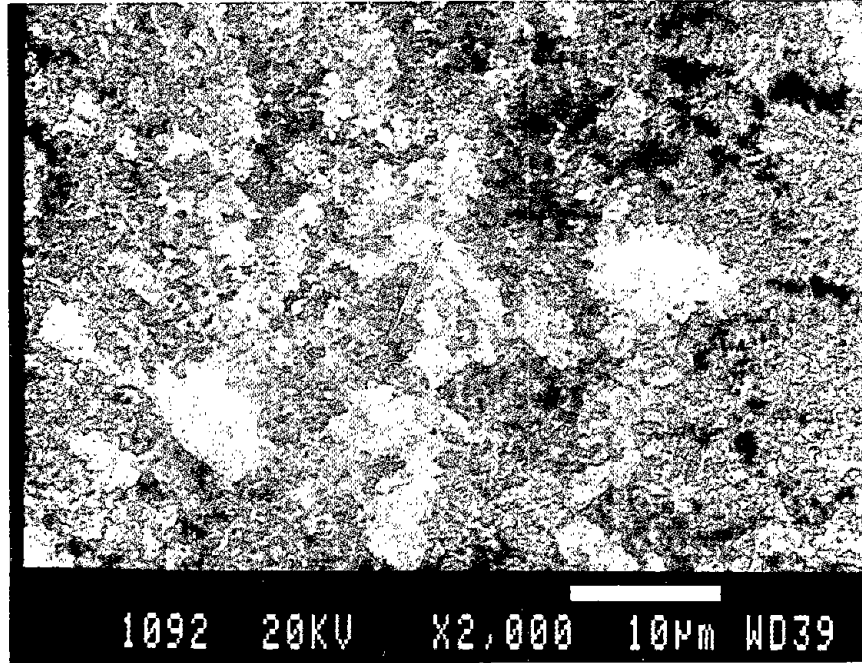


Figure 14. SEM photomicrograph of fine soot deposited on the interior walls of the containment flask.

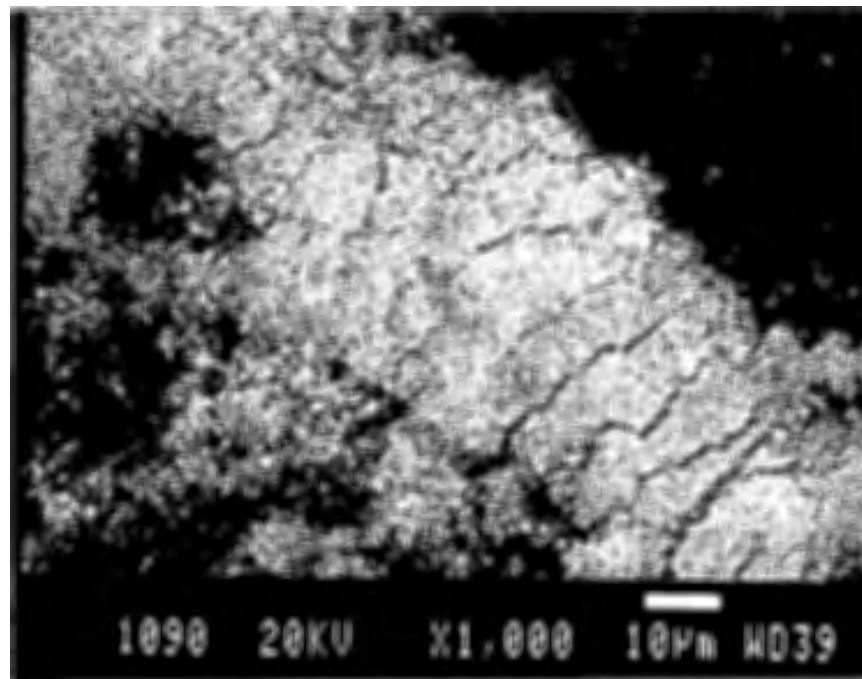


Figure 15. SEM photomicrograph of fine soot deposited on the stainless steel base of the containment flask.

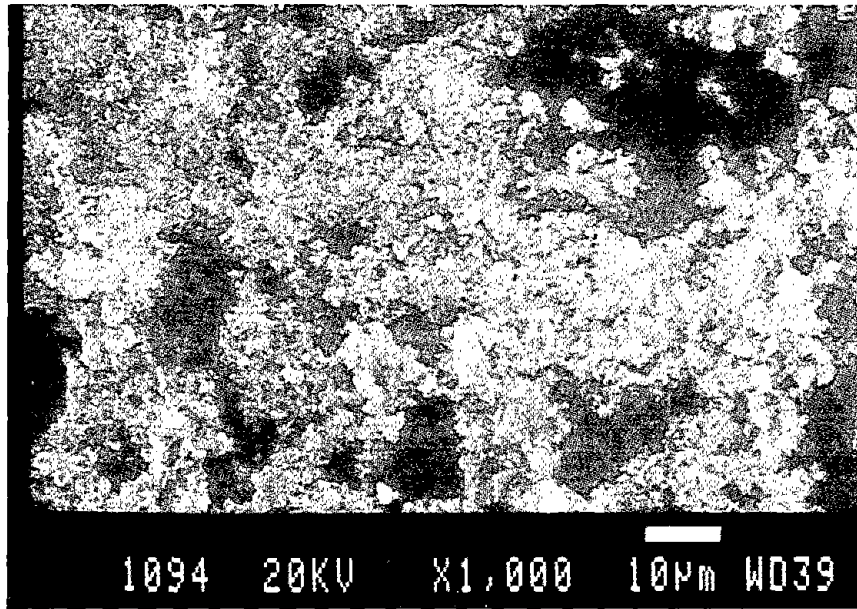


Figure 16. SEM photomicrograph of fine soot deposited on the vacuum seal of the containment flask.

The condition of the painted surface after being subjected to the laser beam for 1 s is shown in figure 17. Several different areas are apparent in the x 10 magnification photograph. The raised black area is where the charred paint has blistered up away from the steel. A portion of the char was broken off, revealing that there is still some residual red lead left on the steel as seen in the upper right-hand corner of the photograph. Some large pieces of soot deposited on untreated green paint are shown at the left and the bottom of the picture.

EDX analysis of soot samples shown in figures 14, 15, and 16 demonstrated that the soot contains lead. The other elements detected by EDX were silicon and aluminum.

Figure 18 is a photograph of the surface after laser treatment. The photograph is at x 7 magnification and shading was produced by the light shining at an angle from the top of the photograph. Several interesting features are apparent. Over most of the treated area, the topcoats were removed leaving red-lead primer. Complete paint removal down to bare metal occurred only over a small area as seen near the top of the treated area. Residual aluminum can be seen along the periphery of the treated area.

The laser tests lead to the following conclusions:

- \* Paint can be removed rapidly by laser treatment.
- \* Care must be taken to ensure complete paint removal.
- \* Large volumes of soot are produced during paint removal using the laser.

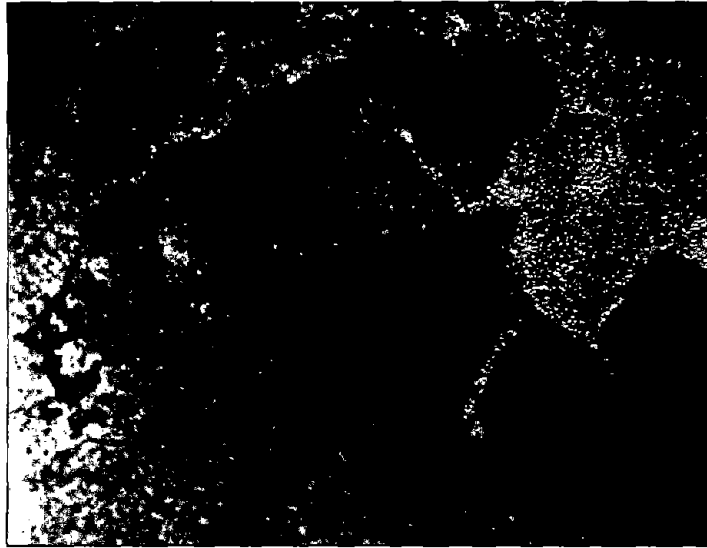


**Figure 17. Photographs at x 10 magnification of two different spots on the surface of the painted steel 1 s after laser treatments prior to cleaning off the char residue.**

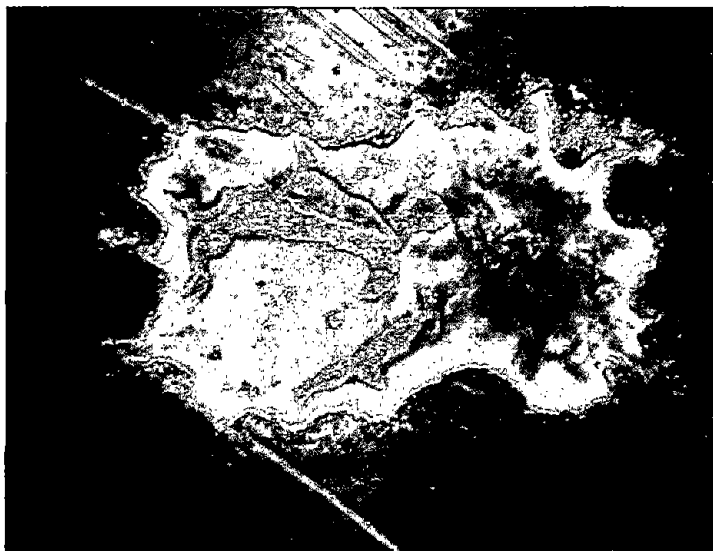


**Figure 18. Photograph at x 7 magnification of a spot on the surface of the painted steel after 1-s laser treatment and after cleaning off the char residue.**

- \* The particle size of much of the soot produced by laser treatment is very fine (less than  $1\mu\text{m}$ ).
- \* The laser-produced soot contains lead and aluminum.

Since the use of heat or light sources to remove the paint would most likely result in similar conclusions to those above, they were not extensively studied.

#### IDOT Paint-Removal Demonstration—Testing Protocol

The Illinois Department of Transportation (IDOT) conducted a paint-removal demonstration program at I-55 between Wood and Damen Streets in Chicago, Illinois, on April 22 and 23, 1993. The project was monitored in this study. The IDOT objective for the program was to familiarize contractors with various aspects of paint removal, including removal methods, Illinois DOT requirements, EPA and Occupational Safety and Health Administration (OSHA) requirements, full-containment structure construction, paint-condition determination, and analysis of paint/blast debris. The objectives of this study were to monitor the removal methods, assess and compare their advantages and disadvantages, obtain samples for TCLP and other analysis, and demonstrate thermal-wave imaging (task F) and electrochemical impedance spectroscopy (task E) as methods of evaluating existing conditions.

Work within this study was divided into three categories: tests before paint removal, tests during the removal processes, and tests after paint removal. All of these tests, which are listed below, provided information directly related to the objectives of task B of this study. In addition, several of the tests, such as 1, 2, 3, and 4, provided information generally required in order to make an economic analysis to fulfill our task A objectives. Several

of the tests (4, 5, 12, and 13) provided the type of data needed to address issues related to task C (Analysis and Disposal of Paint Debris), such as assessment of the degree of hazard and handling procedures for the waste debris. Paint debris samples were taken for TCLP analysis in order to verify results reported by others concerning the ability of steel blast media to stabilize the lead from leaching in the TCLP test. Other tests, such as 2, 3, and 5, provided information relating to task D (Advanced Coatings).

#### Initial Tests

1. Videotape the initial bridge steel surface condition.
2. Measure the paint film thickness using dry film thickness gauge.
3. Conduct paint adhesion tests using an Elcometer.
4. Collect samples of existing paint for metals and chloride analysis.
5. Measure lead (Pb) levels in existing paint using an x-ray fluorescence (XRF) paint analyzer.
6. Collect water samples from web sections of girder to be washed.
7. Document the initial paint surface condition of a section of bridge girder, similar to the one from which paint is to be removed, by thermal-wave imaging.

#### Tests Conducted During the Paint-Removal

8. Collect air samples as near as possible to the blast or tool surface during the paint-removal operations.
9. Collect airborne particulates as near as possible to the blast or tool surface during paint-removal operations using filters and pumps.
10. Measure temperature and humidity.

#### Tests Conducted After Paint Removal

11. Measure lead (Pb) levels remaining on the cleaned surfaces using XRF.
12. Collect samples of paint debris from each removal method and submit for total Pb analysis and toxicity characteristic leaching procedure (TCLP) testing.
13. Laboratory tests:

- a. Analyze air samples taken during paint-removal operations using gas chromatography/mass spectrometry (GC/MS) for volatile organic compounds (VOC) determination.
- b. Analyze particulates collected on filters for metal content and size distribution.

Double containment was used in the demonstration in order to minimize the possible escape of dust from the grit-blast area. The containment structure was recorded on videotape for future reference and is part of the IDOT records, but is not discussed further in this report. Details are available from IDOT. Entrance and exit from the containment area was via an anteroom or change room. The grit blasting was done using G-40 steel grit. The original paint film thickness was measured as 0.15-0.20  $\mu\text{m}$  (6 to 8 mils). It was a three-layer system consisting of a red-lead/alkyd primer, a leafing aluminum/phenolic intermediate coating, and a gray non-leafing aluminum/phenolic topcoat. Adhesion varied significantly from area to area on this structure. Elcometer tests gave adhesion values of approximately 2067 kPa (300 lb/in<sup>2</sup>), but since the paint was brittle, it spalled off while crosshatching during the ASTM D3359-90 test (Measuring Adhesion by Tape Test, Method B - Cross-Cut Tape Test) producing an 0B rating (extremely poor adhesion). Weather conditions were mild throughout the 2-day removal demonstration. Temperatures ranged between 12.8 and 15.6 °C (55 °F and 60 °F), and relative humidities were 35 to 45 percent. Details of the tests relating to task B are discussed below.

#### Analysis of Paint and Steel for Lead by X-Ray Fluorescence

Both the paint and the base steel were analyzed for lead content using a Princeton Gamma Tech (PGT) x-ray fluorescence (XRF) lead-paint analyzer. This work was done by George Cardis of Loyalty Environmental, Inc. of Skokie, Illinois. The XRF method gives results per unit area —it analyzes approximately 1 cm<sup>2</sup> of surface. For lead, it is accurate to  $\pm 0.5$  mg/cm<sup>2</sup>. Paints with lead levels greater than 1 mg/cm<sup>2</sup> are considered hazardous. Analysis of the base steel was needed to obtain a background lead level. The paint contained such large amounts of lead that all paint readings were off scale, i.e., greater than 10 mg Pb/cm<sup>2</sup>. After the various paint-removal methods were demonstrated, the cleaned-surface lead levels were again measured. It was found by visual inspection that grit blasting did drive a small amount of lead from the paint into the cleaned surface. This amount was below 0.5 mg/cm<sup>2</sup> and thus was no longer considered as hazardous. Some concern has been expressed as to the possibility of the presence of sulfur resulting in false lead-concentration measurements by XRF. While it is true that the lead M series line measured at 2.3 keV is interfered by the sulfur K series line, the XRF device used during the IDOT test measured lead concentrations using the lead K series line at 74.9 keV with no interference by sulfur.

Although originally designed for use in homes, schools, and other buildings, the method is finding more and more use with steel structures. This is because the measurements are easy to make, they require only a few minutes to obtain, and the results are known immediately on site. If the owner does not want to purchase the equipment, consultants who will provide the service are readily available.

## Water-Jet Cleaning Results

Water-jet cleaning of bridge girders was demonstrated under various conditions of water pressure and temperature. The chloride levels on the surfaces of the I-beams before and after water-jet cleaning were measured using two different sampling methods. In the first method, a plastic pipe elbow with an o-ring that could be sealed to the painted surface by hand pressure was used. The elbow was filled with 60 mL of deionized water that was allowed to remain in contact with approximately 15 cm<sup>2</sup> of the surface for 30 s and then was poured into a plastic container by rotating the fixture. This method was used to sample the surface of the vertical portions (webs) of the I-beams before and after water-jet cleaning.

In the second method, runoff water from the water-jet cleaning operation was collected at the start of cleaning and at the end of cleaning. The initial sample contained both soluble and insoluble contaminants, including loose rust, loose paint, dirt, and salts coming from the horizontal flange areas as well as from the vertical web area. The final sample contained only soluble materials. The pH of the initial water runoff sample taken under conditions of 17914 kPa (2600 lb/in<sup>2</sup>) water pressure and a starting water temperature of 99.9°C (210°F) was 5.0, while that of the final run-off sample at the end of the cleaning was 5.5. The water-sample analyses are given in table 3.

The chloride content of the starting water was subtracted from each sample analysis and the results were reported in table 3 as milligrams of chloride per square foot of girder surface. The results indicate that the plastic-elbow device gives reasonably reproducible results since the two samples taken before cleaning (1A and 1B) had essentially the same chloride content as did the two samples (2A and 2B) taken after cleaning. Since these samples were taken from a vertical portion of the beam, there was little or no accumulation of salt and dirt on the area sampled. Although the chloride levels were rather low to start with, washing gave approximately a 70 percent reduction in chloride.

The water-jet runoff samples contained much more chloride, probably due to an accumulation of salt on the I-beam flanges. The chloride level in the initial sample was 12953 mg/m<sup>2</sup> (1205 mg/ft<sup>2</sup>). Washing gave a 94 percent reduction in chloride down to a final level of 120 mg/m<sup>2</sup> (11.2 mg/ft<sup>2</sup>). The initial sample also was slightly more acidic than the final sample. In other water-jet cleaning trials conducted in this program and by IDOT, the use of unheated water gave results very similar to those obtained with hot water. As a result, IDOT now requires cleaning with unheated water.

## Air-Sampling Tests for VOC's Generated During Grit Blasting Within Confinement

No volatile organic compounds (VOC's) were found in a vacuum-bottle test of the atmosphere in the confinement area during grit blasting. In addition, no VOC's were collected on a Tenax™ adsorbent tube through which the confinement area atmosphere was continuously cycled during the blasting operation. This is the expected result since there were no organic solvents involved and no heat to cause thermal decomposition of the paint.

Three different air-sampling tests were conducted within the confinement area during the steel-grit blasting procedure. The first test was a vacuum-bottle test in which the valve on an evacuated sampling bottle was opened within the



Table 3. Chloride content of water samples from I-Beam surfaces before and after water-jet cleaning.

Sample No.	Sample Source	pH	Chloride mg/m <sup>2</sup> (mg/ft <sup>2</sup> )
1A	From I-Beam Web Before Cleaning*	-	188 (17.5)
1B	From I-Beam Web Before Cleaning*	-	177 (16.4)
2A	From I-Beam Web After Cleaning*	-	63.4 (5.9)
2B	From I-Beam Web After Cleaning*	-	43 (4.8)
3A	Initial Water-Jet Runoff Sample	5.0	12953 (1205)
3B	Final Water-Jet Runoff Sample	5.5	120 (11.2)

\* Samples taken using plastic-elbow method.

confinement area during blasting to collect an air sample. The objective was to determine whether or not the process produces any significant quantity of VOC's. Analysis of this sample by gas chromatography/mass spectroscopy (GCMS) did not indicate the presence of any VOC's resulting from the blasting.

The second test also was to determine whether or not VOC's are produced during the blasting process. In this test, a small pump was used to continuously draw air through an adsorbent (Tenax™) tube at 20 cm<sup>3</sup>/min. Organic contaminants in the airstream are adsorbed and later in the laboratory are driven from the adsorbent into a GCMS for analysis. This test is better suited to the determination of small concentrations of VOC's than is the vacuum-bottle test since a much larger volume of air is used in this test and the VOC's are concentrated by adsorption. Nevertheless, no VOC's were detected.

#### Airborne Grit-Blast Debris Particulate Sampling and Analysis

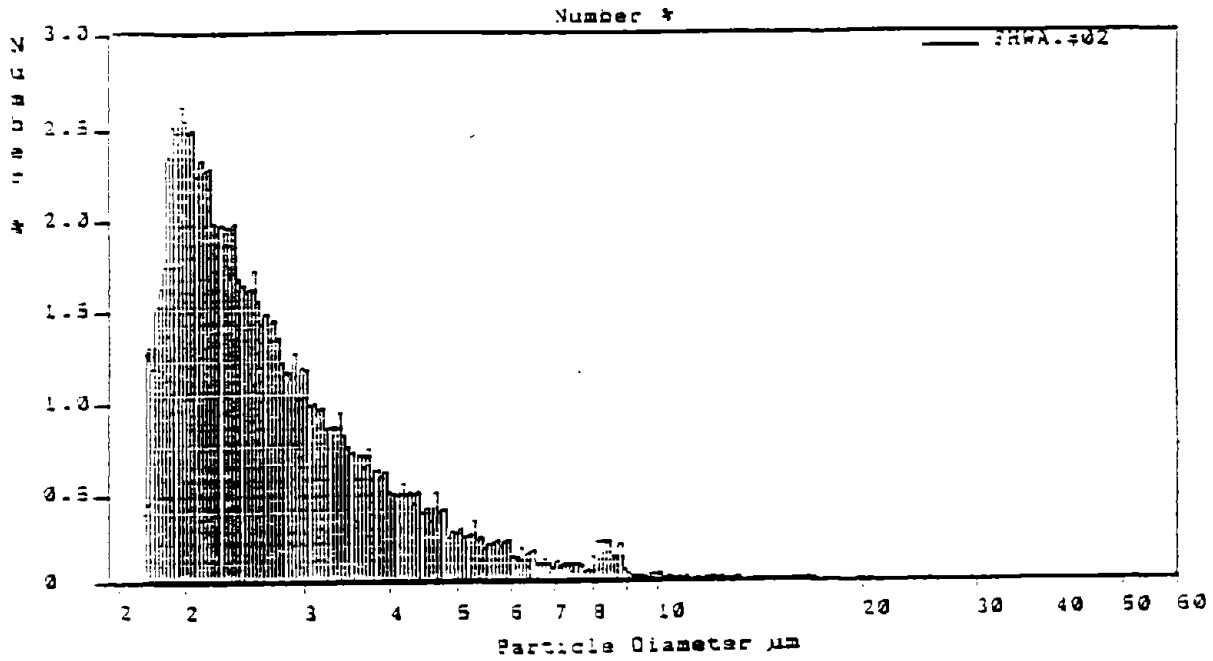
The objective of this air-sampling test was to determine the size distribution and composition of particulates in the air within the confinement area during and after blasting. Samples were collected by drawing ambient air through an 0.8- $\mu$ m mixed cellulose ester (MCE) in-line filter at a rate of 400 cm<sup>3</sup>/min for a total period of 90 min of which only the first 10 min was actual blasting time. The remaining 80 min was time during which blast debris was being vacuumed out of the confinement area. From the weight of the collected residue and the flow of 400 cm<sup>3</sup>/min over the full 90-min period, an average airborne particulate concentration of 280 mg/m<sup>3</sup> is calculated. The residue was analyzed for particle-size distribution by the Coulter technique and by an Elzone™ particle-size analyzer. Particulate size, shape, and composition were determined by scanning electron microscopy (SEM) and energy-dispersive x-ray (EDX) microanalysis. Particle-size analysis results indicate that the presence of many particles having diameters less than the nominal 0.8- $\mu$ m filter porosity are present in the filter cake. This apparently is the result of partial clogging of the filter porosity as the residue built up during the test. The filter cake was thicker in the center of the in-line filter due to the high airflow rate.

Coulter particle-size analysis: Filter-cake particulates were dispersed in a saline solution using an anionic surfactant to prevent the particles from agglomerating. The Coulter Counter particle-sizing system allows for a measurement of a size distribution between certain minimum and maximum particle-size diameters depending on the orifice sizes chosen. A range of 2 to 60  $\mu\text{m}$  was chosen for analysis because preliminary SEM analysis indicated that the smaller particles tended to be more rich in lead. Figures 19(a) and (b) depict the particle-size distribution obtained for two samples taken from different areas on a single filter cake. Sample #1 was taken from an area near the outer edge of the filter, while sample #2 was taken from an area near the center of the filter. The plots in figure 19 are most easily understood by imagining the particles passing through a series of sieves with mesh sizes indicated on the horizontal axis. The height of each vertical line (or bar) represents the number of particles of that size. Neither sample contained many particles with diameters greater than 10  $\mu\text{m}$ . The plot in figure 19(a) indicates that 50 percent of the particles are smaller than 2.5  $\mu\text{m}$  in size. The plot in figure 19(b) indicates that of all the particles measured in the 2- $\mu\text{m}$  to 60- $\mu\text{m}$  range, the largest number occurred at the 2- $\mu\text{m}$  cutoff. Since this strongly suggests that a large portion of the particulates have diameters less than 2  $\mu\text{m}$ , samples were sent out for analysis by the Elzone™ system, which was capable of measuring sizes down to well below 1  $\mu\text{m}$ . These samples were representative of the remainder of the filter cake after having removed the two small samples analyzed in figures 19(a) and (b).

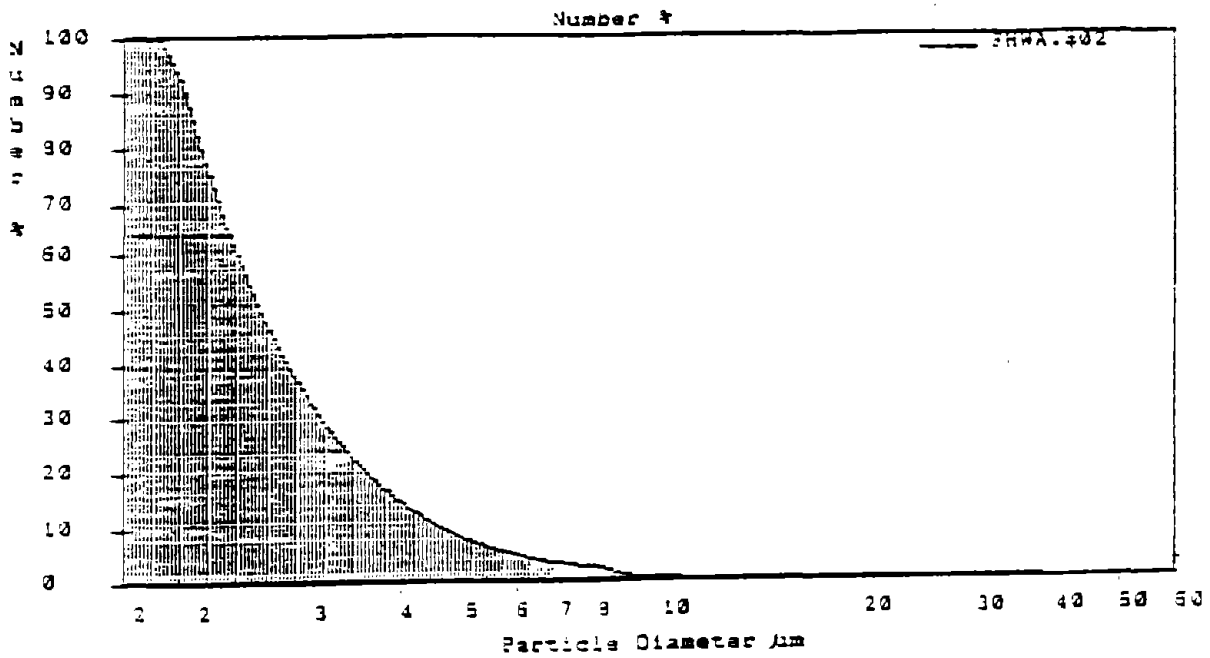
Elzone™ particle-size analysis: The Elzone™ technique is similar to the Coulter technique. The difference was that in the Elzone™ case, a smaller orifice (capable of detecting particle diameters down to 0.6  $\mu\text{m}$ ) was used. Two samples were analyzed and the results are shown as number percentages in figures 20 and 21 and volume percentages in figures 22 and 23. For the sample corresponding to figure 20, more than 50 percent of the particles detected had diameters less than 0.8  $\mu\text{m}$  and the highest number count occurred at 0.65  $\mu\text{m}$ . For the sample shown in figure 21, more than 50 percent of the particles had diameters less than 1.0  $\mu\text{m}$  and the highest number counts occurred between 0.65  $\mu\text{m}$  and 0.73  $\mu\text{m}$ . Although neither sample contained a large number of particles with diameters greater than 6  $\mu\text{m}$ , the larger particles make up a significant volume of the total particulate volume as shown in figures 22 and 23. Note that the sample in figure 22 contained a 10- $\mu\text{m}$  latex marker.

The increased residence time of the smaller particles of aerosol degrades visibility and air quality within the containment zone and raises safety concerns as the particle size approaches the filtering efficiency of different classes of respirators. Neither the Coulter Counter™ nor the Elzone™ system were capable of determining whether or not particles with diameters less than 0.3  $\mu\text{m}$  (the porosity of HEPA filters) were present.

SEM and EDX microanalysis: The air filter was heavily loaded with particulates. Sample particles were prepared for analysis in the SEM using two different techniques. The first technique entailed scooping particulates from the filter and dispersing them in semiconductor-grade acetone. The suspension was then transferred via pipette to a spectroscopically pure carbon plate. The second technique relied on electrically conductive adhesive carbon tape that was gently pressed against the surface of the filter and then mounted on a carbon plate. Both techniques produced satisfactory dispersions as indicated in figures 24(a) and 24(b) that show the acetone dispersion at



(a) Sample #1.



(b) Sample #2.

Figure 19. Coulter number percentage particle-size histogram of airborne dust samples collected within grit-blasting confinement zone during blasting.

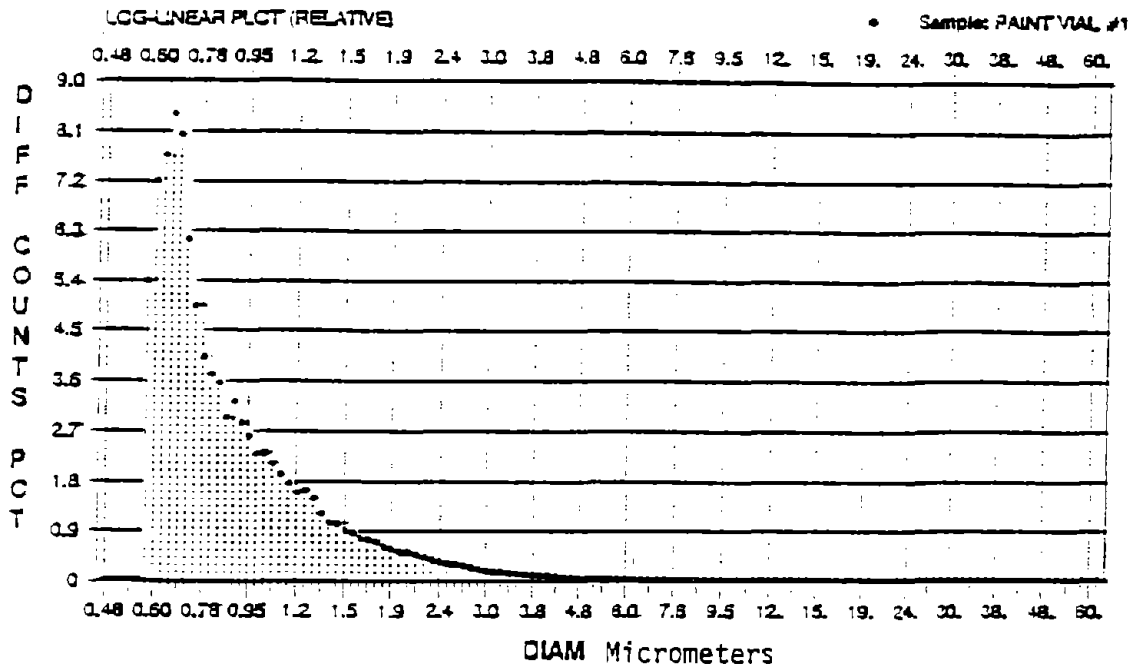


Figure 20. Elzone™ number percentage particle-size analysis of airborne dust sample #1 collected within grit-blasting confinement zone during blasting.

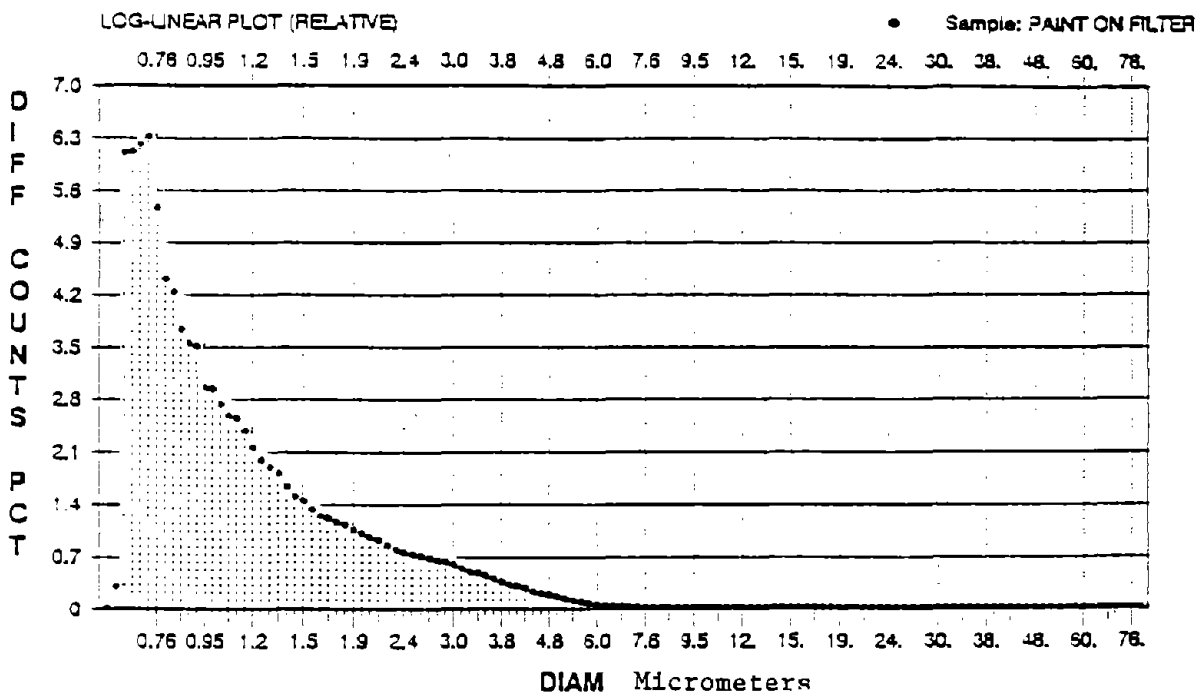


Figure 21. Elzone™ number percentage particle-size analysis of airborne dust sample #2 collected within grit-blasting confinement zone during blasting.

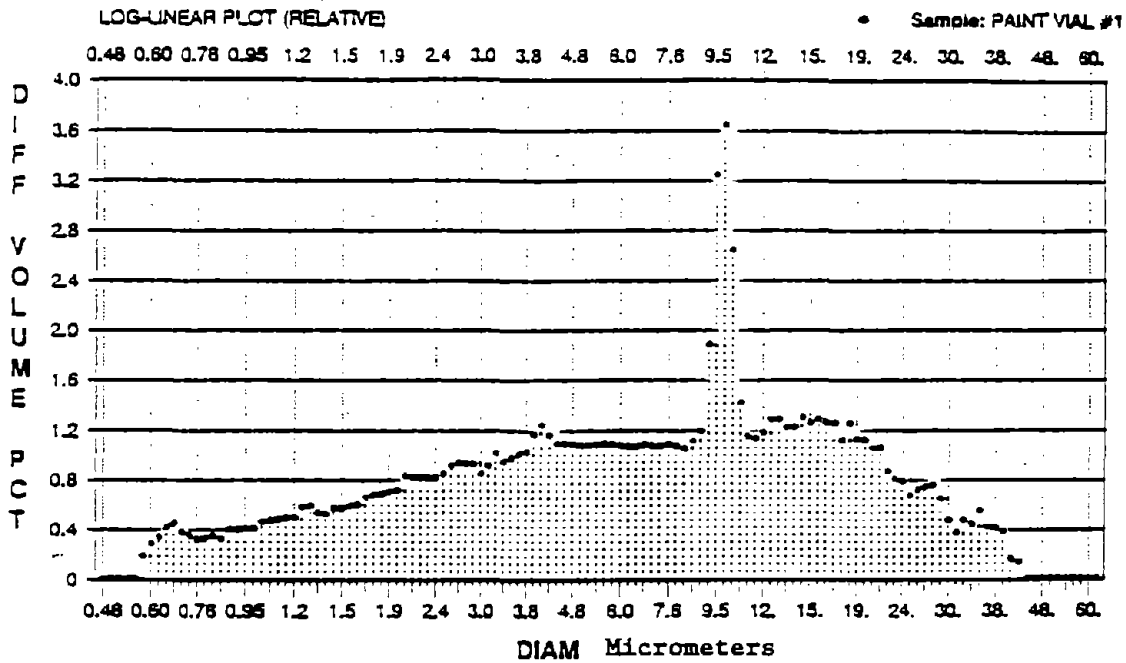


Figure 22. Elzone™ volume percentage particle-size analysis of airborne dust sample #1 collected within grit-blasting confinement zone during blasting.

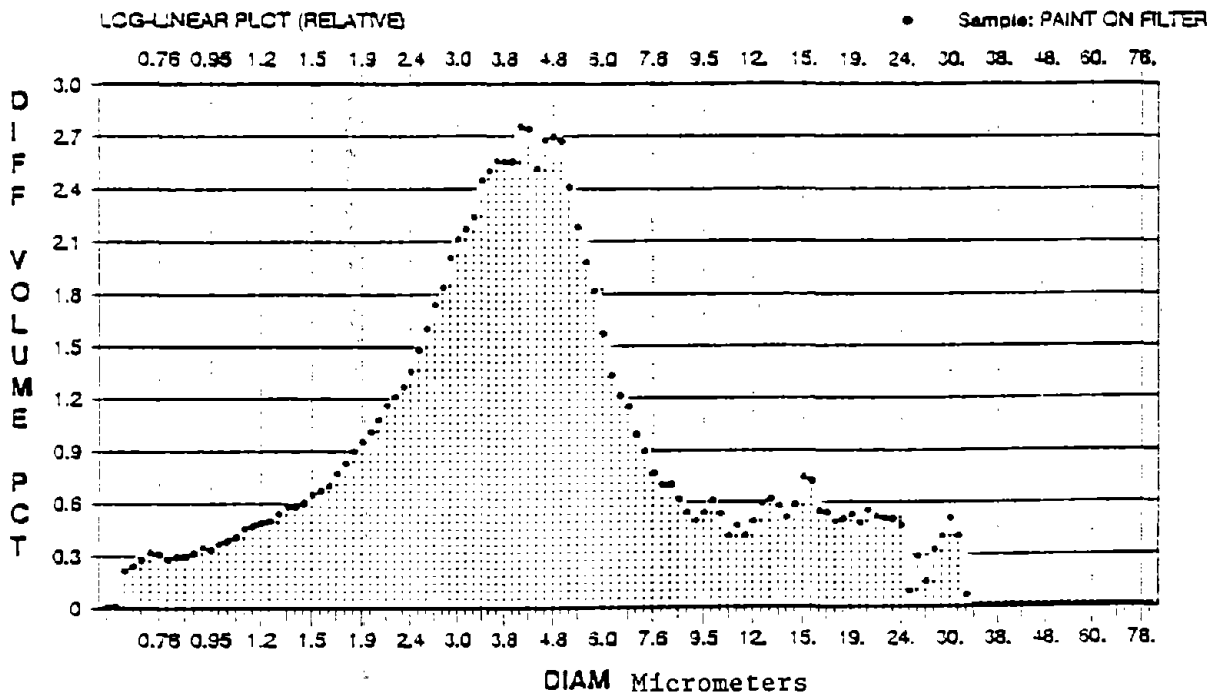
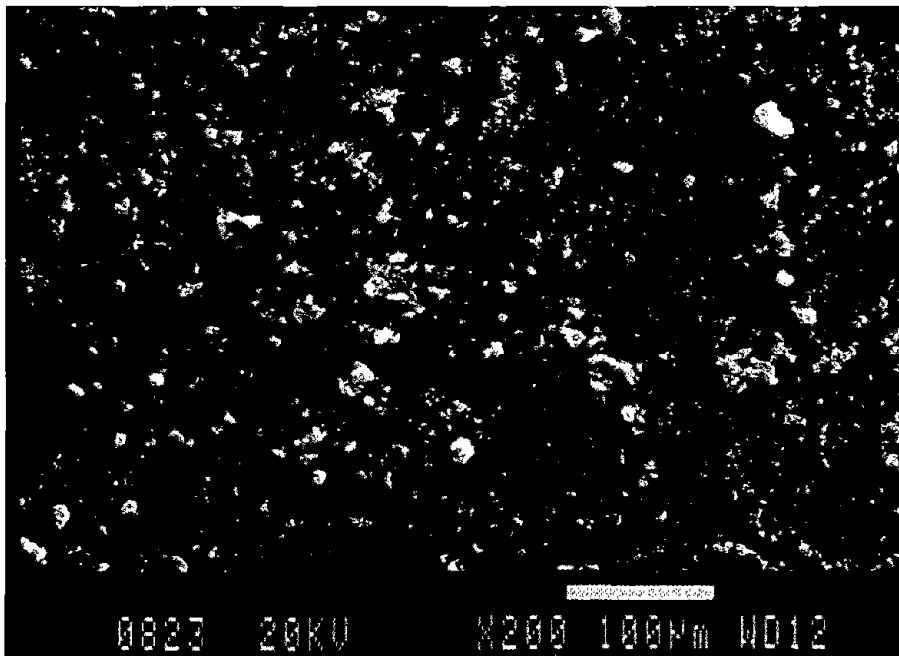
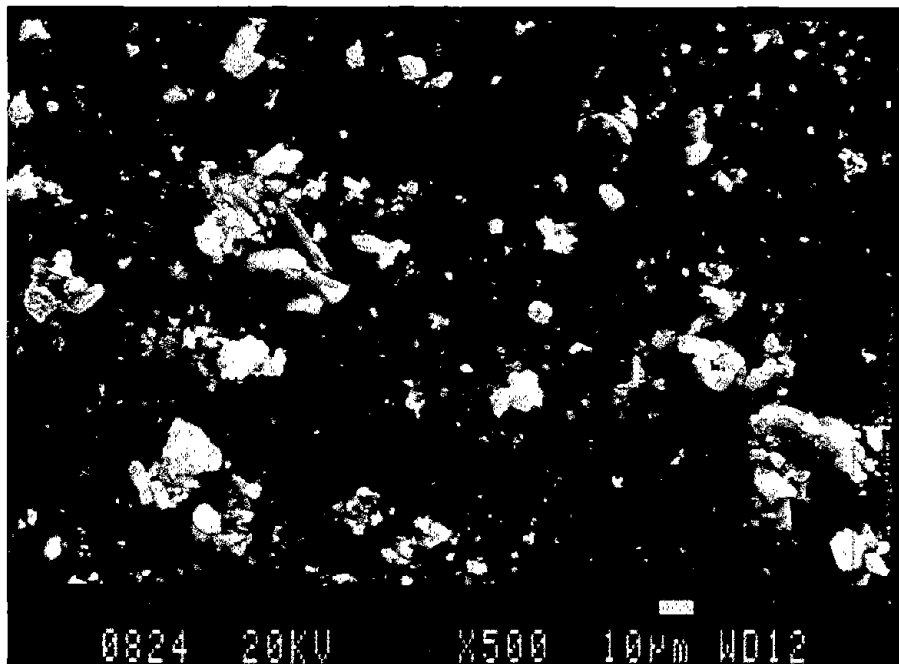


Figure 23. Elzone™ volume percentage particle-size analysis of airborne dust sample #2 collected within grit-blasting confinement zone during blasting.



(a) x 200 magnification.



(b) x 500 magnification.

Figure 24. SEM micrograph showing particle sizes using the acetone dispersion technique.

x 200 and x 500 magnifications and figures 25(a) and 25(b) that show the carbon tape dispersion at x 200 and x 250. The SEM photomicrographs indicate that a wide variation in particle size is present in the airborne grit-blast debris.

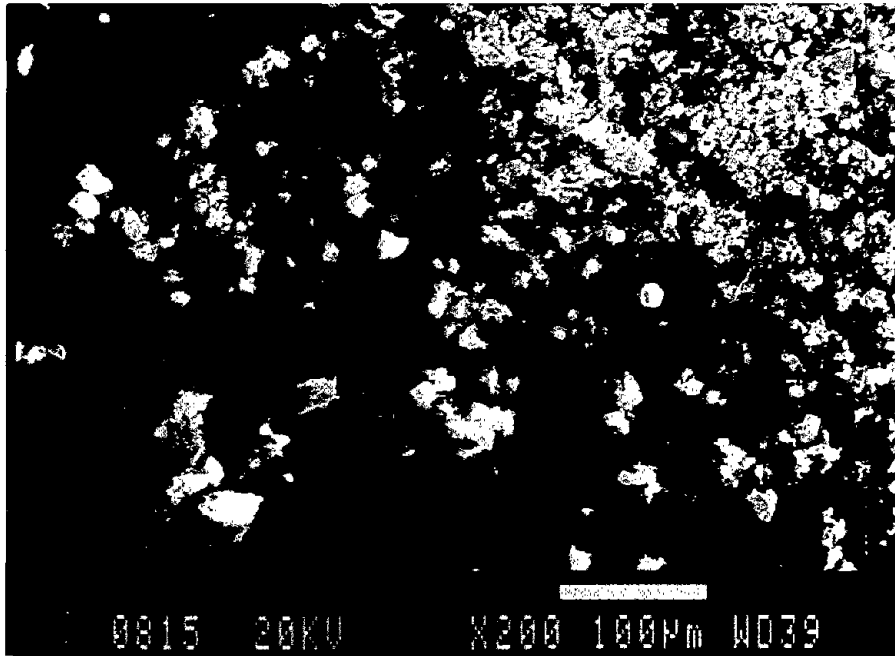
Figure 26 shows the top surface of the filter cake together with its energy-dispersive x-ray spectrum (EDX) and composition. The primary constituents are lead and calcium from the paint; iron from the steel grit and rust, and minor amounts of aluminum and magnesium that may come from the paint or from residual dust. The detection of silicon separately and in combination with aluminum is nearly always due to ambient dust. Note that this x-ray spectrum and the spectra that follow were acquired with an x-ray detector that uses a beryllium window to insulate the x-ray detecting crystal from the vacuum in the SEM. Although the beryllium window ensures proper operation of the detecting crystal, it completely absorbs low-energy x-rays from elements lighter than sodium. Therefore, elements such as oxygen, nitrogen, carbon, and hydrogen are not detectable. Three large fragments of steel grit found in the filter cartridge are shown in figure 27. Note that no lead was detected on the steel grit within the detection limits of the system. Smaller iron-containing particles were also detected, typically in the size range down to approximately 10  $\mu\text{m}$ . Two such particles are shown in figures 28 and 29. The iron-rich particle shown in figure 29 also contains lead and silicon. These two particles may contain significant amounts of rust since they are morphologically different compared with the steel grit in figure 27.

The majority of particles analyzed contained lead, although some did not. Representative samples of particles are shown in figures 30 through 35. The particle in figure 34 contains significant amounts of lead and silicon together with iron, magnesium, calcium, and zinc. It may have come from the topcoat that had dust blown on it before it had cured. Figure 35 shows a particle that is primarily zinc and probably originated from an intermediate layer of paint between the primer and the topcoat.

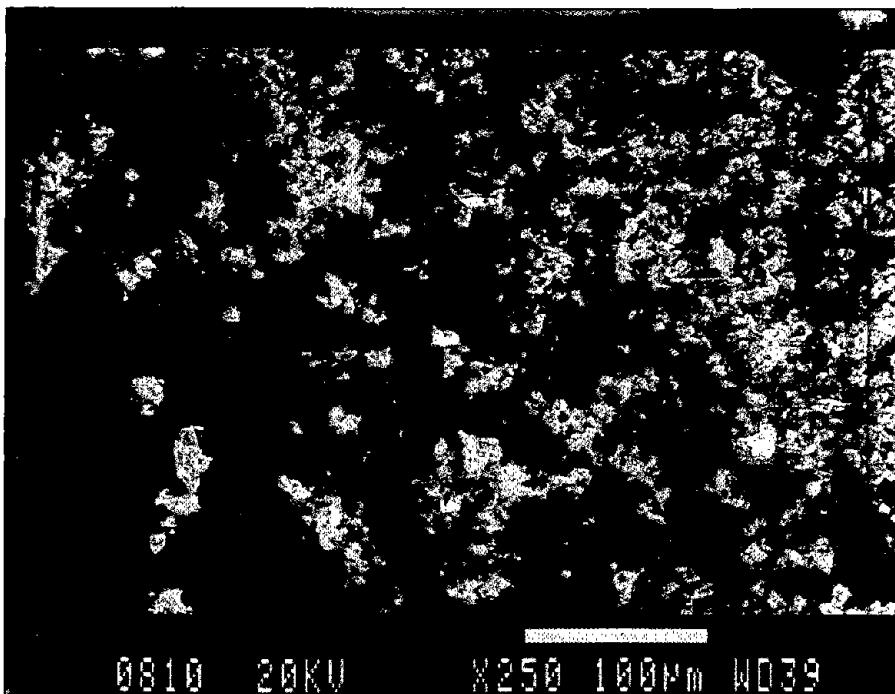
The proportion of particles that contain lead as a major constituent appeared to increase with decreasing size. Smaller particles, down to approximately 1  $\mu\text{m}$ , are shown in figures 36 through 39. The angular morphology, together with the cleavage step appearance of these smaller particles, suggest that they originate from a brittle layer, possibly the primer that is fractured by impingement of steel grit. Table 4 gives the composition of various sizes of particles collected on the filter within the grit-blast confinement area. The figure number of the corresponding SEM and EDX analyses also is listed in table 4.

#### Effectiveness of Paint-Removal Procedures

Three types of paint-removal methods were compared in the demonstration. They were vacuum steel-grit blasting, steel-grit blasting in full containment, and vacuum power-tool cleaning. All blasting was done using G-40 steel grit. Two vacuum power-tool system suppliers demonstrated the use of their equipment. Needle guns, roto-peening, and abrasive-disc cleaning tools were demonstrated by both companies. The debris collected for analysis from each power-tool company's cleaning work was a combination of debris from all three types of tools.



(a) x 200 magnification.



(b) x 250 magnification.

Figure 25. SEM micrograph showing particle sizes using carbon tape dispersion technique.



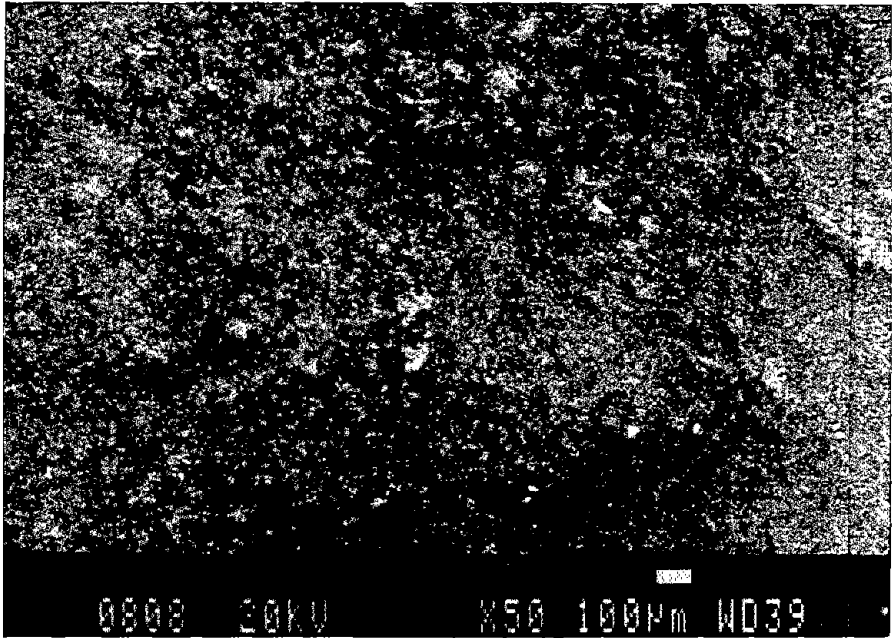
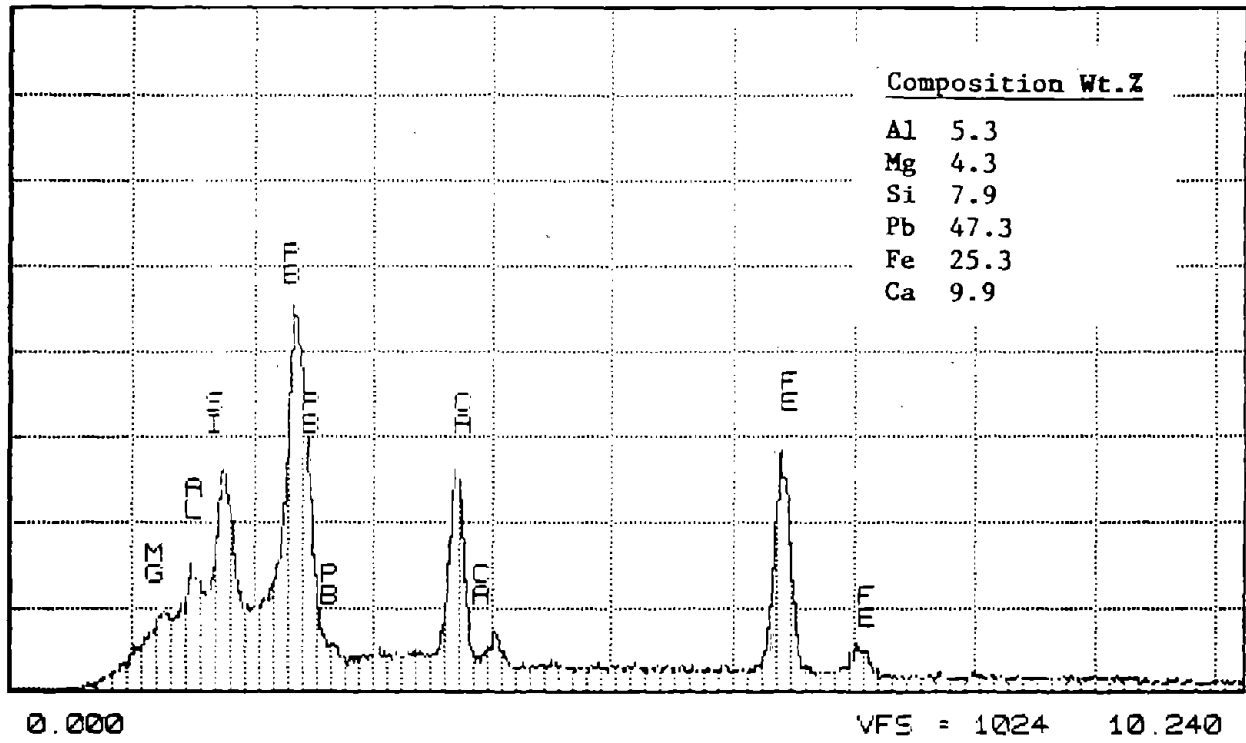


Figure 26. EDX analysis and SEM micrograph of airborne particulates collected within confinement zone during blasting.

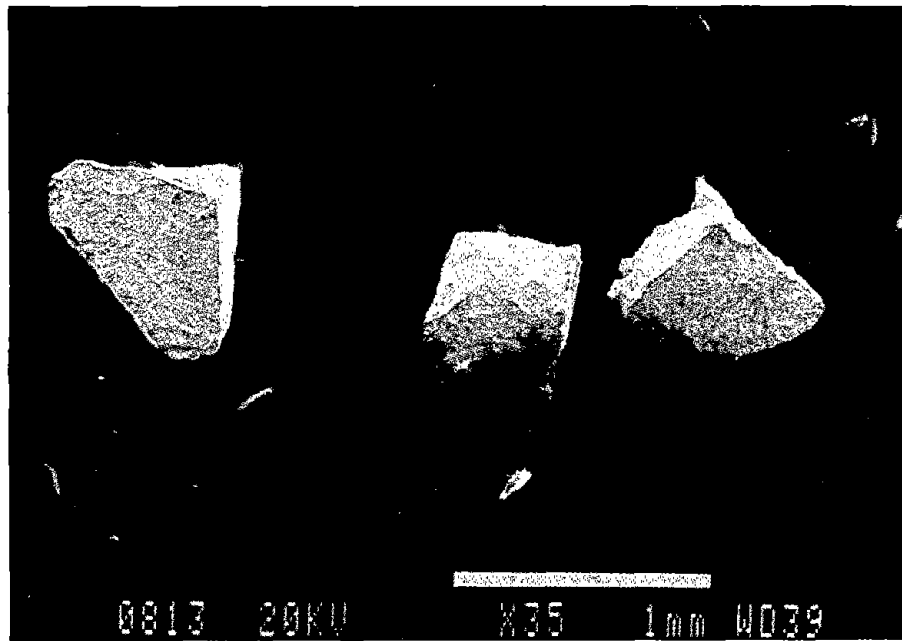
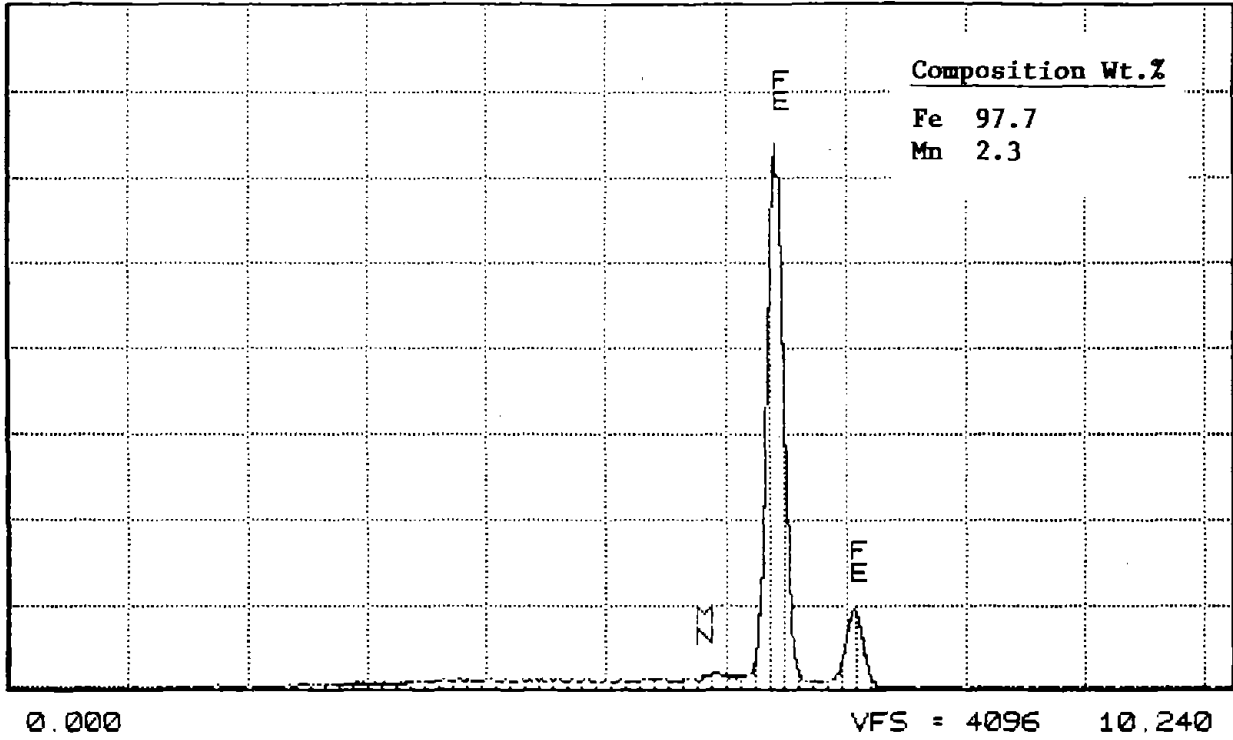


Figure 27. EDX analysis and SEM micrograph of 650- $\mu$ m particles collected on filter within confinement zone during blasting.

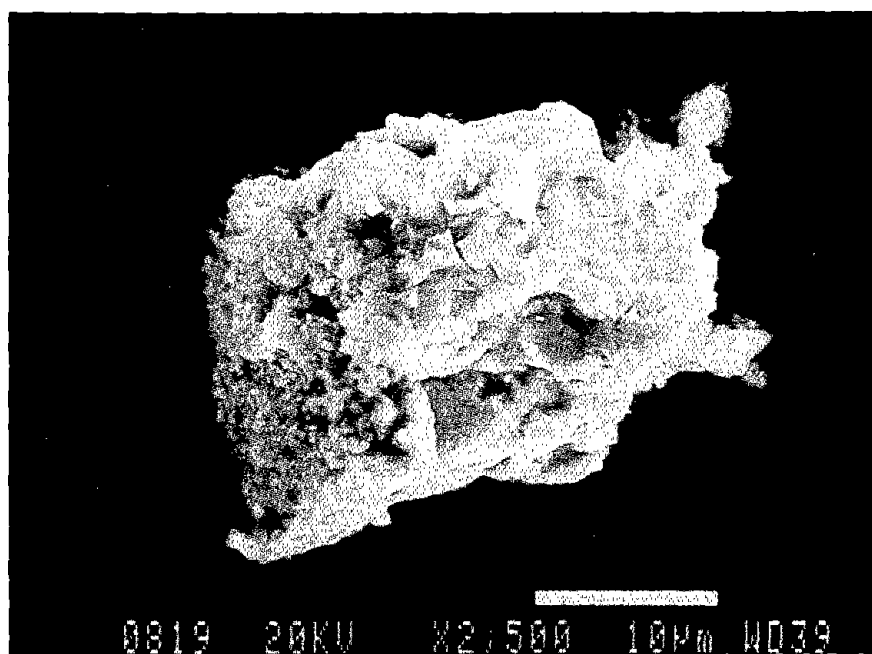
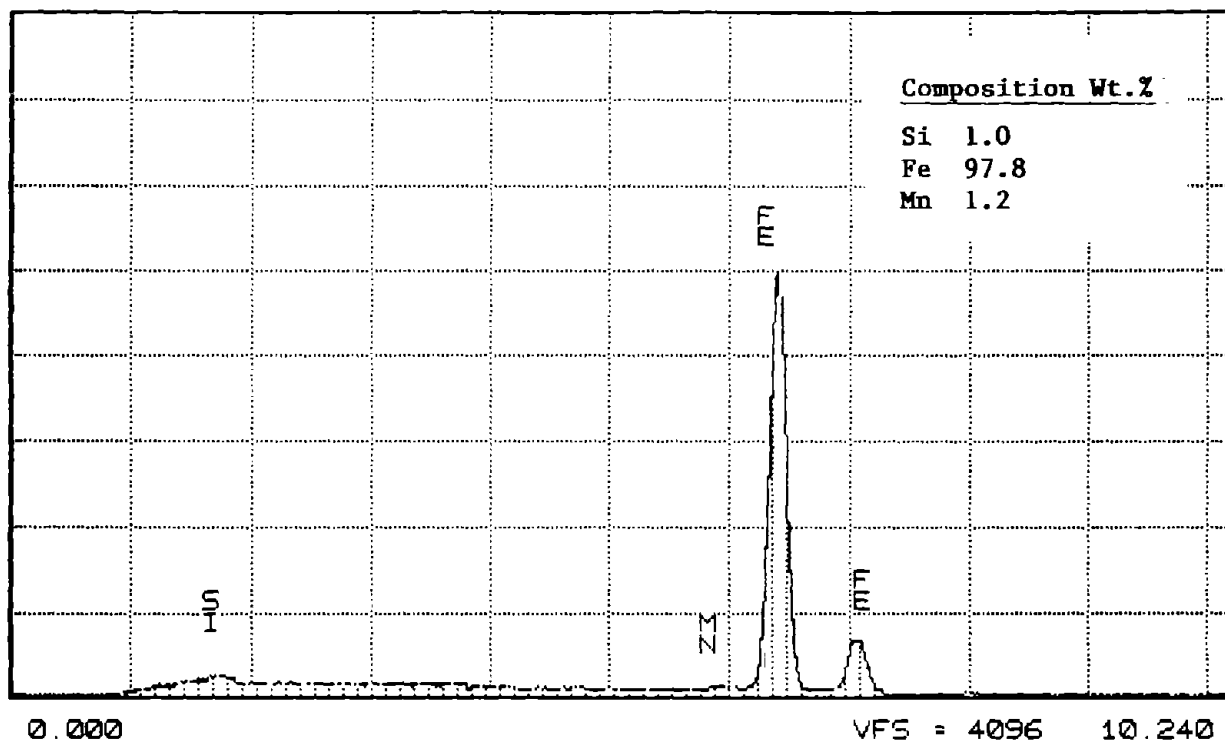


Figure 28. EDX analysis and SEM micrograph of 25- $\mu$ m particle collected on filter within confinement zone during blasting.

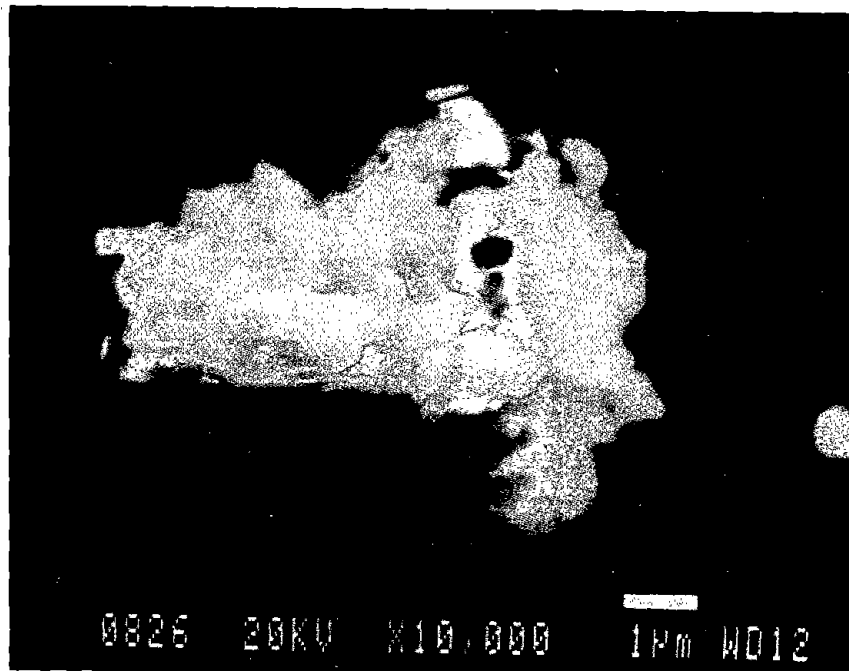
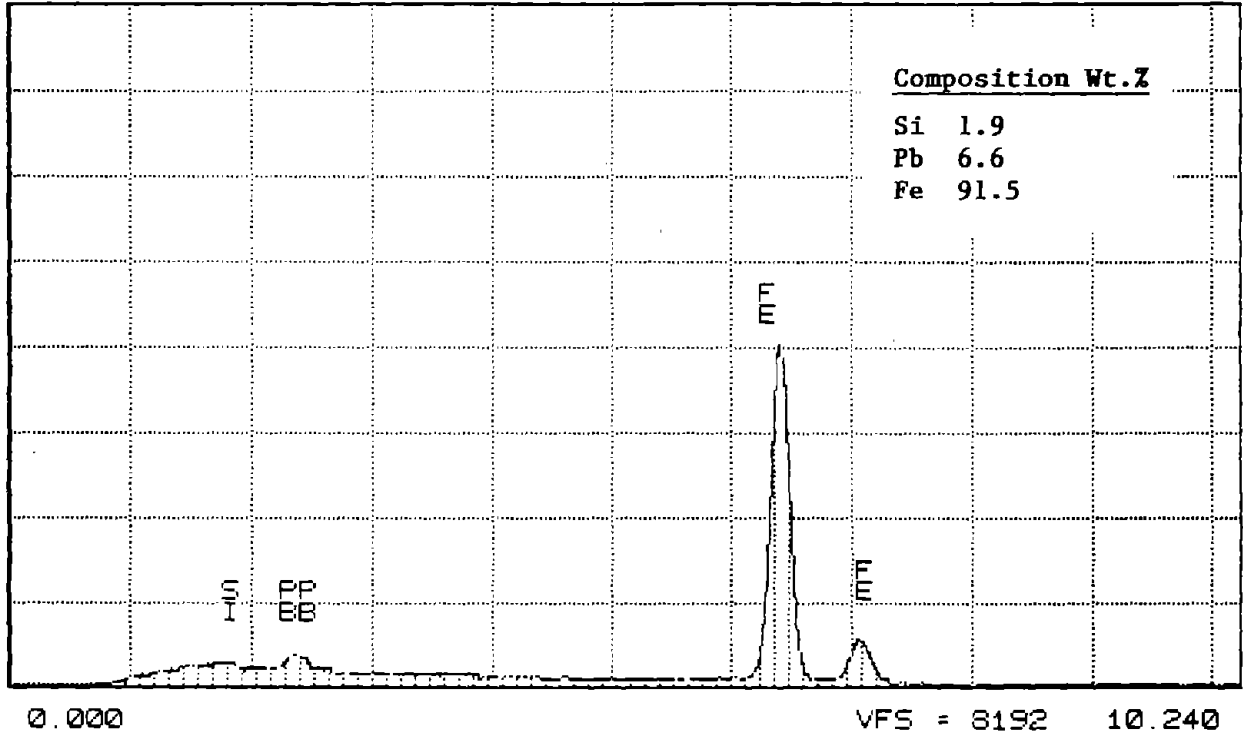


Figure 29. EDX analysis and SEM micrograph of 5- $\mu$ m particle collected on filter within confinement zone during blasting.

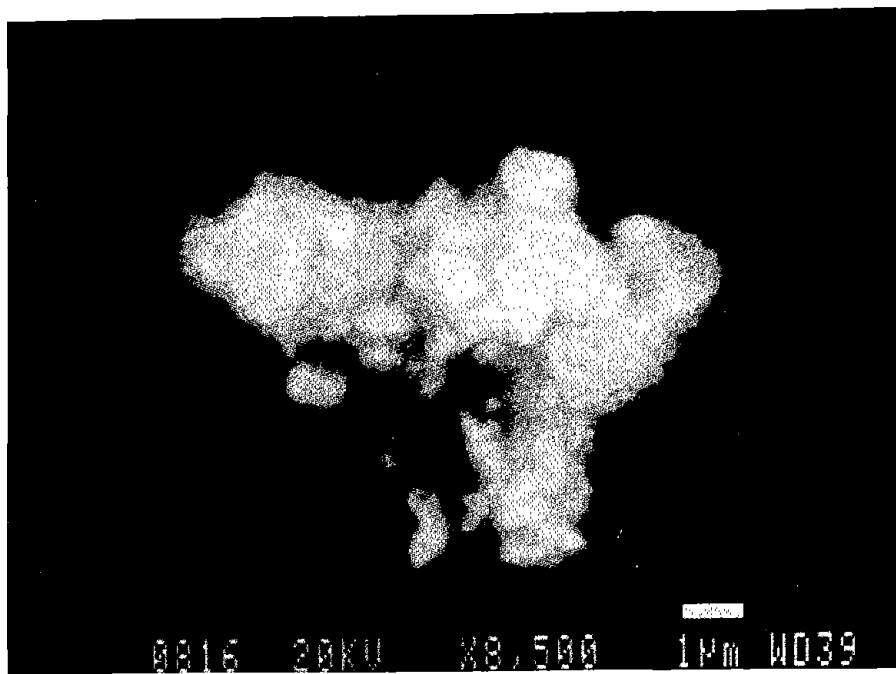
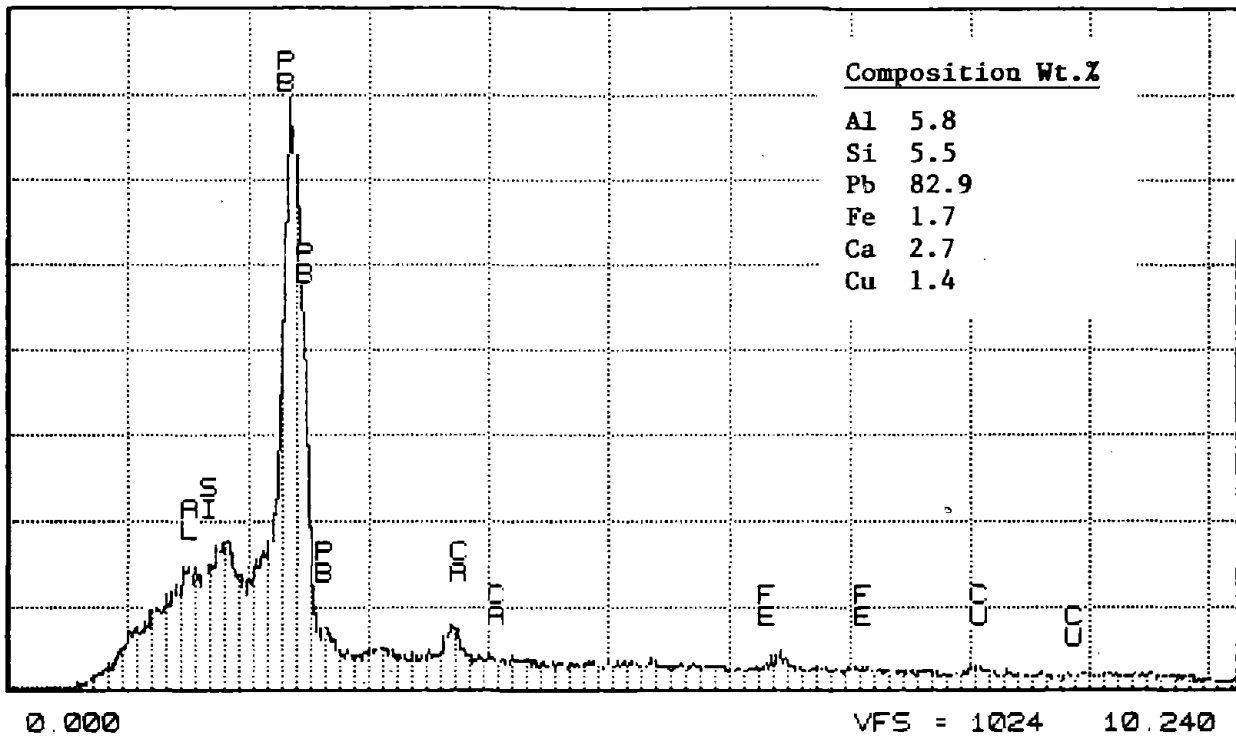


Figure 30. EDX analysis and SEM micrograph of 6- $\mu$ m particle collected on filter within confinement zone during blasting.

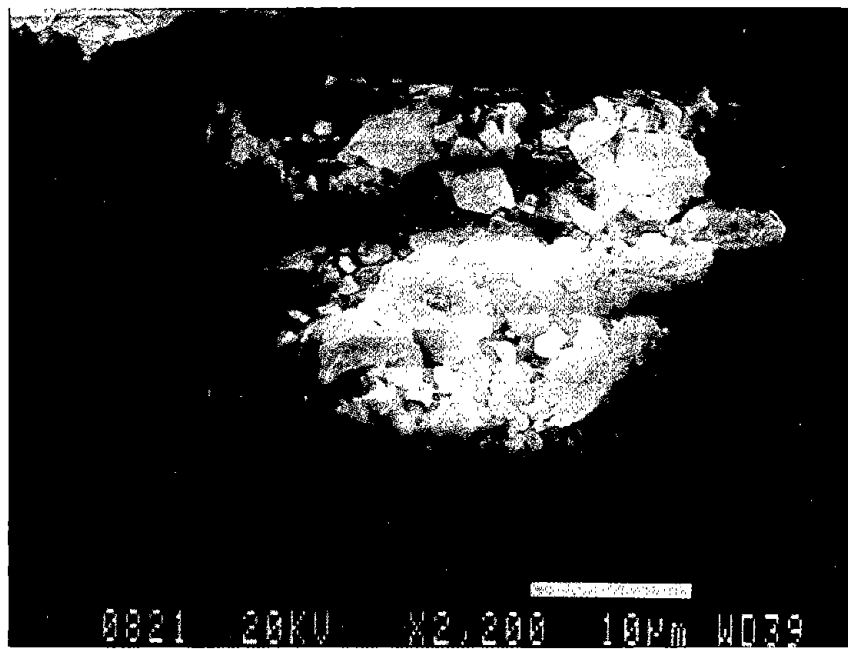
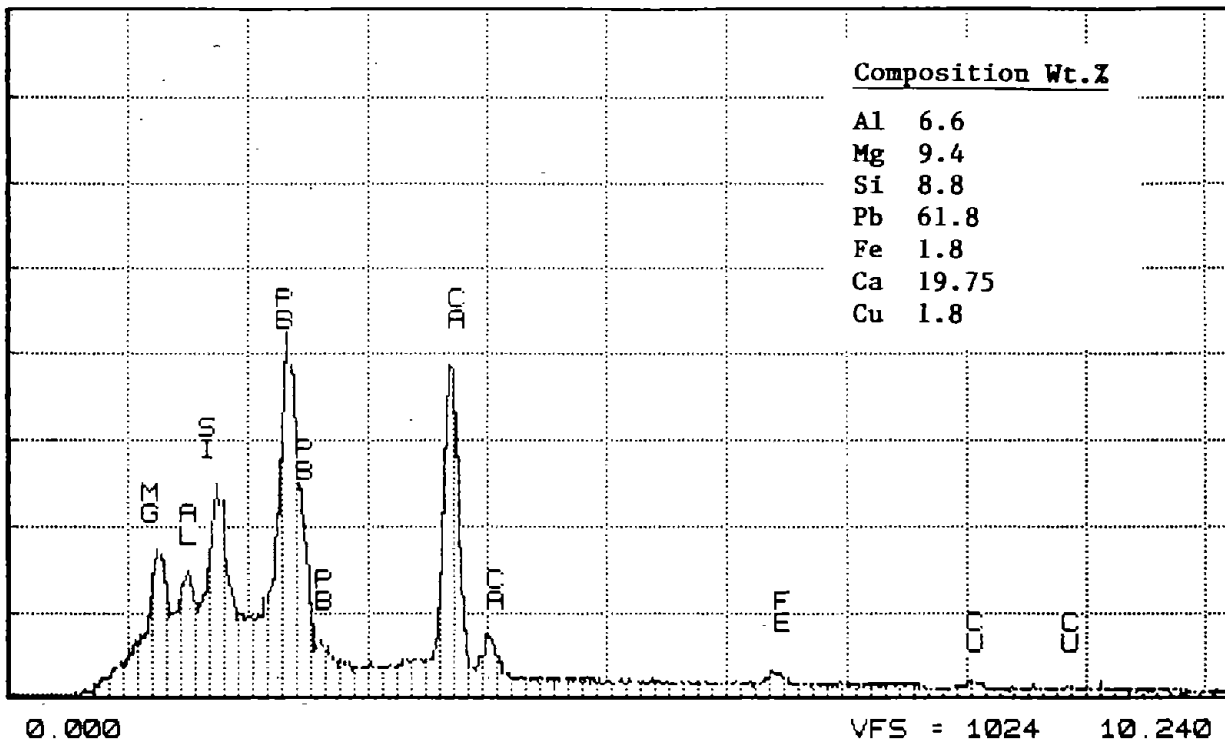


Figure 31. EDX analysis and SEM micrograph of 35- $\mu\text{m}$  particle collected on filter within confinement zone during blasting.

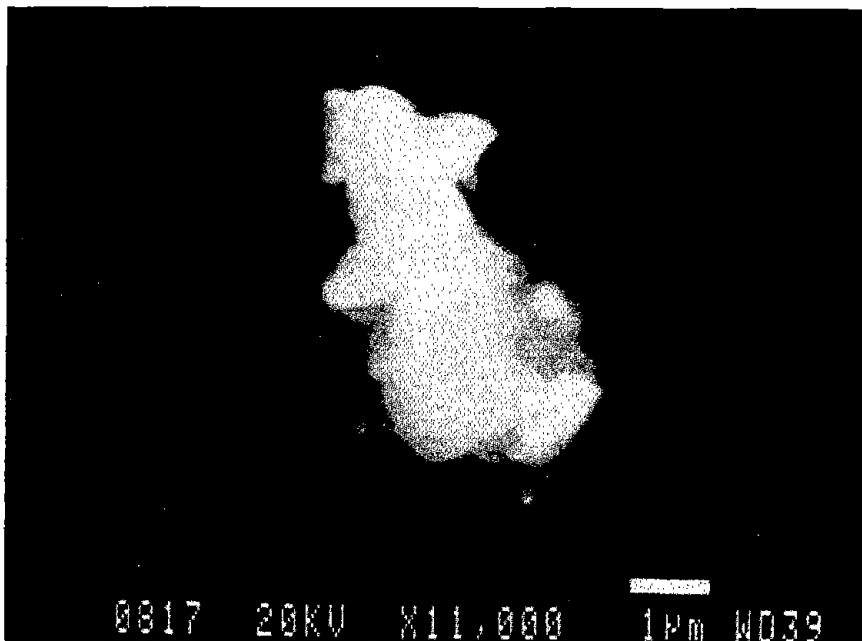
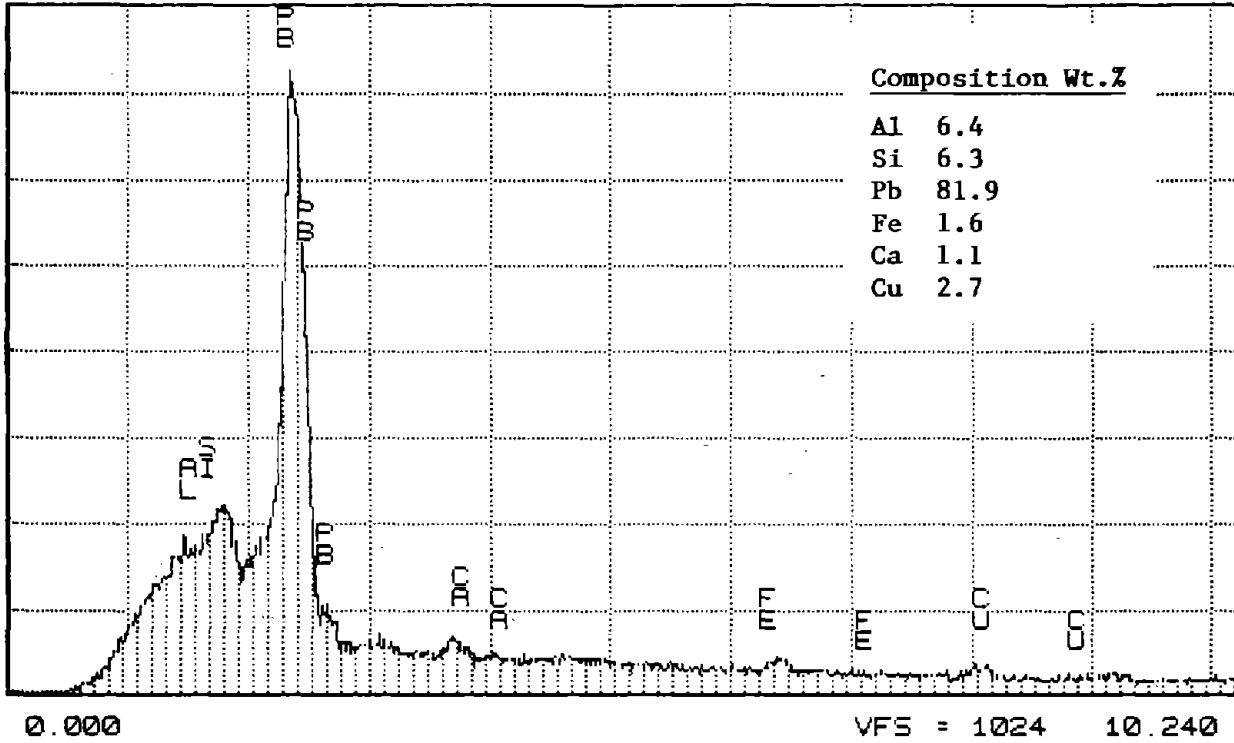


Figure 32. EDX analysis and SEM micrograph of 4- $\mu$ m particle collected on filter within confinement zone during blasting.

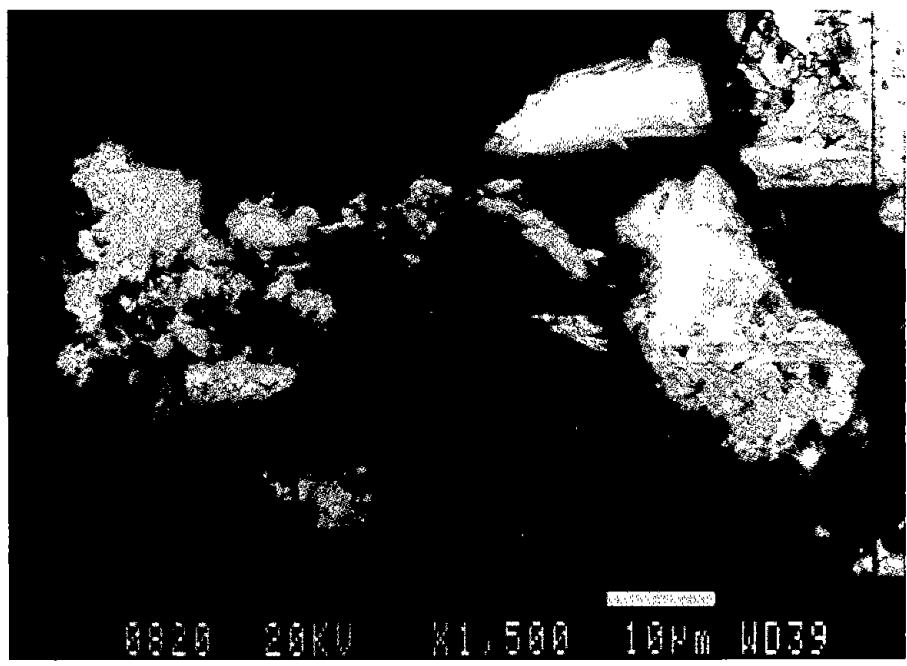
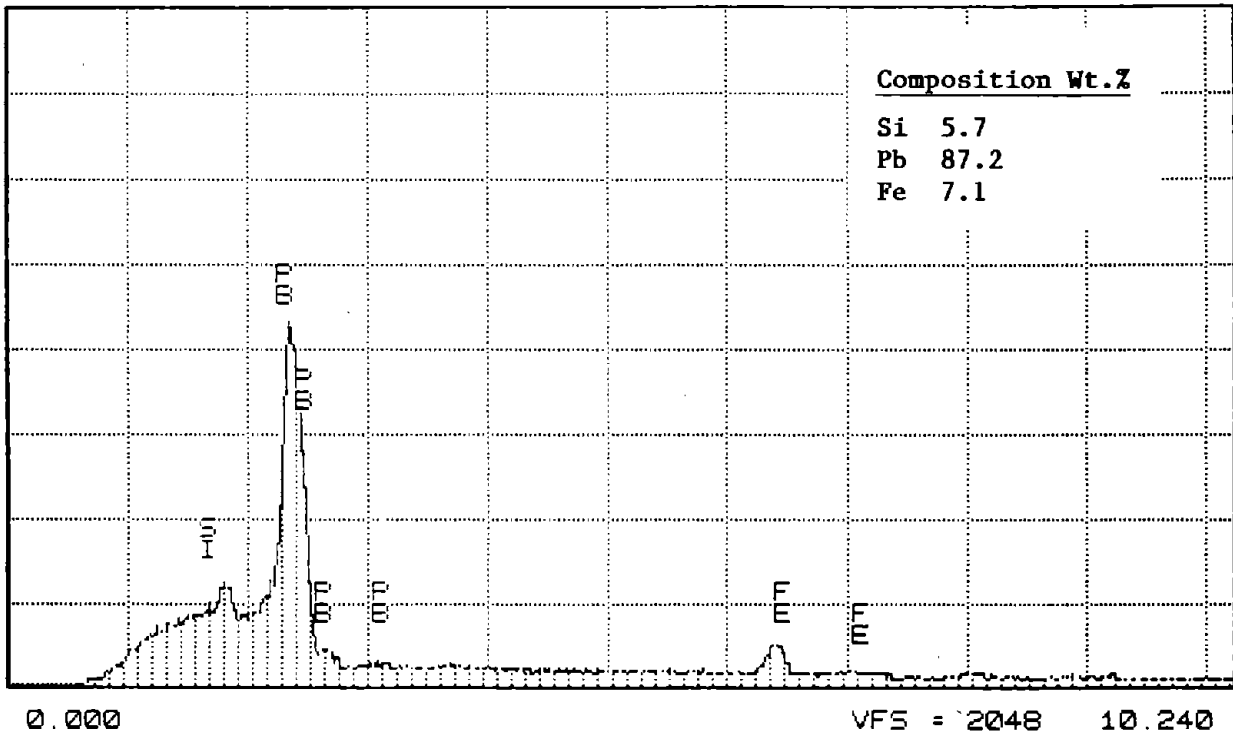


Figure 33. EDX analysis and SEM micrograph, 50- $\mu$ m particle collected on filter within confinement zone during blasting.



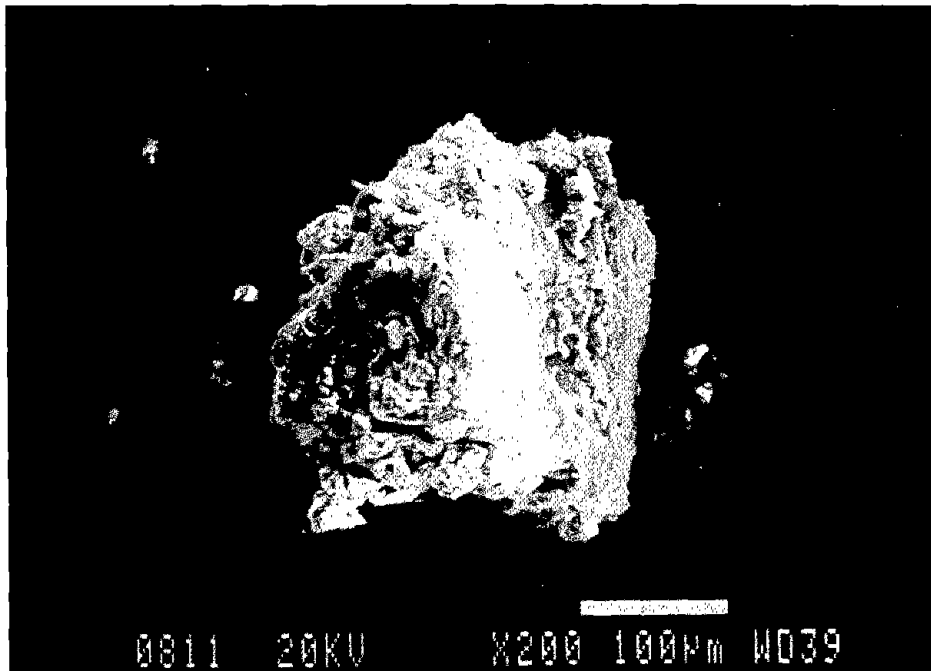
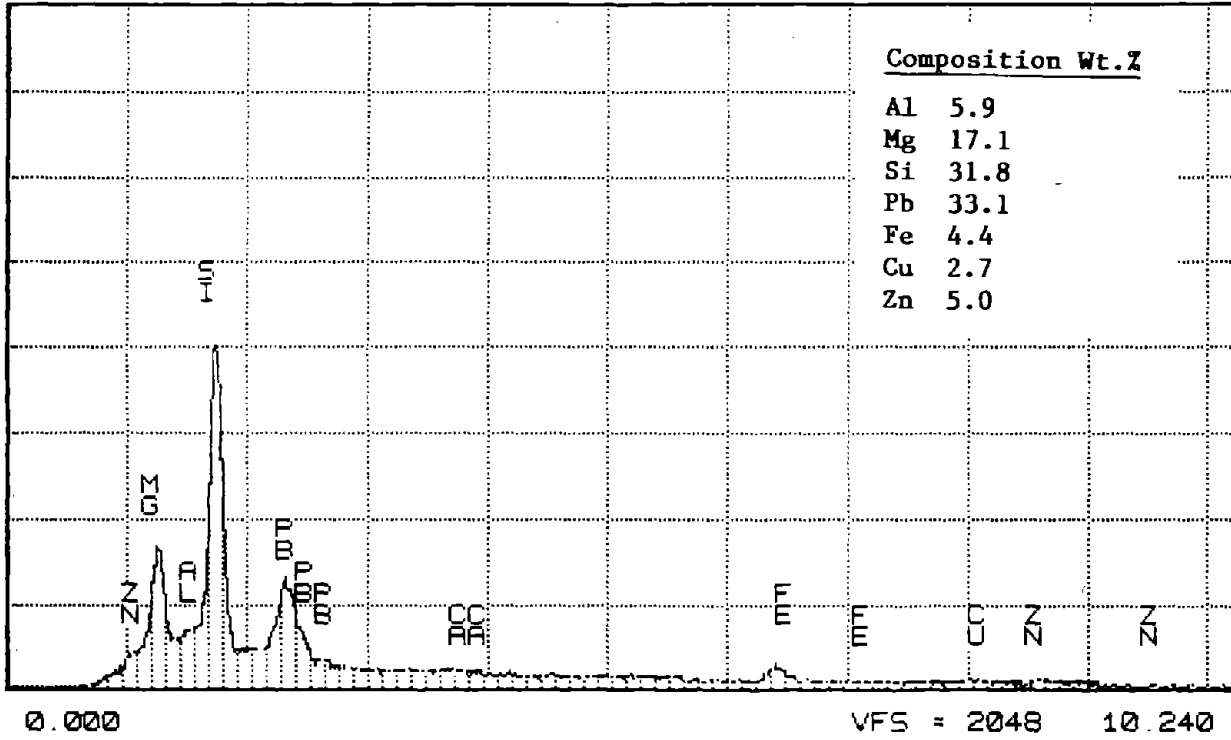


Figure 34. EDX analysis and SEM micrograph of 270- $\mu\text{m}$  particle collected on filter within confinement zone during blasting.

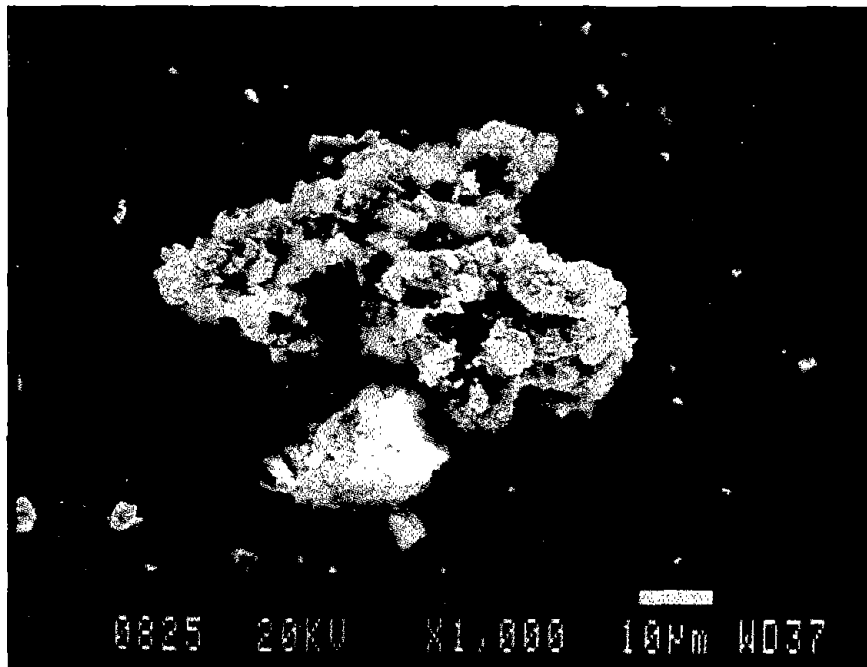
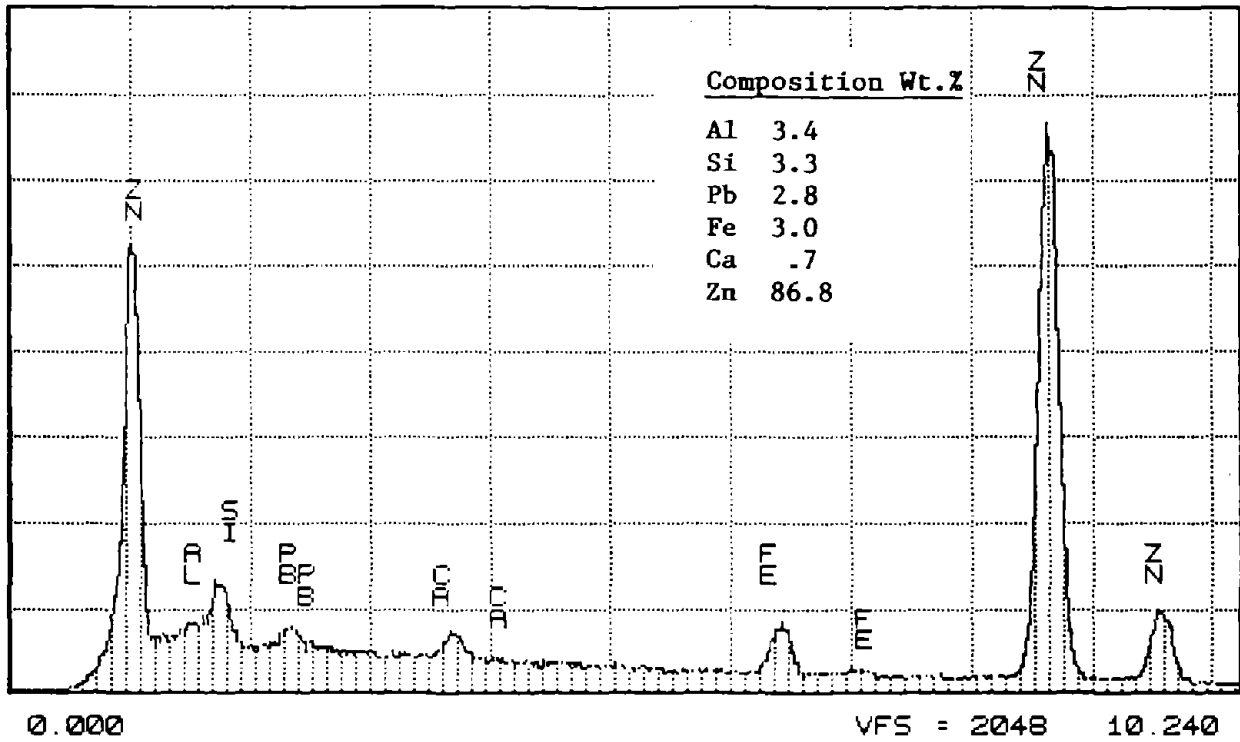


Figure 35. EDX analysis and SEM micrograph of 55- $\mu\text{m}$  particle collected on filter within confinement zone during blasting.

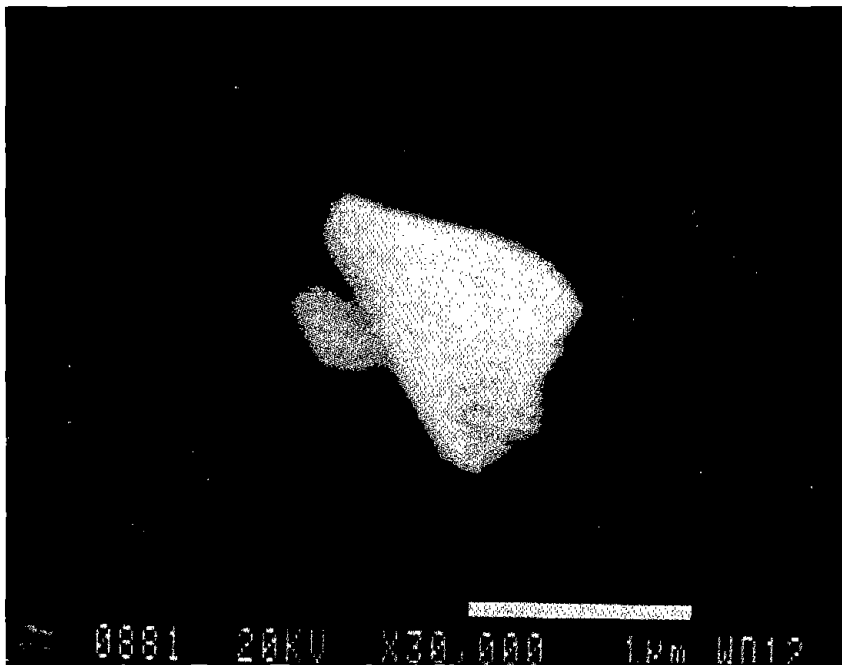
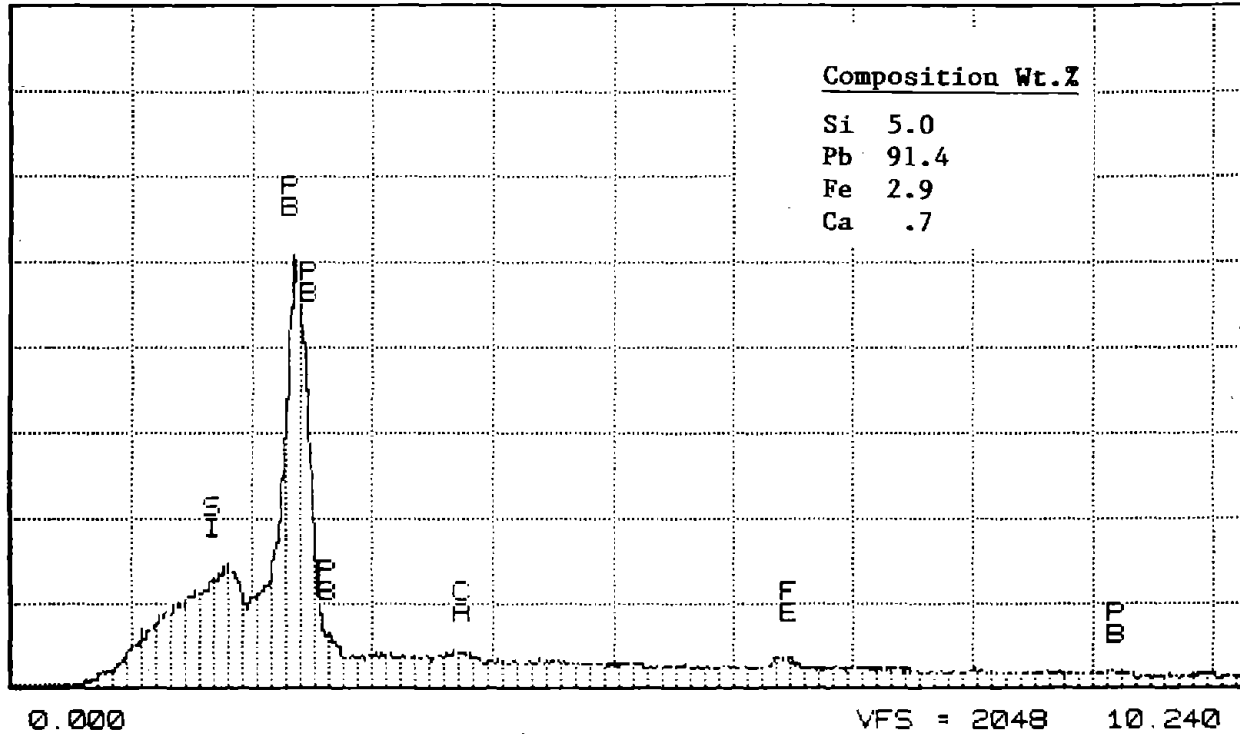


Figure 36. EDX analysis and SEM micrograph of 1- $\mu$ m particle collected on filter within confinement zone during blasting.

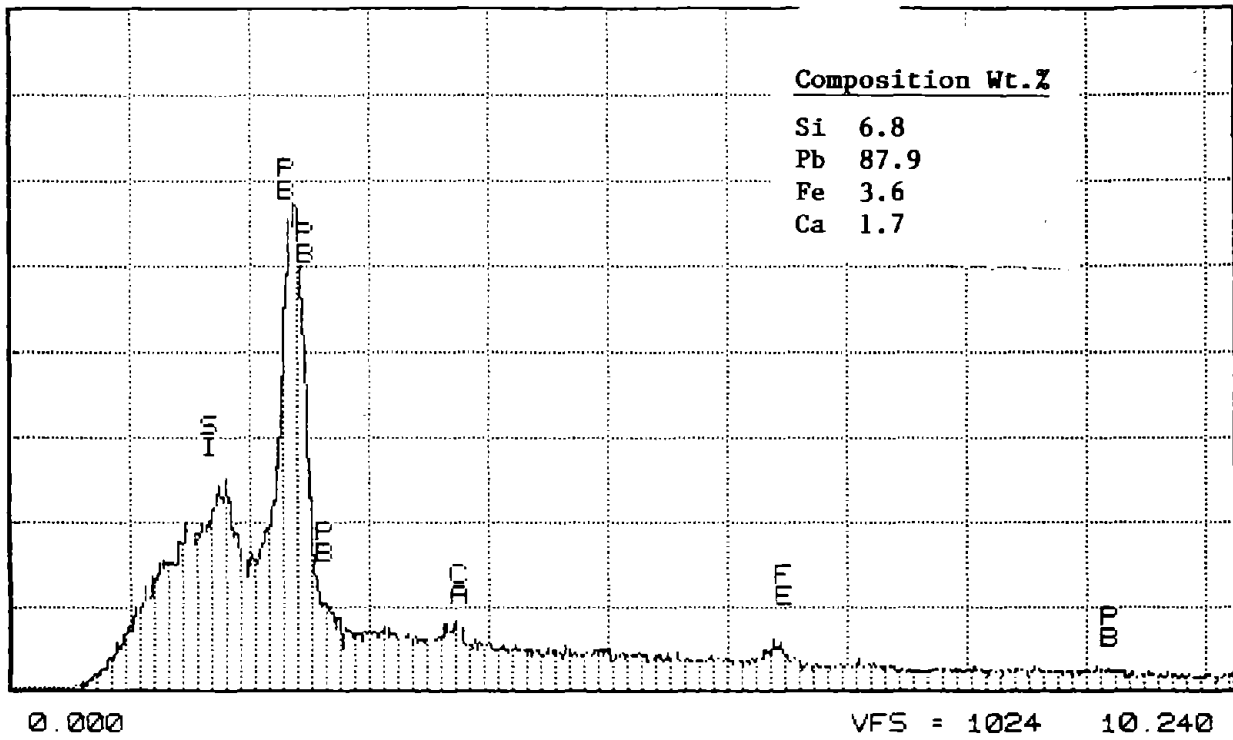


Figure 37. EDX analysis and SEM micrograph of 1- $\mu$ m particle collected on filter within confinement zone during blasting.

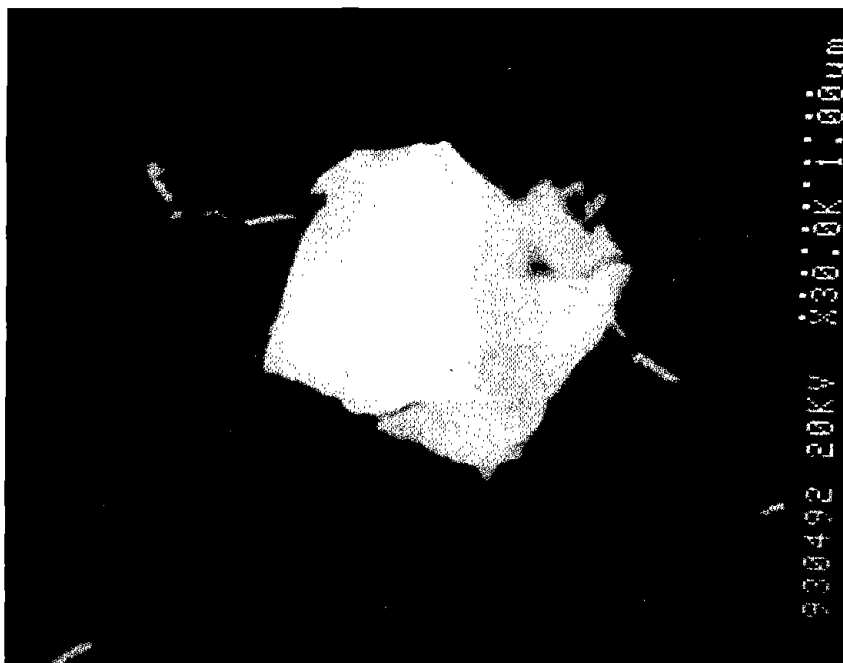
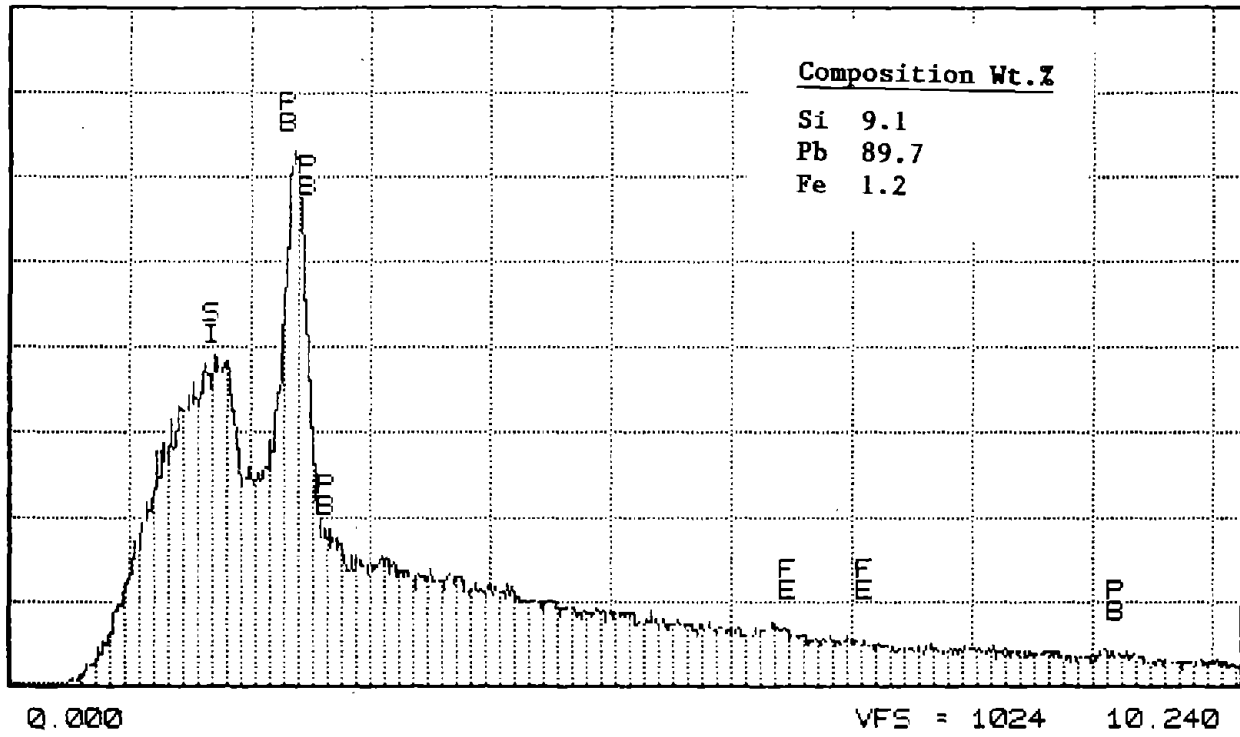


Figure 38. EDX analysis and SEM micrograph of 1- $\mu$ m particle collected on filter within confinement zone during blasting.

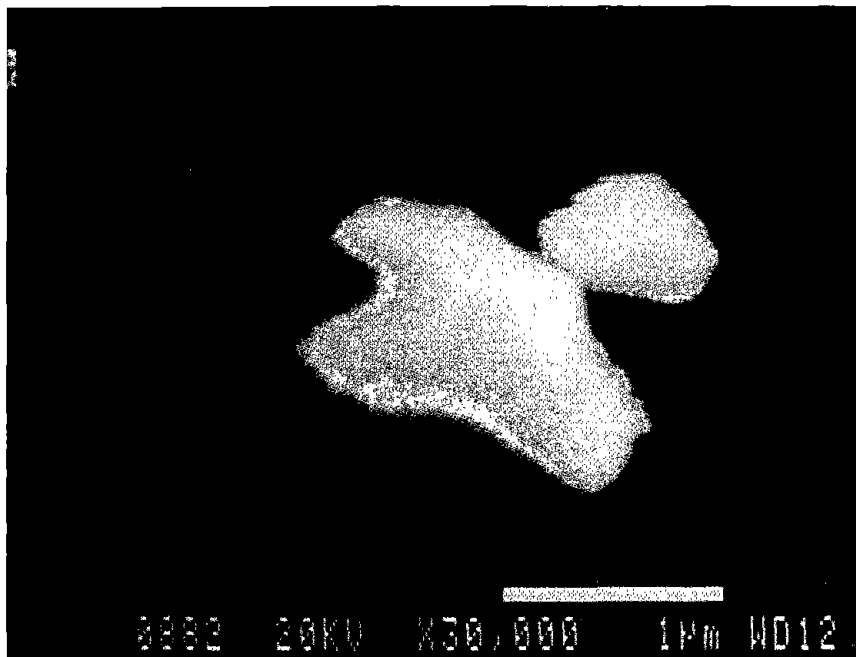
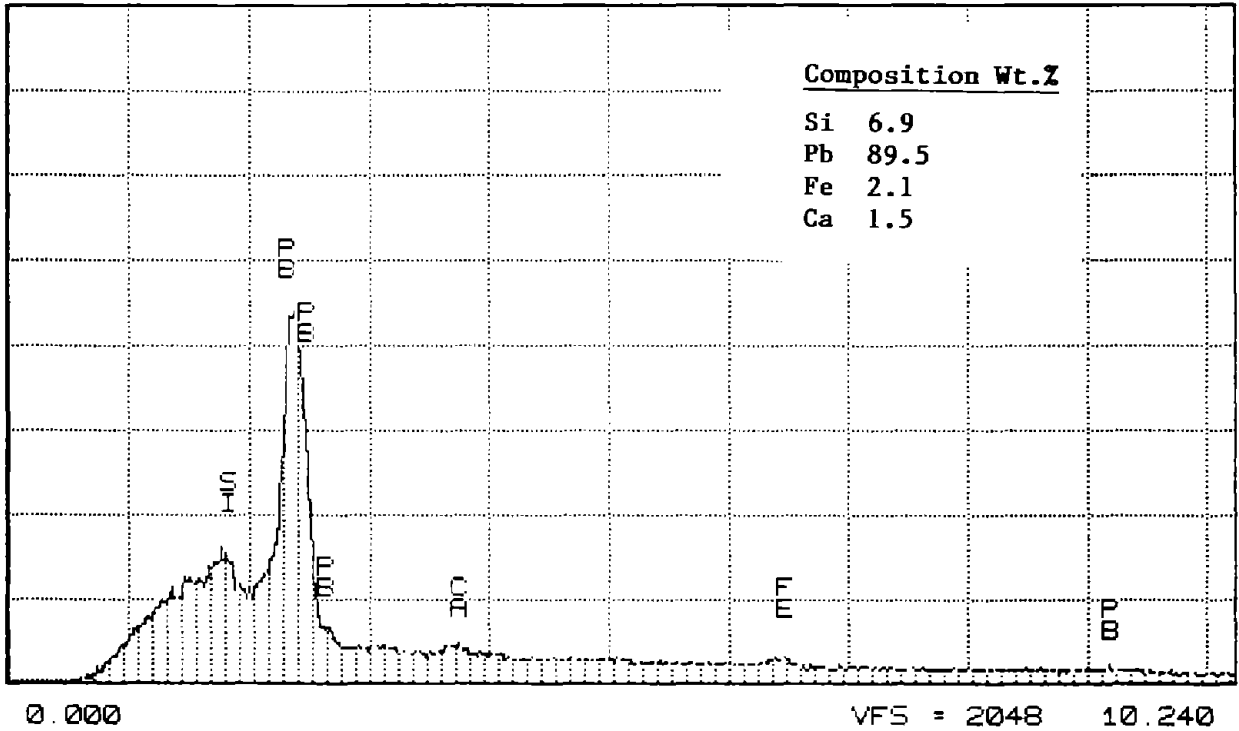


Figure 39. EDX analysis and SEM micrograph of 1- $\mu$ m particle collected on filter within confinement zone during blasting.

Table 4. Composition of various size particles collected on a filter within the grit-blast confinement zone.

Particle Size ( $\mu\text{m}$ )	Figure No.	Composition of Particles in Weight Percentage								
		Pb	Ca	Al	Si	Mn	Fe	Cu	Mg	Zn
1	36	91.4	0.7	-	5.0	-	2.9	-	-	-
1	37	87.9	1.7	-	6.8	-	3.6	-	-	-
1	38	89.5	1.5	-	6.9	-	2.1	-	-	-
1	39	89.7	-	-	9.1	-	1.2	-	-	-
4	32	81.9	1.1	6.4	6.3	-	1.6	2.7	-	-
5	29	6.6	-	-	1.9	-	91.5	-	-	-
6	30	82.9	2.7	5.8	5.5	-	1.7	1.4	-	-
25	28	-	-	-	1.0	1.2	97.8	-	-	-
35	31	61.8	19.8	6.6	8.8	-	1.8	1.8	9.4	-
50	33	87.2	-	-	5.7	-	7.1	-	-	-
55	35	2.8	0.7	3.4	3.3	-	3.0	-	-	86.6
270	34	33.1	-	5.9	31.8	-	4.4	2.7	17.1	5.0
650	27	-	-	-	-	2.3	97.7	-	-	-

A qualitative comparison of these methods is presented in table 5. It is based solely on observations made during the demonstration. Each method has advantages and disadvantages and the method of choice depends on the size, location, and geometry of the bridge being refurbished, as well as the size of the area to be coated, degree of surface preparation required, etc.

#### Julien Dubuque Bridge at Dubuque, Iowa

Paint debris samples were obtained from a paint-removal and recoating project on the Julien Dubuque Bridge over the Mississippi River between Dubuque, Iowa, and East Dubuque, Illinois, done by the Iowa Department of Transportation. The paint-removal method used was steel-grit blasting with full containment. This required bringing a preconstructed scaffolding under the bridge on a barge, raising the scaffolding up under the bridge as shown in figure 40, and putting the confinement structure in place. The grit-recovery system consisted of vibratory grit separation, air washing, and cyclone separation, but did not include a magnetic separation step.

This bridge was originally painted in 1942 using a lead pigment. In 1976, the paint was removed from all the easily accessible areas by grit blasting and the bridge was recoated using a zinc chromate pigment. Paint was removed from the areas not blasted in 1976 using vacuum-blast equipment. This paint debris is a combination of the original lead-based paint and the 1976 zinc chromate system.

Table 5. Comparison of paint-removal methods.

Characteristic	Paint-Removal Method		
	Vacuum Blasting	Confined Blasting	Vacuum Power Tool
Setup Time	Very Short	Time Consuming	Insignificant
Setup Cost	Very Low	Very Expensive	Insignificant
Cleaning Rate	Med. $\approx 5.6 \text{ m}^2/\text{hr}$	Fast $\approx 22 \text{ m}^2/\text{hr}$	Slow $\approx 2.8 \text{ m}^2/\text{hr}$
Surface Quality	Very Good	Excellent	Good
Worker Stress	Heavy Work	Need Breaks	Least Stress
Controllability	Good	Best	Good
Meets EPA Specs	Fair	Good	Good
Meets OSHA Specs		Fair	Fair/Good

The following debris samples were collected: (1) wheelabrator GL40 steel grit, (2) used GL40 grit prior to cleaning, (3) paint waste separated from the used grit by the separation/recycling system, (4) debris obtained by magnetic separation from steel grit initially treated by the separation/recycling system, and (5) a sample of the vacuum blast debris described above. No analysis was done on the first two samples. The other three samples were examined by SEM as shown in figure 41 and by optical microscopy as shown in figure 42. They also were analyzed by EDX and these results are shown in figure 43.

The material magnetically separated from the once-treated grit (see figure 43(a)) is very high in silicon and, in fact, appears to contain glass or sand particles. The other main component identified is iron, which came either from the steel blast media or from the structure itself. The sample was extremely nonuniform in composition and contained some fibrous materials (perhaps wood). It appeared to contain only small amounts of actual paint components, such as red lead and zinc chromate. In fact, several other elements, such as aluminum, magnesium, calcium, and titanium, were found in similar small concentrations. Sieve analysis of this sample showed that despite its very dusty brown appearance, less than 6 percent of the sample by weight was smaller than  $45 \mu\text{m}$  in diameter (passed through a 325-mesh screen sieve).

The paint waste sample (figure 43(b)) is very high in iron. This sample also contains silicon, although at a much reduced level compared to the magnetically separated sample described above. Lead, zinc, and chromium as well as magnesium, aluminum, calcium, and titanium were also found. The relatively low levels of lead in the paint waste are consistent with the fact that most of the lead had been previously removed. This sample contained the largest amount of fines. More than 20 percent of the sample passed through a  $45\text{-}\mu\text{m}$  screen.

The vacuum blast debris sample (figure 43(c)) contains many elements, including lead, chromium, iron, and zinc, that are present in relatively large



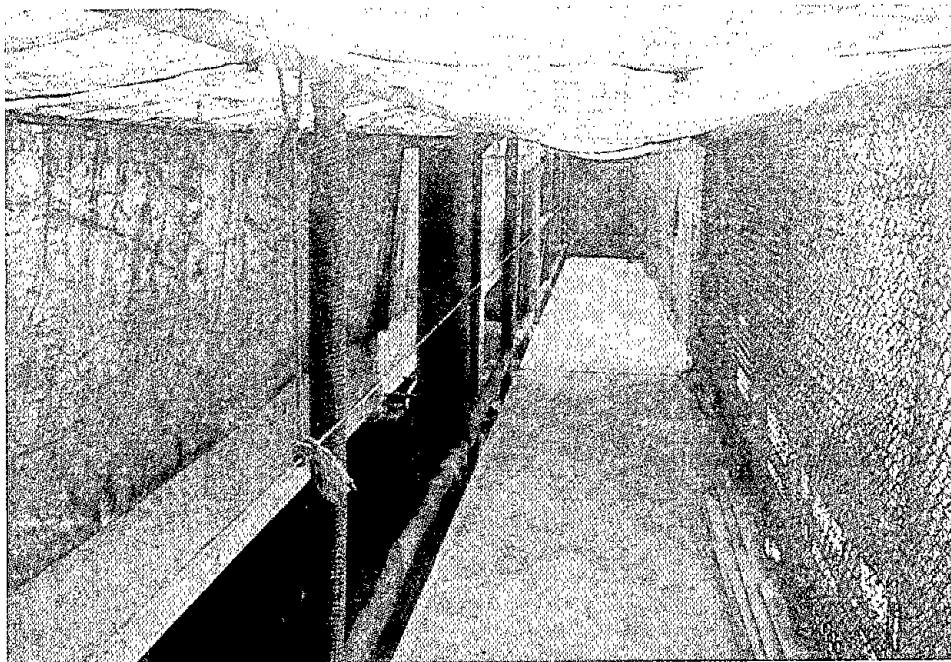
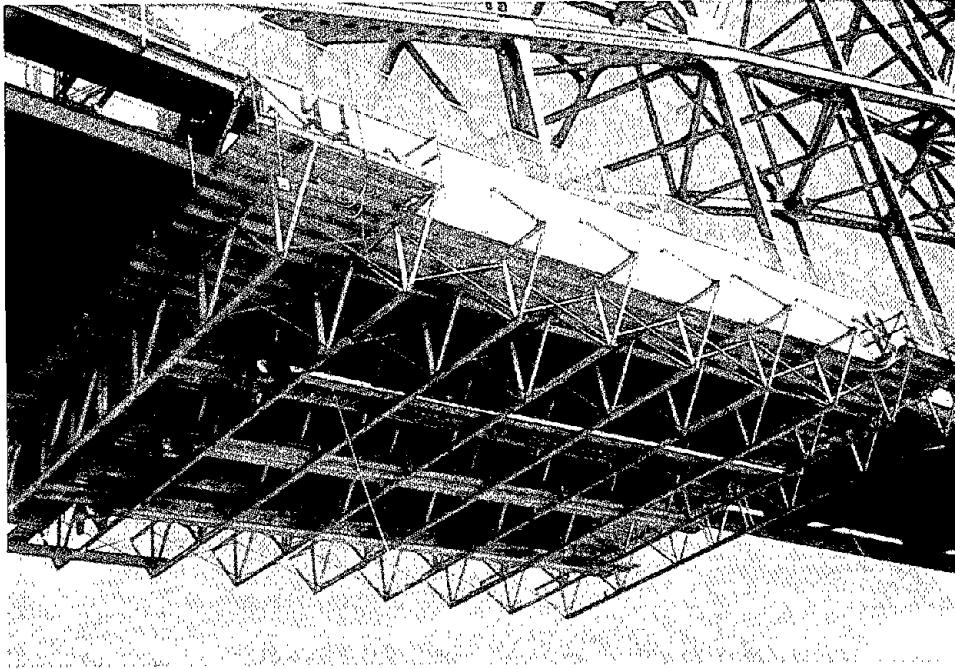
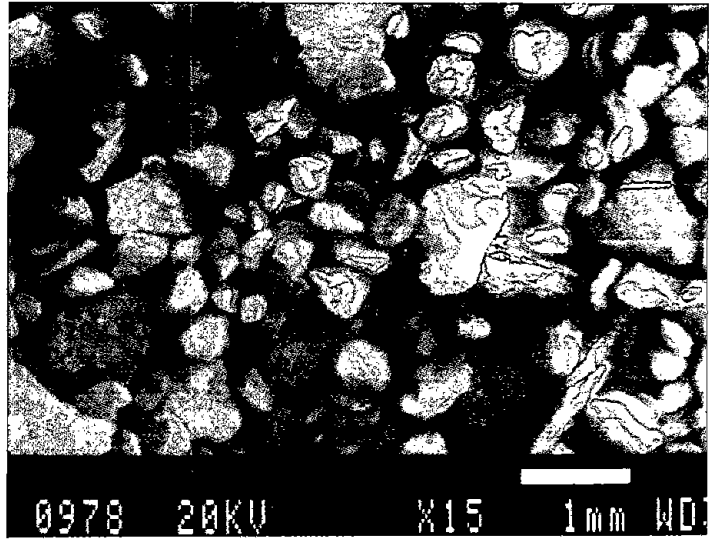
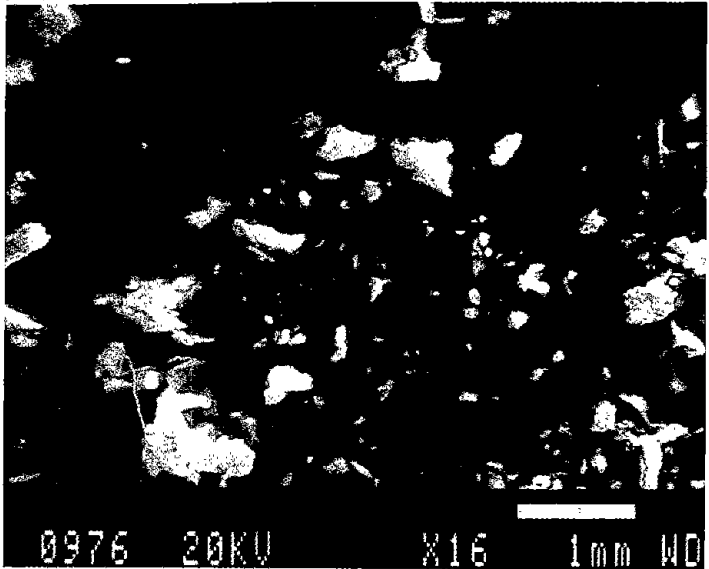


**Figure 40. Scaffolding and grit-blasting confinement structure built for Julien Dubuque Bridge paint-removal job.**

(a) Paint debris separated from steel blasting grit using air separation/recycling.



(b) Debris magnetically separated from steel grit after initial treatment by air separation/recycling equipment.



(c) Paint debris from steel-grit vacuum blasting.

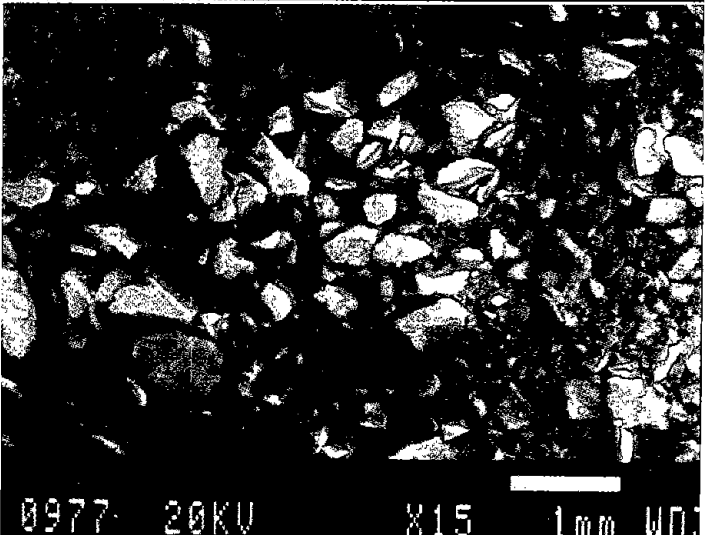
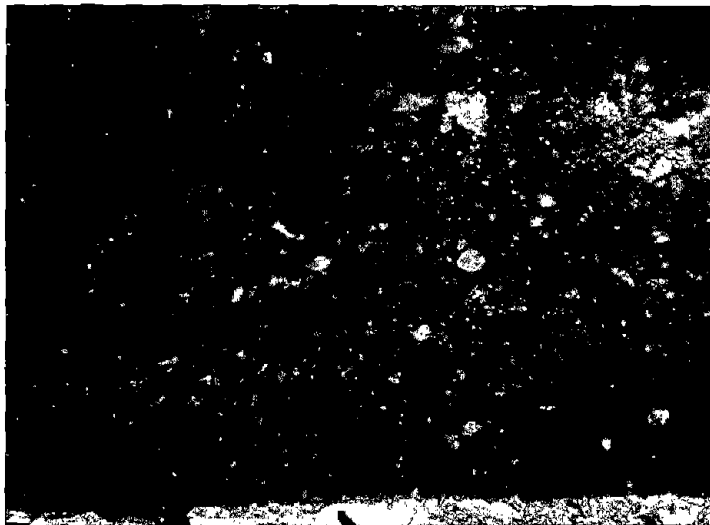
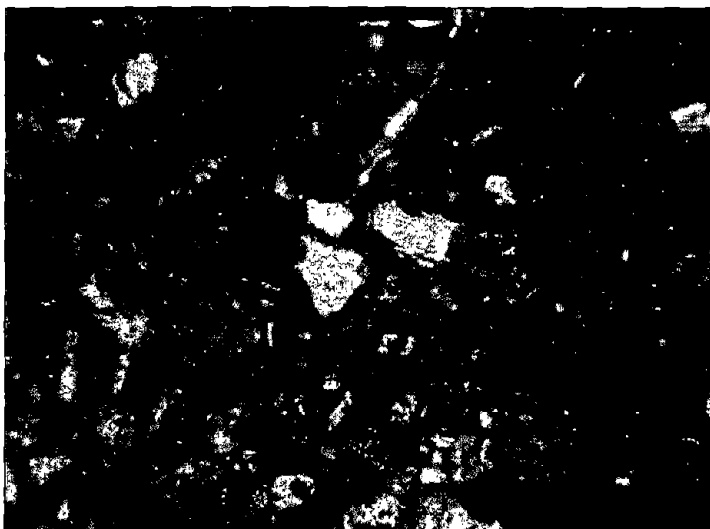


Figure 41. Low-magnification SEM photomicrographs of paint debris samples.

- (a) Paint debris separated from steel blasting grit using air separation/recycling.



- (b) Debris magnetically separated from steel grit after initial treatment by air separation/recycling equipment.



- (c) Paint debris from steel grit vacuum blasting.

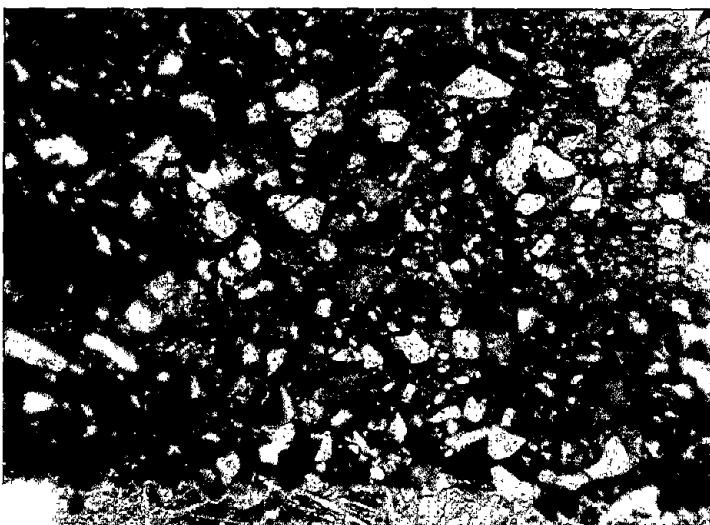
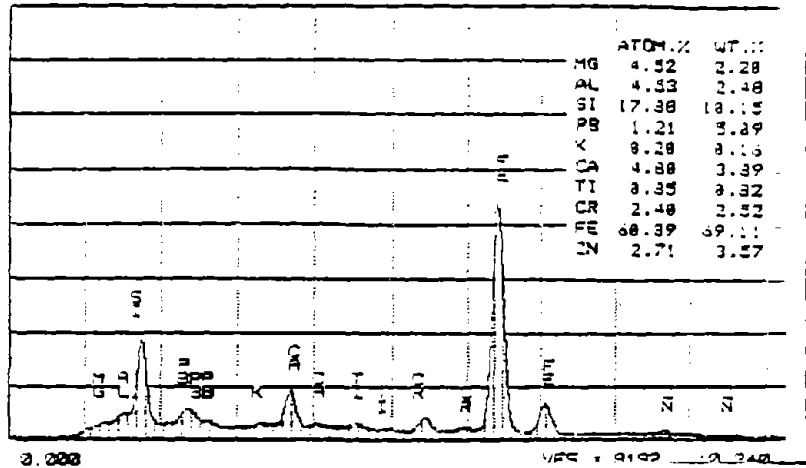
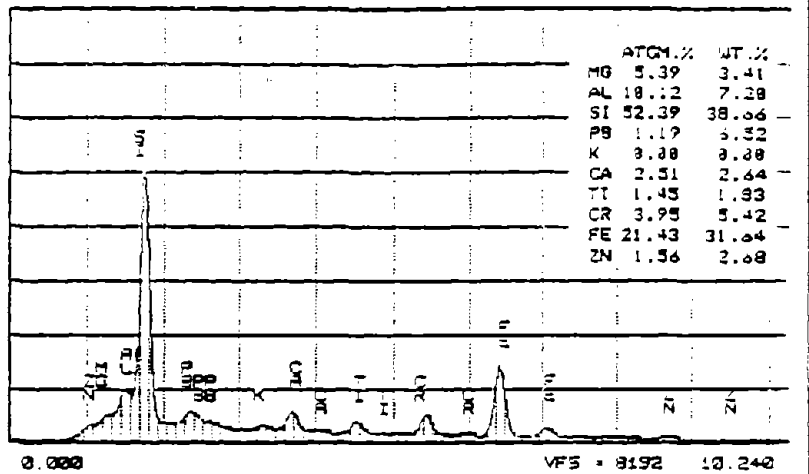


Figure 42. Low-magnification optical photographs of paint debris samples.

(a) EDX of treated grit.



(b) EDX of paint waste.



(c) EDX of vacuum-blast debris.

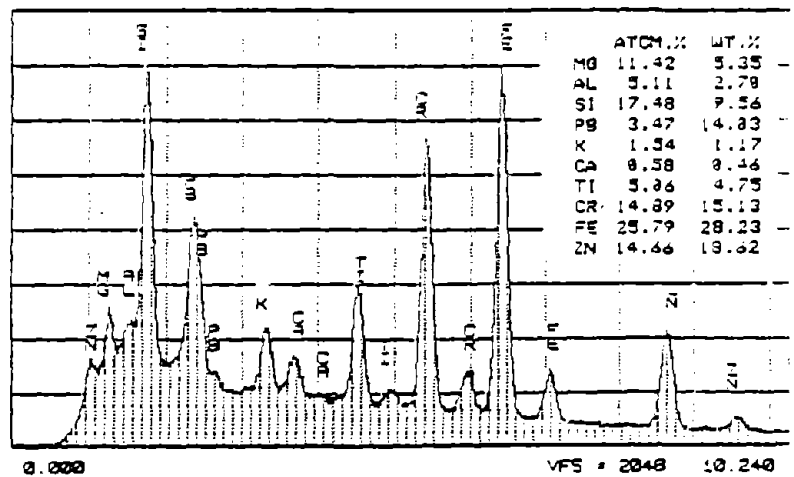


Figure 43. EDX analysis of paint debris samples from Julien Dubuque job.

amounts. This analysis is consistent with the paint records that show that both red-lead and zinc chromate pigments were used in the paints. Again, the iron most likely comes from steel or rust. This is the only paint-waste sample from the Dubuque site that actually looks like it contains paint. Some of these paint particles clearly show four layers of paint under optical microscopic examination. Approximately 16 percent of this sample was finer than 325 mesh (45  $\mu\text{m}$ ).

The fines (the portions that passed through the 325-mesh sieve screen) from each of the above three samples were also examined by SEM. Figure 44 shows the <45- $\mu\text{m}$  particles in the magnetically separated material at magnifications of x 500, x 5,000, and x 50,000. In the x 500 photomicrograph, particles ranging in size from less than 1  $\mu\text{m}$  up to about 30  $\mu\text{m}$  are clearly discernable. The x 5000 photo shows a less than 0.5- $\mu\text{m}$  particle nest to an approximately 10- $\mu\text{m}$ -diameter particle. The x 50,000 photo shows only the 0.4- $\mu\text{m}$ -wide particle.

Figure 45 shows a similar set of photomicrographs for the paint-waste particles that passed through the 325-mesh screen. Figure 46 presents the results for the vacuum blast fines. In each of the three sets of figures, the particle featured at x 50,000 can be identified in the x 5,000 and x 500 photos upon close examination. Particles smaller than 0.3  $\mu\text{m}$  in diameter appear to exist in each of the samples, but since this size is near the limit of resolution of the instrument, further study is needed to establish whether or not such small particles are present, and if so, how many.

Two particles, approximately 0.5  $\mu\text{m}$  in diameter, from each of the above three samples were analyzed by EDX. The results are presented in figures 47, 48, and 49. For the paint-waste samples separated from the grit by air and magnetically, one particle contained lead and the other did not. For the vacuum blast debris, both particles contained lead. Again, these results demonstrated that the fine particles produced during grit-blasting operations contained lead.

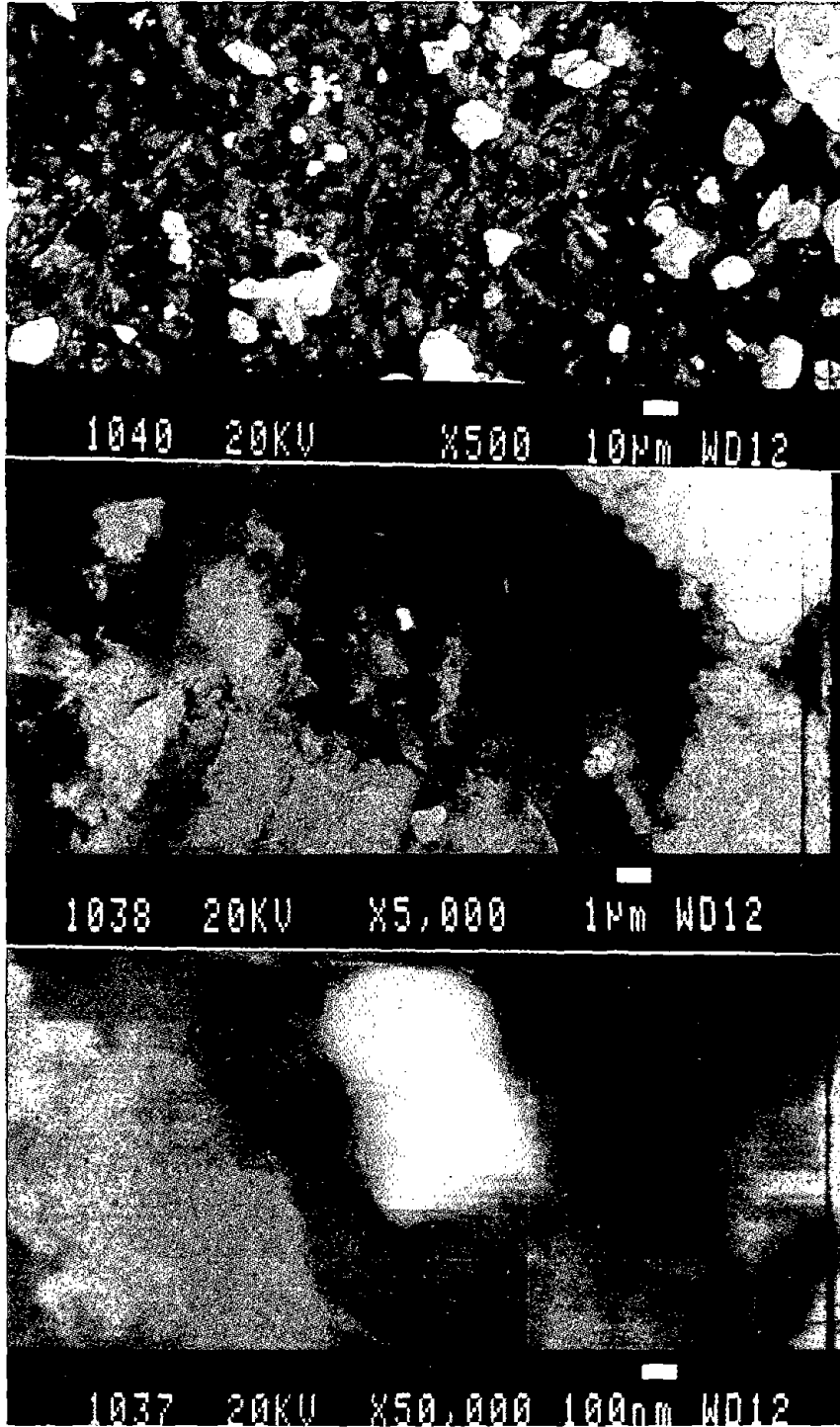


Figure 44. SEM photomicrographs of magnetically separated paint debris particles <math>< 45 \mu\text{m}</math> in diameter at magnifications of x 500, x 5,000, and x 50,000.

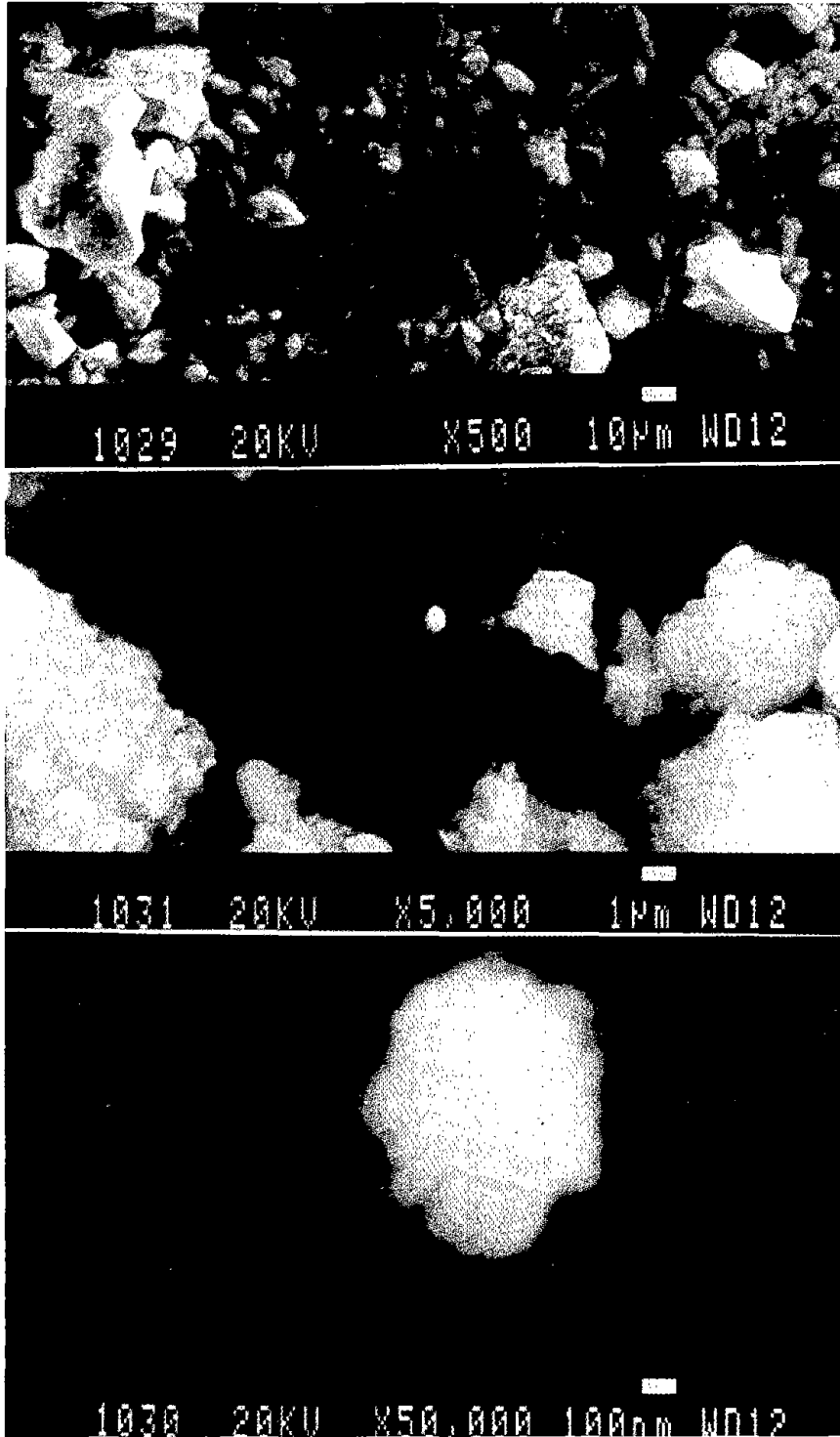


Figure 45. SEM photomicrographs of air-separated paint debris particles < 45  $\mu\text{m}$  in diameter at magnifications of x 500, x 5,000, and x 50,000.

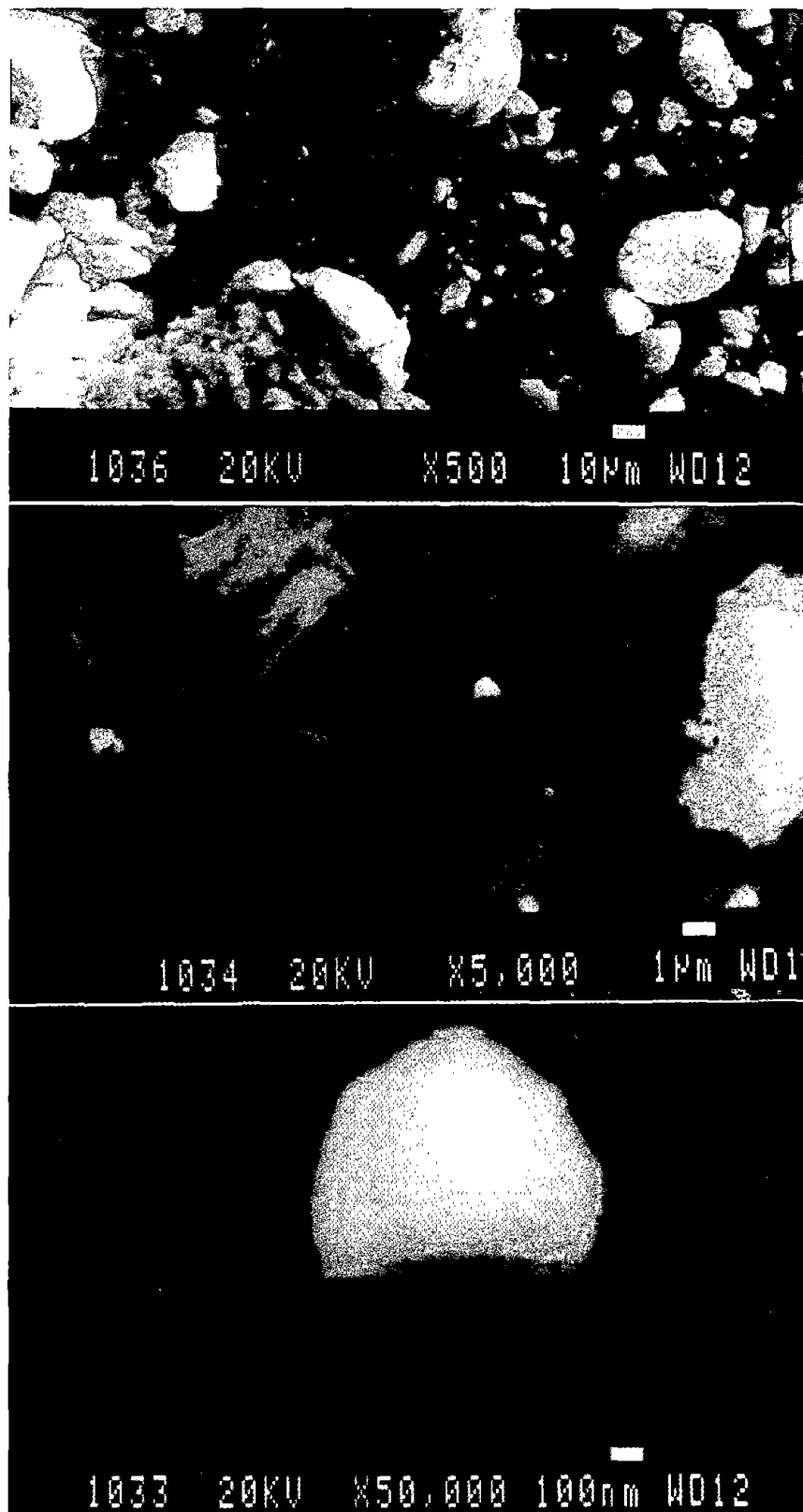


Figure 46. SEM photomicrographs of vacuum-blast paint debris particles < 45 μm in diameter at magnifications of x 500, x 5,000, and x 50,000.



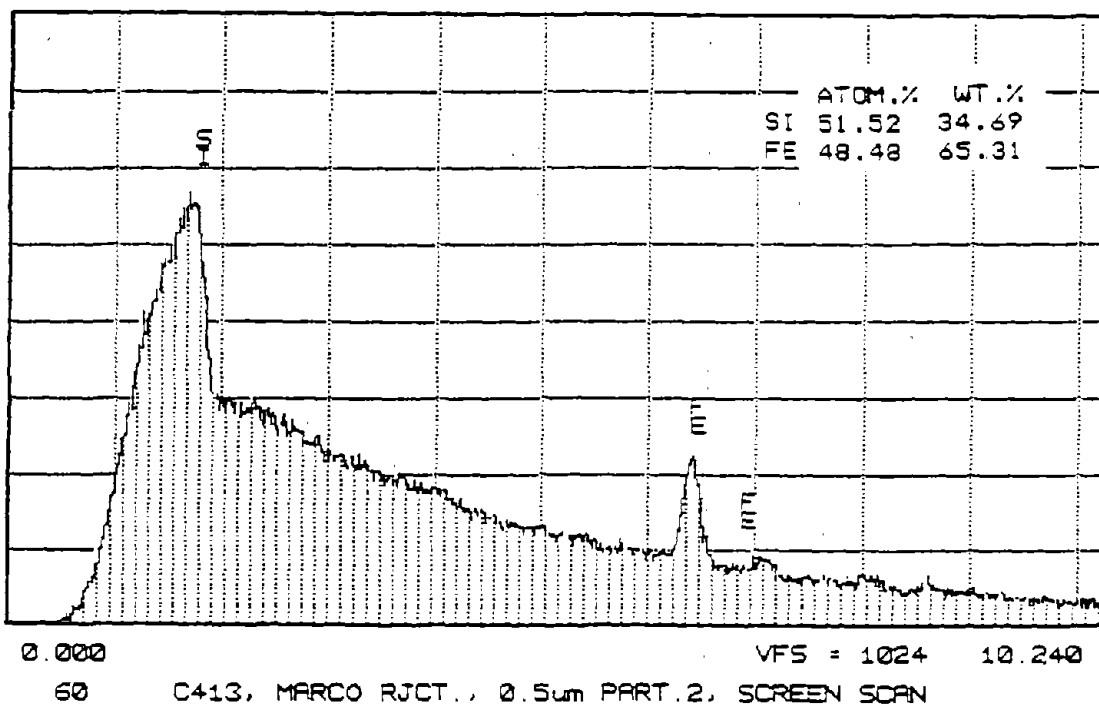
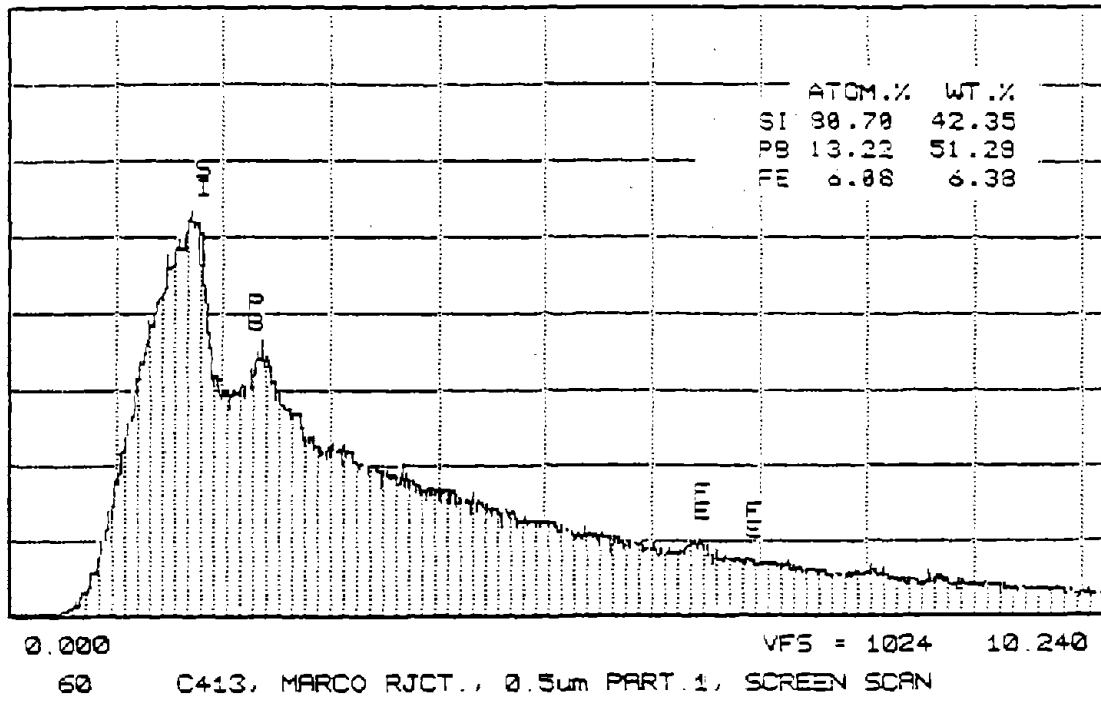
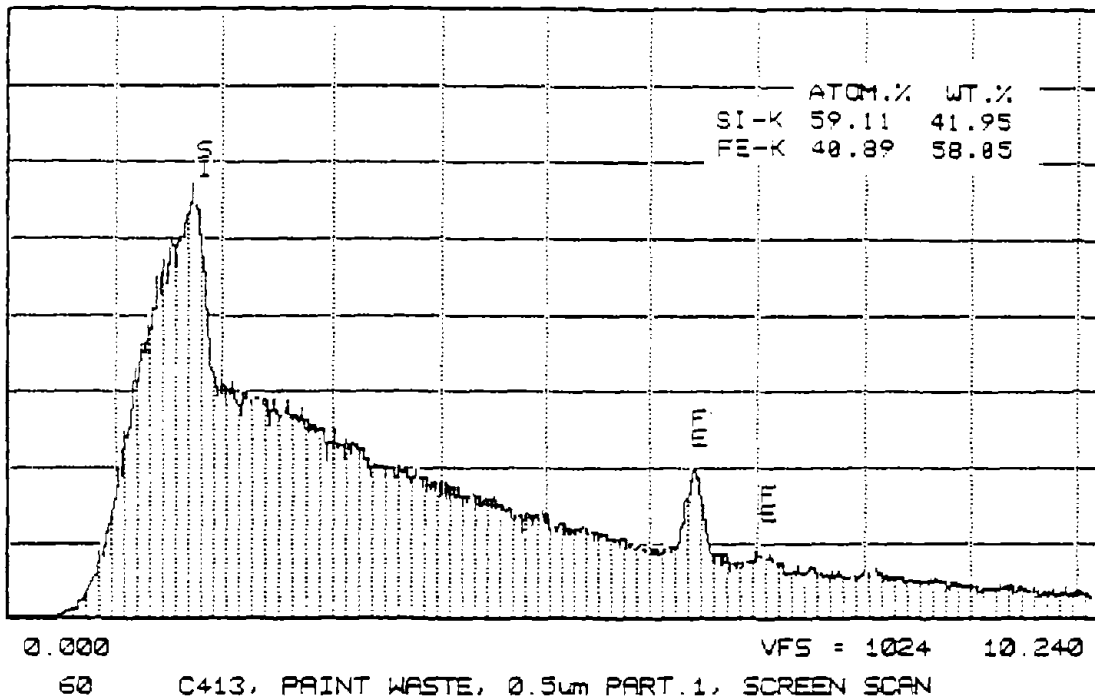


Figure 47. EDX analysis of 0.5- $\mu$ m magnetically separated particles.



BASIC INDUSTRY RESEARCH LAB / NW UNIV. FRI 21-NOV-83 15:32  
Cursor: 0.000keV = 0

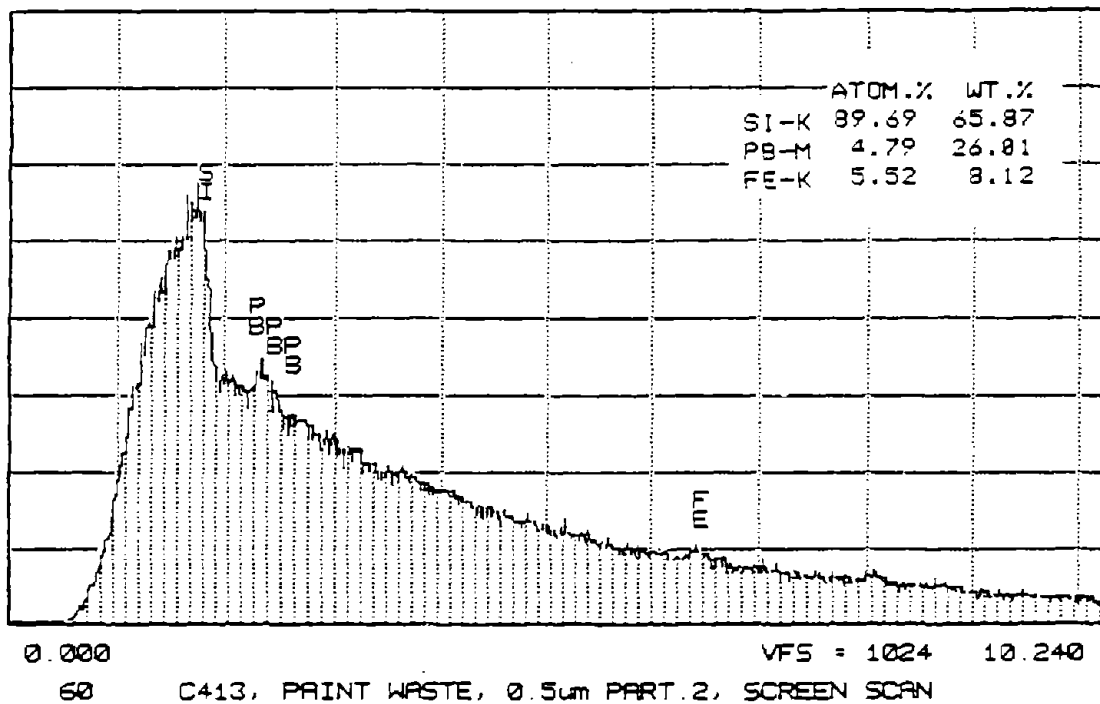


Figure 48. EDX analysis of 0.5- $\mu$ m air-separated particles.

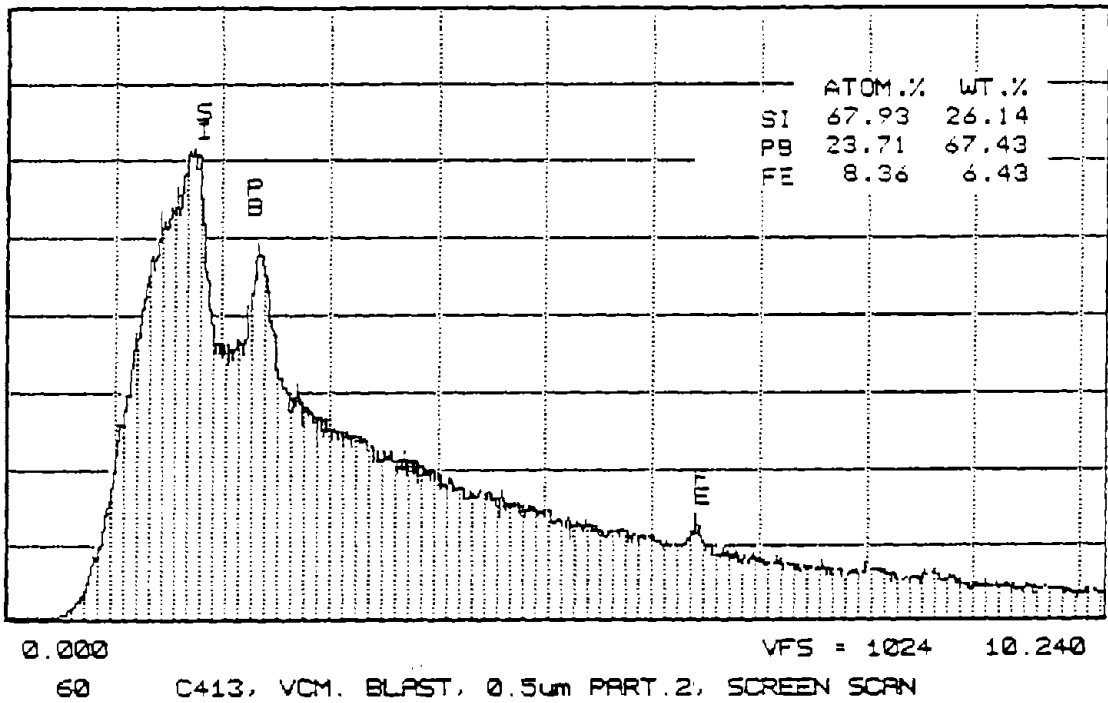
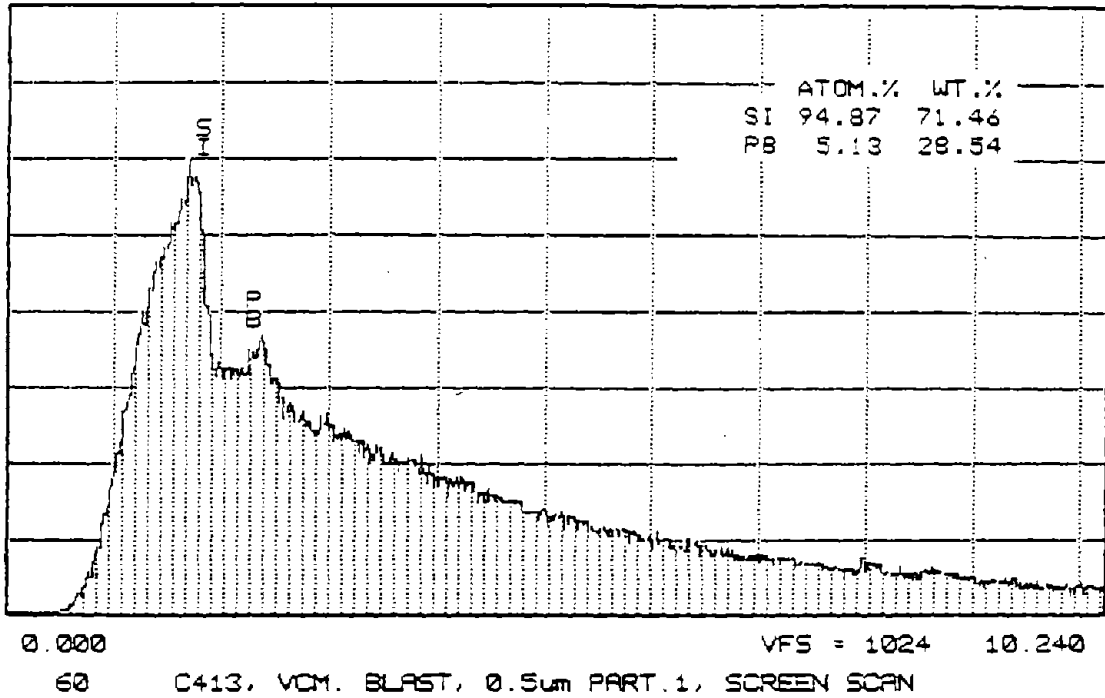


Figure 49. EDX analysis of 0.5- $\mu\text{m}$  vacuum-blast particles.



## CHAPTER 4: TASK C - EVALUATION OF PROCEDURES FOR ANALYSIS AND DISPOSAL OF LEAD-BASED PAINT-REMOVAL DEBRIS

### Introduction

The objective of this task was to review current waste analysis, handling, and treatment procedures, especially with respect to the toxicity characteristic leaching procedure (TCLP) and the effect that iron has on lead leachability. This objective was achieved by: (1) analyzing published reports, (2) discussing results with other investigators, including State DOT's, and (3) analyzing paint debris samples obtained from removal operations, including operations where recyclable steel-grit blasting was used.

Our results are consistent with observations made by others, wherein lead was found to be stabilized against leaching in the TCLP test by using steel blasting grit. The steel (iron) may be present as an additive or as the primary blasting media. The effect appears to be due to the fact that iron is more electropositive than lead, thus reducing the lead ions in solution to metallic Pb that plates out on the iron particles and are subsequently removed by filtration from the leachate being analyzed. Initially, this dramatically reduces solubility, but the permanency of the stabilization of lead-paint debris by iron is questionable on long-term exposure to commercial dump environments. Repeated leaching of the same debris has shown that the rate of leaching increases to where the lead is sufficiently solubilized to fail the TCLP test. As a result, some State DOTs have chosen to treat all paint debris as hazardous waste regardless of whether it passes the TCLP test.

Additives to blast media other than iron are being developed and evaluated. Lead-based paint debris stabilized against leaching by proprietary silicate-based materials such as Blastox™ have proven to be more resistant to the TCLP test conditions than the iron-stabilized debris. This is true both in terms of the initial degree of leachability as well as for repeated leaching. While the long-term stability in commercial waste dumps remains to be demonstrated, work is under way at BIRL and other laboratories to try to define test procedures more nearly representative of natural exposures. Other candidate additives undoubtedly will be forthcoming. These additives will be based on their ease of reaction with the soluble lead compounds in paints to convert them to highly insoluble products.

In the future, environmental regulators may increase the aggressiveness of the TCLP test environments. Consideration is being given to lowering the pH of the test from 5.0 to 1.5, substituting mineral acids for the acetic buffer solution, and lowering the permissible limit of leachability from 5 ppm to 1.5 ppm. But since neither the present TCLP test nor the proposed changes represent long-term commercial dump exposures, the logic behind these changes is questionable. It may be much more realistic to specify a reduction of the debris to a smaller particle-size distribution and to perform longer term, repetitive leaching. An obvious difference between the TCLP test conditions and those present in disposal sites is the availability of oxygen. The disposal site environment is likely to be less oxidizing and this may effect the chemistry that controls lead solubility. Any proposed changes in the TCLP test need to be shown to correlate with containment-site environments before they are implemented.

## Discussion

### Waste Analysis Methods

Analysis of the Existing Paint. Paint analysis should begin with the existing paint to determine if it contains toxic metals such as lead, chromium, etc. The composition of the existing paint may be determined by:

- \* DOT paint history records, or as defined in 15 USC 2601, Section 401.
- \* Onsite x-ray fluorescence analysis.
- \* Laboratory paint chip analysis by atomic absorption (AA) or inductively coupled plasma atomic emission spectroscopy (ICP or ICP-AES).

Each of the above methods has its advantages and disadvantages. Examination of the records should be sufficient provided accurate records have been kept. But since the records probably do not tell how much lead existed in what originally was called a non-lead-based paint or what subsequent contamination from maintenance painting may have occurred, actual analysis is necessary in order to know which precautions need to be taken in removing, handling, and disposing of the paint. Since lead was a common contaminant in zinc, the use of high levels of zinc in paints for corrosion inhibition has been examined to estimate whether or not removal of these paints might lead to a debris that would be a hazardous waste (Journal of Protective Coatings and Linings, 3/93, pp. 24-36). It was concluded that the lead in zinc-rich paints does not pose a significant environmental or public health hazard.

Paint chip analysis is an inexpensive means of determining the amount of lead present. The analysis is done by atomic absorption or ICP after acid digestion to dissolve the lead, and the results are generally expressed as total weight percentage lead in the paint. The disadvantages of paint chip analysis are that the analysis is done off-site and that care must be taken to ensure that the paint is uniformly removed down to the steel substrate without inclusion of any significant amount of rust.

We have found energy dispersive x-ray (EDX) analysis to be a valuable laboratory tool when used in combination with a scanning electron microscope (SEM) to analyze paint chips. The method, although semi-quantitative, is rapid and very informative. Elements heavier than fluorine can be determined by this method. Thus, the presence of elements found in the most common pigments and contaminants can be determined. These include sodium, potassium, chlorine, calcium, silicon, titanium, iron, lead, zinc, copper, aluminum, etc. By analyzing both sides of the paint chip, separate analyses can be obtained for the topcoat and the primer.

### Samples of Existing Paint From I-55

Samples of paint were taken for analysis prior to paint removal. These samples were taken from three different locations. The first sample (no. 414-1) was taken from an area beneath the center of a span. This paint was gray in color and came from an area that later was used to demonstrate vacuum power-tool paint removal. The gray paint was a three-coat system consisting of a red-lead/alkyd primer, a leafing aluminum/phenolic intermediate layer, and a non-leafing aluminum/phenolic topcoat. The second sample (no. 414-2) was taken from the same span, but from an outer beam that was painted green for aesthetics. This paint system also had a red-lead/alkyd primer followed by an intermediate coating that contained aluminum. The green topcoat, however, contained significant amounts of lead and titanium and much less aluminum. The third sample (no. 414-3) was taken from a badly deteriorated area between spans on eastbound I-55, where heavy rusting and loss of adhesion were obvious. Its composition was the same as that of sample no. 414-1 as described above.

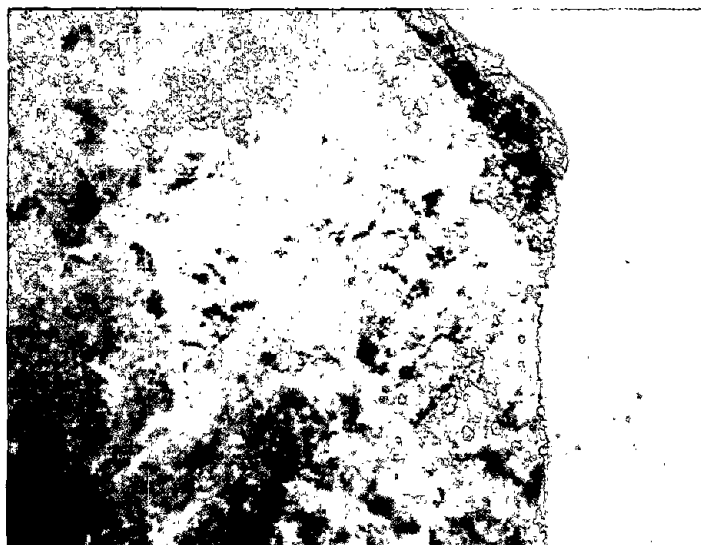
Photographs of the inner (next to the steel) surfaces of the paint chips at x 20 magnification are shown in figure 50. All samples of this surface show the red-lead primer, but to a different degree. Sample no. 414-1 contains a thick, nearly continuous layer of primer, indicating that the primer was more strongly adhered to the rest of the paint than to the steel beneath. Sample no. 414-2 has a large amount of what appears to be rust attached to the primer, indicating that corrosion had taken place beneath the primer. Sample no. 414-3 has little, if any, iron or rust attached to the inner surface and has less red-lead visible, indicating that the primer was more strongly adhered to the steel and separated cohesively.

### Existing Paint Analysis by Energy-Dispersive X-Ray Analysis

The three paint chip samples were analyzed by energy dispersive x-ray (EDX) analysis and the results are given in table 6. Both the outer (exposed to the atmosphere) and the inner (next to the steel) surfaces of each paint chip were analyzed. EDX analysis is a relatively quick and very informative technique that analyzes surfaces to a depth of approximately 1  $\mu\text{m}$ . Since EDX analyzes only a small area at one time and old paint surfaces are not homogeneous, it is important to try to analyze as representative a portion of the surface as possible. Also, it is important to note that only elements with an atomic number greater than 10 (sodium and above) can be determined by EDX. Thus, elements such as C, H, O, and N are not detected by EDX. The results shown in table 6 for two portions of the outer surface of sample no. 414-2 indicate the general degree of variability in going from one spot on the surface to another.

The data presented in table 6 were calculated by the Kevex EDX unit using standardized weighing factors. Trace amounts of other elements were found, but are not listed in table 6. In addition, sample no. 414-3 had potassium (7.2 percent) on its outer surface. Although the EDX analyses reported in table 6 were single-spot results taken on surface areas of approximately 1  $\text{mm}^2$ , they were representative of several such analyses made at different spots on the paint chip surface.

(a) Paint chip sample no. 414-1.



(b) Paint chip sample no. 414-2.



(c) Paint chip sample no. 414-3.

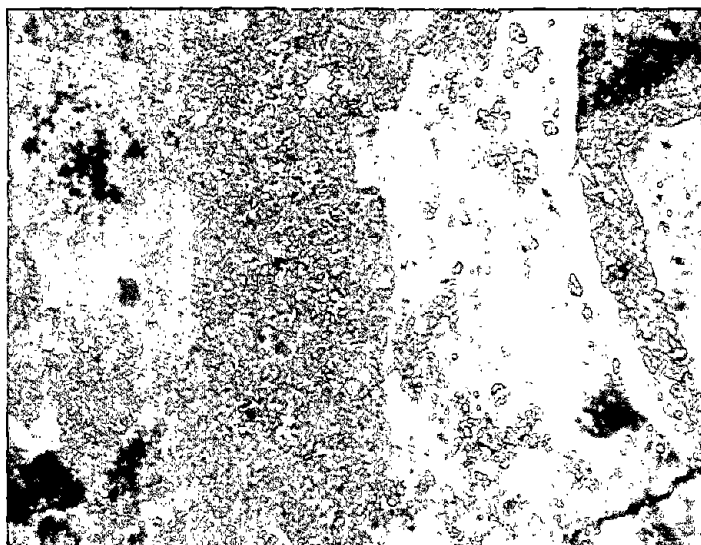


Figure 50. Inner surface of paint chip samples (x 20 magnification).



Table 6. EDX analysis of paint chips from I-55 in Chicago, Illinois.

Sample	%Pb*	%Al	%Fe	%Si	%Ca	%Na	%Cl	%Ti
#414-1 Outer Surface	11.4	37.3	6.4	22.8	4.7	7.0	9.9	0
#414-1 Inner Surface	75.7	3.9	14.8	0	0.4	4.1	0	0
#414-2 Outer Surface-1	30.8	10.9	9.6	14.5	2.2	0	13.7	17.3
#414-2 Outer Surface-2	26.2	10.0	8.5	12.3	1.8	0	12.4	15.5
#414-2 Inner Surface	26.3	0	63.1	1.5	3.8	0	2.6	0
#414-3 Outer Surface	56.5	33.7	6.6	17.9	1.2	0	2.5	0
#414-3 Inner Surface	95.4	1.1	0.3	4.9	0.5	0	0	0

\* The percentages listed are weight percentages based on the total amount of the elements analyzable by EDX.

From the photographs in figure 50 and the EDX results in table 6, the following observations and conclusions can be drawn.

- \* The use of a lead-containing primer is confirmed for all samples. This is consistent with the orange color and also was consistent with IDOT records that identified that a red-lead/alkyd primer was used.
- \* The top coats of all of the paint samples contained aluminum, but the relative concentration in sample nos. 414-1 and 414-3 was more than three times that of sample no. 414-2. Again, this is consistent with IDOT records that show that the gray paint (sample nos. 414-1 and 414-2) consisted of a leafing aluminum/phenolic intermediate layer with a non-leafing aluminum/phenolic topcoat.
- \* The composition of the green paint, sample no. 414-2, clearly was different from the other two samples. It appeared to contain titanium dioxide in addition to aluminum. Furthermore, its lead content was nearly the same on the outer and inner surfaces, indicating that both the primer and the topcoat contained lead. These conclusions also are in agreement with the IDOT records.
- \* Between 5 and 10 percent of the elements found on the outer (topcoat) surfaces of the chips was iron. The source of this iron is not known. It could have come from the pigments, but probably was surface contamination by rust and dirt.

- \* The amount of iron found on the inner (primer) surface varied greatly. A high concentration of iron (63 percent) was found on the inner surface of sample no.414-2. Iron apparently was pulled from the steel along with the chip, suggesting that rusting beneath the primer may have occurred. This was confirmed visually as seen in figure 50.
- \* Chloride was found in significant quantities on the outer surfaces of the paint chips, but generally its concentration on the inner surfaces was quite low. These data indicate that salt, probably from deicing, is mainly on the outer surface and that very little diffusion of chloride through the topcoats to the primer occurred.
- \* The most likely source of silicon, which was found in rather large amounts on the outer paint chip surfaces, is dirt.
- \* Lead chloride crystals were found on the topcoat surface of sample no. 414-2. Of the paint chip samples taken, this sample would have had the greatest exposure to vehicle exhaust fumes. It is possible that the source of lead in these crystals was tetraethyl lead from prior use of leaded gasoline. Alternatively, this may be the result of interaction of lead in the topcoat with deicing salt.

#### TCLP Analysis of the Paint Debris

An analysis of the paint debris to determine if it should be classified as hazardous waste was done by the toxicity characteristic leaching procedure (TCLP) test (EPA Method 1311). It is the required regulatory test to determine if the debris contains sufficient leachable toxic materials to classify the waste as hazardous. Briefly, the test consists of extracting 100 g of the solid debris with 2000 g of aqueous solution, pH adjusted to 5 with acetic acid. The solid sample and the extractant liquid are placed in a bottle and rotated end over end at 30 rev/min for 18 h at 23 °C. The mixture is filtered and the filtrate is analyzed. If the filtrate contains 5 or more ppm lead, the waste is classified as hazardous.

Although the TCLP test was designed to try to simulate dump-site conditions, it suffers from several drawbacks. The test is sensitive to debris particle size, shape, and surface area. Particle size and shape will depend on the method of removal, the type, and the age of the paint. Although grit blasting will tend to produce fine debris particles, the actual size distribution will depend on the type of media used. Vacuum power-tool removal will produce an intermediate size debris, and handtool removal will produce the largest particle sizes. Although the TCLP test specifies a maximum particle size, it probably would be improved by ball milling the debris to a definite screen size range prior to extraction. This would make the test samples more uniform in surface area as well as increase the surface area. The more uniform surface area from one sample to another should make the results more reproducible and, therefore, allow a more precise comparison of sample leach rates. The greater surface area should have two significant effects. The first would be to increase the leach rates because of the increase in surface area exposed to the leachant. The second would be to break up lead-containing

particles that have been encapsulated or complexed by additives such as iron or Blastox™, thus simulating long-term leaching where natural events such as ground shift and chemical interactions occur.

The TCLP test was designed to be mildly aggressive by specifying that the leachant should have a pH of 5, which is slightly acidic. Actual ground conditions in the landfill site, however, may be quite different, not only in terms of pH, but in terms of the soil composition. For example, the TCLP test specifies an acetic acid leachant, whereas the soil may contain other acids and salts and possible chelating agents.

The TCLP test results depend not so much on the amount of lead present as on the form of the lead. Certain lead salts are much more water soluble than others and lead metal is very insoluble. Conversion of more soluble lead salts to less soluble forms will reduce the amount and rate of leaching. It is for these reasons that treatments with iron and proprietary compositions are effective. On the other hand, it is possible that certain contaminant ground components may convert the lead to more soluble forms after disposal.

The TCLP test is widely used, being the best test currently available, and it is the EPA-specified standard. It will continue to be used until a better test is specified. In general, the TCLP test is more aggressive than natural conditions and, therefore, has been thought to represent a worst-case scenario. Recently unreported work by Lloyd Smith and Gary Tinklenberg, however, indicates that a more severe and perhaps more realistic test procedure might be to periodically percolate the leachant solution through a bed of the debris and analyze the effluent for lead concentration. This simulates the effects of natural changes in ground-water flow. Under these conditions, stabilization by iron ultimately fails.

Changes in the TCLP test are being considered by the EPA, both at the State and Federal levels, that would make the test more aggressive. Changes under consideration are: (1) to lower the pH from 5.0 to 1.5, (2) to use mineral acids rather than acetic acid, and (3) to lower the permissible limit for non-hazardous classification from the current 5 ppm to 1.5 ppm or lower. Lowering the pH makes the test more aggressive for two reasons. First, most lead salts become more soluble as the pH is lowered (acidity is increased). Second, the protective nature of lead-stabilizing additives may be reduced because they may dissolve in the acid and may no longer be available to react with the lead salts. Mineral acids being considered are sulfuric and combinations of sulfuric and nitric acids. These acids are strong oxidizers and are very aggressive in terms of their reactions with metals, salts, and the paints themselves. Commercial landfill environments where the pH is below 5 and where large amounts of mineral acids are present are extremely rare and would only occur in the case of an acid spill or if the site was built on an acid runoff area. Lowering of the permissible lead level standard for hazardous waste has been implemented by some States. Illinois and North Carolina classify debris having TCLP leachable lead levels between 0.5 and 5 as special wastes that have to be handled much like hazardous waste.

### Waste Treatment

Paint debris that is determined to be a hazardous waste by the TCLP test must be stabilized against leaching prior to disposal. It is illegal to simply

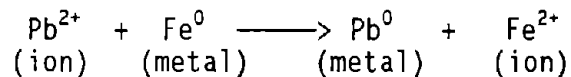
dilute the waste to pass the TCLP test. Stabilization can be accomplished by several means. Onsite post-treatment is legal, but a waste-site analysis plan must be provided and a license must be obtained that may be very difficult to get. Onsite post-treatment methods, therefore, can be avoided by including iron or other materials such as Blastox™ in the blast media, which renders the lead much less leachable. The mechanism of iron stabilization of lead-based paint debris is discussed in the next section. The mechanism of stabilization appears to be conversion of the lead compounds in the paint debris to less soluble forms. As the mechanism of stabilization by other materials becomes better understood, it is expected that new stabilizers will become commercially available.

Post-treatment methods include encapsulation in portland cement, and treatment with lime, lime/fly ash, cement/kiln dust, and proprietary silicates. The most common method is the one based on portland cement. Care must be taken to be sure that these treatments are done properly. For example, if the cement is underhydrated, its effectiveness will be greatly reduced. Also, lime stabilization may not be permanent. An excellent discussion of fixation of metals by cement-based processes is given in *Chemical Fixation and Solidification of Hazardous Wastes* by Jesse R. Conner, Van Nostrand Reinhold, New York, 1990.

#### Iron Stabilization of Lead-Based Paint Debris

The mechanism by which lead is stabilized against leaching when steel-grit blasting media is used has been reviewed by personnel from various DOT and independent laboratories as well as by suppliers and users of blast media. The users and suppliers of blasting media tend not to have any explanation for the reduced leachability in the TCLP test. They view it as good and do not care why it is so. DOT laboratory personnel, such as Rich Kramer of IDOT (private communication), suggest that the effect steel (iron-based) blast media has on leachable lead in paint debris appears to be due to a reduction of lead ions to lead metal by reaction with metallic iron. Others call this a plating-out effect. Since the lead metal is not soluble in the acetic acid leachant, the portion analyzed in the TCLP test, the measured soluble lead is reduced. It should be noted that all of the lead need not be made insoluble to pass the TCLP test. If the exposed surface of the lead in the paint pigment becomes converted to the insoluble metallic form, it will protect the remaining unexposed lead from the leachant. As this protective outer layer erodes away, however, the material may again become soluble and hazardous.

The oxidation potentials for lead and iron are -0.126V and -0.441V, respectively, so the following oxidation reduction reaction occurs:



Since this reaction does not remove lead from the debris, but only changes its solubility state, there exists the possibility that some later reaction will allow the lead to redissolve and therefore become hazardous. If this happens, the co-generators (State/contractor), treater, and anyone in the disposal process becomes responsible.

Other factors that may affect the leachability of lead in paint/abrasive wastes are as follows.

- \* The chemical form of the lead in the paint being removed may have an effect. For example, red lead ( $Pb_3O_4$ ), which is the most common form of lead in the primer, may dissolve in the leachant more or less slowly than lead silicochromate or white lead ( $2PbCO_3 \cdot Pb(OH)_2$ ), which may be found in the topcoat of older paints. Only the soluble surface lead is available to readily react with the iron.
- \* The composition, shape, size, hardness, and oxidative state of the iron-based blast media may play a role in how readily the iron and lead interact.
- \* The effects of other oxidizing and reducing chemicals that may be in the waste being disposed of may determine the degree of conversion of ionic lead to metal as well as how long the lead will remain unleachable.

In 1992, North Carolina removed lead-containing paint from two bridges. For one bridge, 10-percent steel grit was used in their blast media and for the other bridge, no steel was added. The debris generated from the mineral-steel abrasive contained 0.3 to 3.7 percent total lead, but the TCLP leachate contained only 0.3 to 6.3 ppm. The debris where no steel was added in the blast media contained between 0.5 and 1.5 percent total lead and the TCLP leached lead was between 124 and 202 ppm. While the lead may or may not be permanently fixed (made insoluble) by the addition of steel, the initial reduction of lead was impressive. This effect of iron on the reduction of leachable lead has been documented by many investigators, but the long-term insolubility in commercial containment site environments is unknown.

#### TCLP and Optical Analysis of Paint Debris Samples

TCLP test analysis of paint debris obtained via different removal methods are summarized in table 7. The amount of lead found by the TCLP test and the amount of lead remaining in the paint debris after the TCLP testing (residual lead) are reported. The total lead in each sample is the sum of the TCLP lead analysis and the residual lead after TCLP testing. The first four samples in table 7 contain both paint debris and steel grit that was not removed by the vacuum systems. Photos at x 20 magnification of the paint-removal debris for the first, fourth, fifth, and sixth samples in table 7 are shown in figure 51.

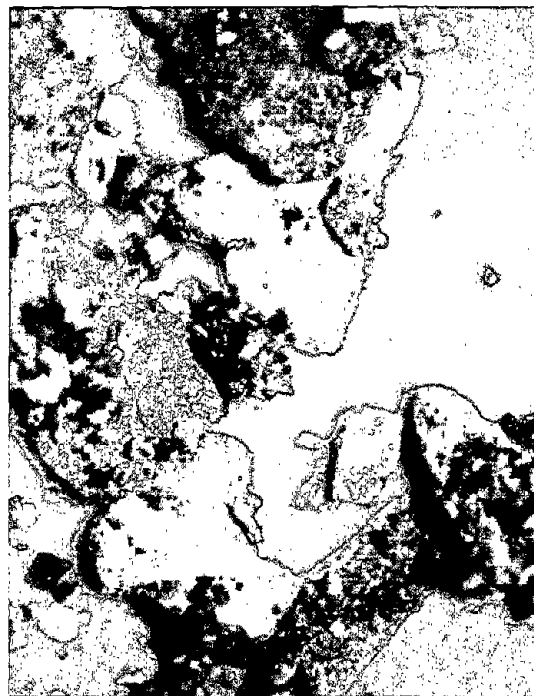
The data clearly show that use of steel-grit blast media within full containment areas (the first three samples in table 7) produces debris that is classified as a non-hazardous waste according to the TCLP test. Even though these samples contain a few thousand parts per million lead, the amount leached was less than the detectable limit of 0.1 ppm. Thus, for the first three samples in table 7, the residual lead determined after TCLP testing is essentially the same as the total lead in the sample. It should be noted that much of the remaining (unleached) lead was encapsulated by paint resin and was not subject to dissolution. Furthermore, use of a non-iron-containing abrasive was not tested in this removal demonstration. Thus, the magnitude of the reduction in leachable lead resulting from the use of steel grit as

Table 7. Analysis of paint debris for lead by the TCLP method.

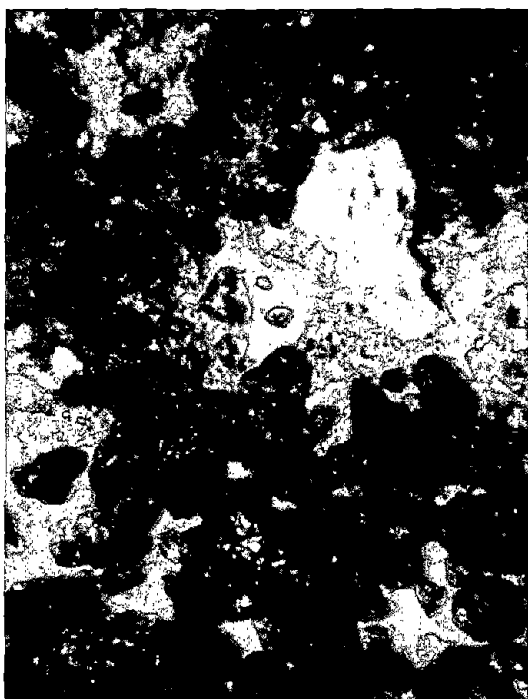
Sample	Lead Analysis (mg/L by TCLP)	Residual Lead (mg/kg After TCLP)
Steel Blast Debris on Containment Floor (I-55)	<0.1	1280
Steel Blast Debris on Containment Flange (I- 55)	<0.1	2060
Steel Blast Debris on Containment Floor (Madison)	<0.1	966
Vacuum Steel-Grit Blast Debris (I-55, Chicago)	133	5570
Vacuum Power Tool No. 1 Debris (I-55, Chicago)	227	22 200
Vacuum Power Tool No. 2 Debris (I-55, Chicago)	246	26 300
Handtool Debris (Illinois River Bridge)	62	31 800



(a) Vacuum power tool #1 debris.



(b) Vacuum power tool #2 debris.



(c) Vacuum blast debris.



(d) Blast debris within confinement.

Figure 51. Paint debris from different removal methods (x 20 magnification).

compared to non-iron-containing grit is not available. Debris picked up on the tarp around the vacuum blast area was found to be a hazardous waste even though the blast media was steel. Debris from the vacuum power-tool operations contained over 200 ppm leachable lead. These paint debris samples are very high in total lead since they are not diluted by blast media (abrasive). Paint debris from handtool removal was high in total lead and leachable lead, but the leachable lead was not as great a percentage of the total lead as it was in debris produced by the power tools. This difference is due to the power tools breaking up the paint to a greater extent than did the handtools, thus exposing more of the paint surface to the TCLP leachant.

### Conclusions and Suggestions

The results of this task study lead to the following conclusions and suggestions. Good paint analysis techniques are available to determine both qualitatively and quantitatively the presence of lead and other hazardous metals in existing paints and in the debris produced by various paint removal methods. They include: (1) x-ray fluorescence (XRF) as an onsite, nondestructive means of determining whether or not the paint should be classified as lead-containing and (2) paint chip analysis done by classical laboratory methods such as atomic absorption (AA and ICP-AA) or energy dispersive x-ray (EDX) analysis to determine total and leachable Pb, Cr, Fe, etc.

- \* The best paint debris analysis method for determining total metal content, including lead, is acid digestion and atomic absorption. This is the accepted regulatory method.
- \* Although the TCLP test has its deficiencies, it is currently the best method and the regulatory specified method of determining if paint debris is to be classified as a hazardous waste.
- \* One of the main deficiencies of the TCLP test is that repeated leach testing often gives different results than originally obtained, such that a waste originally passing the test may later show high soluble lead levels depending upon the waste exposure environment history.
- \* It is suggested that the reproducibility of the TCLP test results could be improved by: (1) specifying reduction of the paint debris to a narrower range and finer particle size distribution, and (2) introducing a periodic percolation of leachant through the debris, either instead of or after the presently specified 18-h leaching procedure.
- \* Despite the fact that steel (iron-based) blast media has the advantages of recyclability and stabilization of lead in paint-removal debris, and that Blastox™ works well as an additive to reduce leachable lead, the search should continue for materials that will stabilize lead efficiently with long-term resistance to aggressive waste containment site environments.



- \* The production of hazardous paint-removal waste should be minimized by the use of recyclable abrasive and the waste generated should be treated by effective methods to ensure its stability in waste containment sites.



## CHAPTER 5: TASK D - ADVANCED COATINGS

### Introduction

The rehabilitation of steel structures, in general, and bridges, in particular, is a significant drain on resources, including manpower and budget. As restrictions on both the permissible methods of paint removal and the VOC content of paint systems increase, the options available to bridge owners diminish.

For years, standard maintenance painting practice for steel bridges has entailed the use of open-abrasive blasting for the complete removal of existing paint prior to repainting. Open-abrasive blasting not only removes the existing paint, but also cleans the steel surface of corrosion products and millscale while providing a roughened surface profile desirable for the adhesion of new paint. In the past, lead-containing paint provided a reliable economical solution to the long-term corrosion protection of these structures without requiring extensive surface preparation, such as the removal of millscale. Recent concerns over the effects of lead as a toxic substance in the environment and the release of VOC's during the application of paints has caused a radical change of direction to be pursued in the painting of steel highway bridges. The primary objective of task D was to investigate advanced coatings that have the potential to meet the changing needs associated with the rehabilitation of steel bridges.

### Background

Organic coatings are applied onto steel surfaces to provide a barrier to minimize the interaction of the steel and corrosive elements of the environment. In order to be successful, these coatings must delay and limit ingress of the aggressive corrosive elements: water, oxygen, and ionic species such as  $\text{Cl}^-$  and  $\text{SO}_4^{2-}$ . These aggressive corrosive elements can reach the substrate/coating interface either by intrusion through defects or by diffusion through the protective coating. While the incidence of defects can be reduced by proper coating application based on good quality control practices, the diffusion of oxygen and salts in solution will always take place. However, the rate of diffusion varies widely, based on the coating system chosen. Considerable research has been performed on the mechanism of coating degradation. However, due to the complexity of metal/coating and coating/environment systems, theories do not exist that quantitatively or even qualitatively describe the coating degradation processes and relate them in a manner that allows the prediction of the performance of coating systems during service. Figure 52 describes one model, developed by NIST, indicating the major factors that they perceive as influencing the durability of a coating system.

Aging is one of the factors that affect coating durability and is a direct measure of the success or failure of the system to provide its stated goal of protecting the substrate. It is primarily aging that determines when, and to what degree, a coating system is removed and replaced.

As mentioned in task A, advanced coatings can benefit the maintenance of steel bridges within the following options: (1) total paint removal and recoating, and (2) partial paint removal and overcoating.

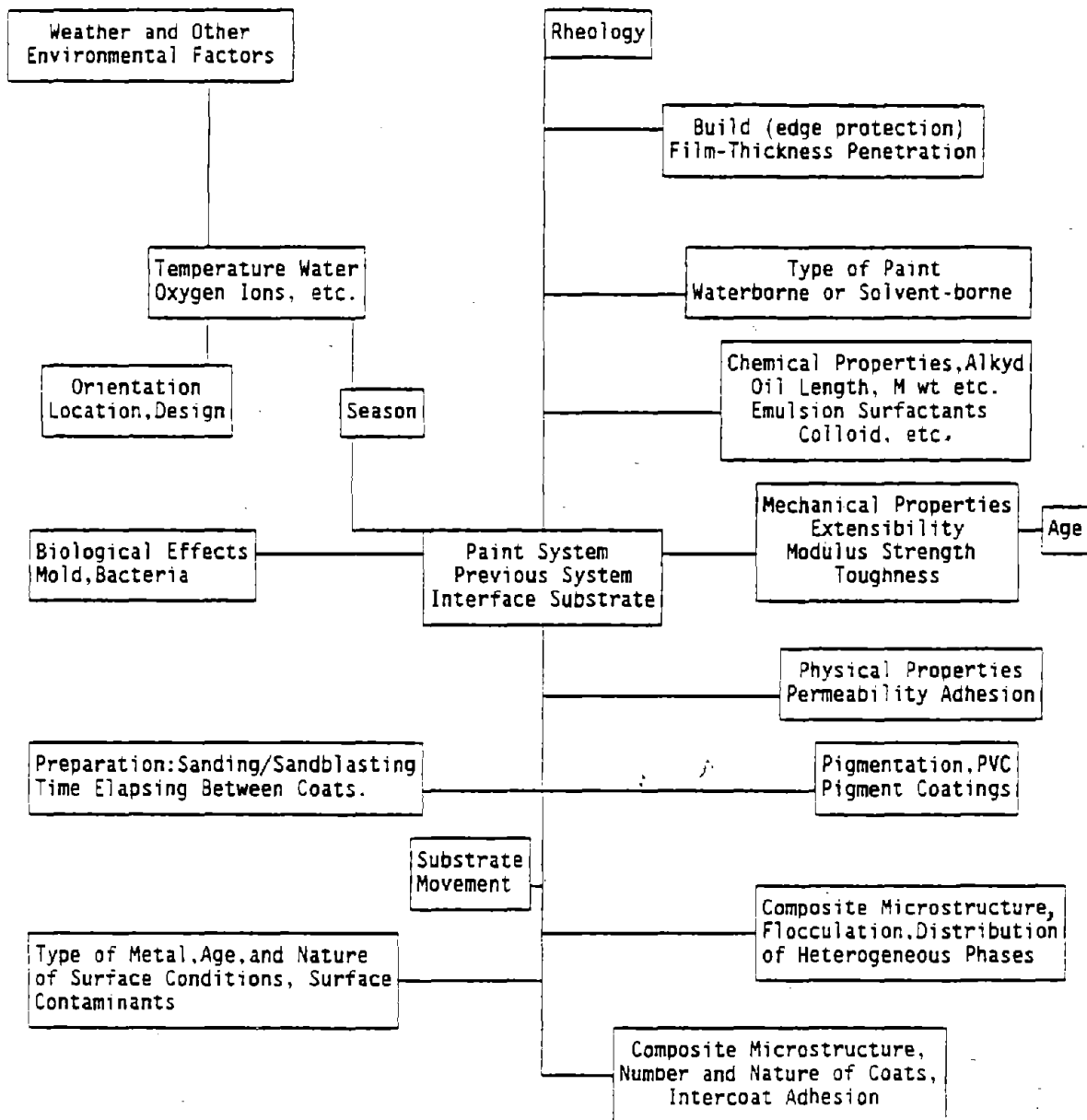


Figure 52. NIST model of elements affecting paint durability.

In addition, advanced coatings can be of benefit during the rehabilitation of steel bridges that require replacement of structural components.

Total paint removal and replacement may be the most economical option if more than 20 percent of its protective coating system has failed. Within the context of total paint removal, several options exist that are based on the integrity of the structural elements. If component replacement is not necessary and/or can be deferred, a VOC-compliant paint system with an expected lifetime comparable to the next planned rehabilitation of the structure can be chosen.

If component replacement is necessary, a coating system applied in the fabrication shop should be chosen such that it can both perform and be repaired in the field. However, fabrication shops have to face increasing challenges in this area, again due to the implementation of ever more stringent VOC requirements as discussed below.

### Dilemmas Facing Fabrication Shops

#### Increased Shop Painting

For many years, highway agencies specified paint systems for new bridges that were reasonably long-lasting and relatively simple for steel fabrication shops to apply. Initially, shop painting involved the application of a primer coat that was supplemented by additional coat(s) of paint applied after the steel was shipped to a job site and erected. Multi-coat paint systems offering enhanced performance have gradually been adopted by many highway agencies, resulting in a desire to limit or eliminate field painting. This is partially due to the increased control of the painting and quality control practices in a shop environment. At least eight highway agencies have adopted the practice of complete shop painting, limiting field painting to touchup work.

#### Containment for Maintenance Painting

Environmental regulations currently prohibit environmental releases of particulates generated by abrasive blasting during maintenance painting of bridges in urban areas. Worker exposure to these particulates necessitates the use of protective respirators, even when abrasive blasting operations do not involve lead-based paints. In the future, it is likely that all bridge maintenance painting incorporating abrasive blasting will require total containment. Highway agencies anticipating that eventuality are currently seeking extremely durable shop coatings to forestall the need for maintenance painting.

#### Fabrication Shop Problems

In the past, fabrication shop personnel considered shop painting as a nuisance, however, it was necessary to sell fabricated steel. In many cases, the quality of painting operations in those shops took a back seat to other activities, such as welding. The forgiving nature of the early oil-alkyd paints promoted that antipathy. The advent of advanced structural steel paints, such as the inorganic zinc/vinyl systems, demonstrated the need for improved quality control. For example, poor control of wet thickness for inorganic zinc paints resulted in "mud cracking." As more highway agencies

have required the shops to perform more painting work using high-performance paint systems, painting has had greater impact on shop profitability and the quality of shop painting has become more critical.

### Regulation of Fabrication Shops

Fabrication shops are point sources of waste generation. As a result, they are easy targets for regulation by State departments of environmental protection (DEPs). Those agencies promulgated regulations restricting the VOC content in paints. In addition, if materials are used that exceed these limits, the fabrication shops are faced with a limit on their total yearly VOC emissions. Highway agencies specifying paints with high-VOC content have been forced to employ lower VOC coatings or the fabrication shops nearing their VOC point-source limits are unable to supply the components.

Current limitations on VOC content of paints and the total allowed yearly VOC emissions by fabrication shops will most likely be tightened in the future. The VOC regulations for paints, as the result of the ongoing regulation-negotiation activities related to architectural industrial maintenance, will most likely reduce the VOC limits on bridge maintenance paints to 336 g/L (2.8 lbs /gal). Most States require for new construction that point sources use paints with a VOC limit of 420 g/L (3.5 lb/gal). In States restricting the total yearly VOC emissions from fabrication shops, those restrictions probably will be more limiting than that for the VOC content.

A solution to the problems of both highway agencies and fabrication shops would be for State highway agencies to specify water-based paint systems such as the acrylic systems now offered by a number of paint companies. However, while these systems may meet present and projected VOC restrictions, they are not as durable, particularly in high-salt environments, as conventional solvent-based systems. In addition, waterborne paints are less application-tolerant than their solvent-based counterparts. They require close control of application conditions (e.g., temperature and humidity) and surface cleanliness (e.g., sensitivity to surface oils and other contamination). Fabrication shops able to apply high-performance solvent-based paints have experienced problems with waterborne systems. Due to shop layouts and the proximity to other operations, some of those problems are difficult to resolve and severely limit painting operations when waterborne systems are employed. Several highway agencies have experienced reduced performance using those systems on new bridges.

Many polymer manufacturers and paint companies have invested heavily in water-based paint technology. With continued research, some of the problems currently experienced with waterborne systems will be remedied over the next 5 to 10 years. However, it is problematical that coating durability of waterborne paints will improve sufficiently to match that of some of the solvent-based systems presently in use, such as inorganic zinc.

The 100-percent solids paint technology employs two-component systems that react chemically and polymerize to form a solid film. The coatings are automatically mixed during the feeding process or internally mixed in the spray-gun head during application. Common two-component systems include epoxies, polyureas, and polyurethanes. The 100-percent solids painting generates no VOC's. Typically, the 100-percent solids paints are applied in

high builds 0.5 to 0.75 mm (20 to 30 mils). The coating components react and dry quickly (typically within 15 to 30 min), facilitating shop handling. Special application and handling equipment, coating materials, and operator training are required. Coating costs will initially be somewhat higher than for conventional solvent-based paint systems. These costs are anticipated to be offset by somewhat longer service lives. The 100-percent solids paints are presently being employed on chemical plants, boat hulls, and railway cars.

The Union Carbide Corporation has developed a proprietary paint application method, the **Unicarb System**, that uses carbon dioxide to replace up to 80 percent of the solvents in conventional solvent-based paint systems. Carbon dioxide gas is introduced in a spray gun during application. It improves paint atomization during spraying and acts as a carrier for the paint. The method has the advantage of being able to employ current solvent-based paint technology, while achieving a significantly reduced VOC release level. The reduced level of VOCs causes the paint to dry fairly rapidly (depending on the paint system), facilitating handling. Special application equipment, coating materials (i.e., compressed gas-carbon dioxide), and operator training are required. Coating costs will initially be slightly higher than for conventional solvent-based systems. The same coatings applied using the **Unicarb System** in place of conventional solvents have had relatively lower permeability. Therefore, longer service lives may be obtained. The **Unicarb System** has been employed for commercial products; it has been demonstrated successfully in several areas, including automotive and aircraft applications. The system as presently employed appears to be more economically attractive for higher production rate, repetitive operations.

### Overcoating

Spot repair and overcoating of compromised coatings involves: (1) cleaning the surface of the bridge with pressurized water to remove salts, soils, and other contaminants, (2) mechanically removing loose corrosion products and paint, (3) spot priming areas where paint and corrosion products have been removed, and (4) applying coats of paint over the entire surface. The conditions required for successful overcoat application are: (1) adequate adhesion and mechanical properties of the old paint, (2) compatibility of the overcoat system to existing coating system, and (3) proper surface preparation. In the past, many highway agencies maintained bridge paint systems by overcoating. Typically, existing lead-based alkyd systems were overcoated with similar or identical paints that provided years of acceptable service. Maintained alkyd paint systems have lasted well over 15 years. Often, oil-alkyd painted bridges were overcoated until they had paint builds as high as 0.75 to 1.0 mm (30-40 mils).

Overcoating has some potential advantages compared to full removal with containment. It minimizes the disturbance of the existing paint, which in turn, limits the generation of (possibly hazardous) wastes and minimizes precautions necessary for preventing waste discharge, worker exposure to lead, and efforts required to dispose of generated wastes. Repair and overcoating operations do not require expensive containment enclosures. Costs for repair and overcoating are low (typically one-fifth to one-third that for full removal with containment) and overcoating. Overcoating may extend the service life of the in-place coating system by 15 years or more. Low initial painting costs coupled with potentially significant extension of service life are very

attractive to State highway agencies strapped with limited painting budgets and large backlogs of bridges needing to be repainted. However, there exists significant danger of short-term failure of the complete system if the original coating system does not have sufficient adhesion/mechanical properties or if a non-compatible repair system is chosen.

The uncertainty with this maintenance option is that long-term experience with many of the newer paint systems as repair material is lacking.

### Factors Affecting Performance and Durability of Overcoating Systems

In the following section, we will discuss the factors that affect the success or failure of an overcoating job. The relative importance of the discussed factors is not clearly understood. Furthermore, in many cases, the current test methods available do not clearly characterize various factors.

#### Adhesion/Cohesion

The use of adhesion tests to rate the ability of an existing paint system to be overcoated and to estimate the durability/compatibility of the repair merit review. Current tests are time-consuming to perform, difficult to repeat, and the meaning of the results are subject to individual interpretation. For example, large differences have been observed between the test results when different methods are used. Existing paints may be brittle and lack cohesion and intercoat adhesive strength (i.e., typically occurring between an alkyd primer and existing intermediate or topcoats of alkyd paints containing aluminum pigments). Knifing adhesion tests such as ASTM D3359-90 (Measuring Adhesion by Tape Test) typically fracture old alkyd paints, causing intercoat (cohesive) failure. The pull-off test, ASTM D-4541 (Standard test Method for Pull-Off Strength of Coatings Using Portable Adhesion Testers), measures adhesion between existing coats or between the primer and the substrate, or the cohesive strength of a specific coat depending upon which component fails first. Brittle alkyds may provide only a 1B or 0B rating using the knifing adhesion test. If used on existing paint that contains several overcoated layers, the knifing adhesion test may provide similar values. However, a pull-off adhesion test on the same system may provide readings in excess of 2067 kPa (300 lb/in<sup>2</sup>).

#### Surface Contamination

The presence of soluble salts on existing paint surfaces and in corrosion products pose a distinct threat to the repair coating's durability. Soluble salts must be removed in order to provide extended paint durability even though their effects are difficult to assess. They are difficult to detect in the field and their concentration may vary depending on the level of deicing salt application, bridge design, and structural location. Currently, the primary tests for chloride surface contamination are wet chemical tests that are slow to perform and are questionable as to accuracy and precision.



## Thermal Spray Technology

### Introduction

As can be seen, the dilemmas facing facility owners and fabrication shops are complex. One potential answer may be thermal spray (TS) technology. TS is a coating process that has been proven in FHWA, National Association of Corrosion Engineers (NACE), U.S. Navy (USN), and other sponsored programs to provide superior long-term corrosion protection in a variety of environments. As part of task D, thermal spray was evaluated by both ongoing field tests and also as part of Task E, Accelerated Testing.

### Thermal Spray Coatings

The term "thermal spray" is commonly used to describe a family of coating technologies associated with the application of thick coatings onto components in order to reduce or eliminate the debilitating effects of wear and corrosion. In general, material in either powder, wire, or rod form is introduced into a region of high enthalpy (figure 53). Within this region, the material is brought to either a plastic or molten state. As part of this process, an expanding gas is used to accelerate the droplets onto the component surface, forming a coating. As the droplets impact onto the surface, they form lenticular splats (figure 54) and form a coating layer. The coating is built up to the desired thickness by multiple passes over the component surface. As with any coating, the surface must be properly prepared in order to ensure coating adherence. In the case of thermal spray coatings applied in open atmosphere, the proper surface preparation is the roughening of the surface either by grit blasting or chemical etching in order to generate the asperities necessary for the mechanical bonding of the coating to the component surface. In addition, thermal spraying is a line-of-sight process with optimum coatings being obtained when the angle of impingement of the molten droplets is perpendicular to the surface being coated. Depending on the process being used, excellent coatings can be obtained when the droplets impinge at angles between 90° and 45° relative to the surface being coated. Below 45°, evaluation of the coating microstructure determines the applicability of a given coating and process to the problem being addressed.

Flame spraying, the oldest form of thermal spraying, has been used since the late 1800's. In its simplest form, it consists of a nozzle assembly wherein a fuel (acetylene, hydrogen, propane, etc.) is mixed either with oxygen or air and undergoes combustion external to the nozzle. The flame front is stabilized by matching the flame propagation speed to the average unburned gas velocity. Heat transferred to the nozzle also aids in anchoring the flame front. For materials in powder form (figure 55(a)), the powder is injected into the flame in a manner designed to optimize the heating of the powder. For materials in wire or rod form (figure 55(b)), the flame is concentric to the wire or rod in order to maximize the uniform heating of the wire rod. A coaxial sheath of compressed gasses around the flame acts to atomize the molten particles and accelerate them toward the substrate. The main advantages of these processes are low capital investment costs and ease of operation. Because of the relatively small size of the equipment and the ease of operation, the process is field-portable, and there is little restriction

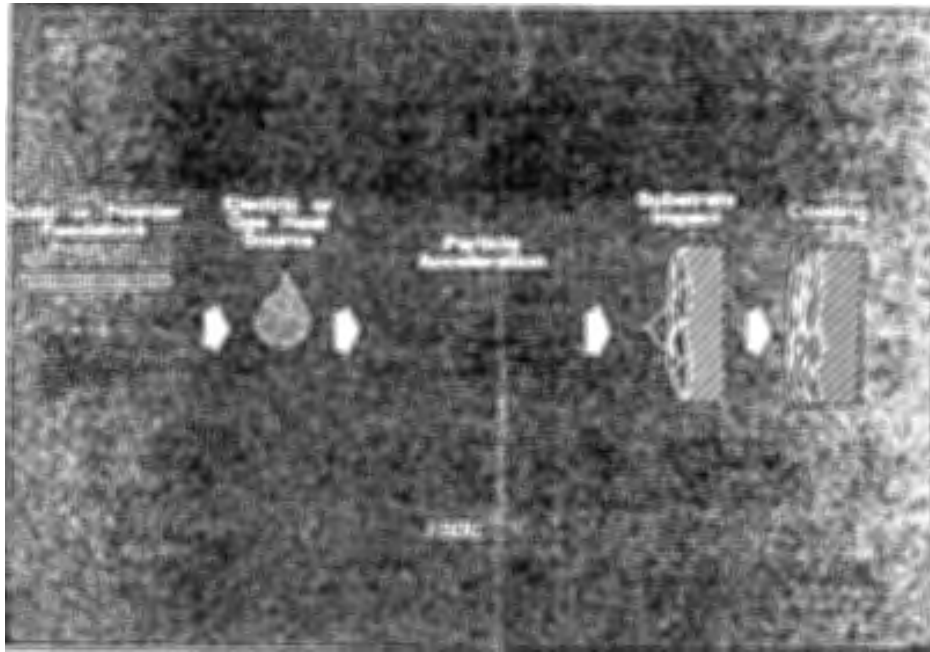


Figure 53. Thermal spray process.

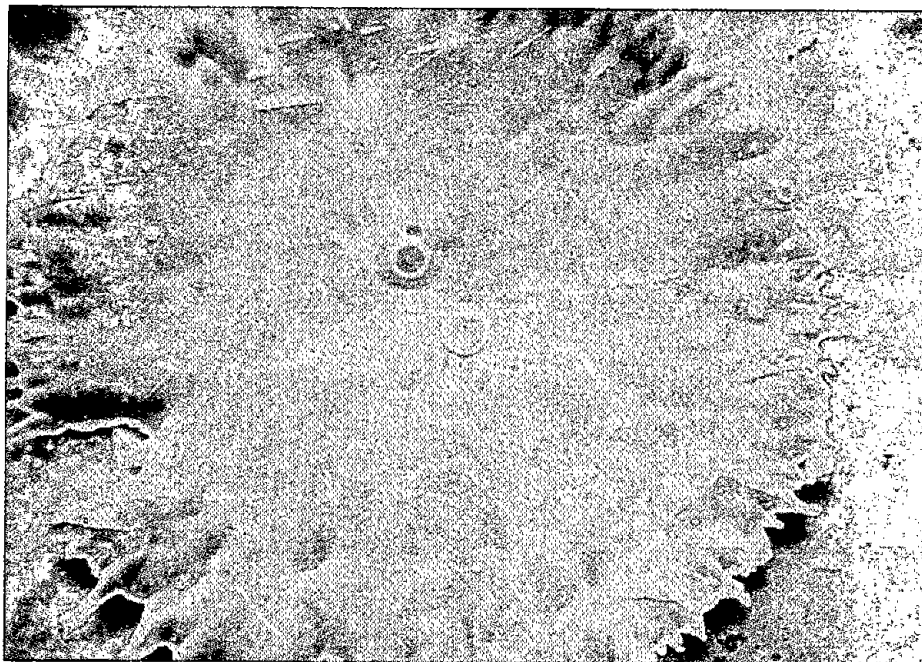
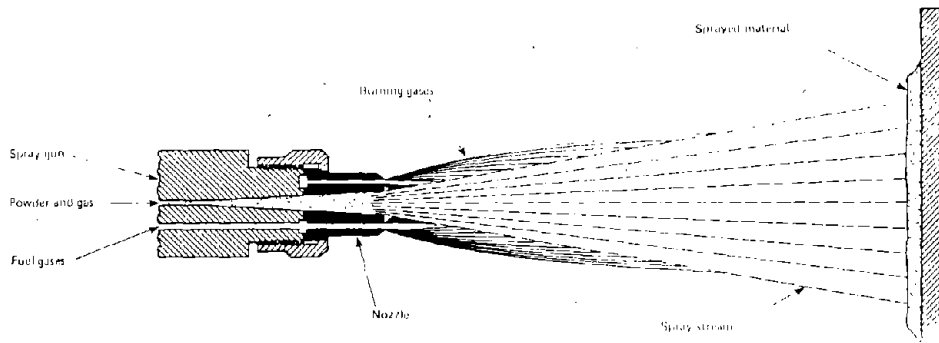
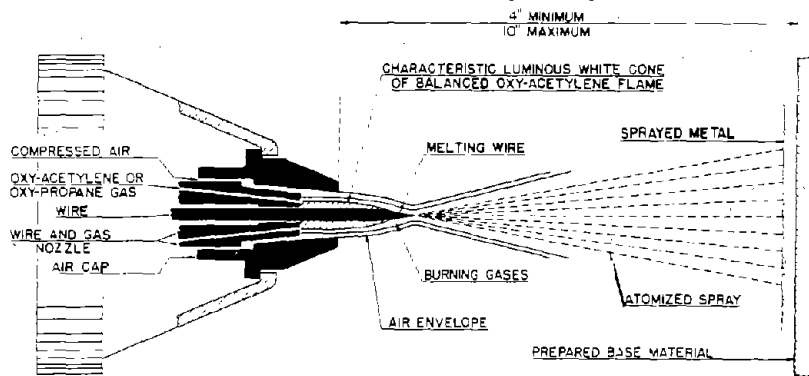


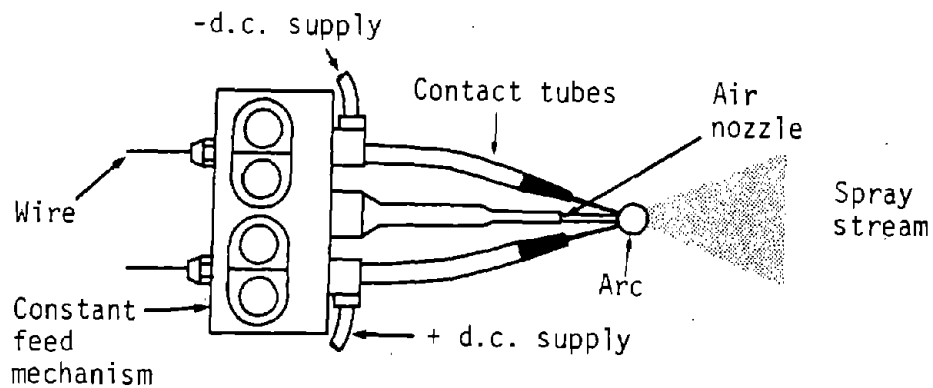
Figure 54. Splat structure.



(a) Powder flame spray process.



(b) Wire spray process.



(c) Wire arc spray process.

Figure 55. Relevant thermal spray processes.

to the size and complexity of components that can be coated. However, particle velocities are relatively low and, therefore, the coating porosity can be as high as 20 percent.

The electric arc process is illustrated in figure 55(c) and involves the continuous feeding of two wires into a device such that the wires converge at a point in space. The wires are held at different electrical potentials, such that an electric arc is generated between them. These wires are, in essence, consumable electrodes and are continuously melted. A jet of gas, usually compressed air, is used to atomize the molten material and accelerate the resultant droplets onto the component surface. It is not necessary for both wires to have the same chemical composition resulting in alloyed coating, however, adjustments to the feeding mechanism are necessary to compensate for these differences. Very high deposition rates are achievable by this process, but the atomization process generates more fumes than other thermal spray processes. In addition, this process frequently results in porosity levels of 25 percent by volume. Recent advances in the design of electric arc equipment have incorporated the use of Coanda accelerators. The Coanda accelerators use the geometry of the flow chamber to enhance the syphoning action of the atomizing gas, thereby increasing the volumetric flow through the same cross-sectional flow area. This results in higher particle velocities and coatings of higher density.

### Thermal Spray Materials

As with any coating process, the proper choice of coating materials may determine whether or not the desired goals are achieved. Historically, thermal spray coating systems have used pure zinc, pure aluminum, and zinc/aluminum alloys for applications involving corrosion protection of steel structures. Being metallic, the coatings offer additional protection in high-wear areas.

Zinc. Zinc provides long-term corrosion protection to steel through galvanic action at the zinc/steel surface as well as by its ability to protect itself with its own corrosion byproducts. Zinc has a lower oxidation potential than iron and will therefore preferentially corrode, preventing the steel from rusting. In addition, this properly provides cathodic protection to any small discontinuities or damage done to the zinc coating that may expose the steel components. Being a reactive metal, zinc readily forms a protective corrosion-product film. When exposed to air, a very thin layer of zinc oxide forms. When exposed to moisture in the atmosphere, the zinc oxide reacts with the moisture to form zinc hydroxide. During the drying process, the zinc hydroxide reacts with carbon dioxide to form an insoluble zinc carbonate layer on the surface, providing excellent protection to the underlying zinc.

Aluminum. Aluminum provides a barrier to the corrosion of steel by the formation of an inert aluminum oxide layer on the surface of the coating. When damaged, this coating is self-healing. Like zinc, aluminum has a lower oxidation potential than steel with respect to iron and therefore provides galvanic protection to the steel substrate. Unlike zinc, pure aluminum has not been extensively thermally sprayed onto steel bridges and structures, although extensive use by the U.S. Navy indicates that aluminum is more corrosion-resistant than zinc in marine environments. Figure 56 describes the estimated service life for aluminum thermal spray coatings.

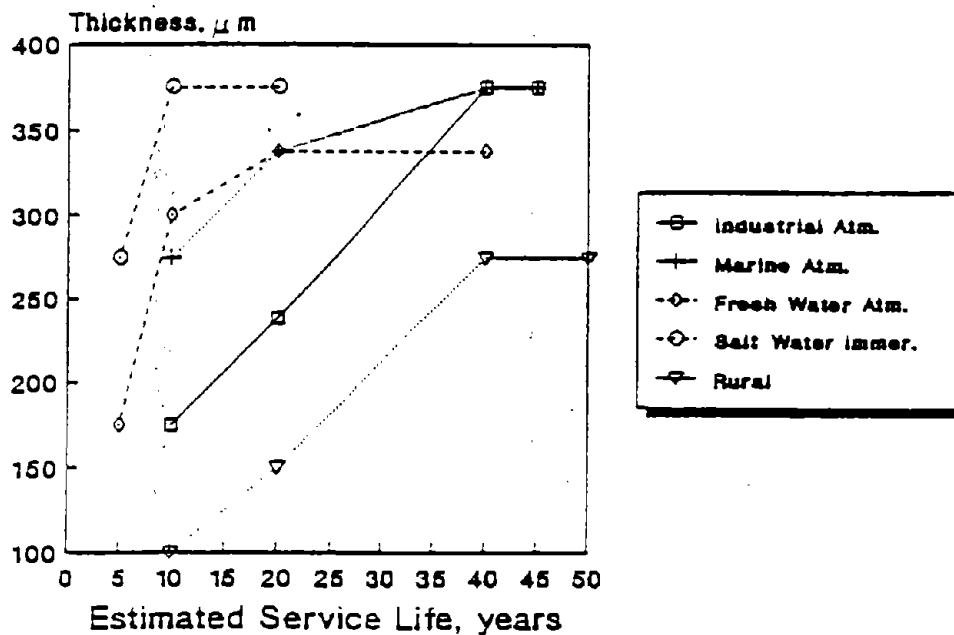


Figure 56. Estimated service life for Al and Al MCC thermal spray coatings.

Zinc/Aluminum. With the proven protection associated with zinc and the implied improved performance of aluminum in salt environments, alloys of zinc and aluminum have been developed. Initial work in Japan indicates that such alloys, particularly 85 percent zinc/15 percent aluminum alloy, have advantages over all-zinc coatings. This alloy has successfully been applied to steel bridges within the United States. Figure 57 describes the estimated service life for Zn and 85/15 Zn/Al thermal spray coatings.

Recently, the application of polymers such as ethylene acrylic acid (EAA) by thermal spray technology has been suggested for corrosion prevention on bridges. Unfortunately, unlike the metallic coatings described above, success has been limited for two reasons. First, control of the substrate temperature is critical for adhesion and to date, no definitive method for ensuring the proper temperature has been proposed. Second, like most paint systems, these coatings are solely barrier coatings without any additional protective mechanisms such as those exhibited by the metallic coatings.

Sealers. Although zinc, aluminum, and their alloys provide galvanic protection, additional protection can be obtained by sealing the porosity with acrylic urethanes, polyester urethanes, vinyls, phenolics, epoxy sealers, or thermally sprayed polymers.

#### Infrastructural Applications of Thermal Spray Technology

There is a history of corrosion protection by aluminum and zinc thermal spray coatings for structural steel work: buildings, bridges, towers, radio and TV antenna masts, steel gantry structures, high-power search radar aerials,

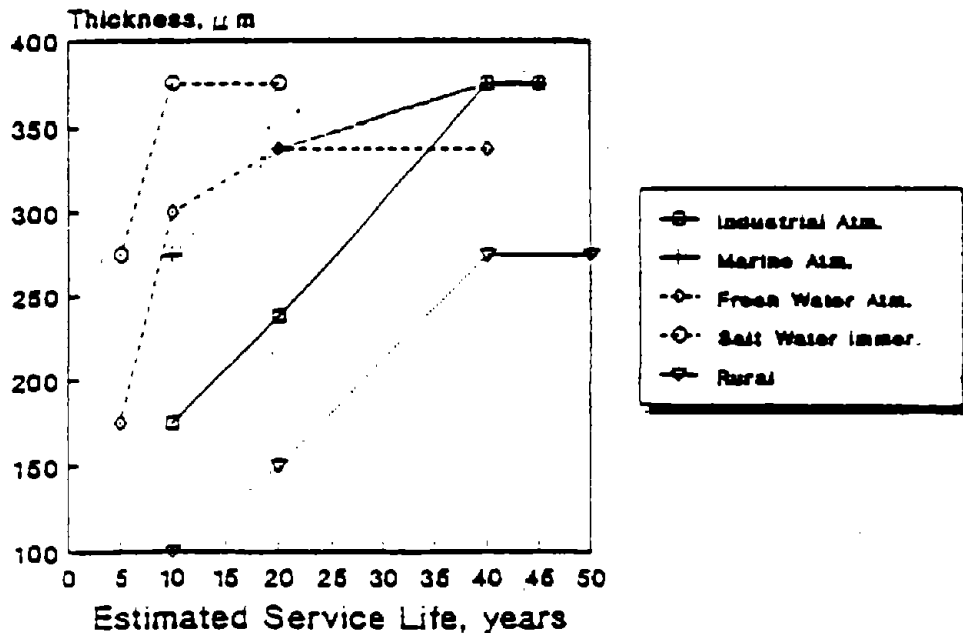


Figure 57. Estimated service life for Zn and 85/15 Zn/Al thermal spray coatings.

overhead walkways, railroad overhead line support columns, electrification masts, tower cranes, traffic-island posts, and street and bridge railings.

The interior of steel-hopper rail cars for hauling coal have been sprayed with aluminum for sulfuric acid corrosion protection and with aluminum composite for both corrosion and abrasion protection. Steel car exteriors have been sprayed with zinc for atmospheric corrosion protection.

Zinc thermal spray coatings used to protect potable water pipelines and storage tanks as specified in ANSI/AWWA D-102-78, American Water Works Association Standard for Painting Water-Storage Tanks.<sup>(5)</sup> Aluminum and zinc thermal spray coatings are used on sluice gates in irrigation systems and canal lock gates in shipping canals. These coated components have required virtually no maintenance for decades.

In marine applications, ship structural areas and components are preserved with aluminum and zinc thermal spray coatings. The U.S. Navy routinely uses aluminum thermal spray coatings in new ship construction and in the overhaul, repair, and maintenance of ship structures and for a wide range of shipboard components, especially those in topside and wet spaces. The British, Australian, and New Zealand Navies use a duplex zinc (base) and aluminum (top) thermal spray coating system.

Zinc thermal spray coatings complement hot-dip galvanizing when fabrications are excessively large or otherwise cannot be hot-dip galvanized. Zinc thermal spray coatings are used for repairing galvanized coating damaged during the fabrication process (e.g., welding, cutting, and joining areas) and for

maintenance recoating. Here, zinc spray is particularly advantageous because it ensures the uniformity and reproducibility of the galvanized coating thickness.

### Thermal Spraying of Steel Bridges: A Short History

Thermal spraying of bridges is not a new idea. Since the 1930's, zinc spraying has been extensively utilized in Europe, and in many countries zinc spraying is specified as the only corrosion protection system for new bridge construction. To date, several hundred bridges have been thermally sprayed to provide long-term corrosion protection. Table 8 lists several significant bridges, the year of metallization, and the last date when the coatings were inspected and found to be intact. In the United States, the oldest known bridge to be thermally sprayed is the Kaw River Bridge in Kansas City, Missouri. In 1936, the bridge was sprayed with between 0.25 to 0.30 mm (10 to 12 mils) of pure zinc. The bridge with the most notoriety is the Ridge Avenue Bridge in Philadelphia, the underside of which was sprayed with 0.25 mm (10 mils) of pure zinc in 1937. The Ridge Avenue Bridge is a railroad overpass and therefore has been subjected to severe corrosion environments due both to its exposure to the effluence of generations of steam and diesel locomotives as well as to road salts. Fifty-five years later, the zinc coating is still effectively protecting the bridge. The Forth Road Bridge in the United Kingdom is noteworthy in that it is the largest structure in the world to have its entire outer surface thermally sprayed. In 1961, over 18140 Mg (20,000 tons) of structural steel was metallized with a 0.125-mm (5-mil) coating of zinc, and upon assembly, supplemented with three coats of paint. The Pierre-LaPorte Bridge, spanning the St. Lawrence River near Quebec City, Canada, is the largest onsite metallized structure in the world. The original construction of the bridge was completed in 1970. The corrosion protection system consisted of painting with a lead silico-chromate, oil, and alkyd system. Maintenance and repainting of the bridge began in 1975. In 1977, the Province of Quebec decided to zinc spray the entire understructure of the bridge [160 000 m<sup>2</sup> (1.8 million ft<sup>2</sup>)]. An economic study concluded that while the paint system would have provided an 8-year lifespan requiring frequent touchups, the alternative zinc spray system would give a probable life of 20 to 25 years, requiring no major touchups. As recently as 1991, the coating was providing superior corrosion resistance on the bridge.

Table 8. Metallized zinc bridges.

STRUCTURE	COATING SYSTEM	YEAR METALLIZED	YEAR LAST INSPECTED
Kaw River (U.S.)	10 mils Zn	1936	1975
Ridge Avenue (U.S.)	10 mils Zn	1938	1984
Forth Road (U.K.)	3 mils Zn + 3 coats paint	1961	1975
Pierre-LaPorte (Canada)	5 mils Zn + 5 coats paint	1977	1985

1 mil = 0.0254 mm

Since 1985, Ohio has coated four bridges with the thermal spray process. The first bridge selected consisted of five lines of 21 WF 62s, 31 m (102 ft) long, over a stream. The surface area of steel to be coated was 309 m<sup>2</sup> (3323 ft<sup>2</sup>). The bridge was to have a new concrete bridge deck constructed on the existing beams. The metallizing of the beams was to be done after the deck was replaced. The beams were required to be sandblasted to a white metal surface (SP 5) and the 85 percent zinc/15 percent aluminum metallizing was to be applied (0.15-2.0 mm (6-8 mils) thick), followed by 0.0375 mm (1.5 mils) of epoxy, and 0.05 mm (2 mils) of a urethane topcoat. The metallizing had to be applied within 4 h of sandblasting to avoid flash rusting of the freshly blasted surfaces. The bid price on this first bridge for surface preparation, metallizing, epoxy intermediate coat, and urethane topcoat was \$30,000 or \$95.35/m<sup>2</sup> (\$9.03/ft<sup>2</sup>). This cost did not include containment of blasting debris since this work was done before containment was a requirement in Ohio. The actual time required for metallizing the beams was 8 working days. To date, this bridge remains in excellent condition and exhibits no rusting of the steel beams.

A second bridge was selected to be metallized in 1985. This structure was considerably more complicated to metallize because: (1) it is a bridge over an Interstate highway and (2) the beams are composed of riveted plates and angles. The bridge consisted of four lines of riveted beams, each being 111m (364 ft) long. Again, this was to have a concrete deck replacement with the metallizing to be done after the deck had been replaced. Containment of the blasting debris was not a requirement on this project. The bid price for cleaning and painting this bridge was \$217,000 or \$87.44/m<sup>2</sup> (\$8.28/ft<sup>2</sup>).

In an effort to better evaluate the effectiveness of the metallizing, it was decided not to topcoat the beams with the epoxy and urethane, but rather only seal the metallized surface with a clear sealer. This bridge, being situated over an Interstate highway, is subject to much salt spray and to date, the beams remain in excellent condition.

At the time of the metallizing of these two bridges, standard paint systems were costing \$36.96/m<sup>2</sup> (\$3.50/ft<sup>2</sup>) and it seemed unlikely at that time that metallizing would ever become cost-competitive on a first-cost basis. However, recent cost increases in standard systems are narrowing the margin between metallizing and conventional painting.

A third bridge, which carries a local road over a four-lane divided highway, was selected for metallizing in 1988. This bridge was also to receive a reinforced concrete deck replacement with the metallizing of the steel beams to be completed after the deck was replaced. The bid price for metallizing the four lines of 30 WF steel beams, 117.2 m (384.5 ft) long, was \$237,000 or \$91.66/m<sup>2</sup> (\$8.68/ft<sup>2</sup>). This price included surface preparation, but not full containment (which was still not required at that time).

#### Test-Panel Preparation

As part of this task, 210 test panels were prepared for field and accelerated testing. Initially, it was proposed that in addition to thermally sprayed test panels, paint systems under testing at the Mathis River Bridge in New Jersey would be included in the testing. This was proposed to provide a baseline comparison between the paint coating systems and the thermally



sprayed coating systems. Unfortunately, many of the paint systems tested at Mathis River are no longer VOC-compliant and, therefore, it was decided that paint systems meeting existing and proposed VOC limits would be used in this study. Table 9 details the thermally sprayed samples prepared and table 10 details the paint systems samples prepared.

All coatings were applied onto standard 102-mm by 152-mm by 4.76-mm (4-in by 6-in by 3/16-in) A-36 steel panels purchased from KTA Tator. All samples were degreased in a vapor degreaser/ultrasonic bath containing 1,1,1 trichloromethane. They were then grit-blasted using 36 grit aluminum oxide at 511 kPa (80 lb/in<sup>2</sup>) to a SP-5 white metal finish with at least a 0.051-mm (0.002-in) profile as shown in figure 58. Using ANSI/AWS C2.18-93, *Guide for the Protection of Steel with Thermally Sprayed Coatings of Aluminum, Zinc, and their Alloys and Composites*, the zinc (figure 59), aluminum (figure 60), and 85/15 zinc/aluminum (figure 61) samples were prepared. The EAA coating (figure 62) was applied using manufacturer supplied parameters. In addition, the paint systems were applied following manufacturers' guidelines.

A typical set of samples for field testing was composed of one each of paint systems 1 through 5 and one each of the thermally sprayed zinc, aluminum, and 85/15 zinc/aluminum. In addition, one each of the zinc, aluminum, and 85/15 zinc/aluminum test samples had one-half of each panel sealed with the cycloaliphatic/aliphatic amine epoxy. Finally, one each of the 85/15 zinc/aluminum test samples had one-half of each panel thermally sprayed with the EAA copolymer. One set of test panels has been deployed to the I-55 bridge with three remaining sets to be deployed in early 1994. Follow-on evaluation of these panels will occur as part of an ongoing 4-year program on overcoating. The remaining samples were supplied for evaluation under task E.

### Conclusions and Recommendations

The most critical factor in the implementation of advanced coatings is the relative lack of history as it pertains to the durability of these coatings, with the exception being thermally sprayed coatings. One difficulty with the implementation of thermally sprayed coatings is the relative age of the infrastructure and limited access to portions of the bridges where advanced corrosion has occurred.

Table 9. Thermally sprayed samples.

MATERIAL	NO. OF PANELS	SEALED	OTHER
Zinc	68	(1)	No
Aluminum	58	(1)	No
85/15 Zn/Al	45	(1)	(2)

- (1) On one-half of four panels, a modified cycloaliphatic/aliphatic amine epoxy [VOC's 9.6 g/L (0.08 lb/gal)] was applied as a sealer with 0.025 to 0.0375 mm (1 to 1.5 mils) dry film thickness.
- (2) On one-half of four panels, a thermally sprayed ethylene acrylic acid copolymer [VOC's 0.0 g/L (0.01lb/gal)] was applied with 0.254 mm (10 mils) thickness.

Table 10. Paint systems.

PAINT SYSTEM 1			
PRIMER	MIDCOAT	TOPCOAT	# OF PANELS
Epoxy Amidoamine	None	Acrylic Aliphatic Polyurethane	4
VOC (lb/gal)	0.7	NA	2.4
Dry Film Thickness (mils)	1-2	NA	2-3
PAINT SYSTEM 2			
Epoxy Amidoamine	Aluminum Epoxy Mastic	Acrylic Aliphatic Polyurethane	4
VOC (lb/gal)	0.7	0.74	2.4
Dry Film Thickness (mils)	1-2	4-5	2-3

NA=Not Applicable

Table 10. Paint systems (continued).

PAINT SYSTEM 3			
Epoxy	None	Epoxy	4
VOC (lb/gal)	0.0	NA	0.69
Dry Film Thickness (mils)	1-2	NA	4-8
PAINT SYSTEM 4			
Calcium Sulfonate Alkyd	None	Calcium Sulfonate Alkyd	4
VOC (lb/gal)	2.3	NA	2.4
Dry Film Thickness (mils)	4-5	NA	3-4
PAINT SYSTEM 5			
Alkyd	None	Alkyd	4
VOC (lb/gal)	2.69	NA	2.72
Dry Film Thickness (mils)	3-6	NA	2-4
PAINT SYSTEM 6			
Zinc-Filled Epoxy	Aluminum Epoxy Mastic	Acrylic Aliphatic Polyurethane	29
VOC (lb/gal)	2.52	0.74	2.4
Dry Film Thickness (mils)	3-4	3-6	2-4

NA-not applicable    1 mil=0.025 mm  
 1 lb/gal=120 g/L

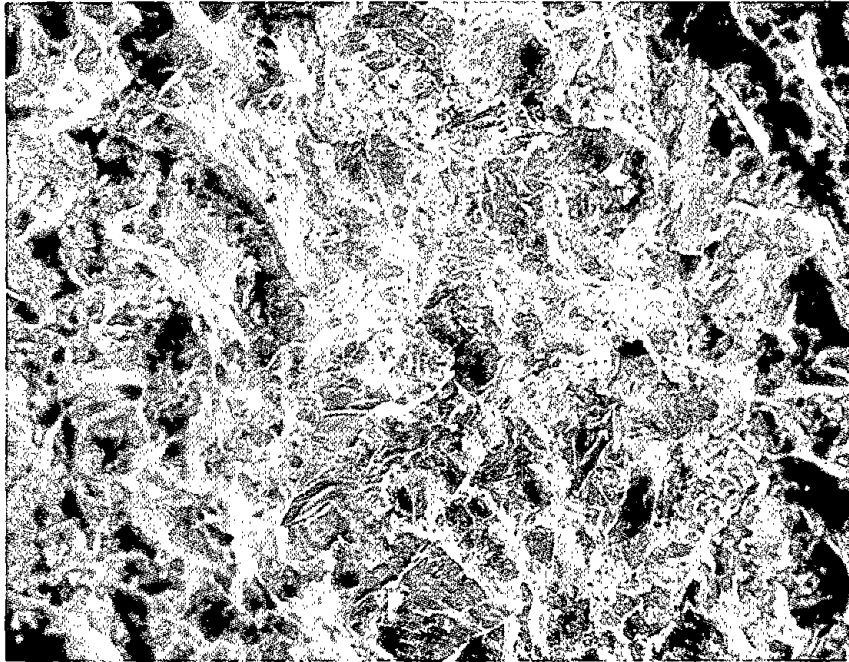


Figure 58. Grit-blasted surface of steel plate.

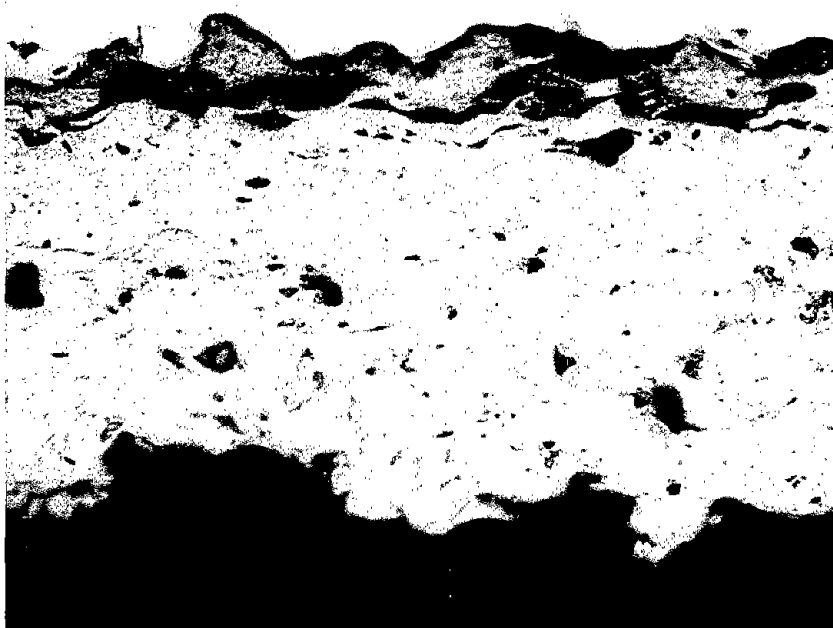


Figure 59. Thermally sprayed zinc coating.

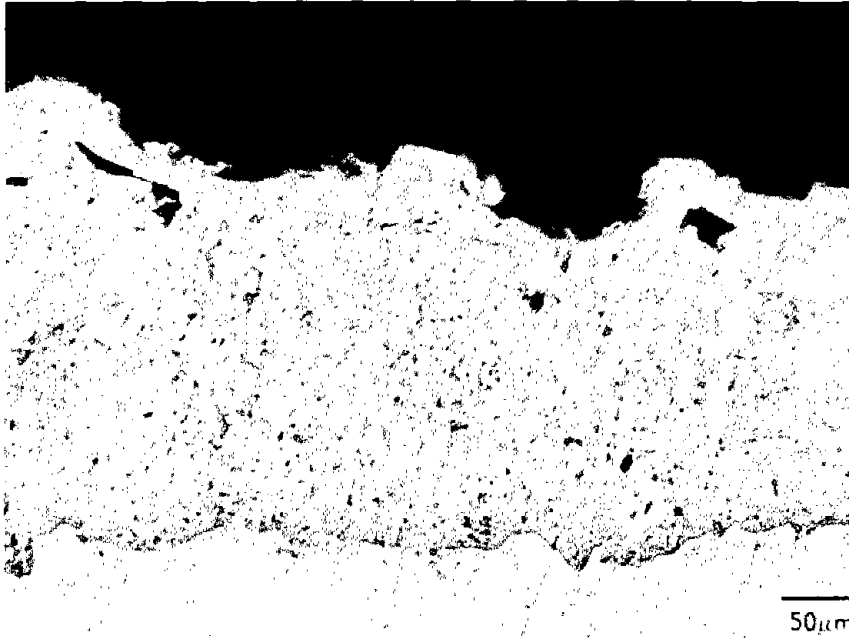


Figure 60. Thermally sprayed aluminum coating.



Figure 61. Thermally sprayed 85/15 zinc/aluminum alloy.



**Figure 62. Thermally sprayed EAA copolymer.**

Since many bridges have suffered loss of cross section, the application of thermally sprayed coatings retard corrosion, but cannot replace lost steel. In addition, since the regions of most serious corrosion are in the area of expansion joints and bearing areas, thermal spray technology's need for line of sight can limit the quality of coating applied. This should not preclude use of this technology when the above-mentioned limitations do not contraindicate its use.

Two immediate areas where thermal spray technology can be implemented are in structural replacement and fabrication. In these applications, if the steel at an expansion joint was sprayed with 85/15 Zn/Al, it would provide long-term corrosion protection and minimize loss of cross section.

The use of paint for overcoating requires an understanding of the durability of these paint systems and a fuller understanding of the equivalent uniform annual cost as demonstrated in task A. A partial list of companies and State DOTs addressing the technical and economic aspects of overcoating include: Ocean City Research, Inc., BIRL, the industrial research laboratory at Northwestern University, IDOT, KTC, NCDOT, LADOT, VDOT, WI-DOT, etc.

## CHAPTER 6: TASK E – ACCELERATED TESTING

### Background

Corrosion detrimentally affects bridges, reducing section thickness and resulting in a weakened bridge structure that compromises safety. Corrosion control is normally achieved by applying a coating system to the steel bridge. Unfortunately, coating systems do not completely protect and have limited durability. Moisture vapor penetration, water absorption, stress from thermal gradients across the coating, and ultraviolet radiation from sunlight can deteriorate the coating and cause it to fail prematurely. Furthermore, deicing chemicals and salts from the atmosphere can penetrate the coating and allow corrosion to occur at the steel substrate underneath the seemingly intact coating, causing premature blistering and delamination.

### Types of Coating Failure

Coatings on bridges can fail in many ways. In general, coating failure is defined as the premature deterioration of the coating system under normal service conditions with subsequent corrosion of the structure's steel substrate. Coating failure may occur because of inadequate substrate preparation, poor adhesion of the coating, improper coating application, formulation problems with the coating, or unsuitable coating selection for a given environment. Additional factors, such as non-flat bridge geometries with hard-to-coat areas and exterior forces such as abrasion of the surface and bridge movement from vehicle traffic, also increase the chance of premature coating failure. Table 11 lists the main factors influencing coating failure as well as the common types of coating failure that occur on coated steel bridges. Three types of coating failure that occur frequently are highlighted below:

Table 11. Important factors and types of coating failure.

<b>Factors Influencing Coating Failure</b>
<u>Coating Application</u> Brush marks, runs and sags, holidays, overspray, pinholes, spatter coat, cratering, improper coating thickness
<u>Bridge Design and Geometry</u> Edges, corners, welds, nuts and bolts, rivets, washers, overlapping joints, plates
<u>Exterior Forces</u> Abrasion, faying surfaces, joint movement
<u>Improper Coating Selection</u> Mixed surfaces, recoating and repair
<b>Types of Coating Failure</b>
<u>Substrate and Adhesion Related</u> Undercutting, delamination, blistering, peeling, flaking
<u>Formulation Related</u> Chalking, checking, cracking, wrinkling, discoloration, pinpoint rusting

- \* Undercutting: Moisture penetration to the steel substrate and buildup of corrosion products underneath a coating can cause disbonding and failure of a coating. Osmosis is an important factor, especially when coatings are subjected to salt exposure, water immersion, frequent condensation, or high-humidity environments. A coating must have strong adhesion to the substrate to be resistant to undercutting. Organic-barrier coatings tend to be less resistant to undercutting than inorganic zinc and thermally sprayed metals. The reason is that adhesion of organic coatings is primarily physical, whereas the adhesion of inorganic zinc and thermally sprayed metals are a result of chemical bonds as well. This combined physical and chemical bond tends to be more durable and more resistant to undercutting.
  
- \* Cracking: Cracking, or breaks in the coating extending from the surface through to the substrate, are caused by stresses in the coating film and between the coating and steel substrate that exceed the strength of the coating. Cracking results in further water penetration and corrosion of the steel substrate. Cracking is caused by polymer chain breakage due to aging and weathering of the paint system as well as premature failure due to exterior forces such as bridge movement between overlapping joints.
  
- \* Holidays: Holidays are bare or thin areas of the coated surface where reduced barrier protection can lead to a concentration of the corrosive environment at the steel substrate and can accelerate corrosion. Holidays and reduced coating thickness are most often found in areas that are difficult to coat and are caused by inadequate coating application. Bridge geometries, such as edges, corners, welds, overlapping joints, and bolted faying surfaces, represent areas where uniform coating application is difficult and non-uniform. Failure of the coating in a critical area, such as a nut-and-bolt or overlapping joints, can lead to rapid corrosion, such as pitting and steel loss that compromises the structural integrity of the bridge. Bridge geometry and design plays an important role in reducing coating durability. However, it is often overlooked in accelerated and long-term field testing procedures because of the difficulty reproducing similar effects in laboratory tests.

### Coating Properties

A protective coating's function is to prevent corrosive service environments (e.g., salt-air atmosphere or deicing chemicals) from contacting the underlying steel substrate and initiating corrosion. To accomplish this function, a coating must have several properties essential to maintaining a proper barrier to the environment. Some of the more important properties are: water permeability resistance, weathering resistance, sunlight resistance, ease of application, good adhesion, and abrasion resistance.



As noted, an important property of a coating is its resistance to water penetration. Two related properties are coating dielectric strength and coating resistance to ionic movement. Water can penetrate a coating either as a liquid or as a vapor. Water penetration decreases the dielectric strength of a coating, decreasing its resistivity and making the coating less insulative. Water penetration can also cause chemical breakdown of the coating, allowing increased ionic movement to the substrate, and further decreasing the useful life of the coating. Moisture also transports oxygen that is necessary for corrosion to occur. Since corrosion is an electrochemical process, ionic and oxygen transport towards the steel substrate increases the chance of corrosion being initiated. Once corrosion has begun, the corrosion products formed can cause undercutting and loss of adhesion of the coating. Water penetration may swell the coating and produce stresses that eventually lift the coating from the substrate. Although water containing naturally occurring salts or deicing chemicals penetrate coatings at a slightly slower rate than pure water, their presence increases the likelihood of coating deterioration and substrate corrosion, since they can accumulate underneath the coating, cause delamination by blistering, or accelerate corrosion of the substrate.

Although immersion of a coating in salt water alone is a severe environment, periods of wetness and dryness and frequent changes in temperature can also cause mechanical damage to a coating. Surprisingly, only small amounts of atmospheric salts, such as ammonium sulfate or sodium chloride, need be present to cause coating degradation because wet/dry cycling tends to enhance ionic movement and concentrate salt in the coating and at the substrate, leading to accelerated corrosion rates.

### Coating Evaluation

The performance and durability of bridge coatings are often evaluated by either an accelerated test, such as a salt-spray fog, or by long-term atmospheric exposure to a particular environment. Condition assessment of bridge coatings is accomplished using ASTM standard methods such as those listed in table 12 to determine the degree of rusting, cracking, blistering, gloss retention, and adhesion to the substrate. Most of the ASTM standard methods require visual inspection of the coating to determine coating degradation and are subjective. In addition, ASTM B-117, the standard salt-spray test, does not correlate well with long-term field exposure. For instance, waterborne coating systems exhibit poor performance using ASTM B-117, but show improved performance in field environments. ASTM D-1014, the long-term field exposure test procedure for coatings, is the best method to judge how well a coating will last in a particular environment. However, it can take years to acquire meaningful data. Current accelerated tests lack credibility as predictors of field service performance.

Electrochemical techniques have also been used to evaluate bridge coatings. Direct-current electrochemical measurements such as linear polarization and potentiodynamic polarization have been attempted on various coating systems, however, the complexity of the coating/steel substrate does not allow accurate interpretation of the data. Electrochemical impedance spectroscopy (EIS) measurements, on the other hand, can resolve these complexities and provide a fast, quantitative method of assessing coating properties related to water penetration and identify the early onset of corrosion of the steel before it

Table 12. ASTM methods for evaluating paint and coating systems.

ASTM Method	Name of Test
D610	Evaluating Degree of Rusting of Painted Surfaces
D661	Evaluating Degree of Cracking in Exterior Paints
D714	Evaluating Degree of Blistering of Paints
D2197	Adhesion by Scratching or Scraping
D3359	Adhesion by Tape Test
D1471	Gloss Measurement
B117	Salt-Spray (Fog) Testing
D1014	Long-Term Field Exposure Test

is seen visually. When used in combination with accelerated tests and long-term field testing, EIS can be a powerful technique for comparing a coating's ability to reduce the corrosion rate of the substrate. In addition, EIS measurements taken on existing bridge coatings in the field and as part of a total bridge management program can provide ongoing data on the condition of the coating. Such information would allow bridge owners to schedule overcoating before severe corrosion of the structure has occurred and ultimately would reduce overcoating costs and increase the life of the coating system.

EIS is capable of probing the electrochemical interface of a coated metal and providing quantitative information on the influence of corrosive environments affecting protective coatings and metallic substrates. For example, an EIS scan of a well-coated sample gives a high electrical resistance ( $R_c$ ) and low capacitance ( $C_c$ ) due to the dielectric property of the protective coating. The steel substrate properties are not measurable and corrosion is not occurring under the coating because the substrate has not been exposed to corrosive elements such as salt and oxygen. If the coating is subjected to an electrolyte by immersion, accelerated salt spray, or atmospheric exposure, the electrolyte can eventually permeate the coating, reducing  $R_c$  and increasing  $C_c$ . The change in these parameters is related to water penetration into the coating and indicates that the coating is degrading. Furthermore, electrolyte and oxygen may penetrate to the steel substrate and initiate corrosion of the steel substrate. At this point, the polarization resistance ( $R_p$ ) and capacitance ( $C_p$ ) properties related to the steel corrosion rate will become measurable. EIS parameters, such as  $R_p$ ,  $C_p$ ,  $R_c$ , and  $C_c$ , can be plotted versus time to determine how well they correlate with the rate of deterioration and the onset of corrosion for each coating.

Another important EIS parameter that has been used to correlate steel corrosion is the frequency at maximum phase angle ( $\omega_{max}$ ). The frequency at maximum phase angle is given by the equation:

$$\omega_{max} = \frac{1}{(C_p R_p)} \left(1 + \frac{R_p}{R_s}\right)^{1/2} \quad (5)$$

This equation is independent of area because the area dependence of  $R_p$  and  $C_p$ , and  $R_p$  and  $R_s$ , the electrolyte resistance, cancel out each other. The area-independence of  $\omega_{max}$  is a desirable property since the active, corroding steel area under a coating is usually not known. Research by G.T. Ruck et al. has shown that for bare steel pipe in soil,  $\omega_{max}$  stayed relatively constant with

time when the corrosion rate was low and the pipe was protected.<sup>(9)</sup> However,  $\omega_{\max}$  decreased two orders of magnitude when the pipe was not protected and the corrosion rate increased. The same decreasing trend of  $\omega_{\max}$  can be used to determine the onset of corrosion underneath a coating. Further details on the EIS technique and the important parameters measured are given in appendix A.

### Objectives and Approach

The objectives of this task were: (1) to identify potential accelerated test methods that improve the evaluation of bridge coating performance and (2) to use these methods to evaluate the corrosion resistance and weathering performance of several coatings.

Three accelerated test procedures were identified and used to evaluate the performance and durability of five bridge coatings: (1) a cyclic salt-spray exposure test, (2) a test combining cyclic salt-spray exposure, a freeze/thaw cycle, and carbon-arc, ultraviolet-light exposure, and (3) an electrolyte immersion test. Four of the five coatings studied were thermally sprayed zinc, aluminum, and zinc/aluminum, and a three-part VOC-compliant coating system. Test panels were also cut from a bridge section removed from service that contained a naturally weathered, red-lead primer/alkyd topcoat. In addition to flat test panels, non-flat panels were constructed to simulate a welded section and a bolted faying surface configuration commonly found on bridges. EIS was performed periodically on the test panels in the immersion experiments and before, during, and after the two cyclic tests to quantify coating resistance and capacitance ( $R_c$  and  $C_c$ ), polarization resistance and capacitance ( $R_p$  and  $C_p$ ), and the frequency at maximum phase angle ( $\omega_{\max}$ ). Consumption rates of the metallic coatings and corrosion rates of the steel substrate were calculated from  $R_c$  and  $R_p$ . Visual and photographic inspection of the test panels were also performed before and after testing.

### Materials and Procedures

#### Test-Panel Preparation

Experimenters prepared 99 coated test panels for exposure in the 3 accelerated tests. Of these test specimens, 94 were 10.0-by 15.0-by 0.64-cm (4-by 6-by 0.25-in), ASTM A36, hot-rolled, carbon steel plates that were either grit-blasted with a G-40 grit to a white-metal finish (SP-5), or were left with as-received millscale. The remaining five test panels were cut from a coated bridge section that had been taken out of service. Of the test panels, 52 contained either of 2 modifications: a welded steel support or 2 right-angle brackets welded to the panel and attached to each other with 2 nuts and bolts (as shown in figure 63). The non-flat geometries were used in the two cyclic tests to simulate welded sections and bolted, faying configurations (surfaces that are difficult to coat properly). Table 13 summarizes the test specimens used in the experiments. The flat panels and flat panels with the welded steel supports were purchased from KTA-Tator Company. Additional KTA-Tator-supplied flat panels were modified to construct the welded and bolted right-angle bracket configurations.

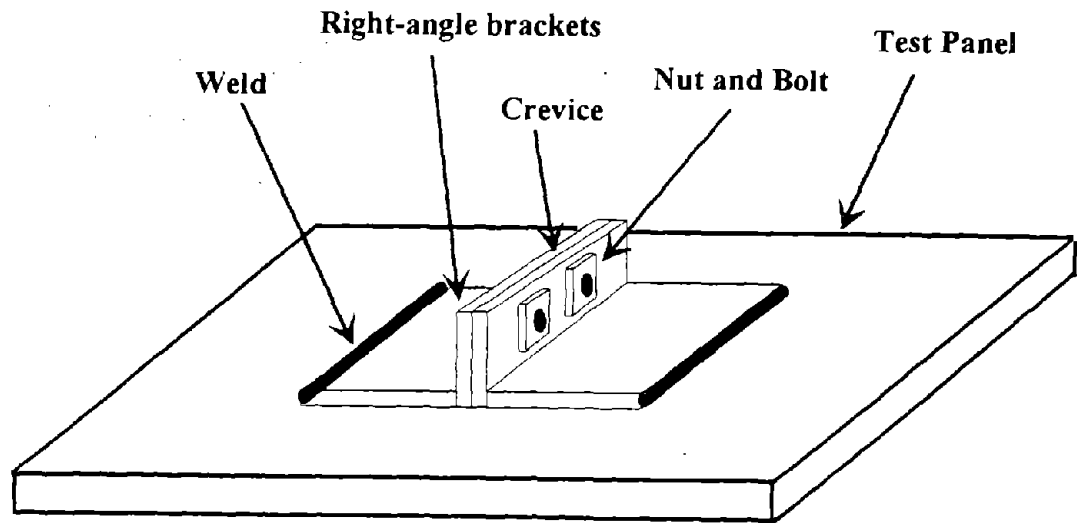


Figure 63. Steel test panel with typical bridge geometries.

Table 13. Summary of experimental materials.

TEST SPECIMENS	
·Materials	ASTM A36 steel plate
·Size	10 by 15 by 0.6 cm (4 by 6 by 0.25 in)
·Surface condition	White-metal grit-blast (SSPC-10), millscale
·Geometry	-Flat plate -Flat plate with welded support -Flat plate with welded and bolted right-angle brackets
COATING TYPES	
<ul style="list-style-type: none"> <li>·Red-lead primer/alkyd topcoat (naturally weathered)</li> <li>·VOC-compliant 3-layer system: organic zinc primer, aluminum epoxy mastic intermediate coat, polyurethane topcoat</li> <li>·Thermally sprayed zinc</li> <li>·Thermally sprayed aluminum</li> <li>·Thermally sprayed 85% zinc/15% aluminum</li> </ul>	
ELECTROLYTE	
<ul style="list-style-type: none"> <li>·0.40% wt. ammonium sulfate</li> <li>·0.05% wt. sodium chloride</li> </ul>	

## Coating Type and Application

Five coatings systems were evaluated in this task: thermally sprayed (TS) zinc, aluminum, and 85/15 Zn/Al, a VOC-compliant coating system; and a weathered, red-lead primer/alkyd topcoat taken from a bridge section that had been removed from service. The VOC-compliant coating system consisted of a three-component, zinc-filled, epoxy primer [VOC, 302 g/L (2.52 lb/gal)]; a two-component, high-build, modified aluminum epoxy mastic intermediate coat [VOC, 89 g/L (0.74 lb/gal)]; and a high-gloss, high-solids, aliphatic polyurethane topcoat [VOC, 288 g/L (2.4 lb/gal)]. The bridge section containing the red-lead primer/alkyd topcoat was obtained from the Illinois Department of Transportation (IDOT). Further information on the thermally sprayed metal coatings are given in the previous task. Application of the coatings was done following either manufacturing recommendations or standard practices. Prior to coating, the test panels were ultrasonically cleaned in trichloromethane to remove any grease or dirt on the surface. After coating, thickness measurements were performed using either an Elcometer thickness gauge or a Positector-2000 thickness gauge. Wet thickness was also measured on the VOC-compliant coating as recommended by the manufacturer.

Linear polarization, potentiodynamic polarization, and EIS were made on ASTM A36 carbon-steel rods that were left bare or were thermally sprayed with zinc, aluminum, or Zn/Al. Initial consumption rates of the metallic coatings and initial corrosion rates of the steel substrate were obtained for comparison with values obtained from the three accelerated exposure tests. Any change in the metallic coating consumption rate or steel corrosion rate would mean that the metallic coating has become ineffective and that significant corrosion of the steel is occurring.

The carbon-steel rods were grit-blasted to a white-metal finish (SSPC-10) or left with original millscale. The electrolyte used was 0.40-percent ammonium sulfate and 0.05-percent sodium chloride. Two, thermally sprayed coating thicknesses were put onto the steel rods (75  $\mu\text{m}$  (0.003 in) and 150  $\mu\text{m}$  (0.006 in)). The 75- $\mu\text{m}$  thickness represents a coating of minimal through-porosity and the 150- $\mu\text{m}$  thickness represents a flow-through porous coating. The experiments were performed in triplicate and average values of  $R_p$ ,  $C_p$ ,  $R_c$ ,  $C_c$ , and  $\omega_{\text{max}}$  were obtained. Coating consumption rates and steel corrosion rates were calculated from  $R_c$  and  $R_p$ . The carbon-steel rods were thermally sprayed by ASB Industries, Incorporated, Barberton, Ohio.

The linear polarization and potentiodynamic polarization experiments were carried out using the Model 342C Soft corr<sup>TM</sup> corrosion measurement system. The system uses an EG&G Princeton Applied Research Model 273 potentiostat driven by software in an IBM computer. The EIS measurements were performed using the EG&G Princeton Applied Research Electrochemical Impedance System. It consists of an EG&G Model 273 potentiostat, a Schlumberger 1255 Frequency Response Analyzer, and Model 388 software used to control the system and acquire the data. The EIS parameters were calculated from the impedance spectrum using the EQUIVCRT software program from EG&G. A brief overview describing the electrochemical techniques of EIS, linear polarization, and potentiodynamic polarization is given in appendix A.

## Electrolyte Preparation

The electrolyte used in the three accelerated tests contained 0.05-percent sodium chloride and 0.40-percent ammonium sulfate, two salts commonly found in industrial, atmospheric environments. The particular concentrations of the salts have been used in the Mebon Prohesion salt-spray test and are recommended by the Q-Panel Company, Cleveland, Ohio. Reagent-grade sodium chloride and ammonium sulfate were used to make up the electrolyte for the immersion experiments and the salt solution for the cyclic tests.

## Accelerated Test Procedure Identification and Modification

Immersion Experiment. An experiment involving continuous immersion in an electrolyte was chosen for accelerated testing because it provided a severe environment that accelerates water penetration into the coating, a significant failure mechanism that occurs on bridge coatings.

Immersion Test Procedure. To quantify the characteristics of the coating and steel as the coating deteriorates in an electrolyte-saturated environment, 14 flat, coated steel specimens were exposed to an electrolyte containing 0.05-percent sodium chloride and 0.40-percent ammonium sulfate. For each coating and surface condition, two steel panels were used. In addition to the laboratory-prepared samples, two test specimens were fabricated from a weathered bridge section obtained from IDOT. Table 14 lists the number of immersion cells by coating type and surface condition.

**Table 14. Number of test specimens for immersion experiments.**

A36 STEEL		
Coating	White-Metal Blast	Millscale
Red Lead/Alkyd		2
VOC-compliant	2	2
TS Zinc	2	2
TS Aluminum	2	
TS Zn/Al	2	
Total Number of Cells: 14		

The immersion cells consisted of a 20-cm (8-in) long, 8-cm (3-in) diameter, translucent polyvinyl chloride (PVC) pipe to which an 8-cm (3-in) PVC flange was attached. The coated test panels were placed between the flange and tightened with four bolts, as seen in figure 64. A rubber gasket between the upper flange and the coated test panel prevented electrolyte leakage from occurring. A PVC cap was placed on top of the cell to prevent evaporation of the electrolyte. Periodic EIS measurements were performed using a graphite anode and a saturated calomel reference electrode (SCE) placed at the top of the cell.

Cyclic Test I. The cyclic (Prohesion) salt-spray test was chosen for evaluation because wet/dry cycling has been shown to correlate with outdoor weathering exposure more realistically than the standard salt-fog test, ASTM B117. The failure mechanism associated with wet/dry cycling is similar to

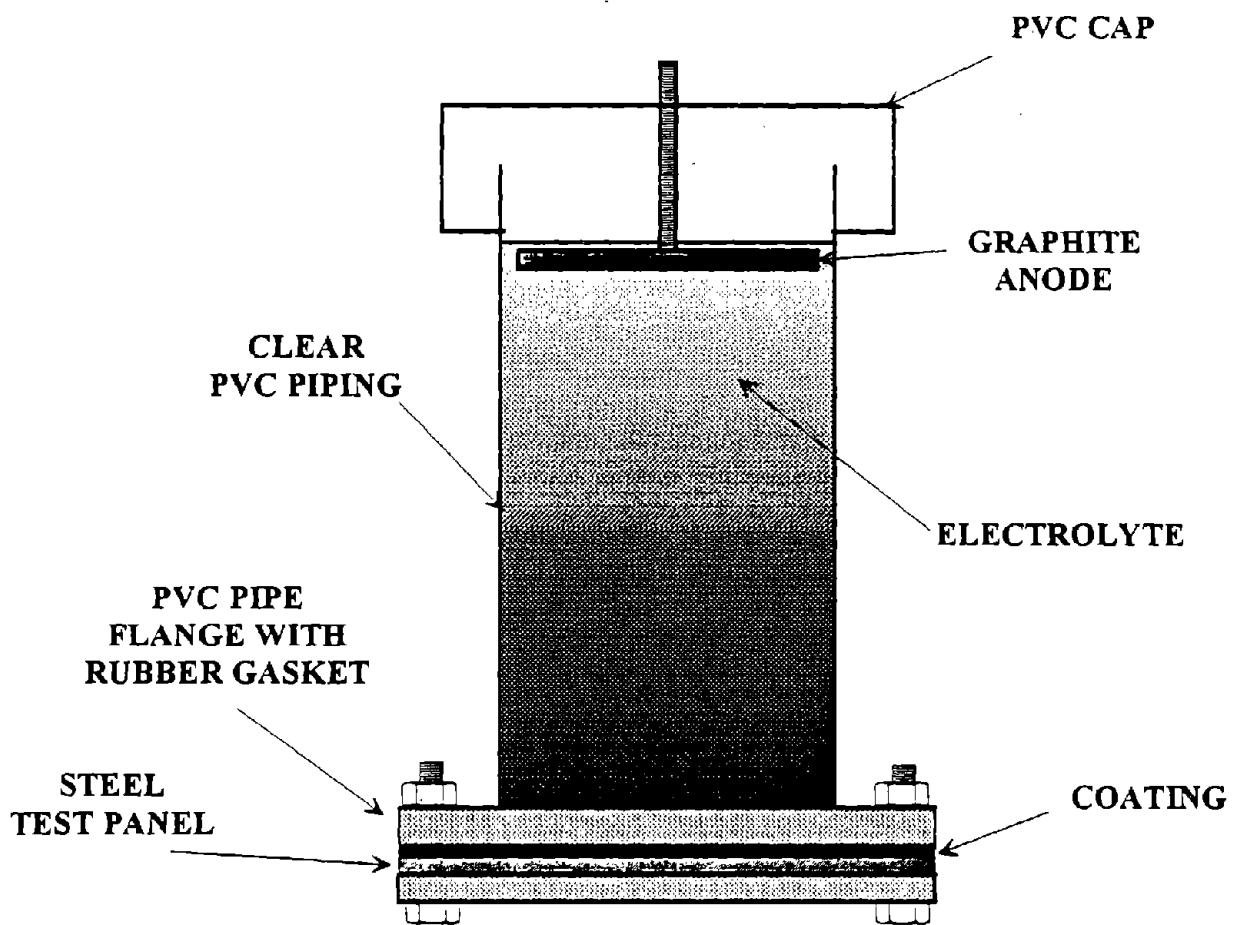


Figure 64. Corrosion cell used in immersion experiments.

water/electrolyte immersion in that osmotic pressure causes water and other ions, such as chloride and sulfate, to diffuse and concentrate in the coating near the steel substrate. Thus, it was thought to be a good alternative test to the immersion experiments. It was decided that a cyclic test with only the salt spray would be run to determine whether the cyclic salt spray alone is a good method for determining coating performance and durability.

Cyclic Test I Procedure. To quantify the characteristics of the coating and steel as the coating deteriorates in a wet/dry cyclic environment, 41 flat and non-flat, steel panels coated with 4 of the 5 coatings were exposed to a cyclic salt fog. The four coatings were the VOC-compliant coating and the thermally sprayed zinc, aluminum, and zinc/aluminum. Two or three coated panels for each coating and surface condition were tested for statistical significance. Table 15 lists the number of panels for cyclic test I by coating, surface condition, and geometry. The salt solution used was an electrolyte consisting of 0.05-percent sodium chloride and 0.40-percent ammonium sulfate.

Table 16 gives a summary of the cyclic experimental procedure. Before testing, the test panels were photographed and initial EIS measurements were run on the flat panels by placing them in an immersion cell filled with an electrolyte of 0.40-percent ammonium sulfate and 0.05-percent sodium chloride. The samples were then placed in the salt-fog chamber and were exposed to a modified cyclic Prohesion salt-spray cycle for 28 d (672 h). The cycle consisted of 1.5 h salt spray, followed by a 1-h dry cycle at 35 °C. This differs slightly from the Prohesion cycle as given by the Q-Panel Company, where the salt spray is for 1 h. It was observed in initial tests with the Prohesion cycle that it took approximately 15 to 20 minutes for the chamber to fill completely with salt fog. The slightly longer spray time allowed the test samples to encounter a more evenly distributed salt spray for a full hour. After 14 d, the flat samples were taken out and EIS measurements were performed. After 28 d, a final EIS measurement was made on the flat panels. All 41 test panels were photographed to show any changes in the coating, and ASTM Standard 610, Evaluating the Degree of Rusting on Painted Surfaces, was performed.

The salt-fog chamber used in the tests was a Q-Fog Corrosion Chamber SF/MP450 manufactured by the Q-Panel Company, Cleveland, Ohio. The test panels were placed in the salt-fog chamber on plastic ledges that were attached to the wall of the chamber, as recommended by the Q-Panel Company for the cyclic test. In addition, flow rate and air pressure were periodically adjusted to maintain an even distribution of salt spray in the chamber.

Cyclic Test II. The cyclic salt-spray, freeze/thaw, and ultraviolet-exposure test was chosen for the same reasons as the cyclic salt-spray test; however, it has the additional benefit of providing thermal stressing due to the freeze/thaw cycle and elevated temperature achieved in the ultraviolet exposure. The ultraviolet exposure also subjects the coatings to possible chemical breakdown of the constituents in the organic coatings. In addition, any water that penetrated the coating in the salt-spray portion of the cycle would freeze in the freeze/thaw cycle and expand in volume and could cause cracking and loss of adhesion. Also, the higher temperatures in the ultraviolet exposure might drive off water from the coating. This continual cycle of water penetration, expansion due to freezing, and evaporation at



Table 15. Number of test panels for cyclic tests.

CYCLIC TEST I						
Coating	White-Metal Blast			Millscale		
	Flat	Non-Flat 1	Non-Flat 2	Flat	Non-Flat 1	Non-Flat 2
VOC-compliant	3	2	2	3	2	2
T-S Zinc	3	3	3	0	0	0
T-S Aluminum	3	3	3	0	0	0
T-S Zn/Al	3	3	3	0	0	0
Total Number: 41 Test Panels						
CYCLIC TEST II						
Coating	White-Metal Blast			Millscale		
	Flat	Non-Flat 1	Non-Flat 2	Flat	Non-Flat 1	Non-Flat 2
Red Lead/Alkyd	0	0	0	3	0	0
VOC-compliant	3	2	2	3	2	2
T-S Zinc	3	3	3	0	0	0
T-S Aluminum	3	3	3	0	0	0
T-S Zn/Al	3	3	3	0	0	0
Total Number: 44 Test Panels						
Non-Flat 1 is flat plate with welded support from KTA-Tator. Non-Flat 2 is flat plate with welded and bolted right-angle brackets.						

Table 16. Summary of cyclic experiments.

-Cyclic Salt Spray	2 h on: Ambient temperature 1 h off: 35 °C
-Cyclic Ultraviolet Exposure	8 h on: 40 to 50 °C 4 h off: Ambient temperature
-Freezing Cycle	20 to 24 h: -23 °C
<b>CYCLIC TEST 1</b>	
(1) Initial EIS measurement, photographs (2) Cyclic salt spray, 14-d exposure (3) EIS measurement on test plates (4) Repeat step 2 for total 28-d exposure (672 h) (5) Final EIS measurement, visual inspection, photographs	
<b>CYCLIC TEST 2</b>	
(1) Initial EIS measurement, photographs (2) Cyclic salt spray, 7-d exposure (3) Freeze cycle, 1-d exposure (4) Cyclic UV exposure, 7-d exposure (5) EIS measurement on test plates (6) Repeat steps 2 through 5 for total 30-d exposure (720 h) (7) Final EIS measurement, visual inspection, photographs	

elevated temperature represents an accelerated cycle of a northern-type exposure of rain or snow, freezing conditions, followed by drying conditions with sunlight and heating of the bridge surface.

Cyclic Test II Procedure. To quantify the characteristics of the coating and steel as the coating deteriorates, 44 flat and non-flat, steel panels coated with the 5 coatings were exposed to a cyclic salt-fog, freeze/thaw cycle, and carbon-arc-generated ultraviolet radiation. The five coatings were the VOC-compliant coating, thermally sprayed zinc, aluminum, and zinc/aluminum, and the weathered red-lead/alkyd topcoat. Two or three coated panels for each coating and surface condition were tested. Table 15 lists the number of panels for cyclic test II by coating, surface condition, and geometry.

Table 16 gives a summary of the cyclic experimental procedure. Before testing, the test panels were photographed and initial EIS measurements were run on the 18 flat panels. The samples were then placed in the salt-fog chamber and were exposed to the modified, cyclic, Prohesion salt-spray cycle for 7 d (168 h). The on/off cycle time was the same as for cyclic test I. After 7 d, the test panels were taken out and placed in a freezer. The initial temperature was slightly above 0 °C (32 °F). The final temperature of -23 °C (-10 °F) was reached in about 2 h and was held for 24 h. After freezing, the samples were immediately taken out of the freezer and were placed in the ultraviolet (UV) weatherometer. The UV exposure period was 8 h on, 4 h off, for 7 d. The temperature in the UV weatherometer was initially at ambient temperature, but rose to about 60 °C (120 °F) in about 1 to 2 h.

After 7 d in the UV weatherometer, the flat panels were taken out and EIS measurements were performed. The cycle was repeated for a total exposure of 30 d (720 h). Afterwards, the test panels were taken out and a final EIS measurement was made on the flat panels. All 44 test panels were photographed to show any changes in the coating, and ASTM Standard 1014, Evaluating the Degree of Rusting on Painted Surfaces, was performed.

The salt-spray experiments were conducted in the Q-Fog Salt-Fog Chamber. The UV-weathering cycle was done in an Atlas Model XW-W weatherometer that uses Sunshine Carbon-Arc Lamps to provide the ultraviolet radiation. The freezer used for the freeze/thaw cycle was a True Manufacturing Company Model T-23F, 0.57-m<sup>3</sup> (20-ft<sup>3</sup>) upright freezer. It was purchased from Pierce Food Service Equipment Company, Countryside, Illinois.

## Results and Discussion

### Immersion Experiments

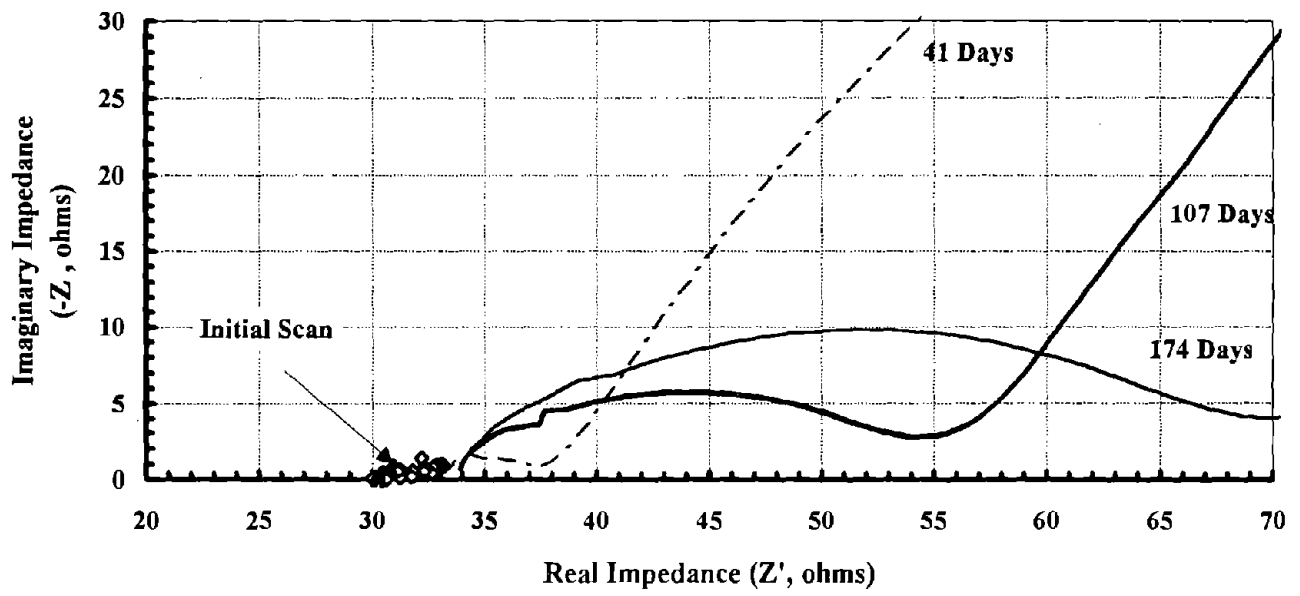
Immersion experiments were performed on eight thermally sprayed (TS) test panels, four test panels coated with a VOC-compliant coating, and two test panels cut from a weathered bridge section containing a lead (Pb) primer and alkyd topcoat. The TS-coated test panels were immersed for 174 d, two each of the VOC-compliant coatings were immersed for 92 and 98 d, respectively, and the two weathered bridge sections were immersed for 72 d. Figures 65(a) through (c) show representative EIS Nyquist plots for the TS-Zinc, Pb/Alkyd, and VOC-compliant coatings as a function of immersion time.

### Thermally Sprayed Coatings

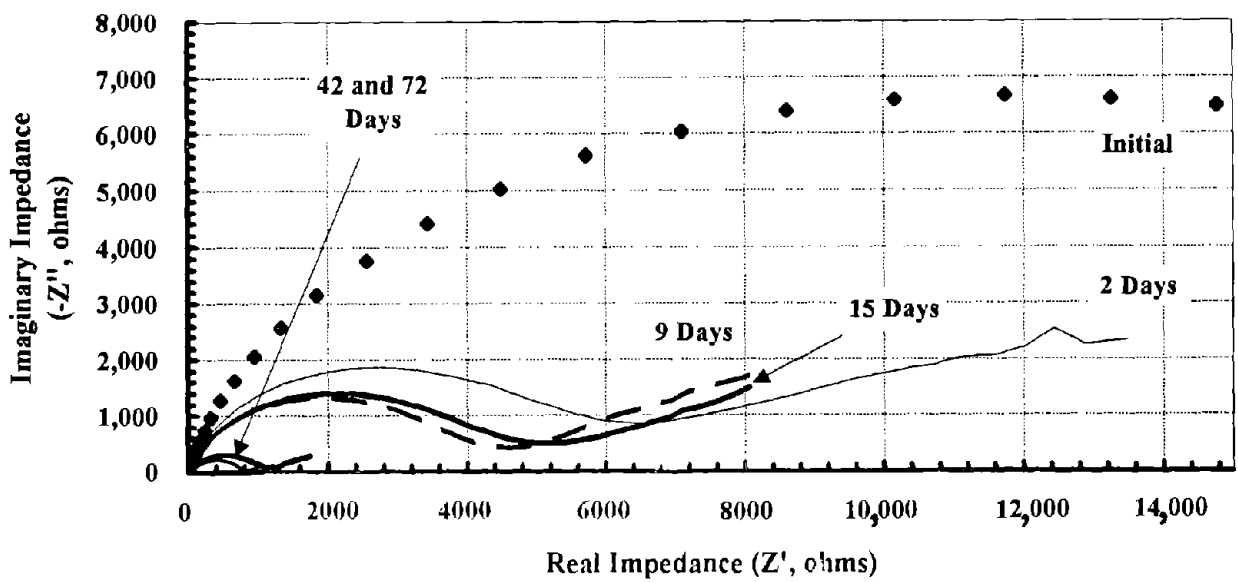
Figure 66(a) shows a plot of the high-frequency section of the EIS scan for a TS-zinc-coated test panel illustrating the increase in coating resistance as given by the increasing semicircle. The straight line going off of the scale is actually a second semicircle at the lower frequencies due to the steel corrosion rate. The second semicircle was absent on the EIS scans for the TS-Al- and TS-Zn/Al-coated test panels, indicating that steel corrosion was not yet measurable on these coatings.

Figures 66(a) and 66(b) show the consumption rate of the thermally sprayed coatings; the corrosion rate of the steel underneath the TS-zinc coating; and  $\omega_{\max}$ , the frequency at maximum phase angle versus immersion time. The TS coatings initially showed a high coating consumption rate of 102 to 635  $\mu\text{m}/\text{yr}$  (4 to 25 mil/yr (mpy)), which decreased with time to approximately 25  $\mu\text{m}/\text{yr}$  (1 mpy). The sacrificial coatings are actively corroding and protecting the steel substrate. Assuming a constant consumption rate, the 300- $\mu\text{m}$  (4-mil) thick coatings would be completely consumed in 12 years of electrolyte immersion. The immersion test has accelerated the coating consumption rate threefold, given an estimated service life of 40 years for a 300- $\mu\text{m}$  thermally sprayed coating thickness.

In addition, corrosion under the thermally sprayed coatings was measurable immediately upon immersion in the electrolyte. The EIS measurements indicated that electrolyte penetrated through the TS-zinc coating to the steel substrate. Initially, the corrosion rate of the steel substrate was 128  $\mu\text{m}/\text{yr}$  (5 mpy), but decreased to 25  $\mu\text{m}/\text{yr}$  (1 mpy) after 20 d. Though it appears that

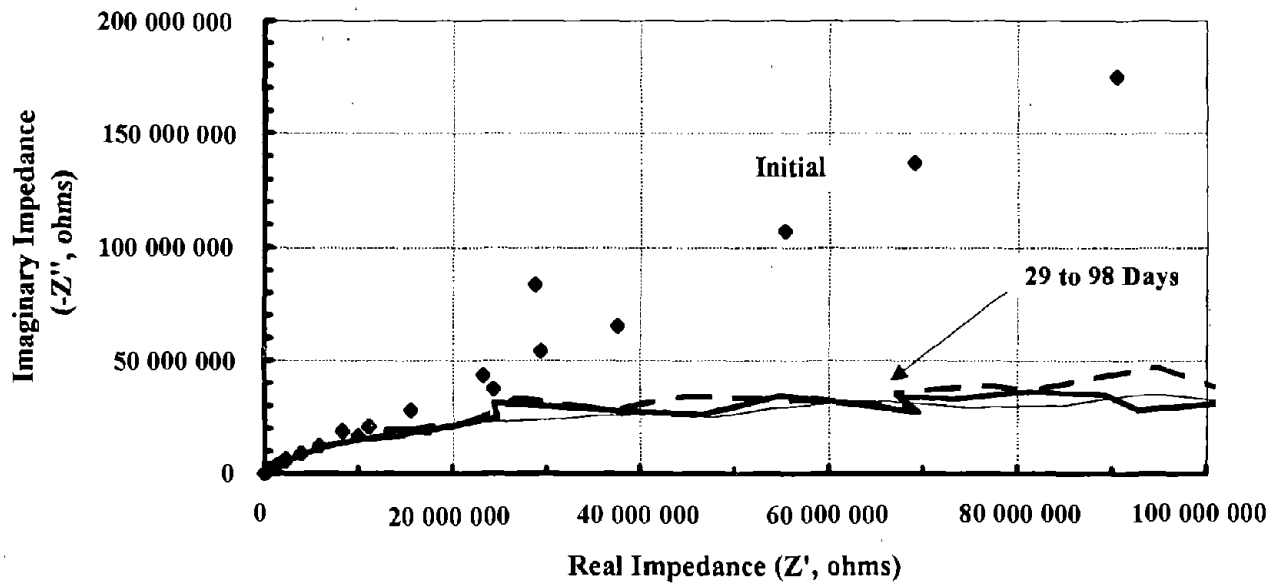


(a) High-frequency detail for thermally sprayed zinc.



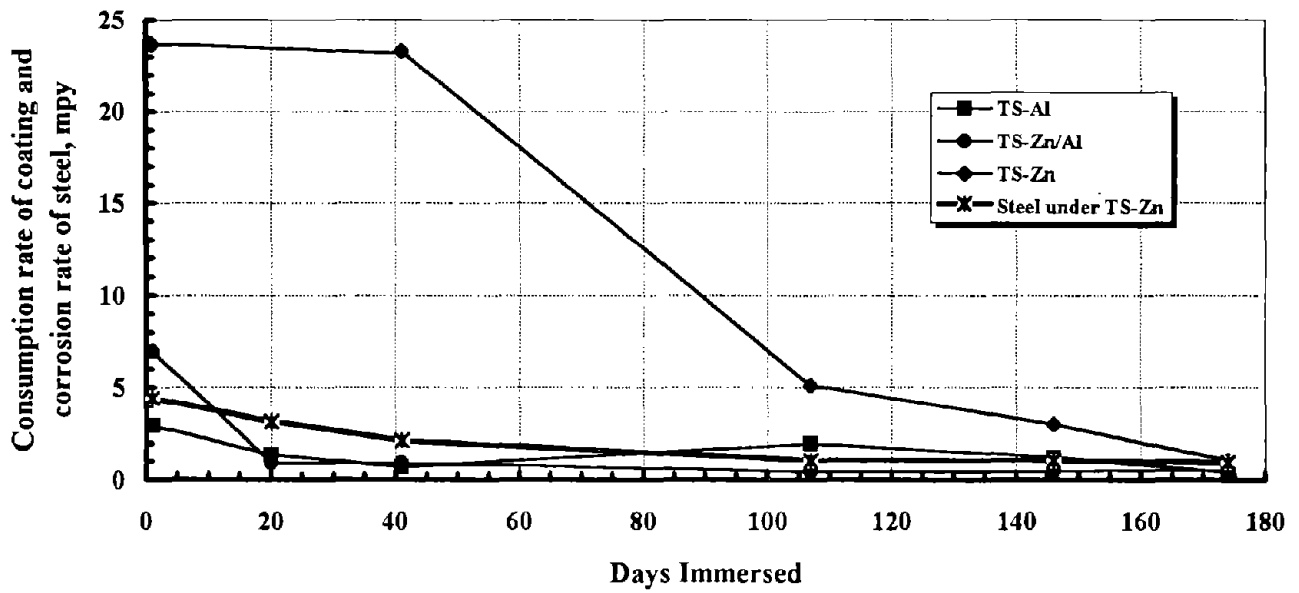
(b) Pb/Alkyd coating from weathered bridge section.

Figure 65. Representative EIS Nyquist plots for the immersion experiments.

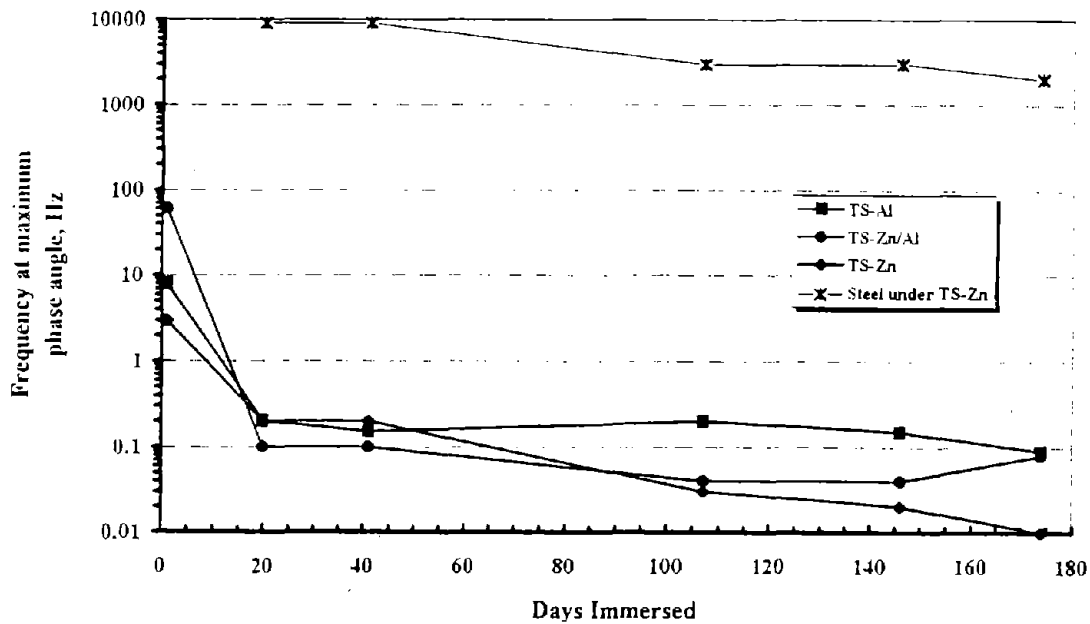


(c) VOC-compliant coating.

Figure 65. Representative EIS Nyquist plots for the immersion experiments (continued).



(a) Consumption rate of thermally sprayed coatings and corrosion rate of steel underneath coating.



(b) Frequency at maximum phase angle.

Figure 66. Electrochemical properties for the thermally sprayed coating in the immersion experiments.

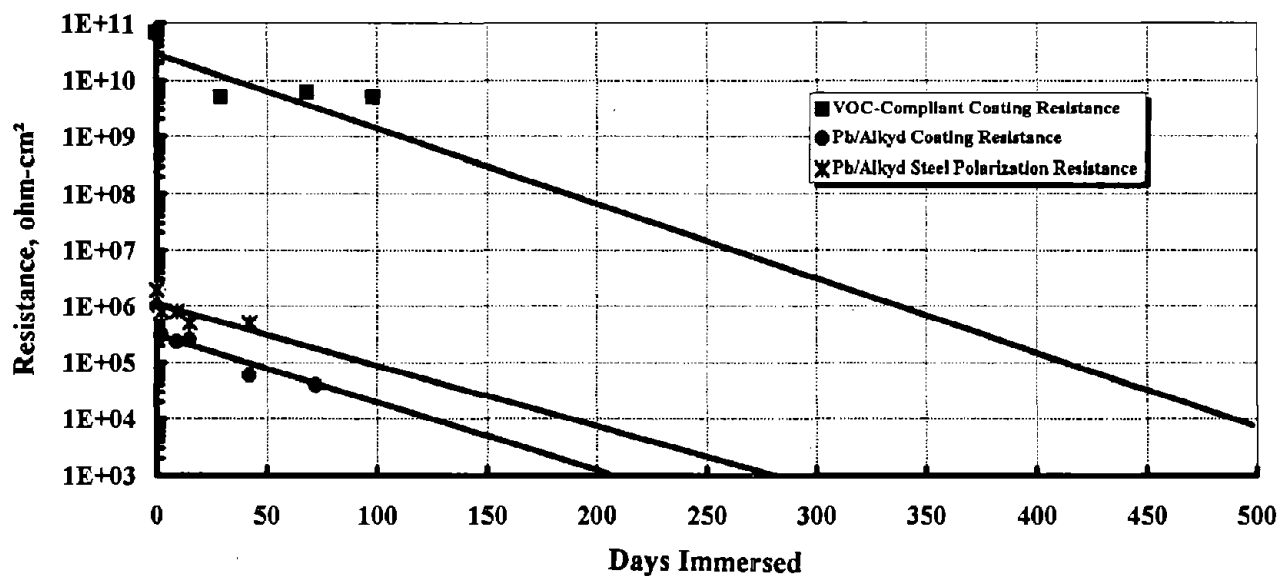
the TS-zinc coating is sufficiently protecting the steel substrate. Corrosion of the steel under the TS-Zn/Al coatings was also not observed. The EIS scan for the TS-Al coating, however, showed an additional diffusional element due to ionic movement in the coating, most likely towards the steel substrate, suggesting that corrosion of the steel may become measurable in a short time.

The frequency at the maximum phase angle,  $\omega_{\max}$ , is plotted in figure 66(b). The  $\omega_{\max}$  decreased with time and with decreasing consumption rate for the thermally sprayed coatings, amplifying the change from a fivefold decrease in consumption rate to a three to four order-of-magnitude decrease in  $\omega_{\max}$ . On the other hand,  $\omega_{\max}$  due to the steel under the TS-zinc coating stayed relatively constant, although the corrosion rate decreased from 128 to 25  $\mu\text{m}/\text{yr}$  (5 to 1 mpy). As noted earlier, the TS-zinc is protecting the steel, which is reflected in the relatively constant value of  $\omega_{\max}$ . A significant change in  $\omega_{\max}$  would probably not occur until the TS-zinc coating had been consumed or was not sacrificially protecting the steel, causing the steel corrosion rate to increase to higher values.

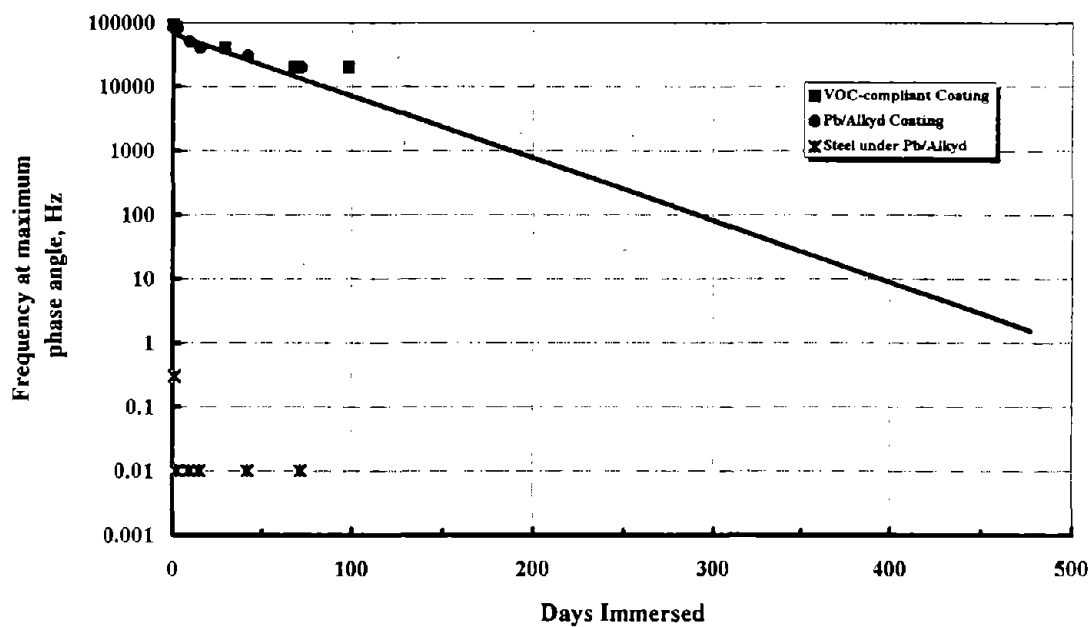
Pb/Alkyd and VOC-Compliant Coatings. Figure 65(b) shows EIS Nyquist plots for the Pb/alkyd coatings as a function of immersion time. Initially, one semicircle was observed. After 2 d of immersion, two semicircles were measured that continually became smaller with time. The first semicircle is representative of the Pb/alkyd coating and the second is due to the steel substrate. Theoretically, for a weathered coating, one would expect an EIS scan with three semicircles representing the alkyd topcoat, the lead primer, and the steel substrate properties. However, visual observation of the test-panel surface under immersion showed areas of exposed steel where significant corrosion was occurring. This provides evidence that the second semicircle on the EIS scan is due to steel corrosion and not to the lead primer. The Pb/alkyd coating properties appear to be lumped together into a single semicircle on the EIS scans and can be represented by one coating resistance.

Figure 65(c) shows EIS Nyquist plots as a function of immersion time for the VOC-compliant coatings. One high-impedance semicircle was obtained, indicative of a highly insulative coating. However, the high initial coating resistance decreased after 29 d, indicating that there was an initial uptake of electrolyte into the coating. Further changes in the coating resistance were small, but they still indicated further electrolyte penetration into the coating.

Figures 67(a) and (b) show the coating and polarization resistance, and  $\omega_{\max}$  as a function of immersion time for the Pb/alkyd and VOC-compliant coatings. Figure 67(a) shows coating resistance decreasing for both coatings. This is indicative of a coating absorbing electrolyte and becoming less resistive. However, the VOC-compliant coating is still five orders of magnitude higher in resistance than the Pb/alkyd coating, meaning it is still insulative and providing a barrier for moisture penetration toward the steel substrate. Steel corrosion was not observed under the VOC-compliant coatings. On the other hand, the Pb/alkyd coating gave a relatively low coating resistance that continued to decrease with time, indicating that the coating had degraded. In addition, corrosion of the steel substrate was observed from the EIS measurements and confirmed visually. However, the polarization resistance,  $R_p$ , appeared to be high—three orders of magnitude higher than obtained from experiments done on bare-steel rods of known area in the same electrolyte. A



(a) Coating and polarization resistance.



(b) Frequency at maximum phase angle.

Figure 67. Electrochemical properties for the Pb/alkyd and VOC-compliant coatings in immersion experiments.



possible reason is that  $R_p$  measured on the test panels is due mostly to the exposed steel areas. However, the total area of the test panel, including the area covered by the Pb/alkyd coating, was used in the calculation. This area is larger than the actual corroding steel area and would give an apparently larger  $R_p$  than the actual value.

More importantly, the EIS measurements are able to distinguish between the highly resistive VOC-coating that is beginning to degrade and the weathered Pb/alkyd coating with corrosion of the steel occurring underneath. Furthermore, the immersion experiments can accelerate coating degradation in a reasonable length of time. Extrapolation of the VOC-compliant coating resistance to values observed with the weathered Pb/alkyd coating give immersion times of 350 to 500 d (1 to 1-1/2 yr). In addition, corrosion of the steel underneath the coating would be measurable before this time. Such a timeframe for an accelerated test is reasonable given that long-term field exposure takes 3 to 5 years before meaningful data is obtained.

Figure 67(b) shows  $w_{max}$  as a function of immersion time for the Pb/alkyd and VOC-compliant coatings. The  $w_{max}$  for the steel under the Pb/alkyd coating shows values indicative of a significant corrosion rate, i.e., above 25  $\mu\text{m}/\text{yr}$  (1 mpy). This confirms that the apparent polarization resistance measured is incorrect due to the area term. On the other hand,  $w_{max}$  for the two coatings shows the same trend even though the coating resistances are much different in value. This suggests that  $w_{max}$  is a useful parameter for determining the onset and extent of steel corrosion underneath a coating, but not necessarily for characterizing the level of coating degradation. Fortunately, however, coating resistance is an excellent parameter to characterize the state of the coating. In addition, the coating capacitance can be used to further quantify water penetration into the coating, however it was not calculated in this task.

In conclusion, it appears that electrolyte immersion combined with EIS is a good method to accelerate coating degradation and corrosion of the steel substrate underneath. EIS measurements allow determination of the consumption rate of sacrificial coatings, quantification of coating degradation, and determination of the onset and extent of steel corrosion. The electrochemical properties of coating resistance and capacitance, polarization resistance, and  $w_{max}$  are good parameters that can be used to correlate the performance of metallic and organic coatings subjected to an accelerated, corrosive environment. Although immersion times of approximately 1 yr are needed to obtain significant coating degradation, the onset of steel corrosion under the coating will occur in a much shorter time.

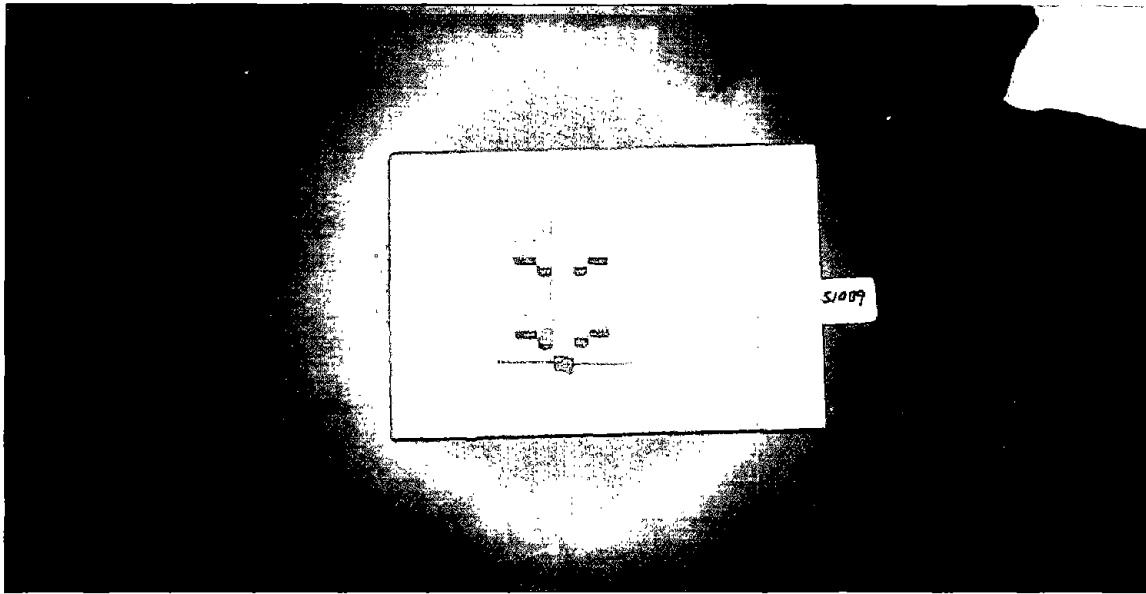
Cyclic Accelerated Tests. Two accelerated tests consisting of a cyclic (Prohesion) salt-spray test (cyclic test I) and a cyclic (Prohesion) salt-spray, freeze/thaw, and carbon-arc UV-exposure test (cyclic test II) were performed on 85 flat and non-flat test panels coated with TS-zinc, aluminum, and zinc/aluminum, and a VOC-compliant, coating system. Flat test panels were also cut from a weathered bridge section taken out of service and that contained a lead primer/alkyd topcoat coating system. The test panels were subjected to cyclic test I for a total of 672 h, and cyclic test II for 720 h. The salt solution used in the salt spray was an electrolyte of 0.4-percent ammonium sulfate and 0.05-percent sodium chloride.

In general, cyclic test I subjected the test panels to a longer salt-spray exposure (twice as long as cyclic test II), which caused more salt solution to penetrate into the coatings. This was especially detrimental to the sacrificial TS coatings, which are porous, and the weathered Pb/alkyd coating that was already naturally degraded. However, the combination of salt spray, freeze/thaw, and UV exposure represented a more severe test that not only allowed salt penetration from on/off cycling of the salt spray, but also allowed chemical and mechanical breakdown of the coatings due to the freeze/thaw and UV-exposure cycle. A longer exposure period for cyclic test II is recommended because it would allow a higher degree of salt penetration, coating degradation, and possible steel corrosion to occur after several salt spray, freeze/thaw, and UV-exposure cycles.

Non-Flat Panel Results. Figures 68(a) through (d) show representative before-and-after photographs of the four coatings on the two non-flat test panels subjected to cyclic tests I and II. Table 17 lists the corrosion rating of each coating and test panel on a scale of 1 to 10 according to the ASTM-D610 visual corrosion rating standard, with 10 representing a coating of excellent performance and durability, and 1 indicating a coating of poor performance and durability.

The VOC-compliant and TS-zinc coating performed the best of the four coatings, showing excellent coating performance. The TS-zinc showed excellent durability and the VOC-compliant coating showed better-than-average durability. Both coatings had visual ratings of between 8 and 10, performing well in the accelerated tests with virtually no corrosion occurring on the surface. Some yellow staining was observed on one of the TS-zinc-coated test panels that was due to the consumption of the zinc. However, several of the VOC-compliant coated test panels showed several small areas of steel corrosion on the welded bracket or the nut-and-bolt area. Though these corroded spots were not enough to decrease the rating significantly, they are noted because they probably occurred due to the difficulty in uniformly coating the non-flat area. The coating thicknesses in these areas were thinner compared to the rest of the flat panel area. In addition, one of the VOC-compliant coated test panels subjected to cyclic test II showed cracking along a nut and bolt as well as on the welded bracket. The cracking was caused by the thermal stressing from the freeze/thaw cycle and subsequent UV exposure at elevated temperatures and this decreased the durability rating of the coating. These results highlight the usefulness of using non-flat test panels to rate coating performance because such observations were not seen on the TS-zinc or VOC-compliant coated flat test panels.

The corrosion rating for the TS-Zn/Al-coated test panels was between 5 and 6, indicating moderate coating performance and better-than-average durability. Although rust from the steel was not observed, the TS-Zn/Al coating showed visible signs of consumption, with many white "pits" where corrosion of the coating had occurred. The surface of the coating was generally rougher than before testing, and the nut-and-bolt area showed fair amounts of coating consumption. This made the coating aesthetically unpleasant. However, overcoating the TS-Zn/Al with a topcoat or a TS-polymer may solve this problem and would also increase coating performance and durability.



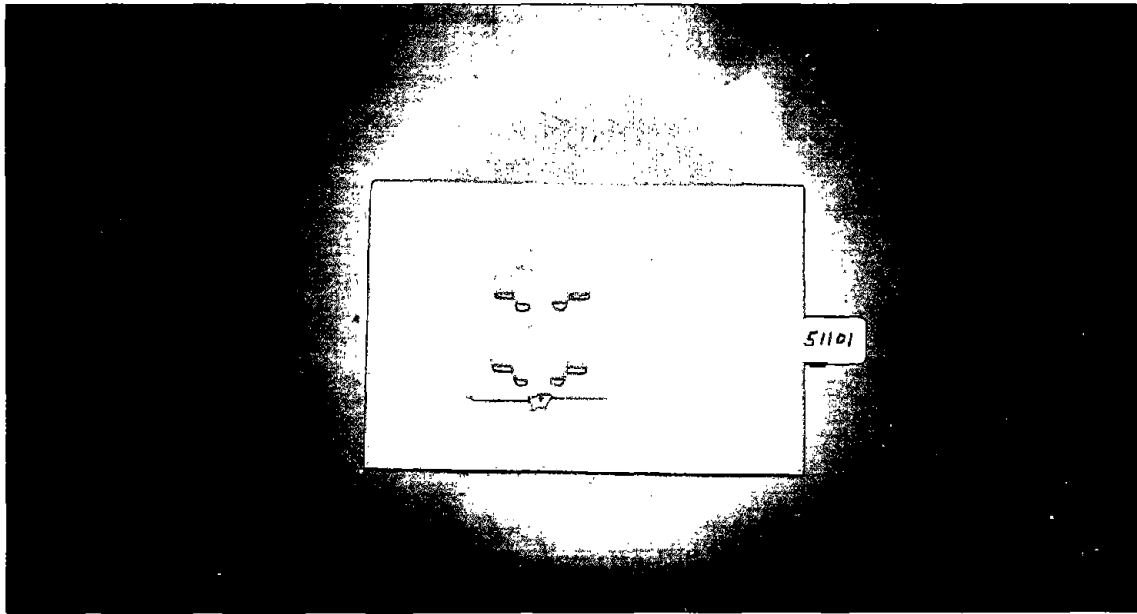
Before



After

(a) Thermally sprayed aluminum, cyclic test I.

Figure 68. Before-and-after photographs of the coated, non-flat test panels subjected to cyclic tests I and II.



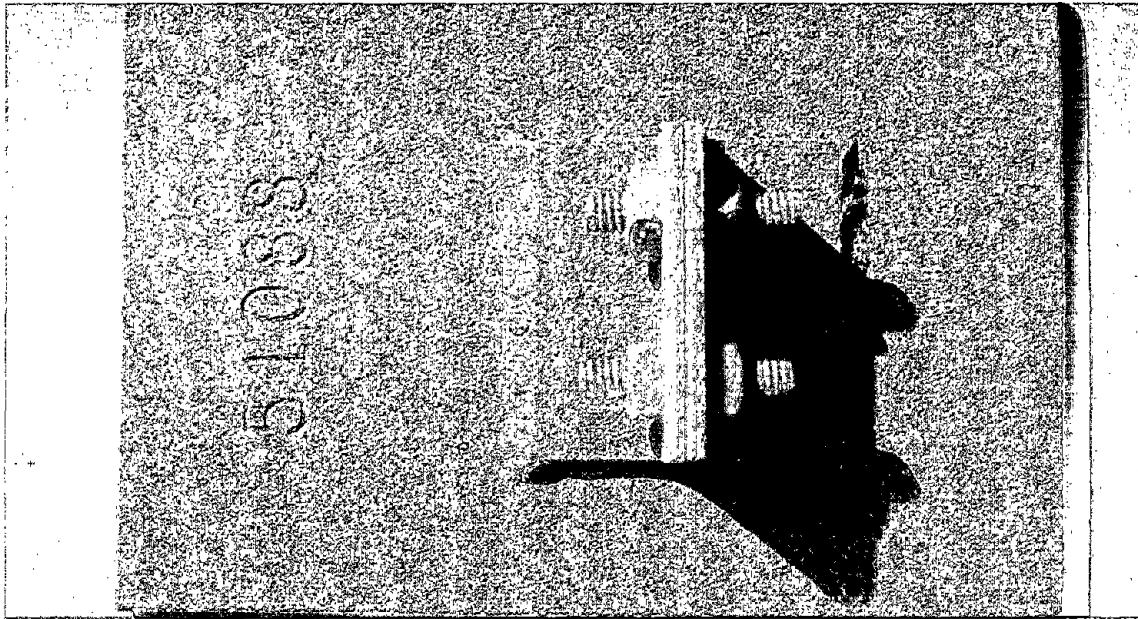
Before



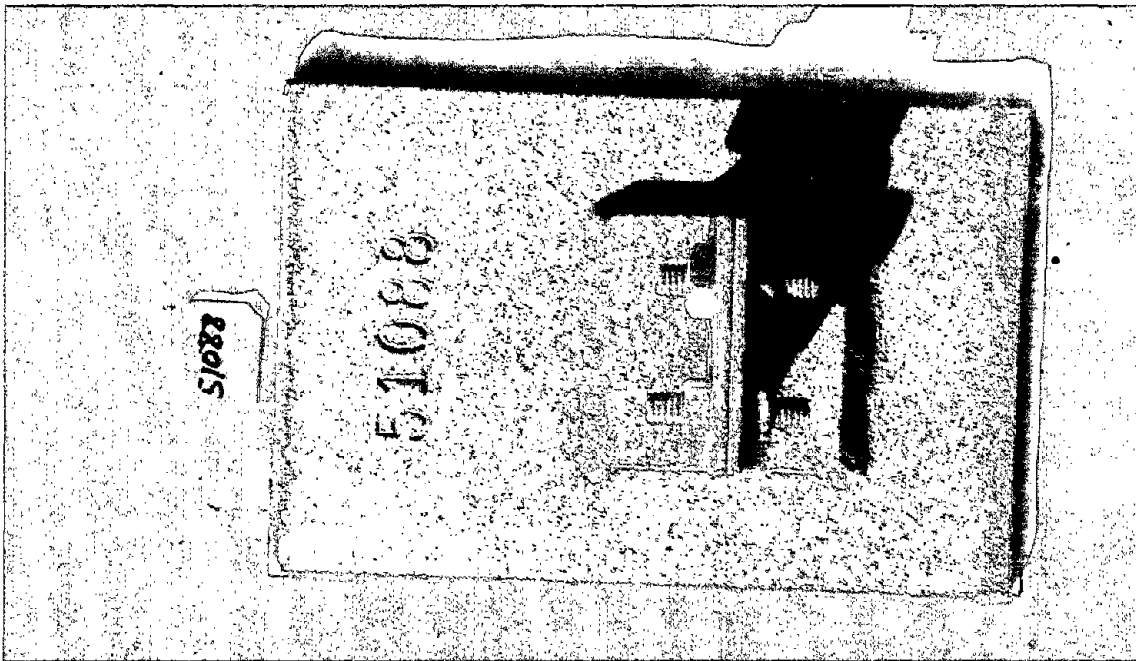
After

(b) Thermally sprayed Zn (85%)/Al (15%), cyclic test I.

Figure 68. Before-and-after photographs of the coated, non-flat test panels subjected to cyclic tests I and II (continued).



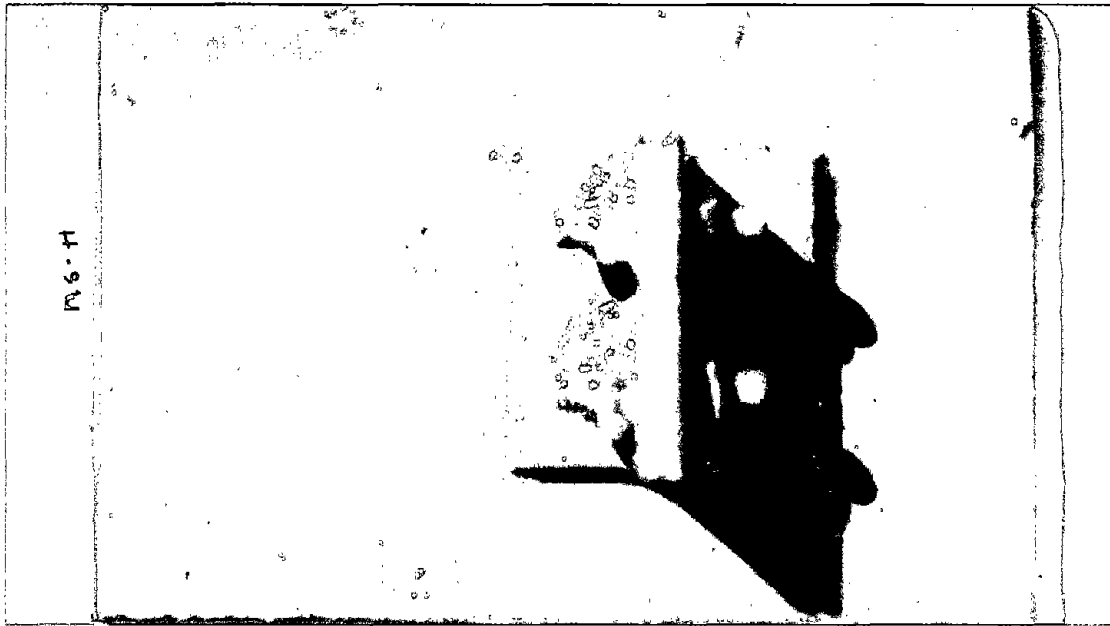
Before



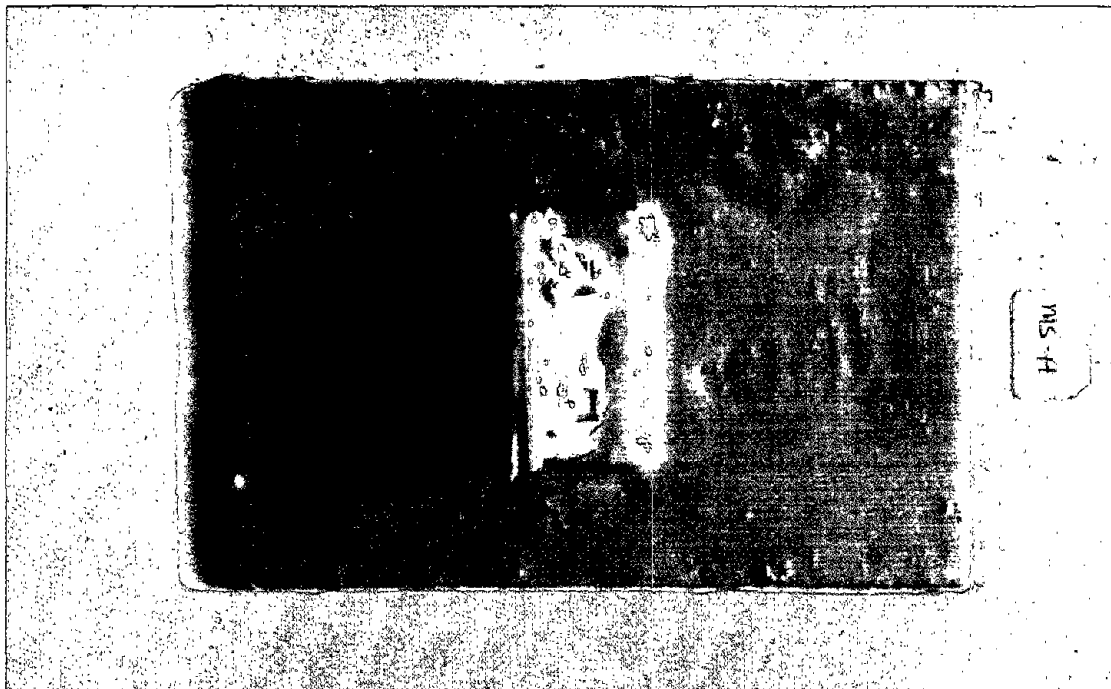
After

(c) Thermally sprayed zinc, cyclic test II.

Figure 68. Before-and-after photographs of the coated, non-flat test panels subjected to cyclic tests I and II (continued).



Before



After

(d) VOC-compliant coating, cyclic test II.

Figure 68. Before-and-after photographs of the coated, non-flat test panels subjected to cyclic tests I and II (continued).

Table 17. ASTM-D610 visual corrosion rating for the non-flat test panels.

Coating	Cyclic Test	Geometry	Corrosion Rating	Comments
T-S Aluminum*	I	Non-Flat 1	3, 2, 2	
	I	Non-Flat 2	5, 5, 3*	
	II	Non-Flat 1	7, 6, 1.5	Heavy Al corrosion product
	II	Non-Flat 2	8.5, 1.5, 1.5	
T-S Zn/Al	I	Non-Flat 1	5, 5, 6	
	I	Non-Flat 2	4, 5, 5	
	II	Non-Flat 1	5, 6, 6	
	II	Non-Flat 2	6, 5, 5	
T-S Zinc*	I	Non-Flat 1	10, 10, 10	
	I	Non-Flat 2	10, 10, 10	
	II	Non-Flat 1	10, 10, 10	Yellow staining
	II	Non-Flat 2	10, 10, 8	
VOC-Compliant	I	Non-Flat 1	10, 10, 10, 10**	
	I	Non-Flat 2	10, 10, 10, 10**	
	II	Non-Flat 1	10, 9	Edge chipped Cracking along bolt
	II	Non-Flat 2	10, 9	
Non-Flat 1 is flat panel with welded support.				
Non-Flat 2 is flat panel with welded and bolted right-angle brackets.				
*Corrosion rating reflects coating consumption.				
**One to three steel corrosion areas found on nut-and-bolt area.				

The corrosion rating for TS-aluminum was the worst of the four coatings, with a wide scatter of values between 1.5 and 8.5. Coating performance and durability was moderate to poor. The poor rating was due to significant consumption of the aluminum that caused large amounts of aluminum corrosion deposits on the surface of the coating, as seen in figure 68(a). Steel corrosion was also observed on the nut-and-bolt areas and at the weld and crevice between the two right-angle brackets. As noted for the TS-Zn/Al, an organic or TS-polymer overcoat might solve the problem of coating performance, although it appears that once the overcoat is compromised, significant consumption of the TS-aluminum coating would occur, which would further delaminate the overcoat.

In conclusion, the TS-zinc and VOC-compliant coated non-flat test panels gave the best coating performance and durability of the four coatings. The TS-Zn/Al coating gave moderate coating performance and better-than-average durability; the TS-aluminum gave poor coating performance and durability. The usefulness of the non-flat test panels in cyclic accelerated testing was demonstrated and showed cracking of the coating and significant steel

corrosion at the nut-and-bolt and welded bracket areas, observations that could not have been made on flat panels alone.

### Flat-Panel Results

Visual Rating. Figures 69(a) through (d) show representative before-and-after photographs of the five coatings on the flat test panels subjected to cyclic tests I and II. Table 18 lists the corrosion rating of each coating and test panel on a scale of 1 to 10, according to the ASTM-D610 visual corrosion rating standard.

The VOC-compliant and TS-zinc coatings performed the best of the five coatings, showing excellent coating performance and durability. The TS-zinc coating showed some discoloration due to zinc consumption, but steel substrate corrosion was not observed. The VOC-compliant coatings showed no discoloration, cracking, or rust spots on any of the test panels.

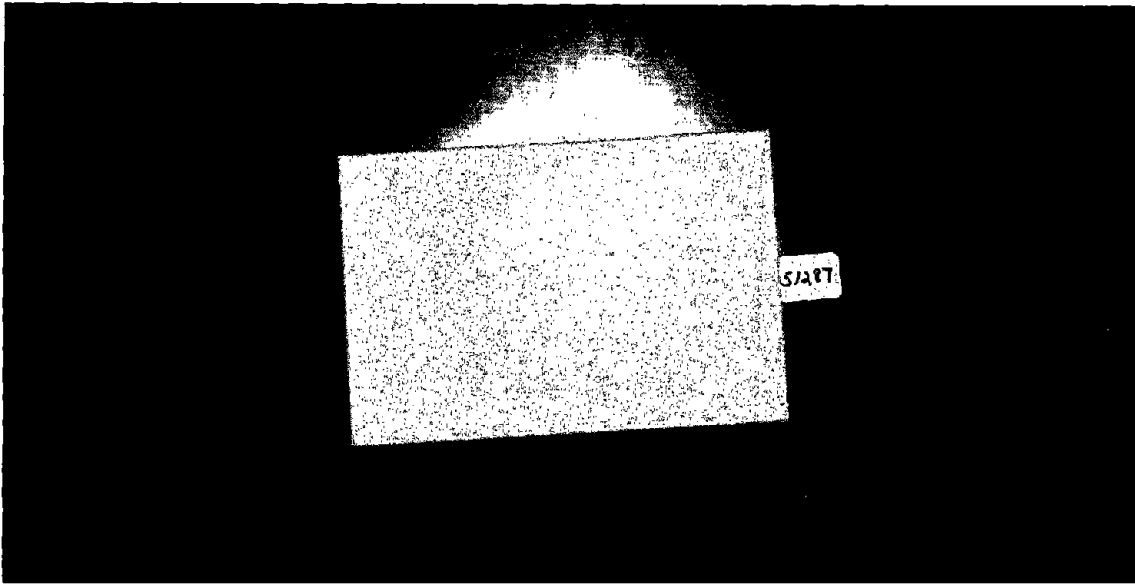
The TS-Zn/Al and TS-aluminum coated test panels showed moderate to better-than-average performance and durability. Alternating areas of a white corrosion product and dark discoloration were observed on the TS-Zn/Al coatings. Discoloration and aluminum corrosion pits were observed on the TS-aluminum coatings. However, steel corrosion rust spots were not observed on the test panels.

The Pb/alkyd coated test panels showed poor performance and durability of the coating. Significant steel corrosion was observed on the surface where the steel substrate appeared to have been exposed. However, discoloration of the alkyd topcoat was not observed.

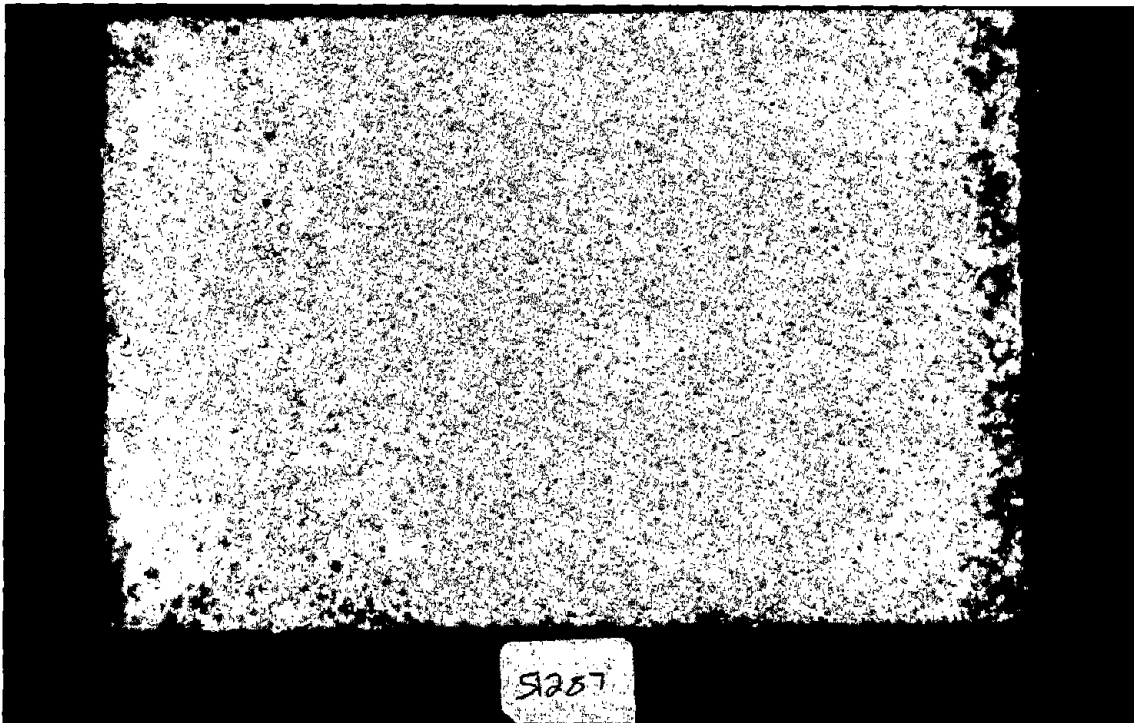
EIS Analysis. Figures 70(a) through (c) show the consumption rate of the thermally sprayed coatings, the corrosion rate of the steel underneath the TS-coatings, and  $\omega_{\max}$  (the frequency at maximum phase angle) for cyclic tests I and II. The TS-zinc coating gave negligible consumption rates throughout cyclic test I, as shown in figure 70(a). This corroborates with the excellent rating given by the visual observations and indicates that salt or water has not penetrated to the steel substrate. On the other hand, the TS-aluminum and TS-Zn/Al coatings gave initial coating consumption rates of 127 to 190  $\mu\text{m}/\text{yr}$  (5 to 8 mpy), which decreased with time to approximately 25 to 114  $\mu\text{m}/\text{yr}$  (1 to 4 mpy). These two sacrificial coatings are actively corroding and protecting the steel substrate. These results are also corroborated by the visual rating that showed significant coating consumption. In addition, steel corrosion rates were observed for the TS-aluminum and TS-Zn/Al after 670 h of exposure. The corrosion rate was less than 25  $\mu\text{m}/\text{yr}$  (1 mpy) for the TS-Zn/Al, but was 241  $\mu\text{m}/\text{yr}$  (9.5 mpy) for the TS-aluminum. Since steel corrosion was not observed visually on the surface of these coatings, corrosion must be occurring under the TS-aluminum coating. Thus, the EIS measurements were able to characterize the early onset of steel-substrate corrosion under the metallic coating before corrosion was observed visually.

Figure 70(b) shows consumption rates for the three TS coatings subjected to cyclic test II. In this case, the TS-zinc showed fairly high consumption rates before, during, and after the test. The TS-Zn/Al and TS-aluminum consumption rates were much lower than the TS-zinc, but were still significant. All three TS coatings are active and are protecting the steel





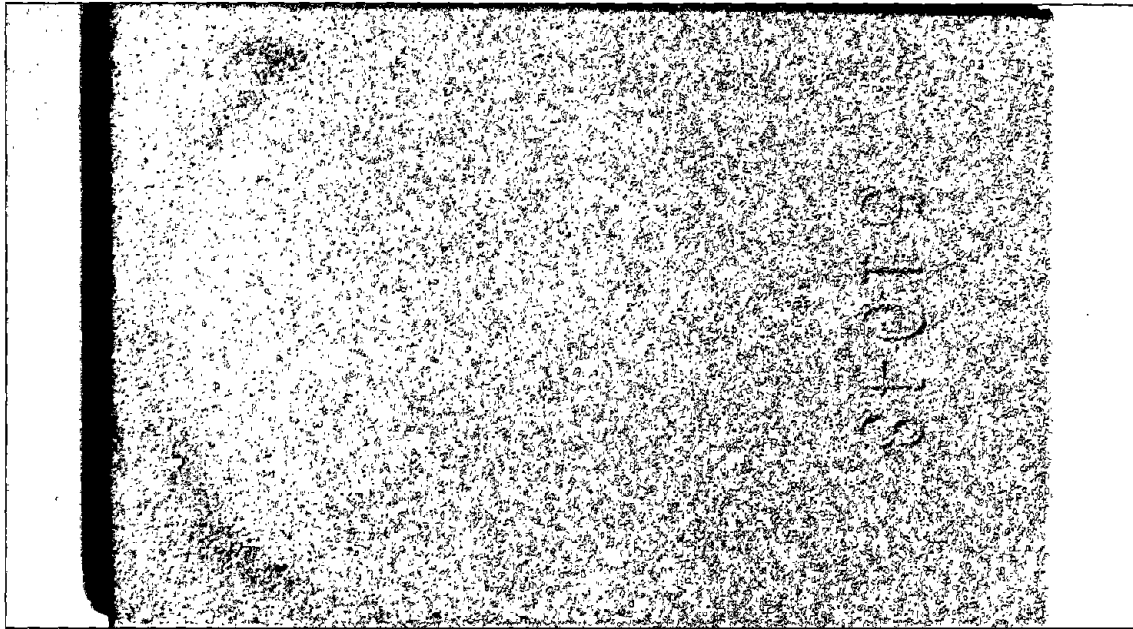
Before



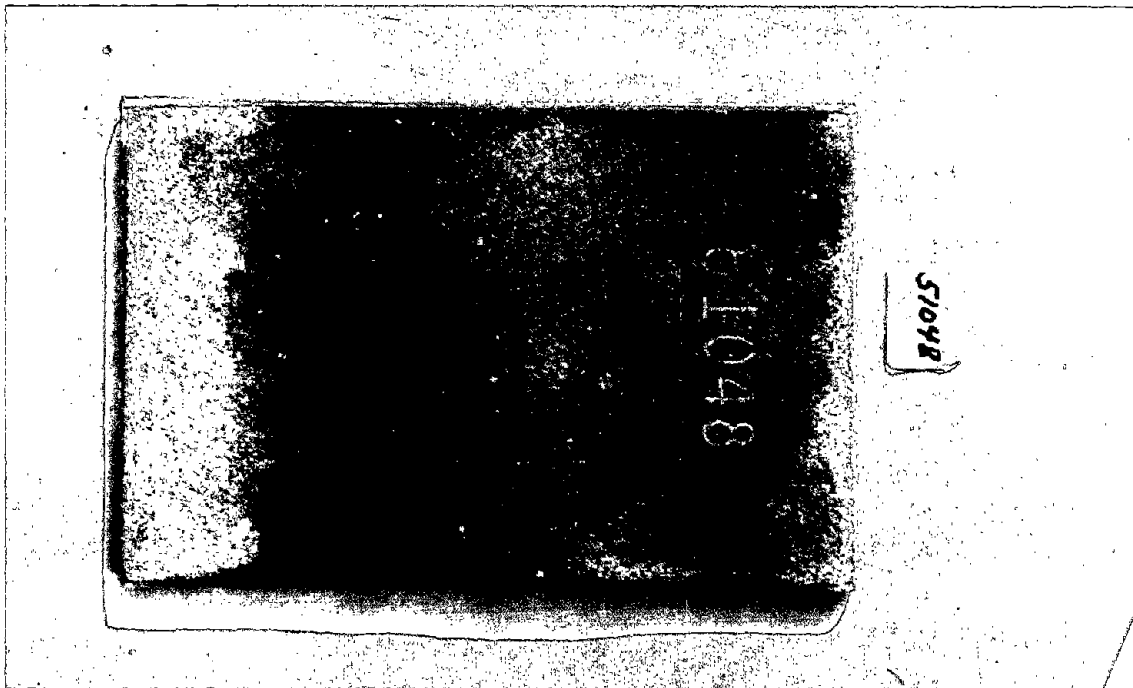
After

(a) Thermally sprayed aluminum, cyclic test I.

Figure 69. Before-and-after photographs of the coated non-flat test panels subjected to cyclic tests I and II.



Before



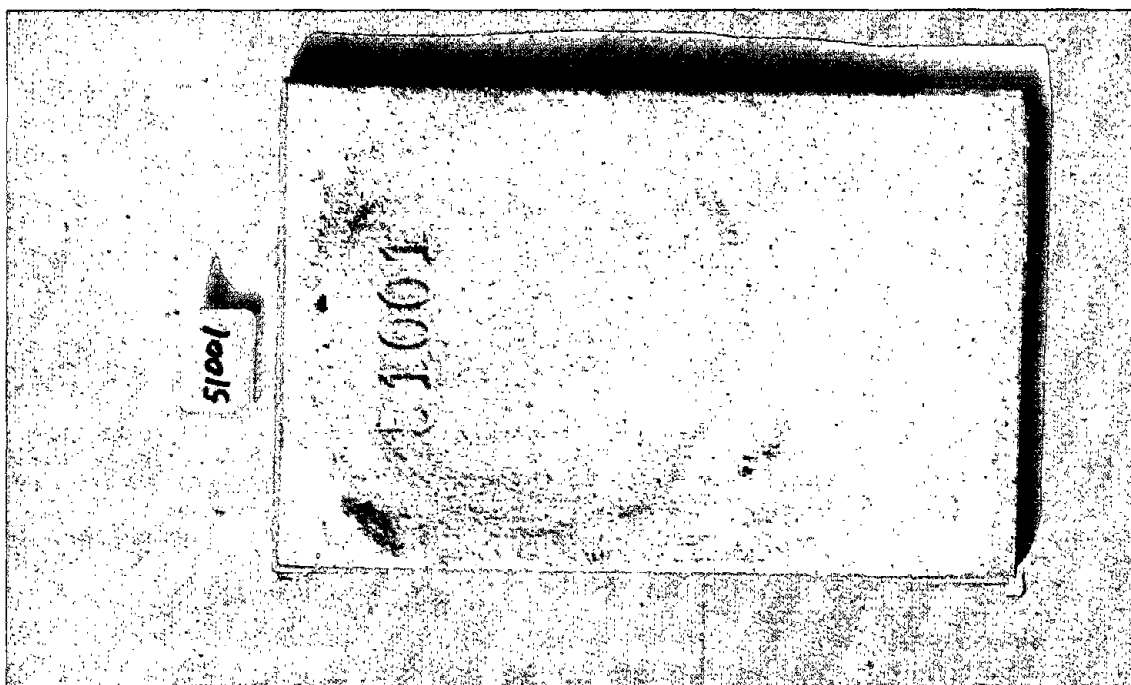
After

(b) Thermally sprayed Zn (85%)/Al (15%), cyclic test I.

Figure 69. Before-and-after photographs of the coated non-flat test panels subjected to cyclic tests I and II (continued).



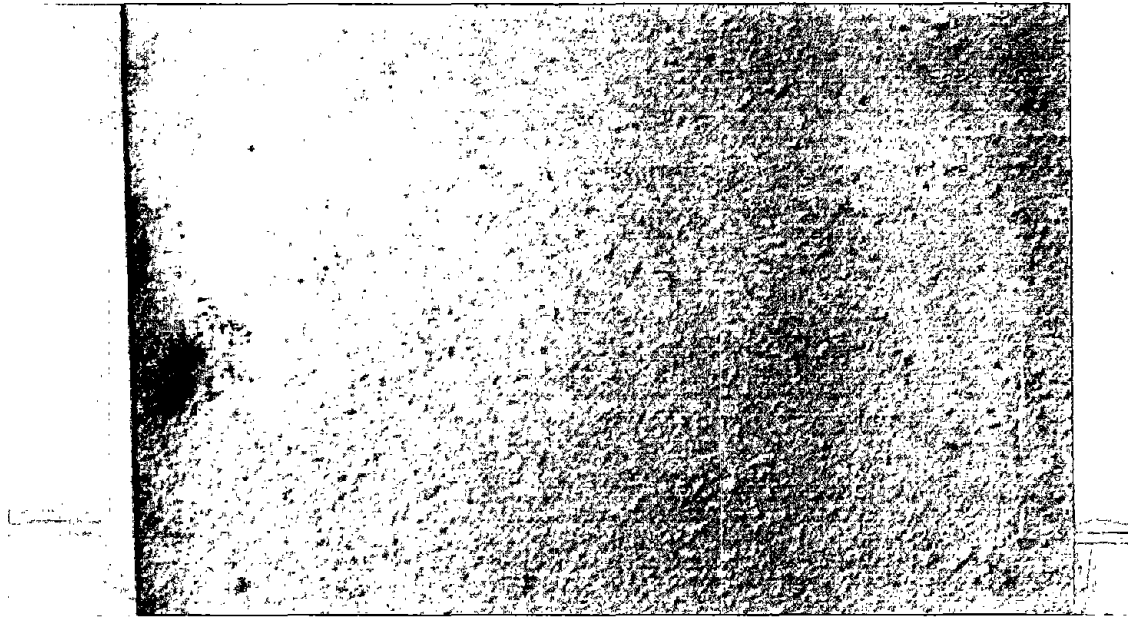
Before



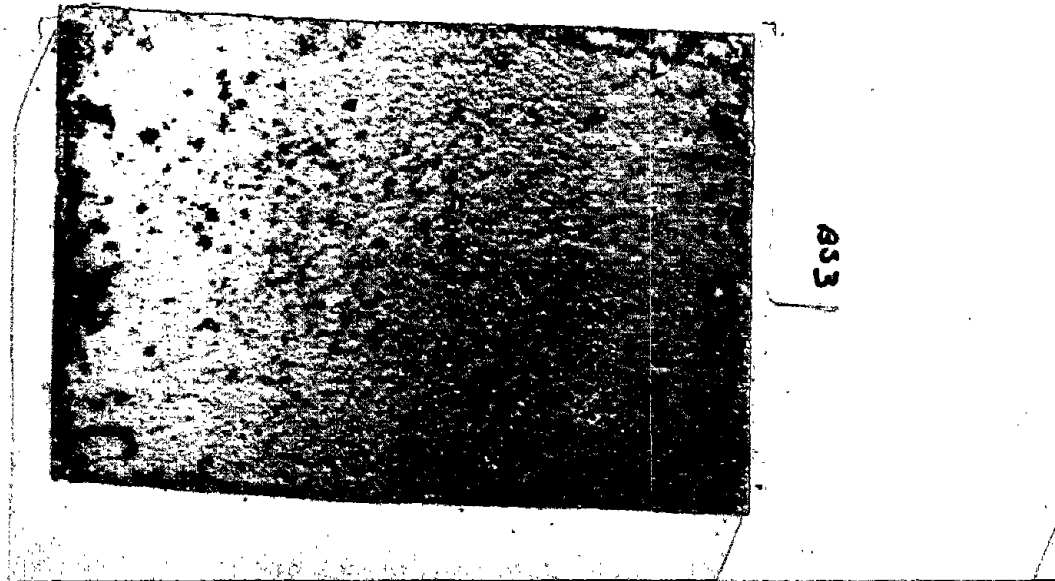
After

(c) Thermally sprayed zinc, cyclic test II.

Figure 69. Before-and-after photographs of the coated non-flat test panels subjected to cyclic tests I and II (continued).



Before



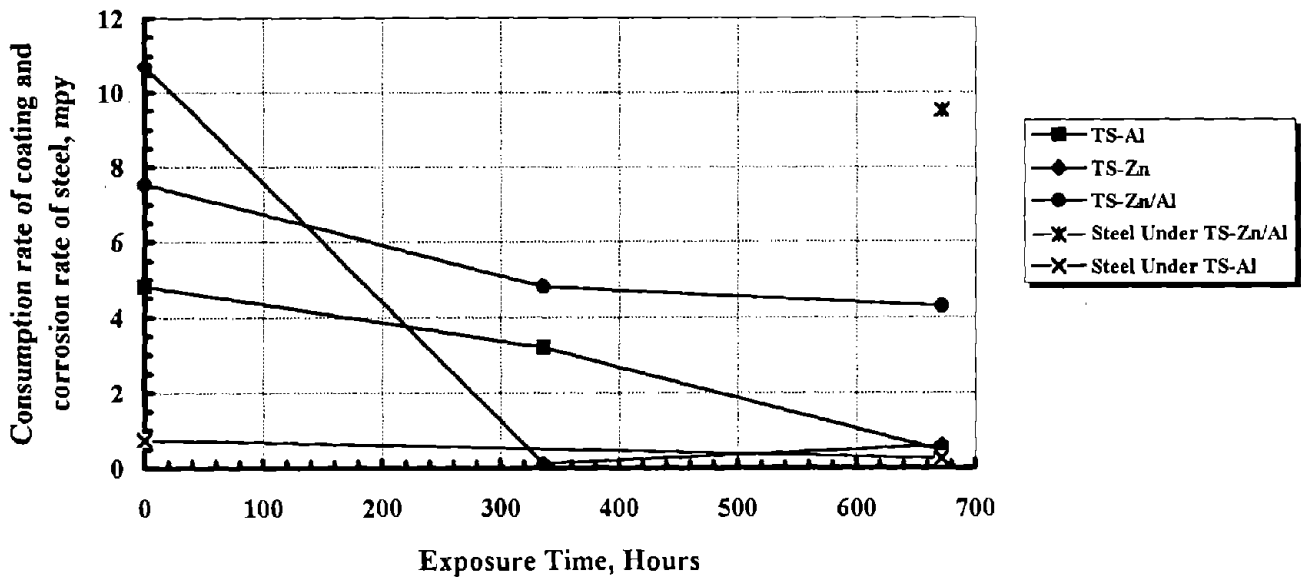
After

(d) Pb/Alkyd weathered coating, cyclic test II.

Figure 69. Before-and-after photographs of the coated non-flat test panels subjected to cyclic tests I and II (continued).

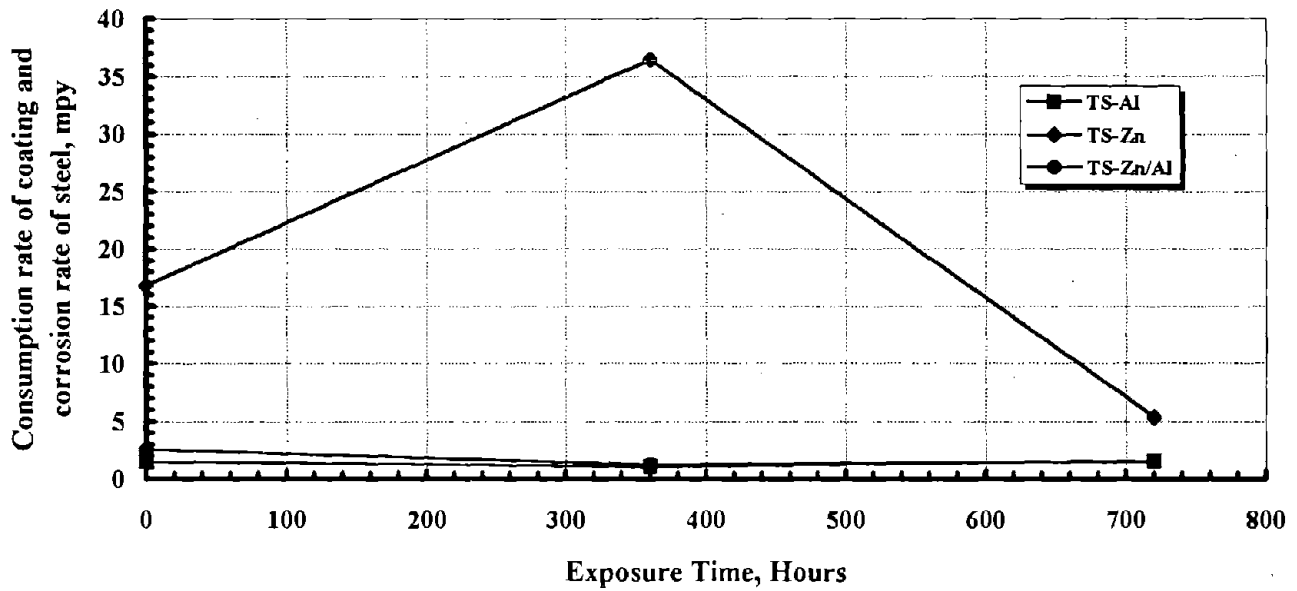
Table 18. ASTM visual corrosion rating for the flat test panels.

Coating	Cyclic Test	Corrosion Rating
T-S Aluminum	I	6, 8, 8
	II	9, 8, 8
T-S Zn/Al	I	7, 8, 8
	II	7, 7, 8
T-S Zinc	I	10, 10, 10
	II	10, 10, 10
Pb/Alkyd	II	2, 2, 3
VOC-Compliant	I	10, 10, 10, 10, 10, 10
	II	10, 10, 10, 10, 10, 10

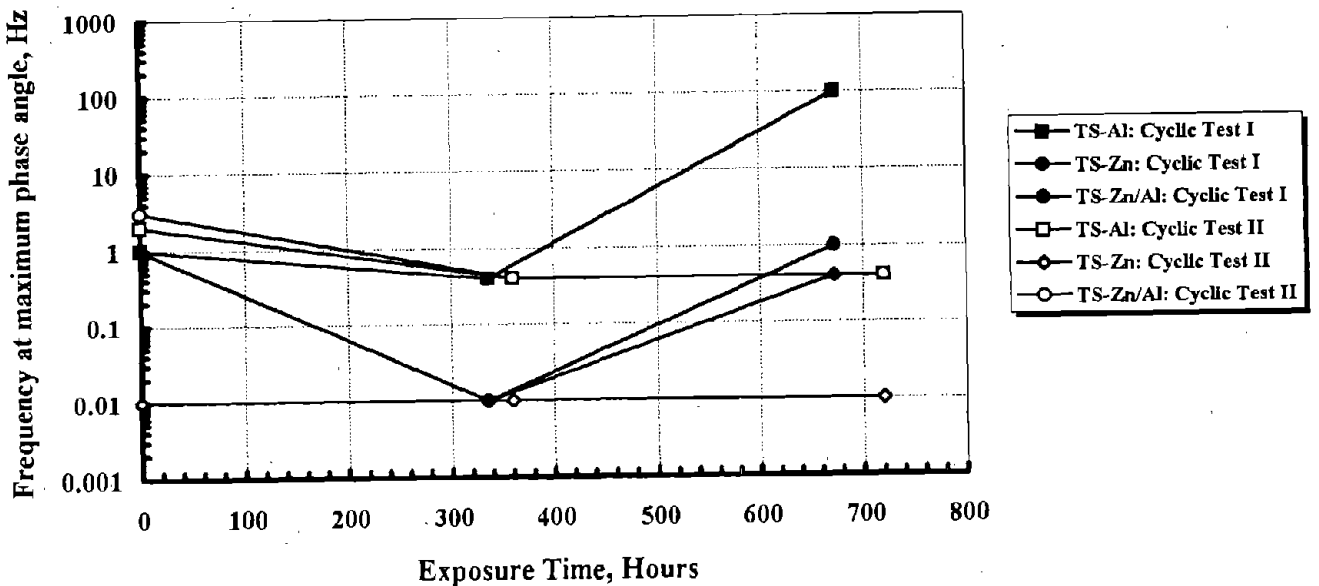


(a) Consumption rate of the coating and corrosion rate of the steel, cyclic test I.

Figure 70. Electrochemical parameters for the thermally sprayed coatings in the cyclic tests.



(b) Consumption rate of coating and corrosion rate of steel, cyclic test II.



(c) Frequency at maximum phase angle.

Figure 70. Electrochemical parameters for the thermally sprayed coatings in the cyclic tests (continued).

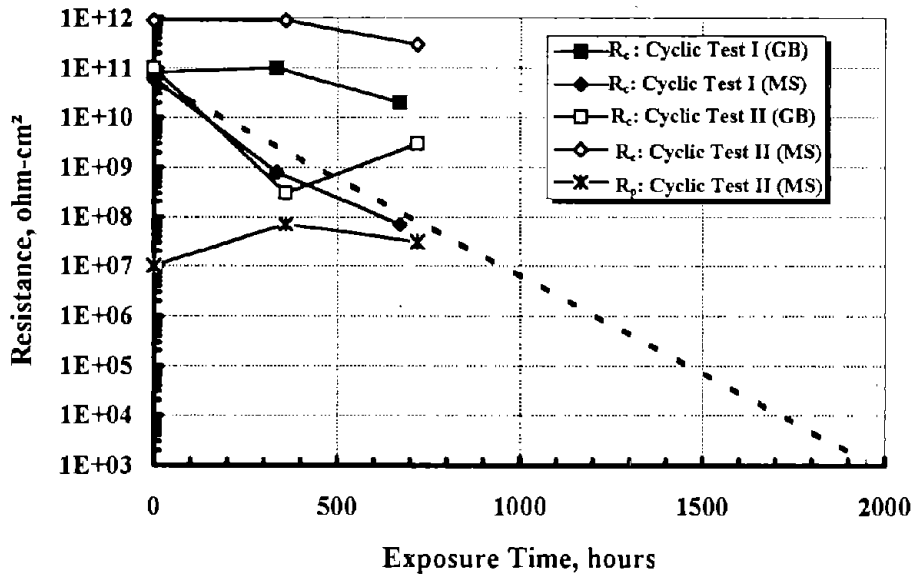
substrate underneath. Steel corrosion rates were not observed for the test panels in cyclic test II, however. As noted earlier, the salt-spray exposure time is half of the cyclic test, or 360 h. Increasing the total exposure time of cyclic test II would provide a longer salt-spray exposure that when coupled with freeze/thaw cycling and UV exposure, would accelerate the onset of corrosion under the coatings.

Figure 70(c) shows  $w_{\max}$  for the three TS coatings subjected to cyclic tests I and II. In general, the low values of  $w_{\max}$  indicate active, corroding metals. The values also agree with the results from the immersion experiments that showed similar consumption rates and values of  $w_{\max}$ . As noted earlier,  $w_{\max}$  appears to be a sensitive indicator of the consumption rates of the TS coatings. In addition, the onset of steel corrosion was observed by EIS in approximately 670 h of accelerated exposure time. Increasing the total exposure time to 1400 h (2 mo) would be sufficient to further quantify steel corrosion underneath the coatings and determine how long the TS coatings can adequately protect the steel substrate.

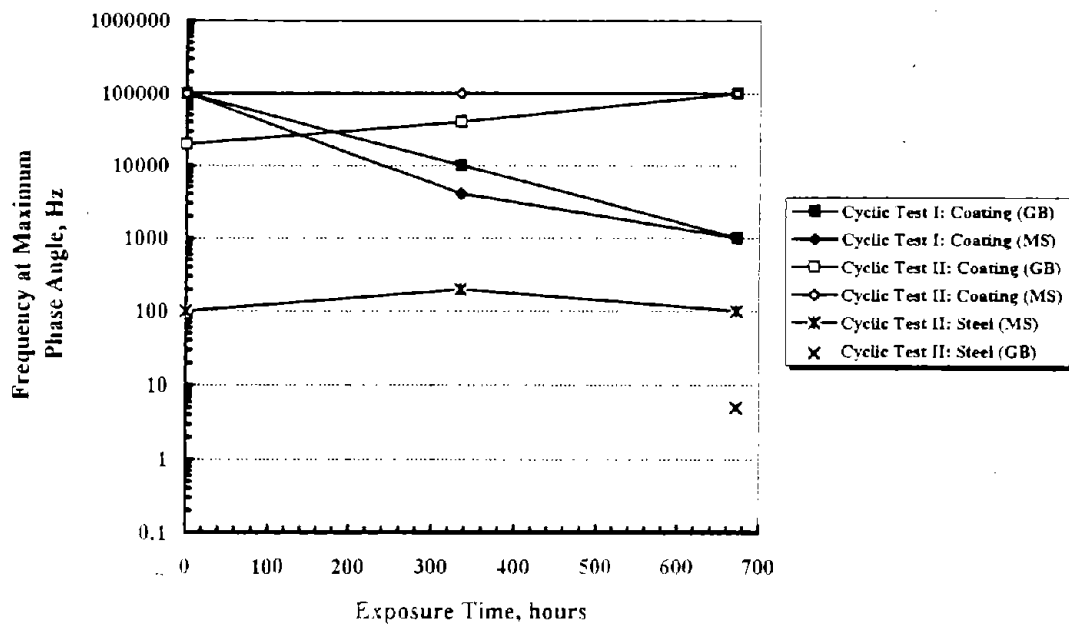
The coating resistance, polarization resistance, and  $w_{\max}$  for the VOC-compliant coating subjected to cyclic tests I and II are given in figures 71(a) and (b). The coating resistance was high for all of the test panels, but decreased by two to three orders of magnitude for several of the test panels. Electrolyte penetration into the coating was occurring, but there did not appear to be any trend for surface condition or accelerated test method. In addition, a test panel with a millscale surface subjected to cyclic test II showed measurable steel corrosion underneath the coating, even though corrosion was not observed visually. Thus, it is necessary to measure the onset of steel corrosion underneath organic coatings before it is visually seen. Still, a longer exposure period is needed to further validate steel corrosion and coating degradation. Extrapolation of the coating resistance for two of the test panels showed that a total exposure time of 1500 to 1900 h (2 to 2-1/2 mo) would be needed to reduce the coating resistance to values similar to a degraded coating.

EIS was able to reduce the coating resistance to values similar to a degraded coating. Steel corrosion underneath the coating would be initiated as well in that time period.

Figure 71(b) shows  $w_{\max}$  for the VOC-compliant coatings subjected to cyclic tests I and II. The  $w_{\max}$  due to the coating decreased two orders of magnitude for the test panels subjected to cyclic test I, following the trend of decreasing coating resistance and indicating that the electrolyte is penetrating the coating. The  $w_{\max}$  due to steel corrosion on a coated panel with a millscale steel surface was low, indicating that significant corrosion was occurring underneath the coating. A coated test panel with a grit-blasted surface gave a measurable  $w_{\max}$  due to steel corrosion after testing, which suggests that the onset of corrosion occurred sometime between 360 and 720 h of exposure time.



(a) Coating and polarization resistance.



(b) Frequency at maximum phase angle.

Figure 71. Electrochemical parameters for the VOC-compliant coating in the cyclic tests (GB means grit-blasted surface, MS means millscale surface).



## Conclusions and Recommendations

Based on the research performed in this task, it can be concluded that:

- \* The cyclic exposure tests and immersion experiments combined with EIS measurements provide an early indication of coating degradation, degree of water penetration, and the onset of steel corrosion underneath a coating before it is visually seen in a relatively short period of time.

EIS measurements performed on the flat test panels in the cyclic salt-fog test, the cyclic salt-fog, freeze-thaw, and UV-exposure test, and the immersion experiments allow determination of the consumption rate of sacrificial coatings, quantification of coating degradation, and determination of the onset and extent of steel corrosion, after 1 mo of cyclic exposure and 3 to 6 mo of immersion. EIS was able to distinguish between the highly resistive VOC-compliant coatings that were beginning to degrade and the weathered Pb/alkyd coating with corrosion of the steel substrate underneath. Estimates made from the change in coating resistance and frequency at maximum phase angle with exposure period indicate that cyclic tests of 1400 to 1900 h (2 to 3 mo) and immersion experiments of 12 to 18 mo should provide further verification of coating degradation and steel-substrate corrosion. These measurements can then be correlated with EIS measurements performed on similar coatings subjected to long-term, outdoor exposure to further validate prediction of long-term coating degradation and failure with these methods.

- \* The TS-zinc and VOC-compliant coatings showed excellent coating performance and durability on the flat test panels. The TS-Al and TS-Zn/Al coatings gave moderate to better-than-average results, and the naturally weathered Pb/alkyd coating gave poor results.

The TS-zinc and VOC-compliant coatings performed well in the three accelerated tests, with no visible corrosion of the steel substrate. However, the coating resistance for the VOC-compliant coating decreased with exposure time, indicating that the electrolyte was penetrating into the coating. Corrosion of the steel was also evident from the EIS measurements, but was not observed visually. The TS-zinc coating showed a significant consumption rate. Steel corrosion was not observed visually or by EIS measurements confirming that the TS-zinc was adequately protecting the steel substrate.

The TS-aluminum and the TS-Zn/Al coatings gave moderate coating performance and durability. Strongly adhered corrosion deposits on the coating surface provided evidence of aluminum consumption for the test panels subjected to 1 mo of cyclic salt-fog exposure. Corrosion of the steel substrate was measurable on both coatings, even though it was not observed visually.

The weathered bridge section with the Pb primer/alkyd topcoat performed the worst of the five coatings. The coating resistance was low and steel corrosion was evident visually and from the EIS measurements. The results provide a baseline for a weathered coating further subjected to accelerated weathering. The changes in the EIS parameters due to accelerated testing can be compared with EIS parameters of coatings still in service to identify their state of coating degradation and possibly to predict future degradation and failure.

- \* The TS-zinc and VOC-compliant coatings gave better-than-average to excellent coating performance and durability on the non-flat panels containing welded and bolted brackets. The TS-Zn/Al gave moderate coating performance and the TS-Al showed poor results.

Modifying the flat test panel to include a nut and bolt and a welded bracket allowed coating performance and durability to be simulated on non-flat areas of a bridge, such as overlapping joints and welded supports. Rust spots and cracking were observed on the nut-and-bolt area and on the edges of the welded brackets, whereas the flat sections of the panels were usually corrosion-free. The TS-zinc and VOC-compliant coatings gave the best performance, with visual ratings of 8 to 10 observed on the test panels. Cracking of the coating and evidence of steel-substrate corrosion at the nut-and-bolt area were observed for the VOC-compliant coated test panels subjected to the cyclic salt-fog, freeze-thaw, and UV-exposure test. Thermal stresses appear to have been sufficient to cause coating delamination. The TS-Zn/Al gave moderate coating performance and better-than-average durability. White pits of corrosion products and roughness of the surface due to coating consumption were observed. The TS-aluminum coating gave poor coating performance and durability, with considerable amounts of aluminum corrosion deposit seen and steel corrosion observed due to aluminum consumption on the nut-and-bolt areas of the panel.

Based on the conclusions from this task, the following recommendations for future work are given:

- \* Perform additional experiments using a longer cyclic exposure and immersion period.

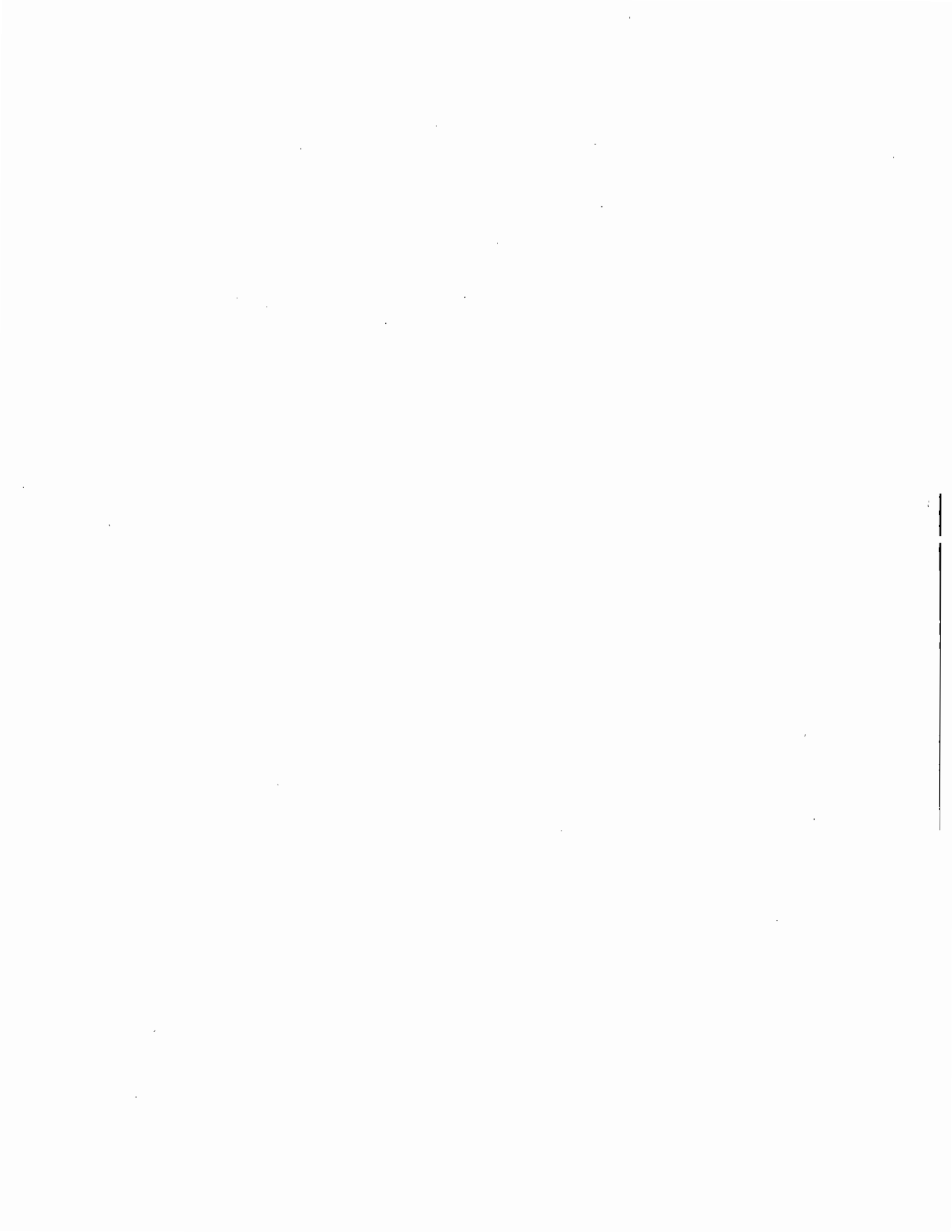
Based on estimates from the EIS parameters, a longer cyclic exposure and immersion period would further verify coating degradation and the onset of substrate corrosion. The experiments should also include additional analysis on the coated test panels, such as optical and surface analysis, to provide supplementary evidence of coating degradation. In addition, further refinement of the accelerated tests can be accomplished by performing serial experiments. Test panels will be taken out periodically and analyzed to determine the shortest exposure period needed to determine coating degradation and failure.

- \* Conduct accelerated experiments on additional thermally sprayed and organic coatings.

In addition to the TS-zinc, TS-aluminum, and TS-Zn/Al, a combination of thermally sprayed metal and polymer should be investigated using the accelerated tests. Such a coating system would typically be used on a bridge, since it combines the sacrificial properties of the metallic coatings with the barrier characteristics of the polymer. In addition, other VOC-compliant organic coatings should also be studied to quantify their coating degradation characteristics and to determine whether the onset of steel corrosion can be predicted.

- \* Conduct EIS measurements on field-exposure test panels and on coated steel bridges to evaluate the viability of field EIS measurements and their correlation with cyclic accelerated tests.

EIS measurements taken on coated test panels subjected to long-term outdoor exposure as well as measurements taken on coating systems presently applied to steel bridges and in various states of degradation, should be performed. Such measurements would allow the investigation of the viability of field EIS measurements and the determination of whether results from cyclic accelerated tests can be correlated with field-obtained EIS parameters such as coating resistance, polarization resistance, and  $\omega_{\max}$  (the frequency at maximum phase angle).



## CHAPTER 7: TASK F - PRODUCTIVITY IMPROVEMENT

### Introduction

The objective of this task was to apply state-of-the-art technology with the goal of improving productivity and enhancing quality control. After discussions with various DOT's, contractors, consultants, and paint suppliers, it was determined that the application of sensors to the maintenance, repair, and replacement of coating systems offered an immediate opportunity to improve productivity through increased performance of coating systems. Although estimates vary, it is believed that over 70 percent of coating-system failures are the result of improper surface preparation or poor coating application techniques. It is apparent that improvements in quality control of the painting application process would reduce coating failures. In addition, it would also have a major impact on the reduction of life-cycle costs for the bridge maintenance system through increased durability of a quality paint application. This chapter presents brief discussions of several techniques, including both monochrome and color-visible techniques as well as near-infrared imaging. The increased availability of low-cost digital imaging devices coupled with the availability of rugged low-cost powerful computers make these techniques practical for their application in the field. The utilization of sophisticated signal-processing techniques will allow these imaging devices to provide easily interpreted results that can be generated by inspection personnel with minimal technical training.

The techniques described below are global in nature, allowing inspection of significant areas of the bridge structure. They have the potential to provide a quantifiable assessment of the quality of the paint prior to surface preparation and, subsequently, the quality of the application of the paint system. Finally, the examples presented are the results of application of the techniques in the laboratory on coated steel panels and work in the field.

### Degree of Surface Rusting

ASTM has developed a standard method for the evaluation of the degree of rusting on painted steel surfaces.<sup>(10)</sup> A scale of rust grades ranging from 0 to 10 that correspond to 100-percent rust for grade 0, and no rust or less the 0.01 percent of surface rusted for grade 10. The following photographic standards—labeled 4, 6, 8, and 9, which correspond to 10-, 1-, 0.1-, and 0.03-percent rust, respectively, were used in this study. The application of this standard requires that the inspector judge the rust grade by visual comparison of the actual bridge with these standards. It is relatively simple to apply image-processing techniques to a digitally recorded image of the surface and quantitatively measure percentage of rusting. This concept was explored using a monochrome digital camera to record the images of the photographic standards discussed above. The application of a simple threshold (assigning 0 or 1 based on gray scale) followed by a count of picture elements (pixels) could be used to quantitatively measure percentage of rust. The primary difficulty with this method is the sensitivity, where a shift in threshold results from shifts in the gray scale of the obtained image. A better approach would be to compute the contour of each rusty point and then measure its size, followed by a total count of the contoured areas. This approach tends to be more tolerant to gray scale variations. An example of the results obtained using the Steel

Structures Painting Council (SSPC) photographic standards as test samples is shown in figures 72 through 75. A contouring algorithm was used to compute the percentage of rust in an area and the corresponding rust grade is automatically printed in the upper left-hand of the recorded image. This approach can be made to easily sort the photographic standards. After calibration to the ASTM D610-85 photographs, verification of the technique was performed on actual steel panels used as an equivalent National Association of Corrosion Engineers (NACE) standard. How well it will function on actual bridge areas where the contrast and the recorded gray scales may not be as good as these photographic standards needs to be determined. This technique needs to be applied to actual bridge surfaces or pieces of bridges where comparison to manually measured rusted area can be performed. Tests of this type would allow evaluation of performance under conditions that include aged or faded paint, dark colors, and surface contaminants such as grease or dirt stains. Tests also need to be performed under typical field conditions to determine minimum lighting requirements.

#### Evaluation of Blast-Cleaned Surface

The degree of cleanliness of a steel surface prior to paint application is critical to the durability of the paint. This quality in the maintenance painting process is frequently not maintained. A means of objectively evaluating the blasted surface prior to painting would be a valuable aid in improving the quality control of the process. Current practice makes use of the visual degree of cleanliness standard.<sup>(11)</sup> Ultimate responsibility lies with the inspectors and is critically dependent on their skills and dedication. If a paint failure occurs, there is no traceable data other than what has been documented by the inspector. A stored digital image should be capable of providing a quantitative real-time and permanent record of the surface condition. The simple monochrome techniques described previously may have differentiation problems associated with the subtleties of the cleaned surface. A technique based on color measurement would be more applicable. An example of this approach can be seen in figures 76 through 78. These histograms show the distribution of pixel values for the red, blue, and green elements of images recorded from the A SP-10 and A SP-5 standard photographs of blast-cleaned surfaces. The vertical axis in the figures represents the number of pixels that have a specific value (intensity). The x-axis represents intensity with 0 being black and 300 saturation. The histograms of the A SP-10 and A SP-5 standards show that the centers of the distributions are distinctly shifted for each color component. Furthermore, the green component, figure 78, shows a clear difference between the peaks of the distributions for the two test samples. These results show that color measurements have promise for detecting subtle differences in cleaned surfaces. The approach should also allow the percentage of rust to be measurable despite the presence of paints having similar coloring.

#### Quantitative Measurement of Damaged Area

A visual evaluation procedure has been developed (based on the red/green/blue techniques described above) and tested that can determine the percentage of rusted and/or damaged paint. In this procedure, the image is acquired by use of a color CCD camera (figure 79). The recorded images are enhanced by state-of-the-art techniques pioneered by NASA and the military. These techniques

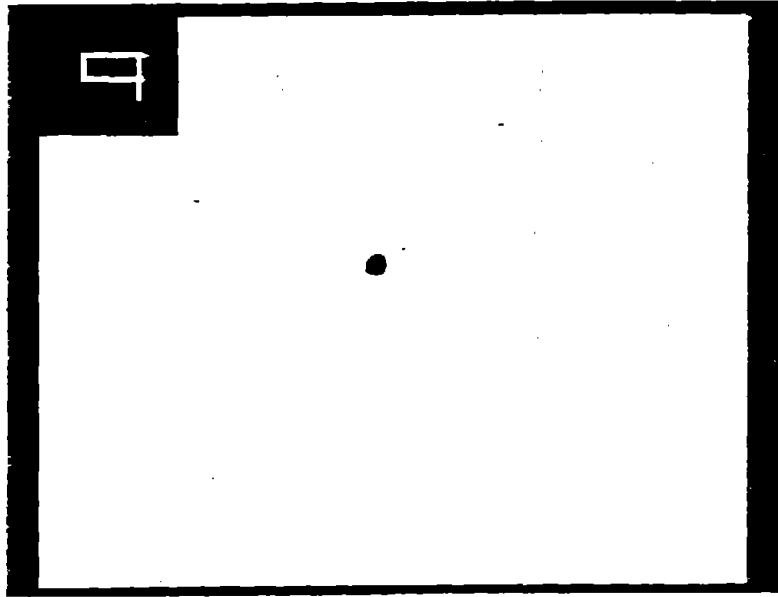


Figure 72. Results of image analysis of standard for rust grade 9 (0.03-percent rust).

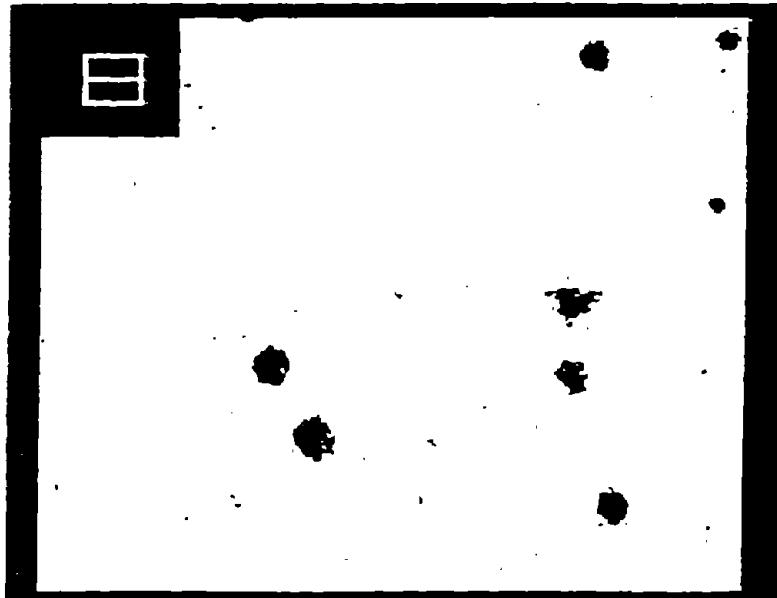


Figure 73. Results of image analysis of standard for rust grade 8 (.01-percent rust).

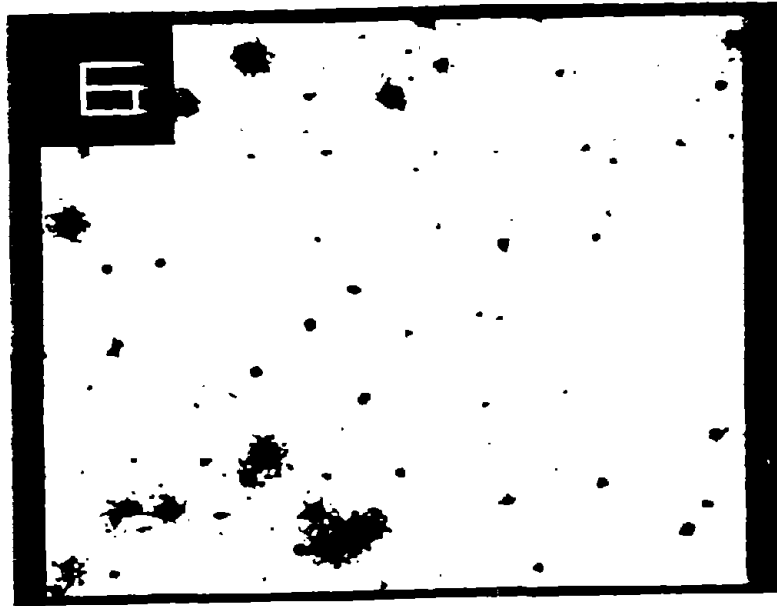


Figure 74. Results of image analysis of standard for rust grade 6 (1-percent rust).



Figure 75. Results of image analysis of standard for rust grade 4 (10-percent rust).



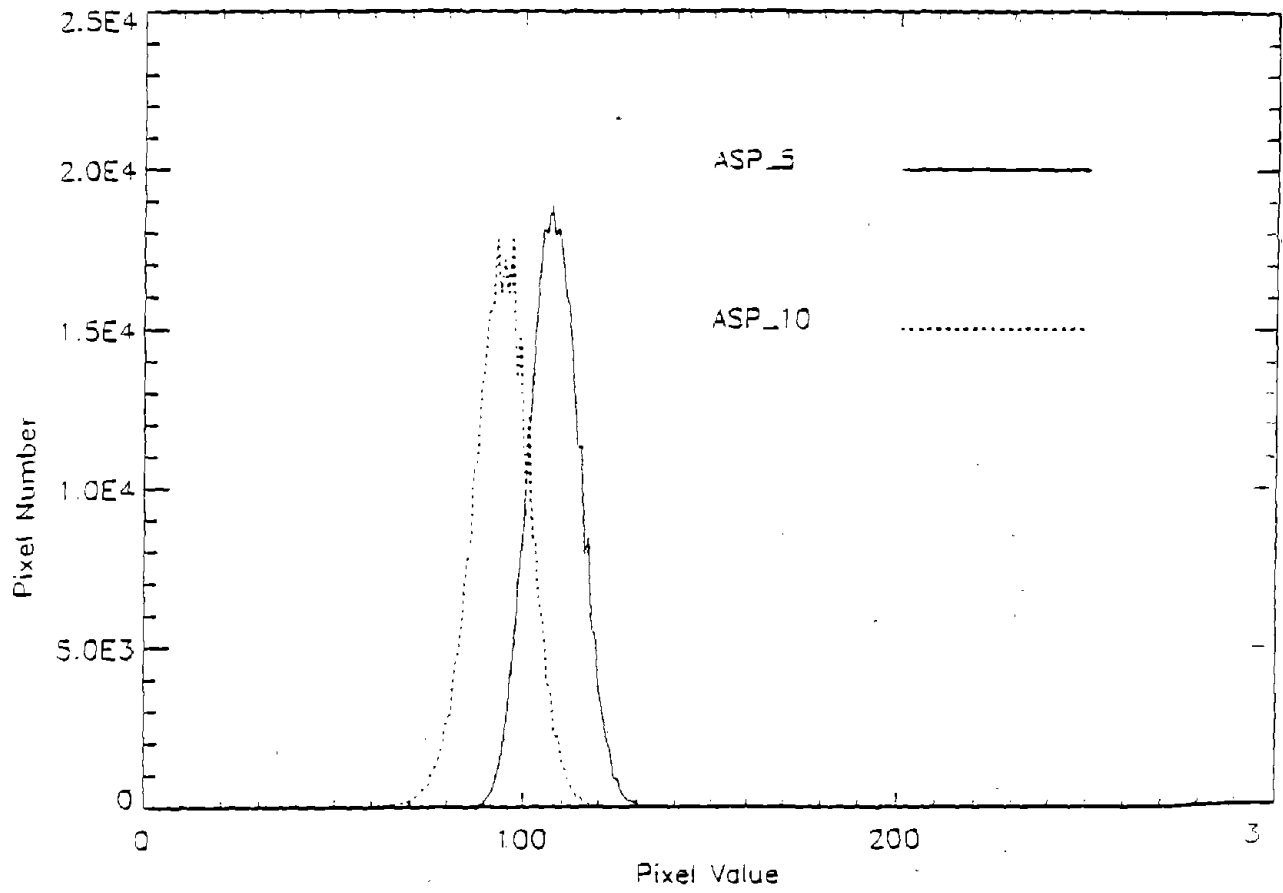


Figure 76. Histogram of red element.

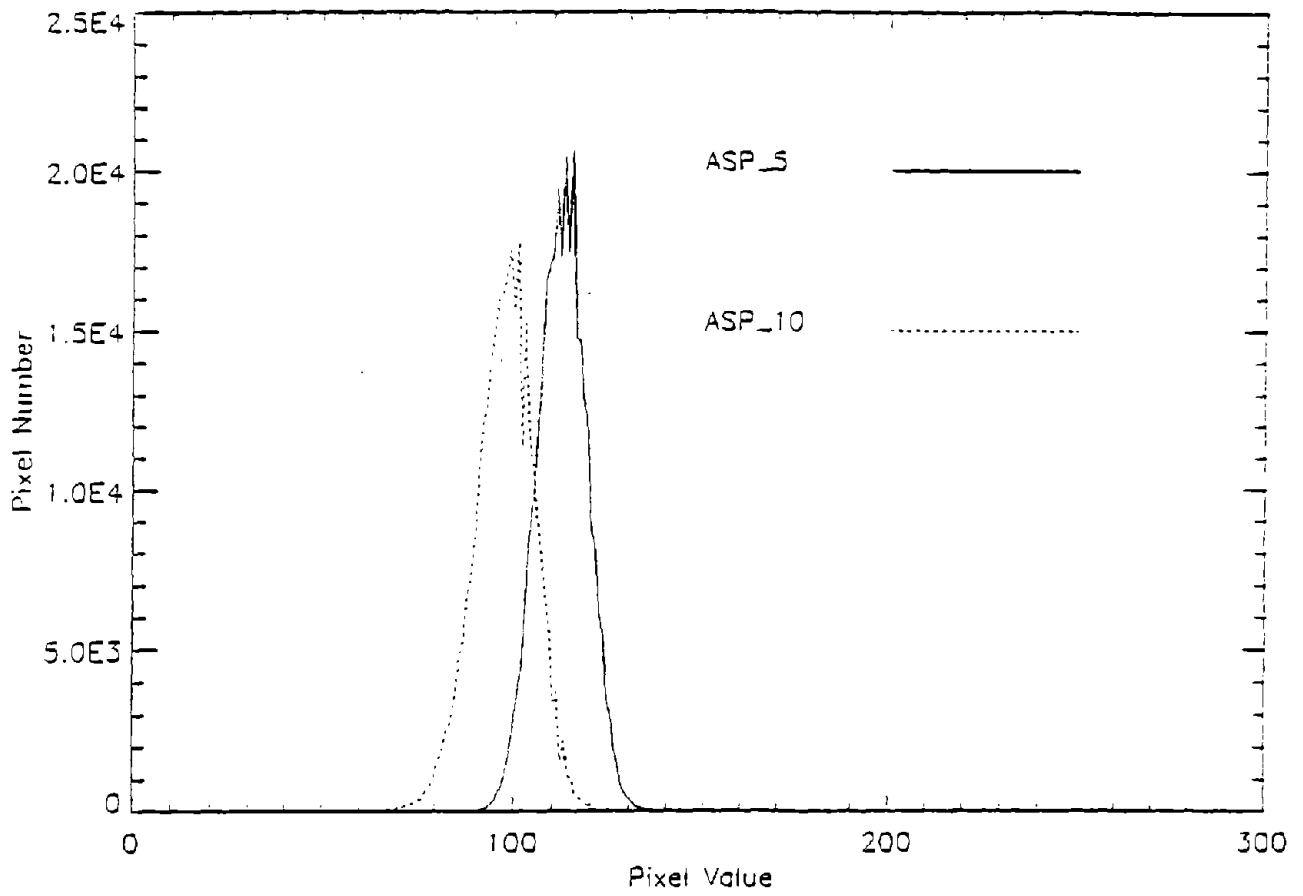


Figure 77. Histogram of blue element.

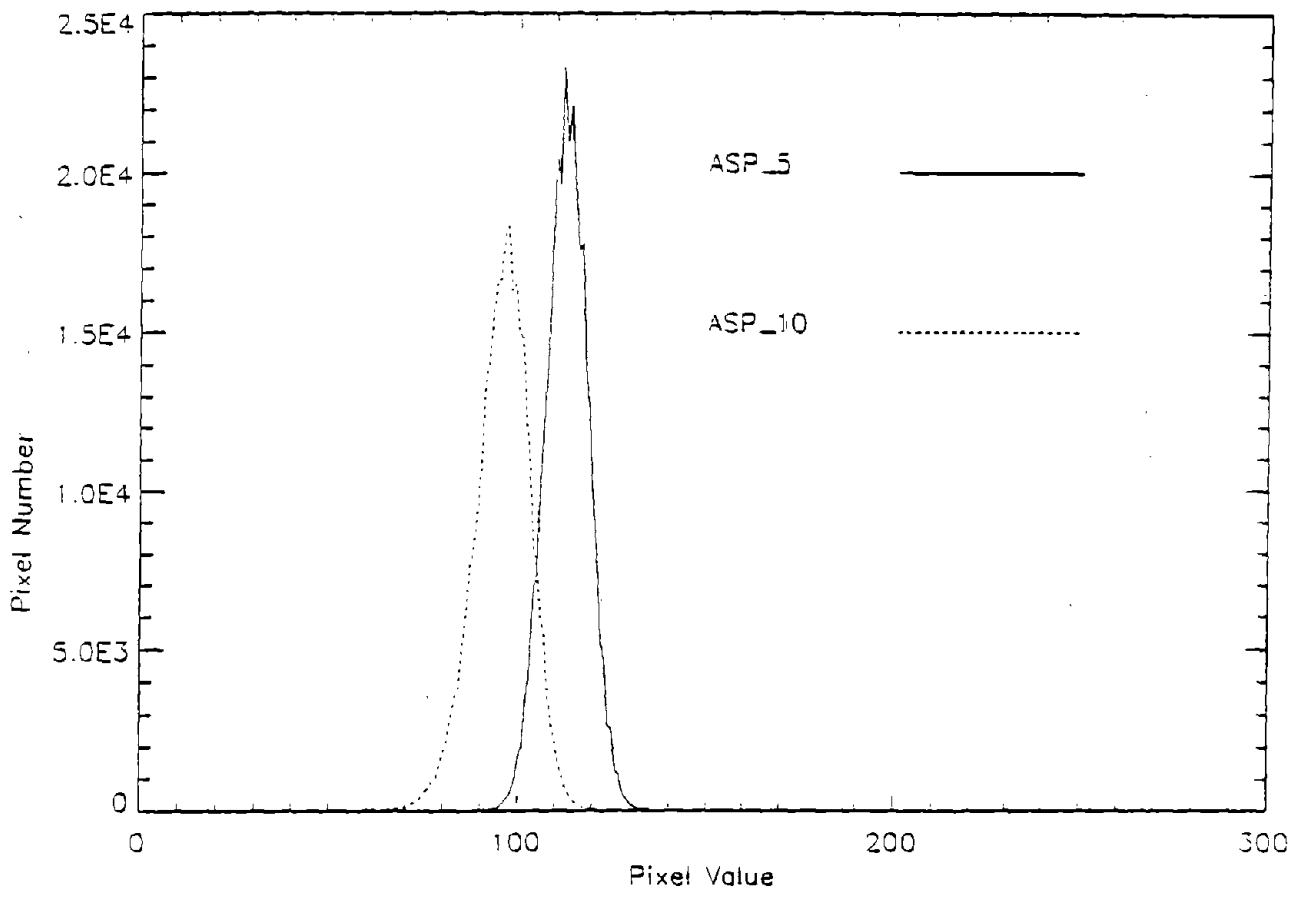


Figure 78. Histogram of green element.

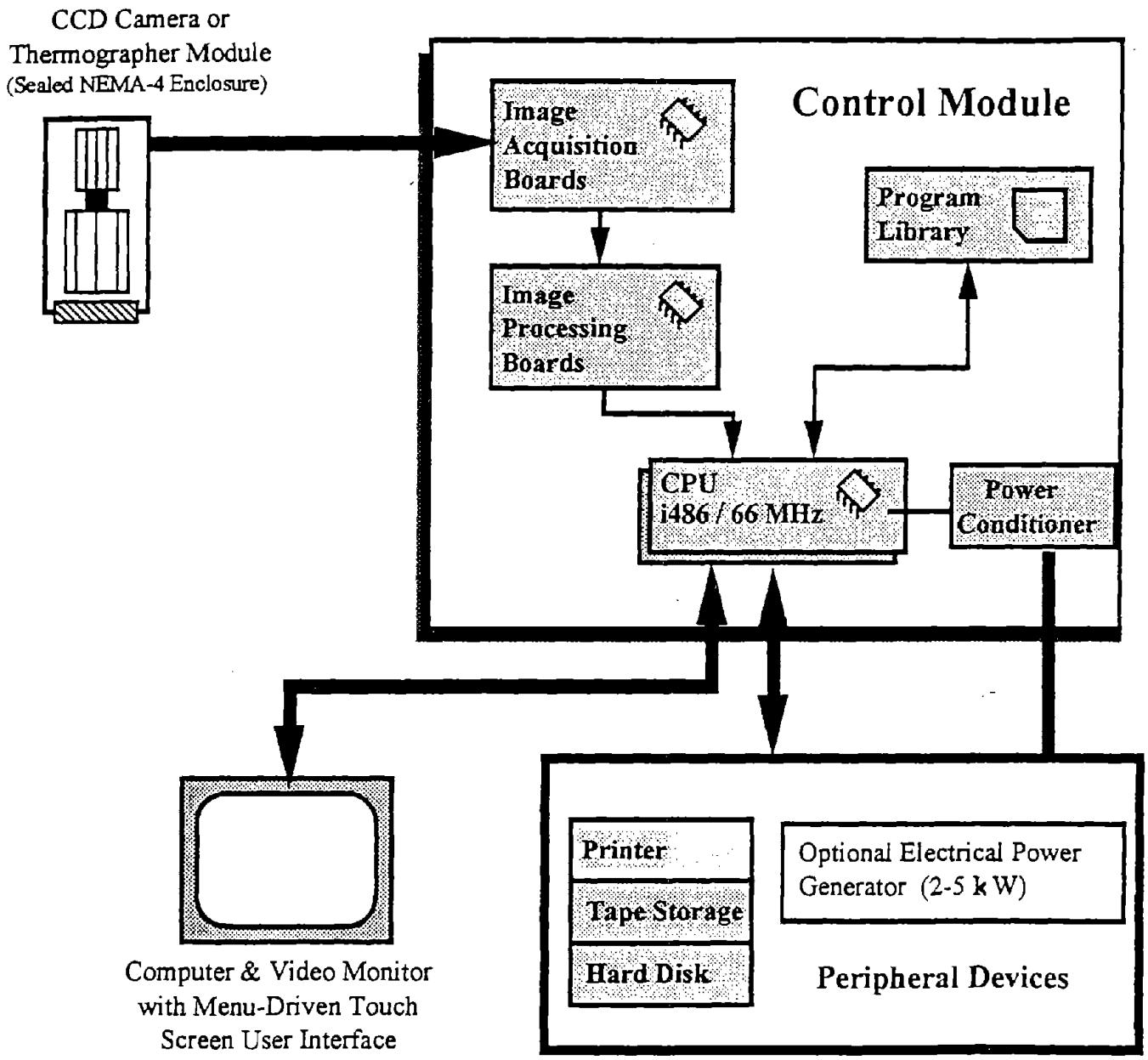


Figure 79. Schematic of color CCD camera system to measure damaged area.

have been integrated into a software package designed to assess the percentage of damaged area in real time.

All image pixels that have values that are lower than a selected threshold are considered representative of damaged area and are assigned a value of 1. The remaining image pixels that have values that are greater than or equal to the threshold value are assigned the value of 0. The resulting binary image shows the damaged area of the original image. The percentage of damaged area is calculated by first counting the number of pixels that have a value of 1 and then dividing that sum by the total number of pixels. A portion of a girder (figure 80) from the IDOT storage yard was used to evaluate the technique and the results are shown in figure 81.

## Infrared Thermography

### Introduction

As demonstrated above, visual techniques can quantify damaged areas within the visible spectrum. However, the ability to detect delaminations, voids, and other non-visual phenomena requires a technique to monitor an expanded electromagnetic spectrum. One such technique is thermography. Infrared (thermal) imaging is often referred to as thermography, an optical technique for remote detection of a scene's thermal radiation. Physically, it is based on thermal radiation laws and technically, it is similar to infrared thermometry. A completely non-invasive technique, it does not require any contact with an object and can be used to measure the temperature distribution of remote or moving targets. Various ranges of spectral response and optical configuration gives this technique a considerable level of flexibility in adapting it to a wide spectrum of applications. It is a unique tool for measurement, visualization, and analysis of various steady-state and transient heat-transfer phenomena. Analysis of the emissive and heat-transfer properties often provides a unique "signature" of various physical structures, processes, or objects. These capabilities have made infrared thermography an indispensable diagnostic tool for variety of industrial, military, and scientific applications, including materials non-destructive evaluation; aerial and vehicle-based testing of structures and buildings; and online inspection and non-destructive testing of electrical installations and nuclear, chemical, and petrochemical industrial complexes. In many of applications, infrared imaging allows early detection and quantitative diagnostic analysis of faults and failures of structures and materials, thus making feasible establishment of preventive maintenance scheduling.

In the last few years, applications of infrared thermography have been even further broadened due to immense developments and enhancements in the field of infrared sensing, image acquisition, and computer-processing hardware.

### Disbondment of Existing Paint Systems

The evaluation of the strength of the bond of paint and the identification of delaminations and voids present a complex problem. Spot measurements may be made by using magnetic dry film thickness gauges to assess the thickness of the original paint system. Similarly, the determination of its bond strength may be made by using one of several standard tests. The basic problem is that these tests give a reading only at the point of measurement with no given



Figure 80. Photograph of girder section showing damaged paint.

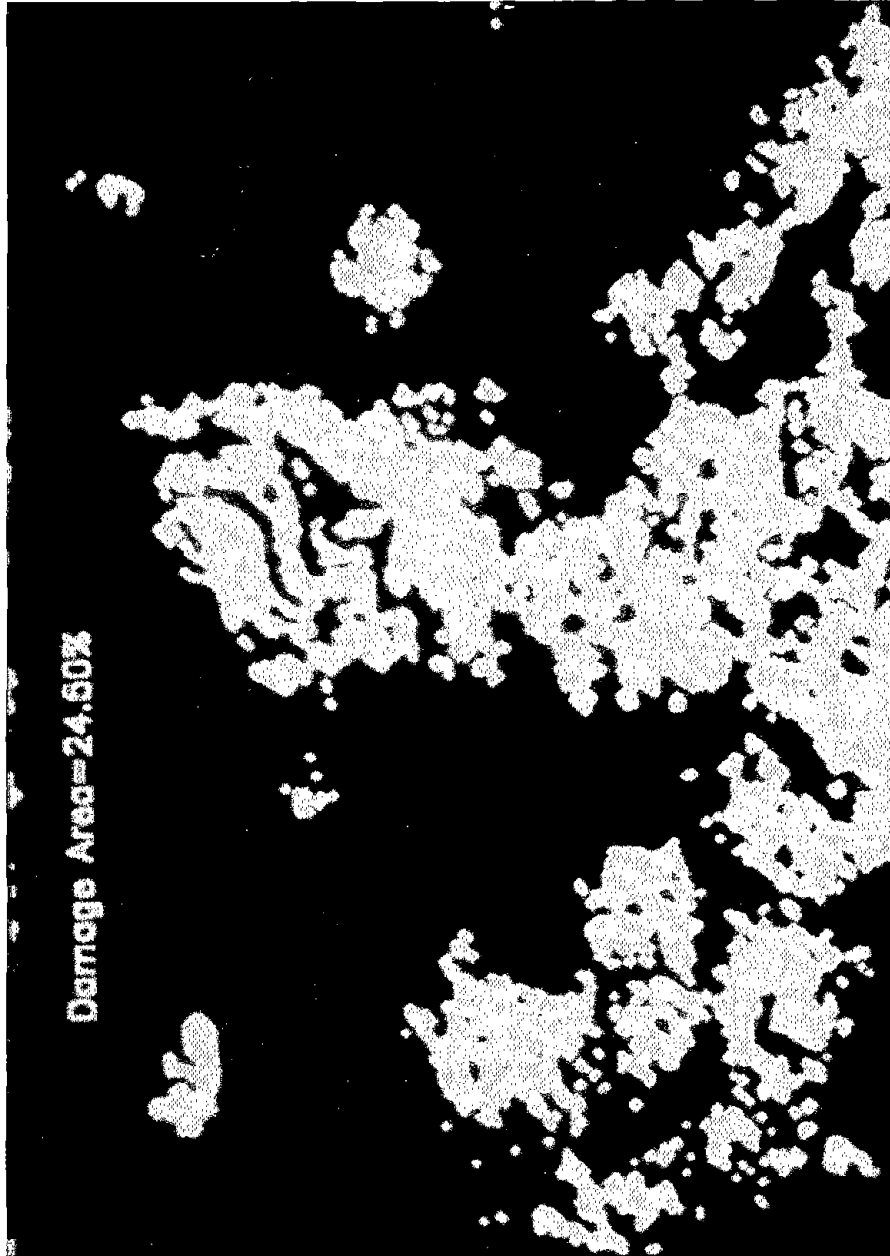


Figure 81. Calculated damaged area.

assurances that they are an accurate gauge of any zone or of the entire structure. The need exists for a global method that will detect the differences in the bond condition of the overall surface and direct the inspector to suspicious areas where additional point measurements can be made of the coating bond strength. In this case, thermography makes use of the fact that the bond strength affects the heat-transfer properties of the insulating paint bonded to a conductive substrate. This technique involves applying heat or cooling to the surface, either in the form of a continuous source or as a transient pulse, and observing differences in temperature from one location to another with an infrared sensor as the surface either heats up or cools down. The choice of heat source depends on a combination of conditions, including ambient temperature and the heat-transfer properties of the coating and the substrate. On a bridge, the heat source might be a heat lamp, torch, or flash lamp. One interesting possibility would be to use the thermal gradients resulting from solar heating. In this case, observations would be made either during sunrise or sunset on the areas of the bridge that are of interest. An imaging infrared sensor would allow temperature differences to be mapped. Hot areas, where the cooling rates were slower, would indicate areas of poor bond strength. These areas could be marked for later reference and review. An important factor to keep in mind with this technique is that absolute measurements are not required and only temperature gradients are required to pinpoint suspicious areas.

Thermal-wave imaging was evaluated to determine its ability to detect debonded paint areas. The thermographic system is schematically represented in figure 82 and is employed not only as an infrared sensor, but also as a high-resolution color camera. The camera is used to identify an area and act as a reference for the thermographic image. The panels used in this evaluation were obtained from a bridge girder supplied by IDOT. The surfaces were in a bad state of degradation. Figure 83 shows a typical sample area. As can be seen, there are areas of bare metal, rust, millscale and blister, and intact original paint. After the panel was heated, the image was obtained and enhanced by computer software. The areas of damaged and delaminated paint are easily seen (white and light shaded areas (figure 84)). In the preceding example, a continuous heat source was employed. However, if it had been replaced by a pulsed source and the gradient of heat flux was monitored, it would be possible to identify and differentiate between voids and delaminations and also to determine relative bond strengths.

### Conclusion and Recommendations

Preliminary evaluation has demonstrated the applicability of digital image analysis for paint inspection, including distinguishing and measuring of damaged paint areas. Image texture and color information were successfully used for evaluation of the damaged area, and the results have shown the sensitivities of color image features to certain paint characteristics. The image analysis technique based on accurate color image acquisition can be a useful and effective tool for laboratory as well as field paint assessment and can provide a permanent record of the results. However, it is essential to apply the knowledge of paint experts to the analysis of color images, and additional work with a greater number of paint samples is needed in order to establish consistent correlations between color image features and paint characteristics.



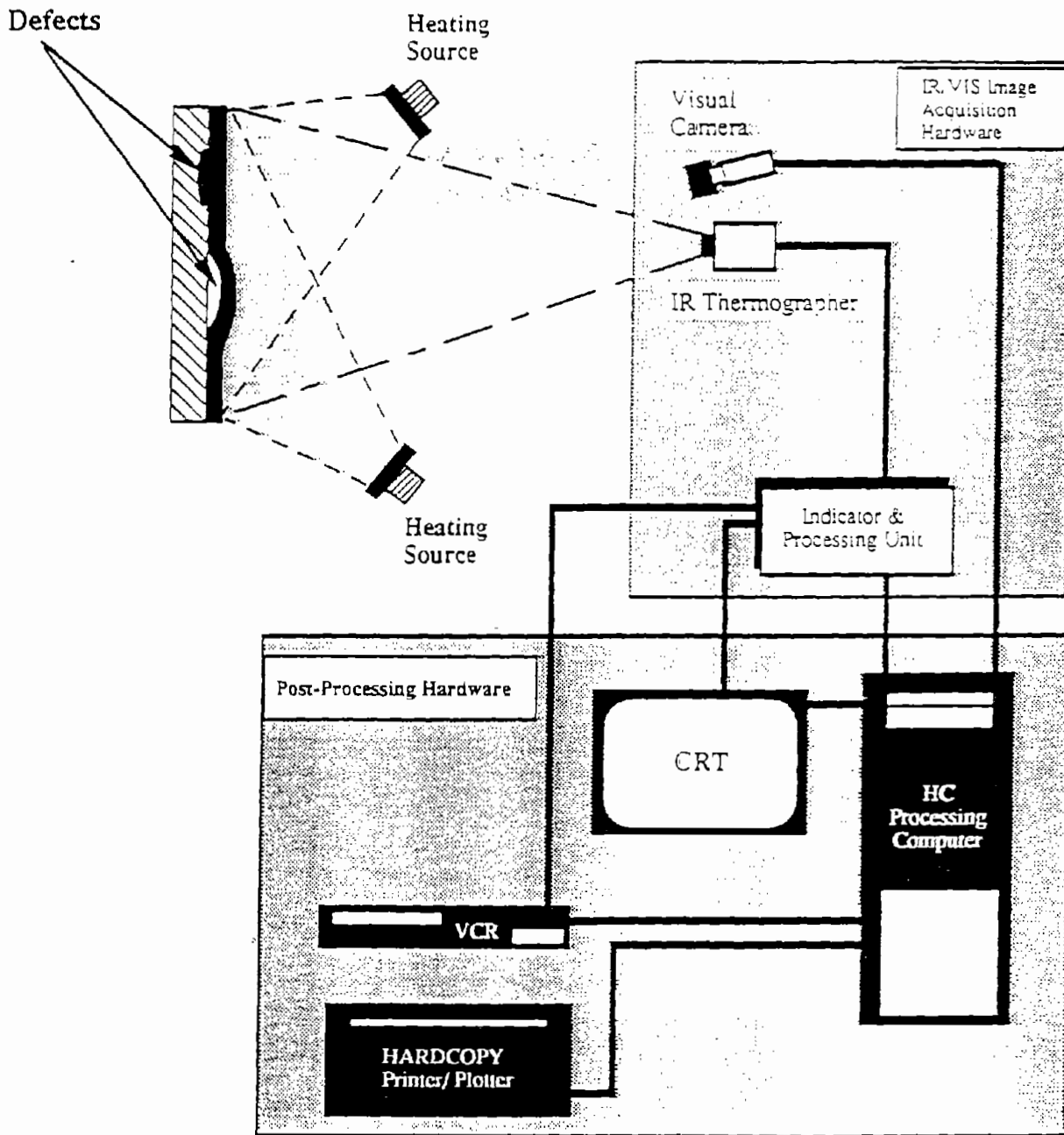


Figure 82. Schematic of infrared thermography system.

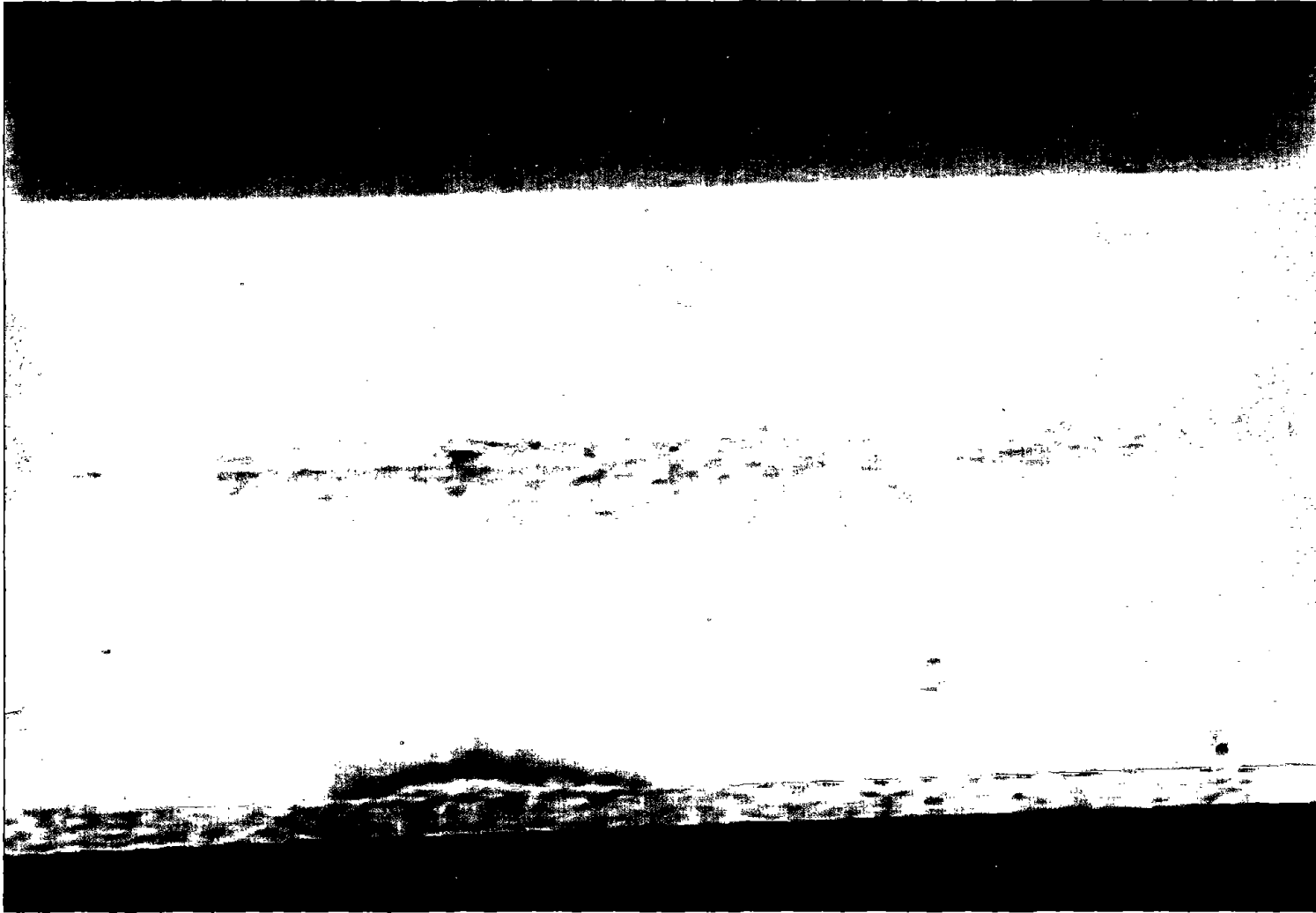
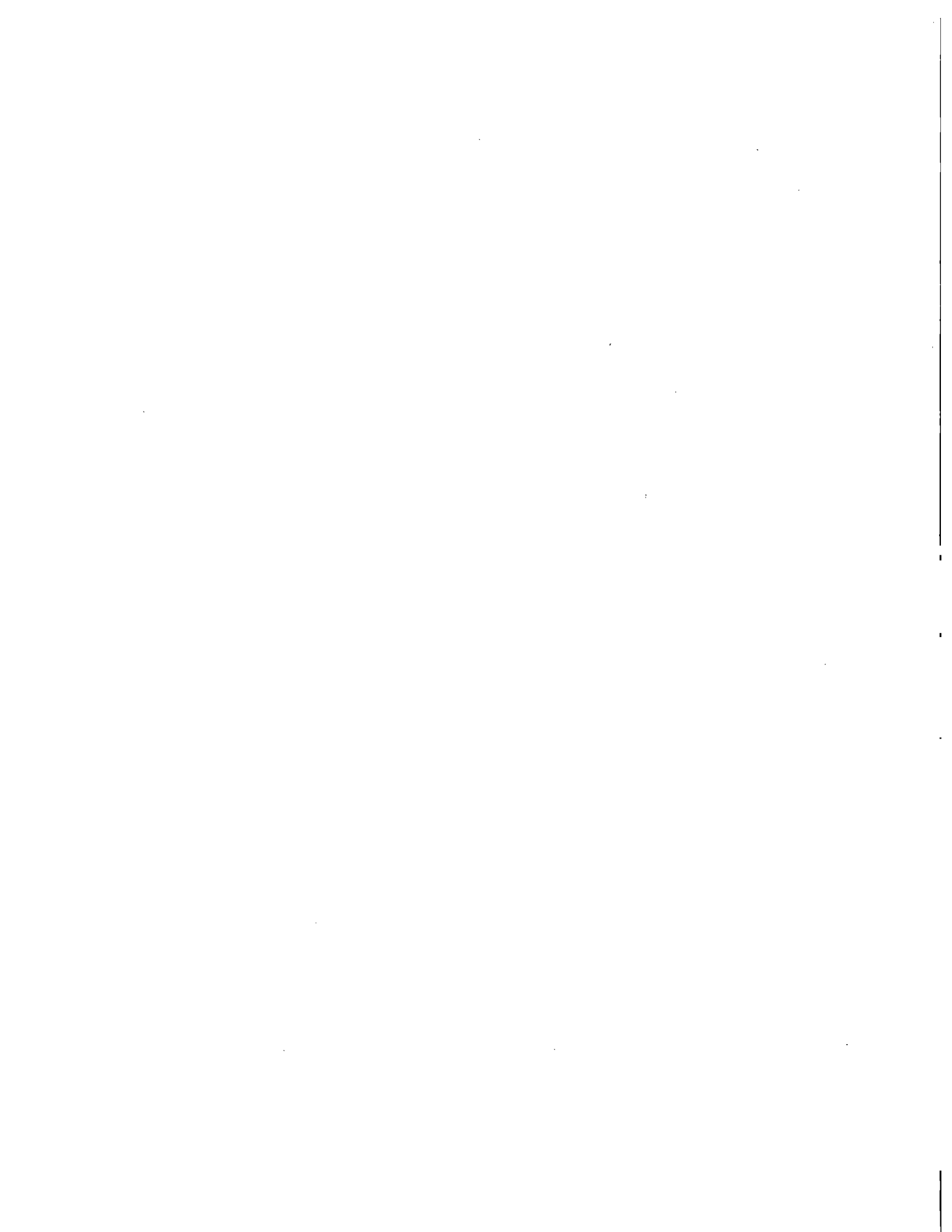


Figure 83. Section of girder used to evaluate infrared thermographs.



Figure 84. Delaminated paint on the I-Beam.



## APPENDIX A: DESCRIPTION OF ELECTROCHEMICAL TECHNIQUES

Given below is a short description of the three electrochemical techniques utilized in this study: electrochemical impedance spectroscopy (EIS), linear polarization, and potentiodynamic polarization.

### Electrochemical Impedance Spectroscopy

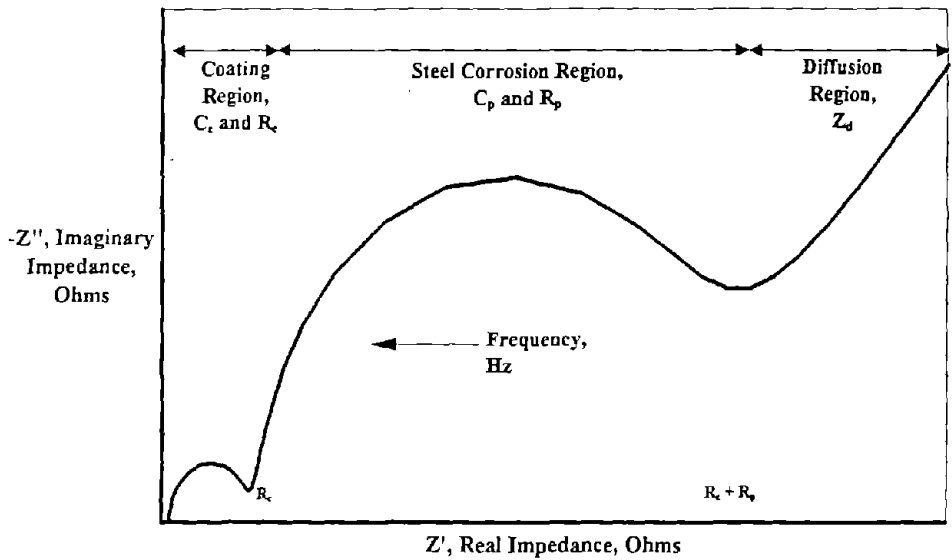
EIS is a technique where a small amplitude signal, usually a voltage between 5 to 50 mV, is applied to a specimen over a range of frequencies. Normally for corrosion systems, the frequency range is 0.001 Hz to 100,000 Hz, since most of the relevant information regarding the corrosion reaction occurs over this range. The EIS instrumentation records the real (resistive) and imaginary (capacitive) components of the impedance response of the system,  $Z'$  and  $Z''$ , respectively. Figure 85(a) shows an idealized Nyquist plot for a metal coated with a porous coating. The high-frequency limit on the left side of the plot gives the ohmic resistance of the electrolyte,  $R_s$ . At lower frequencies, two semicircles representing the corrosion reaction at the metal/electrolyte interface can be seen. One represents the coating resistance and capacitance,  $R_c$  and  $C_c$ , and the other represents the polarization resistance and capacitance,  $R_p$  and  $C_p$ . At even lower frequencies, a straight line is sometimes observed that is related to the mass transfer resistance ( $Z_d$ ) of the process. In the case of a coated metal surface, this parameter is related to the diffusion of electrolyte through the coating. Thus, from one experiment, relevant physical characteristics of a corrosion system (such as coated steel) can be found.

An important part of the EIS analysis is to create an "equivalent circuit" of the system using resistors and capacitors in series and in parallel. The physical behavior of the corrosion system can be simulated and quantified with this circuit to gain insight into the important processes of the corrosion system. Figure 85(b) shows an equivalent circuit simulating the ideal Nyquist plot for the metal coated with a porous coating shown in figure 85(a).

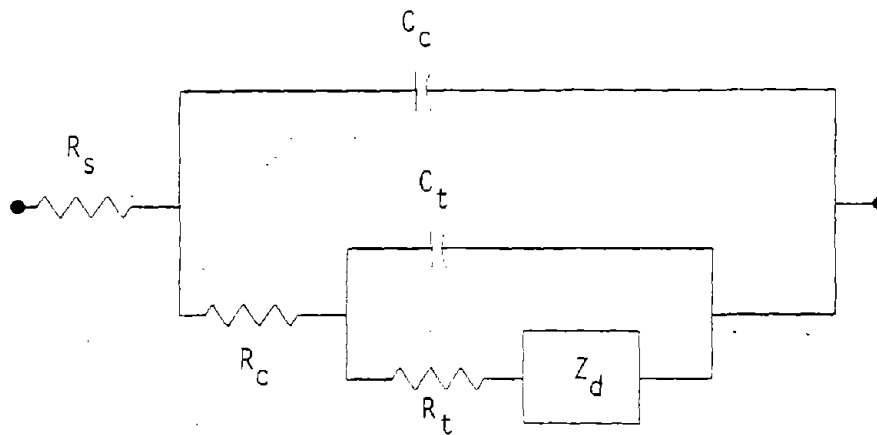
The EIS spectrum can also be presented in the Bode plot form, which gives the logarithm of the impedance,  $|Z|$ , and the phase angle,  $\phi$ , versus the logarithm of frequency. Figure 86(c) shows an idealized Bode plot for a metal coated with a porous coating. The Bode plot is useful when determining the frequency at maximum phase angle,  $\omega_{max}$ , because the maximum phase angle is immediately apparent on the plot. In the case of a metal with a porous coating, there are two maxima, one representative of the coating and the other representative of the corrosion reaction. The change in frequency at maximum phase angle can then be followed as the coating degrades and corrosion begins to occur.

### Linear Polarization

Linear polarization is a well-established electrochemical technique where a potential scan of 20 mV, positive and negative, of the free-corrosion potential (the open-circuit potential) is imposed on a metal sample and the current is recorded. The current/potential relationship is linear in this voltage range, and the slope ( $\Delta E/\Delta i$ ) is the polarization resistance ( $R_p$ ). Polarization resistance is defined as the resistance of the metal to oxidation during the application of an external potential. The corrosion rate is directly related to  $R_p$  and can be calculated from it by knowing the anodic and

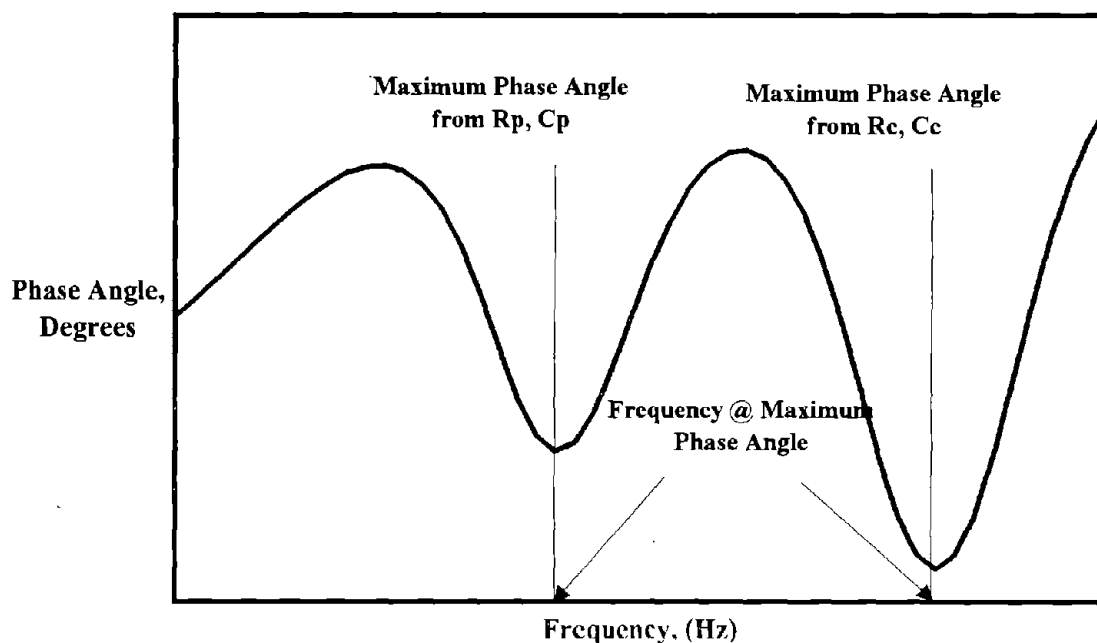
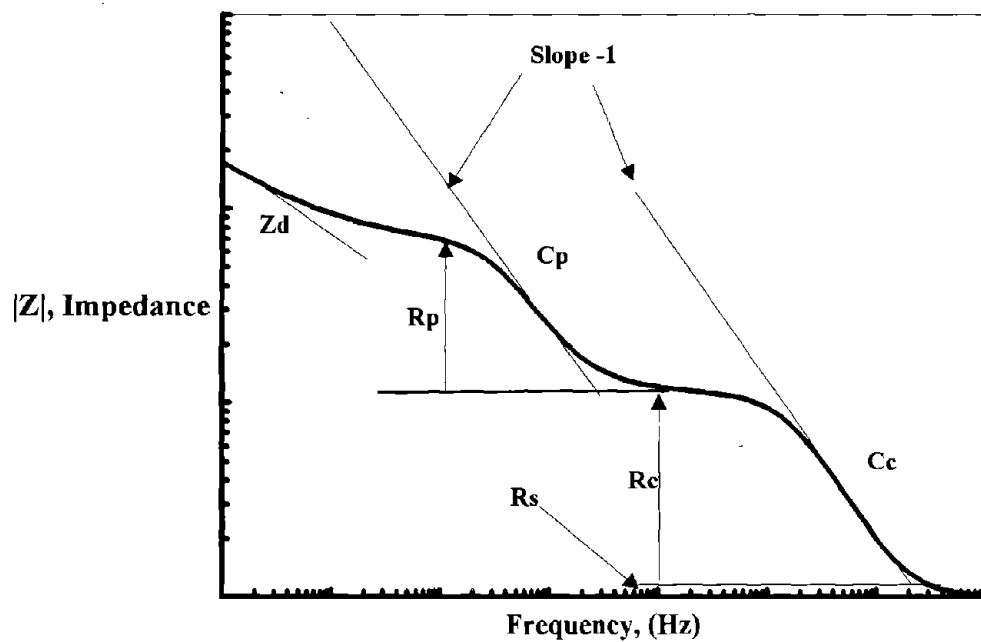


(a) Idealized Nyquist plot.



(b) Equivalent circuit for the idealized Nyquist plot.

Figure 85. Some elements of electrochemical impedance spectroscopy.



(c) Idealized Bode plot.

Figure 85. Some elements of electrochemical impedance spectroscopy (continued).

cathodic Tafel slopes, which can be obtained from potentiodynamic polarization measurements. The equation for calculating the corrosion rate is:

$$\text{CorrosionRate} = \frac{0.13 (E.W.)}{Ad} \frac{\beta_a \beta_c}{2.3 R_p (\beta_a + \beta_c)} \quad (6)$$

where E.W. is the equivalent weight of the metal, A is the area, d is the metal density, and  $\beta_a$  and  $\beta_c$  are the anodic and cathodic Tafel slopes, respectively.

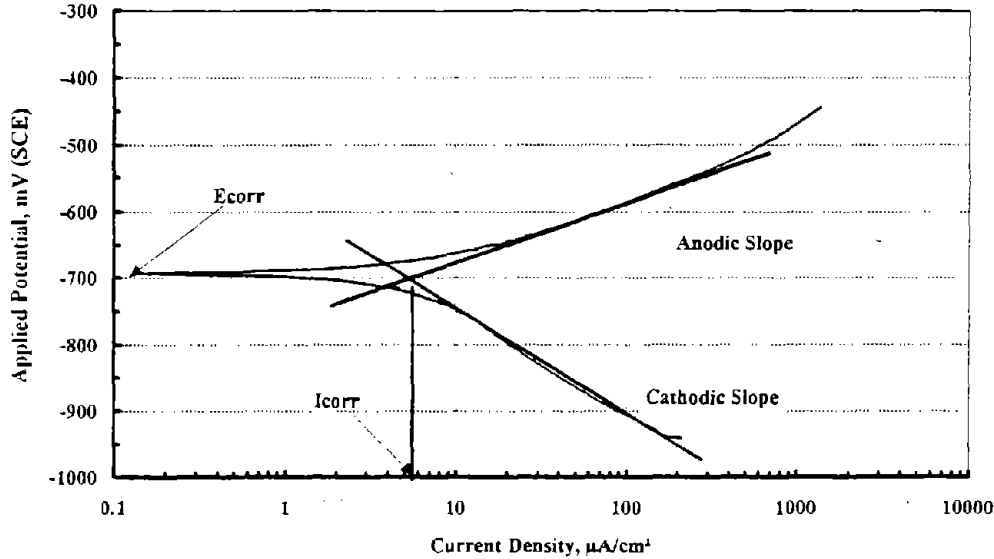


Figure 86. Representative potentiodynamic polarization scan for mild-steel rod in electrolyte.

### Potentiodynamic Polarization

Potentiodynamic polarization is a well-established electrochemical technique where a potential scan of 250 mV, positive and negative, of the free-corrosion potential is imposed on a metal sample and the current is recorded. The current in this potential range varies logarithmically with potential. Figure 86 shows a typical potentiodynamic polarization scan for a mild steel rod in electrolyte. The Tafel slopes of the anodic and cathodic reactions are obtained from the linear portions of the scan and together with the corrosion current,  $i_{corr}$ , the corrosion rate can be calculated. The corrosion current is obtained from the plot where the two slopes join, which is at the free-corrosion potential. In addition, the anodic and cathodic Tafel slopes can be used with  $R_p$ , obtained from linear polarization, and a corrosion rate can also be calculated.



## REFERENCES

1. "Better Roads 1993 Bridge Inventory", Better Roads, November 1993.
2. "Special Provision for Cleaning and Painting Existing Steel Structures, Complete Removal (Modified SSPC SP-10) Surface Preparation", Illinois Department of Transportation, July 1, 1992.
3. "Special Provision for Cleaning and Painting Existing Steel Structures, Partial Removal (Modified SSPC SP-6) Surface Preparation", Illinois Department of Transportation, July 1, 1992.
4. "Special Provision for Cleaning and Painting Existing Steel Structures, Partial Removal (Modified SSPC SP-3) Surface Preparation," Illinois Department of Transportation, July 1, 1992.
5. "Itemized Bids", Oregon State Highway Division, 1991.
6. "Costing Considerations for Maintenance and New Construction Coating Work", Gordon H. Brevoort, Brevoort Consulting Associates, Inc., Ridgewood, NJ, Paper 335, NACE Annual Conference, 1992.
7. "Costing Considerations for Maintenance and New Construction Coating Work", Gordon H. Brevoort, Brevoort Consulting Associates, Inc., Ridgewood, NJ, Paper 335, NACE Annual Conference, 1992.
8. "Cost Summary for Ohio Bridge", A. Kay, personal correspondence, November 1992.
9. G.T. Ruck et al., *Effectiveness of Cathodic Protection*, Gas Research Institute, Final Report, Contract No. 5082-271-0759, November 1985.
10. Standard Method of Evaluating Degree of Rusting on Painted Steel Surfaces, ASTM D610-85, 1986.
11. *Visual Standard for Abrasive Blast-Cleaned Steel*, SSPC-VIS-1-89, SSPC, Second Printing 1992.

